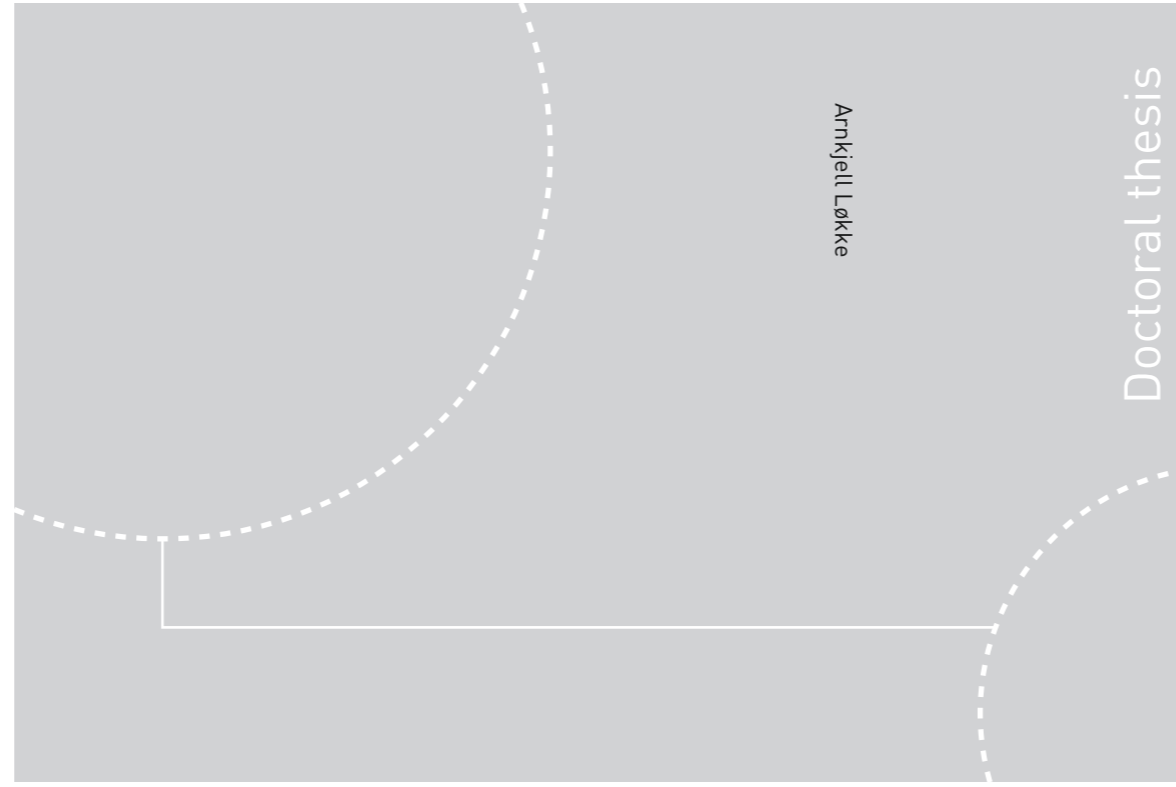


ISBN 978-82-326-3294-7 (printed ver.)
ISBN 978-82-326-3295-4 (electronic ver.)
ISSN 1503-8181



Doctoral theses at NTNU, 2018:252

NTNU
Norwegian University of Science and Technology
Thesis for the Degree of
Philosophiae Doctor
Faculty of Engineering
Department of Structural Engineering



Doctoral theses at NTNU, 2018:252

Arnkjell Løkke

Direct finite element method for nonlinear earthquake analysis of concrete dams including dam-water-foundation rock interaction

Arnkjell Løkke

Direct finite element method for nonlinear earthquake analysis of concrete dams including dam–water–foundation rock interaction

Thesis for the Degree of Philosophiae Doctor

Trondheim, September 2018

Norwegian University of Science and Technology
Faculty of Engineering
Department of Structural Engineering



Norwegian University of
Science and Technology

NTNU
Norwegian University of Science and Technology

Thesis for the Degree of Philosophiae Doctor

Faculty of Engineering
Department of Structural Engineering

© Arnkjell Løkke

ISBN 978-82-326-3294-7 (printed ver.)
ISBN 978-82-326-3295-4 (electronic ver.)
ISSN 1503-8181

Doctoral theses at NTNU, 2018:252

Printed by NTNU Grafisk senter

ABSTRACT

Evaluating the seismic performance of concrete dams requires nonlinear dynamic analysis of two- or three-dimensional dam–water–foundation rock systems that include all the factors known to be significant in the earthquake response of dams. Such analyses are greatly complicated by interaction between the structure, the impounded reservoir and the deformable foundation rock that supports it, and the fact that the fluid and foundation domains extend to large distances. Presented in this thesis is the development of a direct finite element (FE) method for nonlinear earthquake analysis of two- and three-dimensional dam–water–foundation rock systems. The analysis procedure applies standard viscous-damper absorbing boundaries to model the semi-unbounded fluid and foundation domains and specifies at these boundaries effective earthquake forces determined from a ground motion defined at a control point on the ground surface.

Part I develops the direct FE method for 2D dam–water–foundation rock systems. The underlying analytical framework of treating dam–water–foundation rock interaction as a scattering problem, wherein the dam perturbs an assumed "free-field" state of the system, is presented, and by applying these concepts to a bounded FE model with viscous-damper boundaries to truncate the semi-unbounded domains, the analysis procedure is derived. Step-by-step procedures for computing effective earthquake forces from analysis of two 1D free-field systems are presented, and the procedure is validated by computing frequency response functions and transient response of an idealized dam–water–foundation rock system and comparing against independent benchmark results.

This direct FE method is generalized to 3D systems in Part II of this thesis. While the fundamental concepts of treating interaction as a scattering problem are similar for 2D and 3D systems, the derivation and implementation of the method for 3D systems is much more involved. Effective earthquake forces must now be computed by analyzing a set of 1D and 2D systems derived from the boundaries of the free-field systems, which requires extensive book-keeping and data transfer for large 3D models. To reduce these requirements and facilitate implementation of the direct FE method for 3D systems, convenient simplifications of the procedure are proposed and their effectiveness demonstrated.

Part III of thesis proposes to use the direct FE method for conducting the large number of nonlinear response history analyses (RHAs) required for Performance Based Earthquake Engineering (PBEE) of concrete dams, and discusses practical modeling considerations for two of the most influential aspects of these analyses: nonlinear mechanisms and energy dissipation (damping). The findings have broad implications for modeling of energy dissipation and calibration of damping values for concrete dam analyses. At the end of Part III, the direct FE method is implemented with a commercial FE program and used to compute

the nonlinear response of an actual arch dam. These nonlinear results, although limited in their scope, demonstrate the capabilities and effectiveness of the direct FE method to compute the types of nonlinear engineering response quantities required for PBEE of concrete dams.

Keywords: Concrete dams; nonlinear earthquake analysis; dam–water–foundation rock interaction; absorbing boundaries; response history analysis; three-dimensional analysis

ACKNOWLEDGMENTS

First and foremost I would like to express my deepest gratitude to my main academic advisor Professor Anil K. Chopra at UC Berkeley for sharing his extensive insight into the theory of dynamics of structures and earthquake analysis of concrete gravity dams; for his steady guidance, encouragement and challenging of my ideas; and for being a mentor and role model. His contributions during our countless meetings and discussions over the last three years are gratefully acknowledged. I would also like to thank my advisors at NTNU: Professor Svein Remseth for making it possible for me to write this thesis for NTNU in collaboration with the UC Berkeley and to Adjunct Professor Amir Kaynia for his guidance and support, and for always finding the time to answer my many questions.

I am also grateful to several other individuals who have all contributed to this research in different forms:

- Dr. Ushnish Basu for his advice and contributions to the development of the direct FE method and its numerical implementation.
- Dr. Frank McKenna for his help with implementing 2D and 3D fluid–soil–structure interacting models in OPENSEES.
- Dr. Neal Simon Kwong for providing a critical outside view of my research, and for making lunch time discussions at campus such an enjoyable experience.

Last but not least, I am forever grateful to my loving wife Sarah. Your encouragement, patience and dedication to seeing this through, even when it meant moving half way around the world, means everything to me. Without your support, this PhD thesis would have never happened.

TABLE OF CONTENTS

INTRODUCTION.....	1
Motivation.....	1
Objectives and scope.....	2
Organization of this thesis.....	2
PART I DIRECT FE METHOD FOR NONLINEAR EARTHQUAKE ANALYSIS OF TWO-DIMENSIONAL DAM–WATER–FOUNDATION ROCK SYSTEMS	
1 Introduction	6
2 System and ground motion.....	8
2.1 Semi-unbounded dam–water–foundation rock system.....	8
2.2 Modeling of unbounded domains	9
2.3 Governing equations.....	9
2.3.1 Dam and foundation domain.....	9
2.3.2 Fluid domain	10
2.3.3 Dam–water–foundation rock system	12
3 Dam–foundation rock system.....	13
3.1 Dam–foundation rock interaction as a scattering problem.....	13
3.2 Viscous-damper absorbing boundaries.....	14
3.3 Equations of motion.....	15
3.4 Free-field earthquake motion.....	16
3.5 Computing effective earthquake forces	17
3.5.1 Bottom boundary	17
3.5.2 Side boundaries.....	18
3.5.3 Relation to the Domain Reduction Method	20
3.6 Numerical validation	21
3.6.1 Dam on rigid foundation rock.....	23
3.6.2 Dam–foundation rock system	23
3.6.3 Ignoring effective earthquake forces at side boundaries.....	24
3.6.4 Can foundation mass be ignored?.....	25
4 Dam–water system.....	27
4.1 Dam–water interaction as a scattering problem.....	27
4.2 Viscous-damper absorbing boundary	28
4.3 Equations of motion.....	29
4.4 Computing effective earthquake forces at Γ_r	30
4.5 Numerical validation	31

4.5.1	Hydrodynamic forces on rigid dam	32
4.5.2	Dam–water system.....	34
4.5.3	Ignoring effective earthquake forces on fluid boundary Γ_f	35
5	Dam–water–foundation rock system	36
5.1	Dam–water–foundation rock interaction as a scattering problem	36
5.2	Equations of motion.....	37
5.2.1	Approximating water–foundation rock interaction.....	38
5.2.2	Dam–water–foundation rock system	39
5.3	Summary of procedure	39
5.4	Numerical validation	41
5.4.1	Frequency response functions for dam response	42
5.4.2	Response to transient motion	43
5.4.3	Influence of water–foundation rock interaction.....	44
6	Conclusions	47
PART II DIRECT FE METHOD FOR NONLINEAR EARTHQUAKE ANALYSIS OF THREE-DIMENSIONAL DAM–WATER–FOUNDATION ROCK SYSTEM		
1	Introduction	50
2	System and ground motion.....	52
2.1	Semi-unbounded dam–water–foundation rock system.....	52
2.2	Earthquake excitation	55
3	Equations of motion	59
3.1	Governing equations.....	59
3.2	Interaction as a scattering problem	60
3.3	Approximating water–foundation rock interaction	63
3.4	Final equations of motion	64
4	Computing effective earthquake forces.....	66
4.1	Forces at bottom boundary	66
4.2	Forces at side boundaries.....	67
4.2.1	Computing forces at side boundaries: uniform canyon	67
4.2.2	Computing forces at side boundaries: arbitrary canyon geometry	69
4.3	Forces at upstream fluid boundary	71
5	Numerical validation of the direct FE method	74
5.1	Reproducing free-field motion in foundation rock.....	74
5.1.1	Free-field motion at flat box surface (the flat box test)	74
5.1.2	Free-field motion at canyon surface	75
5.2	Dynamic response of Morrow Point Dam	77
5.2.1	System analyzed.....	77

5.2.2	EACD3D-08 model for substructure method	79
5.2.3	Frequency response functions for dam response	79
5.2.4	Response to transient motion	82
5.3	Frequency response functions for spatially uniform motion	83
5.3.1	Dam on rigid foundation rock	84
5.3.2	Dam–foundation rock system	84
5.3.3	Dam–water system	86
5.3.4	Dam–water–foundation rock system	86
6	Simplifications of the direct FE method	88
6.1	Using 1D analysis to compute effective earthquake forces at side foundation boundaries	88
6.2	Ignoring effective earthquake forces at side foundation boundaries	92
6.3	Avoiding deconvolution of the surface control motion	95
6.4	Ignoring effective earthquake forces on upstream boundary of fluid domain	97
7	Summary of procedure	99
8	Conclusions	101

PART III MODELING AND PRACTICAL IMPLEMENTATION OF THE DIRECT FE METHOD FOR PERFORMANCE BASED EARTHQUAKE ENGINEERING OF CONCRETE DAMS

1	Introduction	106
2	Performance based earthquake engineering of dams	107
2.1	The Pacific Earthquake Engineering Research Center PBEE framework	107
2.2	Seismic hazard analysis	109
2.3	Structural analysis	110
2.4	Damage analysis	111
2.5	Loss analysis	112
2.6	Modeling of uncertainty	113
3	Modeling of concrete dams by the direct FE method	115
3.1	Modeling of nonlinear mechanisms	115
3.1.1	Cracking of concrete	115
3.1.2	Opening and closing of vertical contraction joints	118
3.1.3	Sliding and separation at lift joints and concrete-rock interfaces	119
3.1.4	Discontinuities in the foundation rock	120
3.2	Modeling of energy dissipating mechanisms	120
3.2.1	Material damping	120
3.2.2	Radiation damping	121
3.2.3	Energy dissipation at the reservoir boundaries	122
3.2.4	Calibration of damping values	127

4	Nonlinear earthquake analysis of Morrow Point Dam	130
4.1	System and ground motion	130
4.1.1	FE model of dam–water–foundation rock system	130
4.1.2	Nonlinear modeling parameters	131
4.1.3	Static and dynamic loads	132
4.2	Implementation of the direct FE method with ABAQUS	133
4.3	Results from nonlinear dynamic analysis	134
5	Conclusions	138
CONCLUSIONS AND FUTURE WORK		141
	Summary and conclusions	141
	Future work	142
REFERENCES		145
NOTATION		153
APPENDIX A SELECTION OF DOMAIN SIZE FOR TWO-DIMENSIONAL DAM–WATER–FOUNDATION ROCK SYSTEMS		157
APPENDIX B THE DOMAIN REDUCTION METHOD FOR SEISMIC INPUT IN SOIL–STRUCTURE-INTERACTION ANALYSES		169
APPENDIX C COMPUTING FREQUENCY RESPONSE FUNCTIONS IN THE TIME DOMAIN		175
APPENDIX D APPLYING UNIFORM GROUND MOTION IN THE DIRECT FE METHOD.....		179
APPENDIX E COMPUTING BOUNDARY TRACTIONS FROM 1D STRESS-STRAIN RELATIONS		183

INTRODUCTION

Motivation

Concrete dams are critical structures that provide important services in the form of power generation, flood control, irrigation and recreation. There are also catastrophic consequences for life and property in the case of a failure of these structures. However, most existing dams in seismic regions were designed by methods that are now considered inaccurate and obsolete. The damage sustained by the few concrete dams that have been subjected to intense ground motions, e.g., Koyna Dam in India, Hsinfengkiang Dam in China, Sefidrud Dam in Iran, and Pacoima Dam in the United States, together with the growing concern of the seismic safety of critical facilities, has led to considerable interest in reevaluating existing dams using modern analysis and experimental procedures. In recent years, interest has also increased on how to apply the principles of Performance Based Earthquake Engineering (PBEE) to concrete dam evaluations.

Earthquake analysis of concrete dams is greatly complicated by interaction between the structure, the impounded reservoir and the deformable foundation rock that supports it, and the fact that the fluid and foundation domains extend to large distances. To overcome the difficulties in modeling dam–water–foundation rock interaction and semi-unbounded domains in the finite element method (FEM), the dam engineering profession has often employed an expedient solution: the foundation is modeled in limited extent and assumed to have no mass, hydrodynamic effects are approximated by an added mass of water moving with the dam, and the design ground motion at the surface is applied directly to the bottom fixed boundary of the foundation domain. This modeling approach has become popular in actual dam engineering projects because it is easy to implement in commercial FE codes; however, research has demonstrated that such oversimplified analyses can overestimate stresses by as much as a factor of 2 to 3, thus leading to overly conservative design of new dams and the incorrect conclusion that an existing dam is unsafe and needs retrofitting.

Clearly, this situation is not satisfactory. Evaluating the seismic safety of concrete dams requires accurate and robust analysis procedures that recognize dam–water–foundation rock interaction and the semi-unbounded sizes of the water and foundation domains, and consider nonlinearities such as opening and closing of vertical contraction joints and cracking of concrete during intense earthquake motion. However, recognizing that most dam engineers may – for various reasons – be predisposed to use a particular FE program, it is also important

that such analysis procedures are general enough to be used with any FE program without requiring undue efforts from the user.

Objectives and scope

The overall objective of this research is to develop a procedure for nonlinear response history analysis (RHA) of semi-unbounded dam–water–foundation rock systems that is accurate, robust, and general enough to be used with any commercial FE program without modification of the source code. In particular, the objectives are to:

- Extend the "standard" finite element model of dam–water–foundation rock systems to include absorbing boundaries at the upstream end of the fluid domain and bottom and side boundaries of the foundation domain to model their semi-unbounded geometries.
- Develop a practical procedure for determining the seismic input to the analysis procedure starting from a free-field control motion specified on level ground.
- Validate the accuracy of the analysis procedure by comparing against analytical and semi-analytical unbounded domain models using the substructure method of analysis for 2D and 3D dam–water–foundation rock systems.
- Develop guidelines for implementation of the procedure in commercial FE software, as well as recommendations for practical modeling choices such as the sizes of the foundation and fluid domains to be included in the FE model, modeling of nonlinear mechanisms, and modeling of energy dissipating mechanisms (damping).
- Demonstrate the usefulness of the analysis procedure for conducting nonlinear RHA of concrete dams in commonly used commercial FE programs.
- Advocate use of more accurate analysis procedures for earthquake analysis of concrete dams in the dam engineering community.

Organization of this thesis

This thesis is written in three parts, each corresponding to a paper that has been published in international peer-reviewed journals (Parts I and II) or has been submitted for such publication (Part III). The content in this thesis is more extensive than the journal papers however, because it also contains several parts (derivations, validation results, etc.) that were left out of the papers due to space limitations.

Part I presents the analytical framework underlying the direct FE method, develops the analysis procedure for earthquake analysis of two-dimensional dam–foundation rock, dam–water, and ultimately dam–water–foundation rock systems, and derives the equations of motion for these systems. Then, procedures for computing effective earthquake forces starting from a free-field ground motion defined at a control point on the foundation surface are

developed. Several examples are presented to validate the accuracy of the direct FE method applied to a wide range of 2D systems.

Part II generalizes the direct FE method to three-dimensional systems, which is fundamentally more challenging to analyze because of their complicated 3D geometry. The equations of motions for 3D systems with absorbing boundaries are derived, procedures for computing effective earthquake forces from a set of 1D and 2D analyses are presented, and several numerical examples are presented to validate the accuracy of the direct FE method applied to 3D systems. To facilitate implementation of the procedure for 3D systems, convenient simplifications are proposed and their effectiveness demonstrated.

Part III proposes to use the direct FE method for conducting the large number of nonlinear RHAs required for PBEE of concrete dams. A brief introduction to PBEE in the context of concrete dams is presented, the most significant nonlinear mechanisms that can develop in concrete dams are discussed, and the various types of energy dissipation (damping) in the dam–water–foundation rock system are reviewed. Recommendations for how to model these features in the direct FE method are presented. Finally, the capabilities of the direct FE method are demonstrated by computing the nonlinear earthquake response of Morrow Point Dam using a commercial FE code.

This thesis also includes five appendices: Appendix A presents guidelines for selecting an appropriate size for the foundation domain to be included in 2D dam–water–foundation rock models. Appendix B outlines the use of the Domain Reduction Method for seismic input to soil–structure interaction analyses and demonstrates that – when based on the same assumptions – the DRM and direct FE method will give identical results. Appendices C and D provides details on the computational procedures used to calculate frequency response functions in the time domain and to apply uniform ground motion in the direct FE method, respectively. Lastly, Appendix E presents equations for computing effective earthquake forces from one-dimensional stress-strain relations.

In addition, two contributions from this research are not documented in this thesis. The first is the development of several sets of scripts and computer code to implement the direct FE method for nonlinear RHA and to facilitate the benchmark analyses using the substructure method for 2D and 3D systems implemented in the Fortran77 programs EAGD84 and EACD3D-08. These scripts will be made publicly available online through the NISEE e-library websites. The second is the objective of advocating the use of more accurate analysis procedures in the dam engineering community. This has been achieved through presentations at international conferences and workshops on concrete dams and earthquake engineering.

PART I

**Direct finite element method for nonlinear
earthquake analysis of two-dimensional dam–water–
foundation rock systems**

1 Introduction

Evaluating the seismic performance of concrete gravity dams requires dynamic analysis of two- or three-dimensional dam–water–foundation rock systems that include all significant factors in the earthquake response of concrete dams [1]: dam–foundation rock interaction including inertia effects of the rock [2,3]; dam–water interaction, including water compressibility and energy absorption at the reservoir bottom [4–6]; radiation damping due to the semi-unbounded sizes of the reservoir and foundation domains [3,7]; and nonlinear behavior of the dam and foundation rock [8–16];

Analysis procedures based on the *substructure method* have been available since 1984 for 2D frequency-domain analysis of dam–water–foundation rock systems [17]. This method models the semi-unbounded domains rigorously and specifies the ground motion directly at the dam–foundation rock interface; however, it is restricted to homogeneous material properties and simple geometry of the reservoir and foundation domains. More importantly, the substructure method is restricted to linear behavior of the entire system. Thus, nonlinear effects such as cracking of concrete and separation and sliding at joints and interfaces cannot be modeled.

The *direct method* of analysis on the other hand, models the entire system directly in the time-domain using finite elements (FEs). Such analyses are often conducted using commercial software that ignores one or several of the above factors to facilitate nonlinear dynamic analysis. For many years, the dam engineering profession used a FE model that included a limited extent of foundation rock, assumed to have no mass, and approximated hydrodynamic effects by an added mass of water moving with the dam. The design ground motion – typically defined at a control point on the free surface – was applied at the bottom fixed boundary of the foundation domain without modification. These approximations are attractive because they simplify the analysis greatly, however, such a model solves a problem that is very different from the real problem on two counts: (1) the assumptions of massless rock and incompressible water – implied by the added mass water model – are unrealistic, as research has demonstrated [1]; and (2) applying ground motion specified at a control point on the free surface to the bottom boundary of the FE model contradicts recorded evidence that motions at depth generally differ significantly from surface motions. In recent years, some engineers have shifted away from this approach.

To eliminate these unrealistic assumptions, the FE model of the dam must be extended to comprise a foundation domain that includes mass, stiffness, and material damping appropriate for rock, and a fluid domain that includes water compressibility and reservoir bottom absorption. The semi-unbounded foundation and fluid domains must be reduced to bounded sizes with appropriate radiation conditions at the domain boundaries to allow propagation of outgoing waves. Development of such *absorbing boundaries* is a vast field

with rich literature [18–34]. The earthquake motion cannot be specified directly at the model truncations as this would render any absorbing boundary ineffective. Instead, *effective earthquake forces* are computed from the earthquake motion and applied either directly at the absorbing boundaries [35–37] or via a layer of elements interior of the boundaries [38–40].

Utilizing these concepts, a direct finite element procedure for nonlinear analysis of dam–water–foundation rock systems was developed by Basu [41]. Here, the high performing Perfectly Matched Layer (PML) [25] was used as the absorbing boundary, and the Effective Seismic Input (ESI) method [38], also known as the Domain Reduction Method (DRM) [40] was used to apply the effective earthquake forces. Although the procedure rigorously incorporates all the above factors significant in the earthquake response of dams, the PML boundary and DRM procedure are currently not available in most commercial FE codes; the only exception is LS-DYNA [42]. Thus, this procedure is not accessible to researchers and practicing engineers who, for various reasons, prefer other FE codes. These limitations can be overcome by modeling the absorbing boundaries by viscous dampers [18] and specifying the effective earthquake forces directly at these boundaries. Both of these features are available in almost every commercial FE code and are therefore chosen herein. A variation of such a procedure initiated by the US Bureau of Reclamation, wherein effective earthquake forces on the side boundaries are ignored, is often used in the dam engineering profession [43–45].

The following chapters develops the formulation for a direct finite element method for nonlinear earthquake analysis of semi-unbounded dam–water–foundation rock systems that incorporates all significant factors for the earthquake response of dams, while ensuring broad applicability by using the well-known viscous damper as the absorbing boundaries. Derivation of the analysis method is founded on the idea of treating interaction as a scattering problem [38,46], and follows a similar outline as the procedure developed by Basu [41] using PML-boundaries and DRM for seismic input. In Chapter 2, the system and ground motion is defined, and the governing equations for each of three subdomains are presented. In Chapters 3 and 4, the direct FE method is developed for dam–foundation rock and dam–water systems, respectively, by utilizing the concept of treating interaction as a scattering problem and formulating the radiation condition for viscous-damper boundaries in a convenient way. These two procedures are integrated to formulate the analysis procedure for the combined dam–water–foundation rock system in Chapter 5. At the end of each of the Chapters 3–5, the analysis method is validated by computing the response of idealized dam–foundation rock (Chapter 3), dam–water (Chapter 4), and dam–water–foundation rock (Chapter 5) systems and comparing against results obtained using the substructure method. In Chapter 5, the importance of including water–foundation rock interaction is also discussed.

A shortened version of this part of the thesis has been published in the journal *Earthquake Engineering and Structural Dynamics*:

Løkke, A., and Chopra, A.K. (2017). Direct finite element method for nonlinear analysis of semi-unbounded dam–water–foundation rock systems. *Earthquake Engineering & Structural Dynamics*, 46.8, 1267-1285.

2 System and ground motion

2.1 Semi-unbounded dam–water–foundation rock system

The idealized, two-dimensional dam–water–foundation rock system (Figure 2.1) has three parts: (1) the gravity dam with nonlinear properties; (2) the foundation rock, consisting of a bounded region adjacent to the dam that can be nonlinear and inhomogeneous, and a semi-unbounded region that is restricted to be linear; and (3) the fluid domain, consisting of a bounded region of arbitrary geometry adjacent to the dam that may be nonlinear, and a uniform channel, unbounded in the upstream direction, that is restricted to be linear. Thus, nonlinear effects such as concrete cracking, sliding and separation at construction joints, lift joints, and concrete-rock interfaces, and cavitation in the fluid may be considered in the analysis.

The earthquake excitation is defined at a control point at the surface of the foundation rock by two components of free-field ground acceleration (Figure 2.1): the horizontal component $a_g^x(t)$ transverse to the dam axis, and the vertical component $a_g^y(t)$. The surface of the foundation rock is assumed to be at the same elevation in the far upstream and downstream directions; this geometric restriction is introduced to define a convenient free-field state of the foundation rock in Section 3.1.

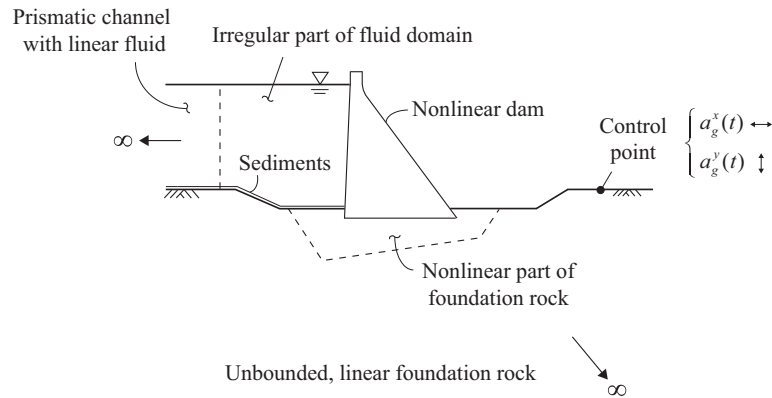


Figure 2.1: Semi-unbounded dam–water–foundation rock system: (1) the dam itself; (2) the foundation rock, consisting of a bounded, nonlinear region and a semi-unbounded, linear region; and (3) the fluid domain, consisting of an irregular, nonlinear, region, and a semi-unbounded prismatic channel with linear fluid. Figure adapted from Ref. [41].

2.2 Modeling of semi-unbounded domains

The dam–water–foundation rock system in Figure 2.1 is modeled by a FE discretization of a bounded system with viscous-damper boundaries to represent the semi-unbounded foundation and fluid domains. The earthquake motion cannot be specified directly at these model truncations as this would render any absorbing boundary ineffective. Instead, effective earthquake forces are computed from the earthquake excitation and applied at the absorbing boundaries.

The size of the foundation and fluid domains included in the FE model is determined by the ability of the absorbing boundaries to absorb outgoing (scattered) waves from the dam. If an advanced boundary such as the PML [25] is used, a small domain is sufficient to model the fluid and foundation domains (Figure 2.2a). In contrast, the simple viscous-damper boundary applied in this formulation requires much larger domains (Figure 2.2b).

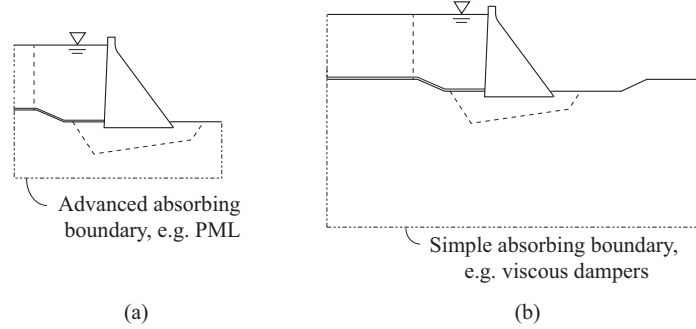


Figure 2.2: Dam–water–foundation rock system with truncated foundation and fluid domains: (a) small domain sizes with advanced absorbing boundary; (b) large domain sizes with simple absorbing boundary.

2.3 Governing equations

2.3.1 Dam and foundation domain

The equations of motion governing the vector of total displacements \mathbf{r}^t in the FE model of the dam with a truncated foundation domain and absorbing boundary Γ_f (Figure 2.3) are

$$\mathbf{m}\ddot{\mathbf{r}}^t + \mathbf{c}\dot{\mathbf{r}}^t + \mathbf{f}(\mathbf{r}^t) = \mathbf{R}_h^t + \mathbf{R}_b^t + \mathbf{R}_f^t + \mathbf{R}^{\text{st}} \quad (2.1)$$

where \mathbf{m} and \mathbf{c} are the mass and damping matrices, respectively; $\mathbf{f}(\mathbf{r}^t)$ is the vector of internal forces which may be nonlinear in the dam and adjacent part of the foundation rock; \mathbf{R}_h^t and \mathbf{R}_b^t are the vectors of hydrodynamic forces acting at the dam–water interface Γ_h and water–foundation interface Γ_b , respectively; \mathbf{R}^{st} is the vector of static forces, including self-

weight, hydrostatic pressures, and static foundation reactions at Γ_f ; and \mathbf{R}'_f are the forces associated with the absorbing boundary Γ_f , which include the effect of the excitation caused by seismic waves propagating from a distant earthquake source to the dam site, and the radiation condition at the boundary. Expressions for the forces \mathbf{R}'_h , \mathbf{R}'_b and \mathbf{R}'_f will be derived later.

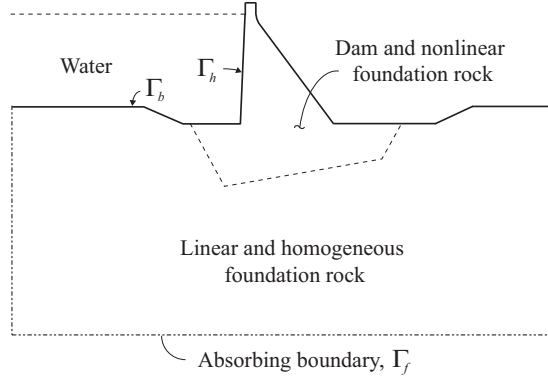


Figure 2.3: Schematic FE model of the dam and foundation rock, with absorbing boundary Γ_f to truncate the semi-unbounded foundation domain.

2.3.2 Fluid domain

The water is modeled as a linear inviscid, irrotational and compressible fluid with hydrodynamic pressures p governed by the acoustic wave equation:

$$\nabla^2 p = \frac{1}{C^2} \ddot{p} \quad (2.2)$$

where C is the speed of pressure waves in water.

Hydrodynamic pressures are caused by acceleration of the boundaries in contact with the reservoir: the upstream dam face Γ_h and the reservoir bottom Γ_b (Figure 2.4). These pressures are related to the total accelerations $\ddot{\mathbf{r}}^t$ at the fluid–solid interface by the boundary conditions:

$$\nabla p \cdot \mathbf{n}_h = -\rho \mathbf{n}_h \cdot \ddot{\mathbf{r}}^t_h, \quad \text{at } \Gamma_h \quad (2.3a)$$

$$\nabla p \cdot \mathbf{n}_b + q\dot{p} = -\rho \mathbf{n}_b \cdot \ddot{\mathbf{r}}^t_b, \quad \text{at } \Gamma_b \quad (2.3b)$$

where \mathbf{n}_h and \mathbf{n}_b are the outward normal vectors to the fluid at Γ_h and Γ_b , respectively; and ρ is the density of water. The second term on the left hand side of Equation (2.3b) is associated with the absorption of hydrodynamic pressure waves in sediments deposited at the

reservoir bottom. This wave absorption is modeled in an approximate way by a boundary condition that allows partial absorption of incident hydrodynamic waves, where the damping coefficient q is given by

$$qC = \frac{1 - \alpha}{1 + \alpha} \quad (2.4)$$

where α is the reservoir bottom reflection coefficient [6,17]. This simplified model is chosen herein to allow for a meaningful comparison with the substructure method [17] in the numerical validations presented at the end of Chapters 3–5. The effects of reservoir bottom sediments can alternatively be included using more sophisticated methods, for example by directly modeling the thickness and extent of sediments discretized by finite elements with a viscoelastic [47,48] or poroelastic [49,50] material model.

At the free water surface the boundary condition is simply $p = 0$; effects of surface waves are not included as these have little influence on the dynamic response of concrete dams [51]. Lastly, an appropriate radiation condition must hold at the absorbing boundary Γ_r .

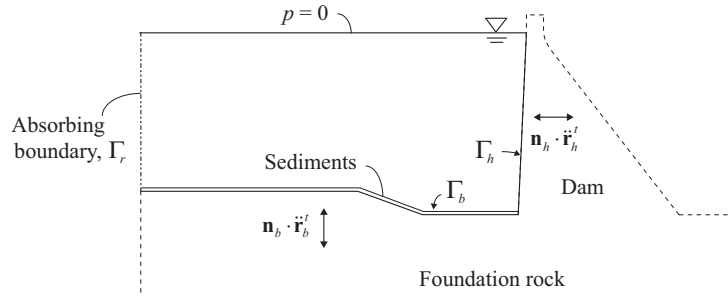


Figure 2.4: Schematic FE model of the fluid domain highlighting the various boundary conditions at the reservoir boundaries.

Discretizing the fluid domain using finite elements and defining \mathbf{p}^t as the vector of total hydrodynamic pressures – where the superscript t has been added for consistency with the notation for the total displacements \mathbf{r}^t – the standard discretization process results in

$$\mathbf{s}\ddot{\mathbf{p}}^t + \mathbf{b}\dot{\mathbf{p}}^t + \mathbf{h}\mathbf{p}^t = -\rho[\mathbf{Q}_h^T + \mathbf{Q}_b^T]\ddot{\mathbf{r}}^t + \mathbf{H}_r^t \quad (2.5)$$

where \mathbf{s} , \mathbf{b} and \mathbf{h} are the corresponding "mass", "damping" and "stiffness" matrices of the fluid [52], and \mathbf{H}_r^t is the vector of forces associated with the absorbing boundary Γ_r . In contrast to the "standard" formulation [52], the damping matrix \mathbf{b} does here not include the effects of the radiation condition because these are represented by the forces \mathbf{H}_r^t . Also included in this term are the forces exerted on the absorbing boundary due to excitation of the

part of the fluid domain upstream of Γ_r that has been eliminated; an expression for these forces will be derived in Chapter 4.

The matrix \mathbf{Q}_h relates hydrodynamic pressures in the fluid to accelerations in the dam at the dam–water interface Γ_h according to the boundary condition of Equation (2.3a):

$$\mathbf{Q}_h = \int_{\Gamma_h} \bar{\mathbf{N}}_h^T \mathbf{n}_h \mathbf{N}_h d\Gamma \quad (2.6)$$

where $\bar{\mathbf{N}}_h$ and \mathbf{N}_h are the shape functions of the dam and fluid nodes, respectively, on the interface Γ_h . The matrix \mathbf{Q}_b is constructed the same way, but integrated over Γ_b .

2.3.3 Dam–water–foundation rock system

The hydrodynamic forces \mathbf{R}'_h and \mathbf{R}'_b in Equation (2.1) that act on the dam and foundation rock, respectively, can be expressed in terms of the hydrodynamic pressures \mathbf{p}' as [52]

$$\mathbf{R}'_h = \mathbf{Q}_h \mathbf{p}' \quad \mathbf{R}'_b = \mathbf{Q}_b \mathbf{p}' \quad (2.7)$$

Substituting this equation into Equation (2.1) and combining with Equation (2.5) gives the equations of motion for the dam–water–foundation rock system with truncated foundation and fluid domains:

$$\begin{aligned} \begin{bmatrix} \mathbf{m} & \mathbf{0} \\ \rho(\mathbf{Q}_h^T + \mathbf{Q}_b^T) & \mathbf{s} \end{bmatrix} \begin{Bmatrix} \ddot{\mathbf{r}}' \\ \ddot{\mathbf{p}}' \end{Bmatrix} + \begin{bmatrix} \mathbf{c} & \mathbf{0} \\ \mathbf{0} & \mathbf{b} \end{bmatrix} \begin{Bmatrix} \dot{\mathbf{r}}' \\ \dot{\mathbf{p}}' \end{Bmatrix} \\ + \begin{Bmatrix} \mathbf{f}(\mathbf{r}') \\ \mathbf{0} \end{Bmatrix} + \begin{bmatrix} \mathbf{0} & -(\mathbf{Q}_h + \mathbf{Q}_b) \\ \mathbf{0} & \mathbf{h} \end{bmatrix} \begin{Bmatrix} \mathbf{r}' \\ \mathbf{p}' \end{Bmatrix} = \begin{Bmatrix} \mathbf{R}'_f + \mathbf{R}^{\text{st}} \\ \mathbf{H}'_r \end{Bmatrix} \end{aligned} \quad (2.8)$$

where the coupling matrices \mathbf{Q}_h and \mathbf{Q}_b have non-zero entries only on the interfaces Γ_h and Γ_b , respectively. Expressions for the unknown forces \mathbf{R}'_f and \mathbf{H}'_r associated with the absorbing boundaries Γ_f and Γ_r will be derived in the subsequent chapters.

3 Dam–foundation rock system

3.1 Dam–foundation rock interaction as a scattering problem

Dam–foundation rock interaction may be treated as a scattering problem in which the dam perturbs the free-field motion in the foundation rock. Procedures based on this idea have been developed for analysis of soil–structure interaction systems [38–40], and of dam–water–foundation rock systems using PML absorbing boundaries and the DRM for seismic input [41]. In this chapter, these ideas will be utilized to formulate an analysis procedure for the dam–foundation rock subsystem with absorbing boundaries modeled by viscous dampers.

Consider the linear foundation rock in its free-field state, i.e., before the dam was constructed or excavation had started (Figure 3.1a). This domain is separated into two subdomains: Ω^0 denotes the region interior of the future absorbing boundary Γ_f , and Ω^+ is the semi-unbounded exterior region. The vector of free-field displacements at nodes in both subdomains is denoted by \mathbf{r}^0 (Figure 3.1a); a procedure to determine this motion will be presented in Section 3.4.

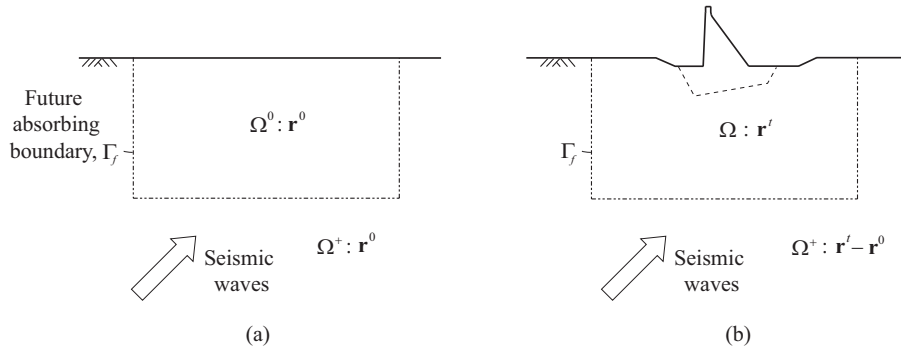


Figure 3.1: Illustration of dam–foundation rock interaction as a scattering problem: (a) foundation rock in its free-field state with displacement field defined by \mathbf{r}^0 in $\Omega^0 \cup \Omega^+$; (b) dam–foundation rock system with displacement field defined by the total motion \mathbf{r}^r in Ω and the scattered motion $\mathbf{r}^r - \mathbf{r}^0$ in Ω^+

The dam–foundation rock system is also separated into two subdomains (Figure 3.1b): Ω denotes the dam and foundation region interior of the absorbing boundary Γ_f , and Ω^+ is the semi-unbounded exterior region, the latter is identical to the exterior region in the free-field system. Following the approach first proposed by Herrera and Bielak [46], the displacement field in the dam–foundation rock system is defined by the variables:

$$\mathbf{r}^r, \quad \text{in the interior region } \Omega \quad (3.1a)$$

$$\mathbf{r}^t - \mathbf{r}^0, \text{ in the exterior region } \Omega^+ \quad (3.1b)$$

where \mathbf{r}^t is the vector of total displacements governed by Equation (2.1), and $\mathbf{r}^t - \mathbf{r}^0$ represents the *scattered motion* in the exterior region Ω^+ , i.e., the perturbation of the free-field motion caused by the presence of the dam. This substitution of variables in Ω^+ will subsequently allow formulation of the governing equations for the absorbing boundary in a way that the forces \mathbf{R}_f^t in Equation (2.1) can be determined from the free-field motion \mathbf{r}^0 .

3.2 Viscous-damper absorbing boundaries

A set of continuously distributed viscous dampers enforces the one-dimensional radiation condition [18]. Assuming that incident waves impinge perpendicular to the boundary, this radiation condition is

$$\sigma + \rho_f V_p \dot{u} = 0 \quad (3.2a)$$

$$\tau + \rho_f V_s \dot{w} = 0 \quad (3.2b)$$

where $\sigma(t)$ and $\tau(t)$ are the normal and tangential tractions; $u(t)$ and $w(t)$ are the normal and tangential displacements[†] (Figure 3.2); ρ_f is the density of the foundation medium; and V_p and V_s its pressure-wave velocity and shear-wave velocity. The viscous damper is a perfect absorber of body waves that arrive normal to the boundary, but only a partial absorber for body wave impinging at an arbitrary angle and for surface waves. However, the accuracy is generally acceptable provided the boundary is placed at sufficient distance from the wave source [20].

The viscous-damper boundary simulates the semi-unbounded foundation region Ω^+ where the displacements were defined by the scattered motion (Equation 3.1b), i.e., $u = u^t - u^0$ and $w = w^t - w^0$. Because the foundation rock in Ω^+ is assumed to be linear, it follows that the boundary tractions associated with the scattered motion are $\sigma = \sigma^t - \sigma^0$ and $\tau = \tau^t - \tau^0$. Substituting for the scattered motion and the corresponding tractions in Equation (3.2) and rearranging terms one obtains:

$$\sigma^t = \sigma^0 - \rho_f V_p [\dot{u}^t - \dot{u}^0] \quad (3.3a)$$

$$\tau^t = \tau^0 - \rho_f V_s [\dot{w}^t - \dot{w}^0] \quad (3.3b)$$

Thus, the total tractions on the absorbing boundary consist of two parts: the free-field tractions, and the product of a damper coefficient and the scattered motion.

[†] Temporarily – for convenience of notation – u and w is used instead of r^t for displacements

forces $\mathbf{c}_f \dot{\mathbf{r}}^f$ and the effective earthquake forces \mathbf{P}_f^0 . The latter consists of two parts: (1) \mathbf{R}_f^0 , the forces consistent with the free-field tractions at Γ_f , and (2) the damper forces $\mathbf{c}_f \dot{\mathbf{r}}_f^0$ determined from the spatially varying free-field motion at Γ_f . Working with the scattered displacements in Ω^+ has thus enabled derivation of Equation (3.7) for the effective earthquake forces in terms of the free-field displacements and tractions.

3.4 Free-field earthquake motion

The free-field motion \mathbf{r}_f^0 required to compute the effective earthquake forces \mathbf{P}_f^0 can be determined by various methods. The standard procedure is to define the ground motion at the control point (Figure 2.1) to be consistent with a design spectrum. This target spectrum may be the Uniform Hazard Spectrum (UHS) determined by probabilistic seismic hazard analysis (PSHA) [53], or a Conditional Mean Spectrum (CMS) [54]. Recorded ground motions are selected, scaled and modified to "match" in some sense the target spectrum; alternatively synthetic motions may be developed for an earthquake scenario. These methods are well developed for a single component of ground motion; work on extending these methods to two- or three components acting simultaneously is in progress.

To determine the required free-field motion at the boundary Γ_f from the ground motion at the control point it is necessary to introduce assumptions on the type of seismic waves and their incidence angle. The simplest assumption, often used for site response analyses and soil–structure interaction analyses, is vertically propagating SH-waves and P-waves [55,56]. This is clearly a major simplification of the actual seismic wave field, that generally consists of a superposition of vertically and horizontally propagating SH-, SV- and P-waves, and horizontally propagating surface waves. This assumption is often justified on the basis that most sites are located relatively far away from the earthquake source, and that the gradual softening of rock and soil towards the earth's surface leads to diffraction of seismic waves towards vertical incidence [57]. It is not obvious that this assumption is appropriate for concrete dams sited on competent bedrock, but at the present time it seems to be the only pragmatic choice.

Under the assumption of vertically propagating waves and homogeneous or layered rock, the free-field motion \mathbf{r}_f^0 at Γ_f can be obtained by deconvolution of the ground motion $a_g^k(t)$ at the control point using standard frequency-domain procedures [55]; software such as SHAKE [58] or DEEPSOIL [59] can be utilized for this purpose. In principle, the deconvolution analysis can provide directly the motion at every nodal point on Γ_f ; however, such an implementation may become cumbersome if output from the deconvolution analysis is required at a large number of elevations. An alternative method that overcomes this problem is presented in the next section.

3.5 Computing effective earthquake forces

3.5.1 Bottom boundary

It was assumed in Section 3.4 that the earthquake motion is caused by vertically incident seismic waves propagating up from an underlying elastic medium. Because the free-field foundation-rock system (Figure 3.1a) is assumed to be linear and homogenous or horizontally layered, the boundary tractions at the bottom of the truncated foundation domain can be expressed as the sum of tractions due to the incident and reflected seismic waves:

$$\boldsymbol{\sigma}^0 = \boldsymbol{\sigma}_I^0 + \boldsymbol{\sigma}_R^0 \quad (3.8)$$

where $\boldsymbol{\sigma}_I^0$ and $\boldsymbol{\sigma}_R^0$ are the normal tractions due to the incident (upward propagating) and reflected (downward propagating) seismic waves, respectively. At the boundary, the radiation condition must be satisfied for both the incident and reflected waves:

$$\boldsymbol{\sigma}_I^0 - \rho_f V_p \dot{u}_I^0 = 0 \quad \boldsymbol{\sigma}_R^0 + \rho_f V_p \dot{u}_R^0 = 0 \quad (3.9)$$

where u_I^0 and u_R^0 are the displacements at the boundary in the normal direction corresponding to the incident and reflected seismic waves. The free-field velocity \dot{u}^0 at the boundary is the sum of the incident and reflected waves, i.e., $\dot{u}^0 = \dot{u}_I^0 + \dot{u}_R^0$. Substituting for \dot{u}_R^0 in Equation (3.9), and inserting the result in Equation (3.8), a new expression for the free-field boundary tractions $\boldsymbol{\sigma}^0$ is obtained:

$$\boldsymbol{\sigma}^0 = \rho_f V_p [2\dot{u}_I^0 - \dot{u}^0] \quad (3.10a)$$

It follows that a similar expression can be derived for the tangential tractions $\boldsymbol{\tau}^0$:

$$\boldsymbol{\tau}^0 = \rho_f V_s [2\dot{w}_I^0 - \dot{w}^0] \quad (3.10b)$$

Such expressions were first derived by Joyner and Chen [60].

Expressing Equation (3.10) in finite element notation to obtain $\mathbf{R}_f^0 = \mathbf{c}_f [2\mathbf{r}_I^0 - \mathbf{r}_f^0]$, substituting the results into Equation (3.7) and cancelling terms, the final expression for the effective earthquake forces at the bottom of the foundation domain is obtained:

$$\mathbf{P}_f^0 = 2\mathbf{c}_f \dot{\mathbf{r}}_I^0 \quad (3.11)$$

where \mathbf{r}_I^0 is the motion at Γ_f due to the incident (upward propagating) seismic waves.

This equation has the advantage that it requires only the motion \mathbf{r}_I^0 of the incident wave, thus avoiding computation of the free-field tractions required if directly using Equation

(3.7). Furthermore, the incident motion \mathbf{r}_i^0 is easily computed as 1/2 the *outcrop motion*[†] at the bottom boundary, which is extracted directly from the deconvolution analysis. The procedure to compute \mathbf{P}_f^0 from Equation (3.11) is summarized in Box 3.1.

Box 3.1: Computing \mathbf{P}_f^0 at bottom boundary of foundation rock.

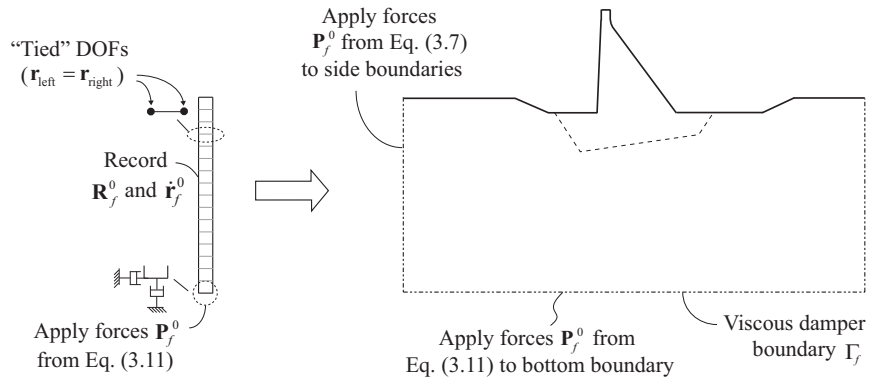
1. Determine the outcrop motion at the bottom foundation-rock boundary by 1D deconvolution of each component of the surface control motion $a_g^k(t)$, $k = x, y$.
2. Compute the incident motion \mathbf{r}_i^0 as 1/2 the outcrop motion at the bottom boundary determined in Step 1 and obtain $\dot{\mathbf{r}}_i^0$ by taking the time derivative of \mathbf{r}_i^0 .
3. Calculate the effective earthquake forces \mathbf{P}_f^0 at the bottom boundary from Eq. (3.11) using $\dot{\mathbf{r}}_i^0$ from Step 2.

3.5.2 Side boundaries

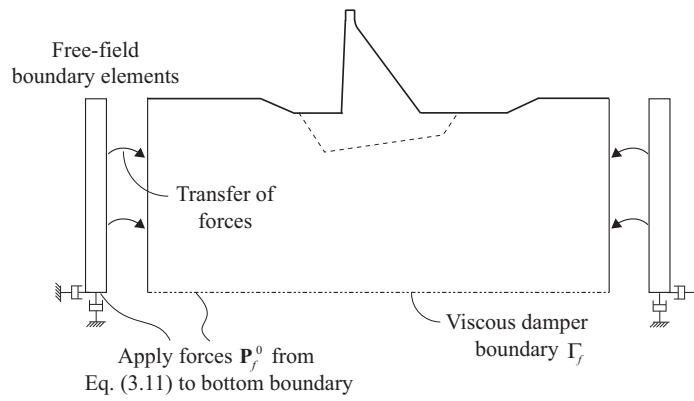
The free-field motion \mathbf{r}_f^0 (and its time derivatives) required to compute the effective earthquake forces \mathbf{P}_f^0 at the side boundaries can be obtained directly from the deconvolution analysis; free-field tractions can then be computed from 1D stress-strain relations and these stresses converted to forces. Alternatively, both quantities can be computed by an auxiliary analysis of the foundation rock in its free-field state (Figure 3.1a). Analysis of this system reduces to a single column of foundation-rock elements with a viscous damper at its base that is subjected to the forces of Equation (3.11) and analyzed to determine $\dot{\mathbf{r}}_f^0$ and \mathbf{R}_f^0 at each nodal point along the height. The procedure is summarized in Box 3.2 and illustrated in Figure 3.3a.

Although straightforward, both of these approaches requires the force histories \mathbf{P}_f^0 at all nodal points on the side boundaries to be stored for later use in setting up Equation (3.7). Clearly, such "book-keeping" may become cumbersome to implement for large models, especially for a 3D system [37]. These difficulties can be avoided by introducing free-field boundary elements in the form of 1D foundation-rock columns at the side boundaries that are solved in parallel with the main FE model (Figure 3.3b) [61]. However, such elements are currently not available in most commercial FE or finite difference codes, the only exceptions are FLAC [62] and PLAXIS [63].

[†] The reflected motion must equal the incident motion at every rock outcrop (stress-free boundary), hence is the incident motion exactly equal to 1/2 the outcrop motion.



(a)



(b)

Figure 3.3: Two methods for application of effective earthquake forces to side boundaries of foundation domain: (a) auxiliary analysis of 1D column to compute $\dot{\mathbf{r}}_f^0$ and \mathbf{R}_f^0 followed by direct application of \mathbf{P}_f^0 ; (b) use of free-field boundary elements.

Box 3.2: Computing \mathbf{P}_f^0 at side boundaries of foundation rock.

1. Determine the outcrop motion at the bottom foundation-rock boundary by 1D deconvolution of each component of the surface control motion $a_g^k(t)$, $k = x, y$.
2. Calculate the effective earthquake forces \mathbf{P}_f^0 at the bottom boundary from Equation (3.11), with the motion \mathbf{r}_l^0 due to the incident (upward propagating) seismic wave computed as 1/2 the outcrop motion extracted from the deconvolution analysis.
3. Develop a FE model for the free-field foundation-rock system: a single column of elements that has the same mesh density as the main FE model at the side boundaries, with viscous dampers applied at the base in the x - and y -directions (Figure 3.3a).
4. Compute the free-field velocities $\dot{\mathbf{r}}_f^0$ and forces \mathbf{R}_f^0 at each node over the height by analyzing the foundation-rock column subjected to forces given by Eq. (3.11) at its base.
5. Calculate the effective earthquake forces \mathbf{P}_f^0 at the side boundaries from Eq. (3.7) using $\dot{\mathbf{r}}_f^0$ and \mathbf{R}_f^0 from Step 4.

3.5.3 Relation to the Domain Reduction Method

The Domain Reduction Method (DRM) [40] is a two-step methodology for modeling earthquake response where large contrasts exist between the physical scales of the background model and a smaller localized feature. The method overcomes the issues of scale difference by subdividing the original problem into two simpler ones where a local feature perturbs the free-field motion in a larger background domain. This same idea was utilized in deriving the equations of motion for the dam–foundation rock system, Equations (3.6) and (3.7), earlier in this chapter.

Although initially developed for large scale geological simulations, the DRM has also been successfully applied to specify the seismic input in soil–structure interaction problems in a layer of FEs interior of the absorbing boundary [41,64]. This has the advantage that it completely de-couples the boundary condition from the method of seismic input, unlike the direct FE method developed above where the effective earthquake forces were derived assuming viscous-damper boundaries. Thus, DRM can be used with any advanced boundary condition and the domain sizes reduced accordingly (Figure 2.2).

When developing a general procedure for earthquake analysis of concrete dams however, this benefit is outweighed by two disadvantages of using DRM: (1) implementation of DRM requires modification of the FE source code, effectively limiting the procedure to users of LS-DYNA, which is the only commercial FE program frequently used by dam engineers where DRM is available; and (2) specifying seismic input for a dam–water–

foundation rock system with small domain sizes (which is the main attractiveness of using DRM) is impractical because it requires auxiliary analysis of a complex water–foundation rock system and extensive book-keeping to set up and store the seismic input forces [41].

To ensure broad usefulness of the direct FE method it was therefore decided to use simple viscous dampers as the absorbing boundaries and specify effective earthquake forces directly at these boundaries. A more comprehensive discussion on this topic, as well as a general introduction to DRM and a comparison between the DRM and direct FE method, can be found in Appendix B.

3.6 Numerical validation

The analysis method developed in the preceding sections is validated by computing the dynamic response of the idealized dam–foundation rock system shown in Figure 3.4. All the direct FE method analyses are implemented in the open source FE program OPENSEES [65] using implicit time integration by the HHT- α method [66] to solve the dynamic equilibrium equations (Equation 3.6).

The idealized, triangular, dam has a vertical upstream face, a downstream slope of 0.8 to 1, and height $H = 120$ m. The dam concrete and foundation rock is assumed to be isotropic, homogeneous, linearly elastic, and in generalized plane stress. This assumption, while strictly speaking not appropriate for the foundation, is dictated by the expected individual vibration of monoliths during intense ground motions. Material properties for the concrete are: modulus of elasticity $E_s = 22.4$ GPa, density $\rho_s = 2483$ kg/m³, and Poisson's ratio $\nu_s = 0.20$; for the foundation rock: $E_f = 22.4$ GPa (i.e. $E_f / E_s = 1$), $\rho_f = 2643$ kg/m³, and $\nu_f = 0.33$. Material damping is modeled by Rayleigh damping with $\zeta_s = 2\%$ and $\zeta_f = 2\%$ viscous damping specified for the dam and foundation rock separately, with the damping matrix for the complete system constructed by assembling the individual Rayleigh damping matrices for the two subdomains [67].

The FE models for the dam and foundation rock both consist of quadrilateral 4-node elements [68]. The FE mesh for the dam has 15 elements across the width and 29 elements over the height (Figure 3.4a). The maximum element size in the foundation rock is limited to less than one-tenth of the shortest wavelength considered in the analysis to ensure satisfactory wave propagation in the mesh [69]. The width (on either side of the dam) and depth of the foundation domain is selected as $4H$ and $2.5H$, respectively. These dimensions are sufficiently large to minimize wave reflections from the viscous dampers for the selected system parameters, and were selected based on a parametric study for determining the required size of the foundation domain when using viscous-damper boundaries (see Appendix A).

The ground motion is specified by the ground acceleration $a_s^k(t)$ at the foundation surface; the free-field motion at depth in the model is obtained by deconvolution of this motion. The effective earthquake forces at the bottom and side boundaries of the foundation

rock are then computed from Equations (3.11) and (3.7), respectively, using the procedures in Boxes 3.1 and 3.2.

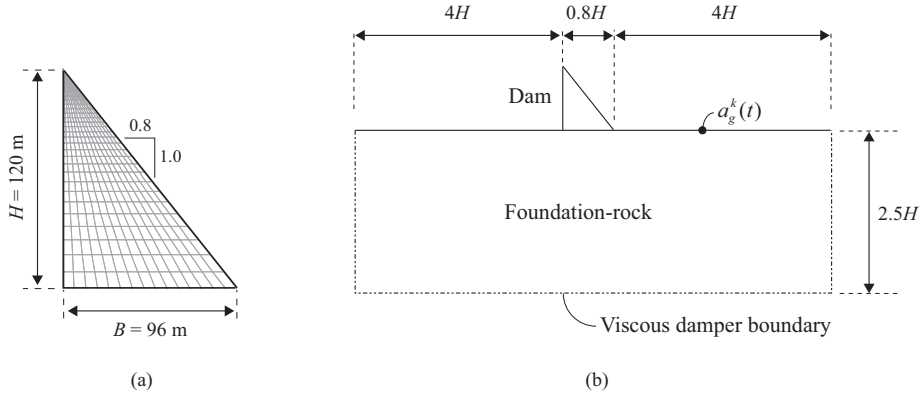


Figure 3.4: (a) Geometry and FE mesh for triangular dam cross section; (b) dimensions of FE model for dam–foundation rock system with viscous-damper boundaries to truncate the semi-unbounded foundation domain.

Frequency response functions are computed by time-domain analysis of the FE system with free-field surface motions $a_g^x(t)$ and $a_g^y(t)$ defined by a harmonic function of unit amplitude. The response of the dam for a single excitation frequency is computed by solving the equations of motion for long enough time to reach steady-state; this is then repeated at a sufficient number of frequencies to produce a smooth plot. More information about this procedure can be found in Appendix C. The semi-analytical benchmark solution, to which the results of the direct FE method is compared, is obtained directly in the frequency domain by the substructure method [17] using the computer program EAGD84 [70] with a set of pre- and post-processing modules in MATLAB [71] that the author has previously developed [72]. In the substructure method, the foundation rock is modeled as a viscoelastic halfspace, the fluid domain is treated as an infinitely long continuum, and the earthquake excitation is specified directly at the dam–foundation interface, thus avoiding the need for artificial model truncations, absorbing boundaries, and deconvolution of the ground motion.

Material damping in EAGD84 is modeled by constant hysteretic damping specified by the hysteretic damping factors $\eta_s = 0.04$ and $\eta_f = 0.04$ for the dam and foundation rock; this corresponds to viscous damping ratios of $\zeta_s = 2\%$ and $\zeta_f = 2\%$. For time-domain analysis in the direct FE method, the Rayleigh coefficients are determined by specifying ζ_s and ζ_f at the excitation frequency $f = \omega / 2\pi$, where ω is the angular frequency of the harmonic excitation, and at $f = 1$ Hz. This unconventional choice defines frequency-dependent Rayleigh damping to be as consistent as possible with frequency-independent hysteretic damping, thus ensuring a meaningful comparison of the frequency response functions from the direct FE and substructure methods. For the response history analyses to earthquake excitation presented

later in Section 5.4.2, ζ_s and ζ_f are specified at the first two natural frequencies of the dam–water–foundation rock system.

3.6.1 Dam on rigid foundation rock

The frequency response function for the amplitude of the relative horizontal acceleration at the crest of the dam on rigid foundation is computed by OPENSEES and EAGD84 and compared in Figure 3.5. The near identical results for both horizontal and vertical excitation confirm the equivalency of the two FE models, and validate that the procedure for selecting Rayleigh coefficients provides material damping that is consistent with the constant hysteretic damping model at a given excitation frequency.

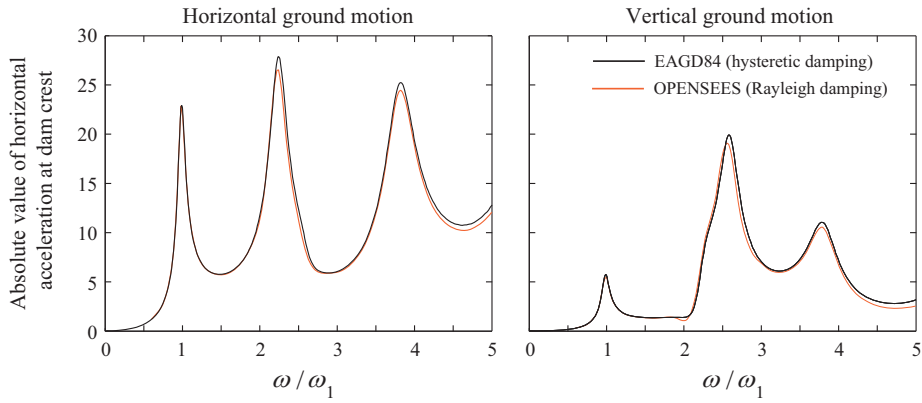


Figure 3.5: Comparison of frequency response functions from OPENSEES and EAGD84 for the amplitude of relative horizontal acceleration at the crest of dam on rigid foundation due to horizontal and vertical ground motion. Results are plotted against normalized frequency ω/ω_1 where ω_1 is the fundamental frequency of the dam on rigid foundation. Material damping in the dam is temporarily set for this analysis as $\zeta_s = 5\%$.

3.6.2 Dam–foundation rock system

The dynamic response of the dam on flexible foundation rock is presented in Figure 3.6 for several values of E_f/E_s , the ratio of modulus of elasticity for the foundation rock to the dam. The results obtained by the direct FE method with viscous-damper boundaries and truncated foundation domain are generally close to the results from the substructure analysis, thus validating the ability of the direct FE method to model the semi-unbounded dam–foundation rock system. The small discrepancies observable at some frequencies are due to the inability of the viscous-damper boundary to perfectly absorb outgoing (scattered) waves from the dam; such discrepancies will generally decrease as the size of the foundation domain included in the FE model increases (see Appendix A).

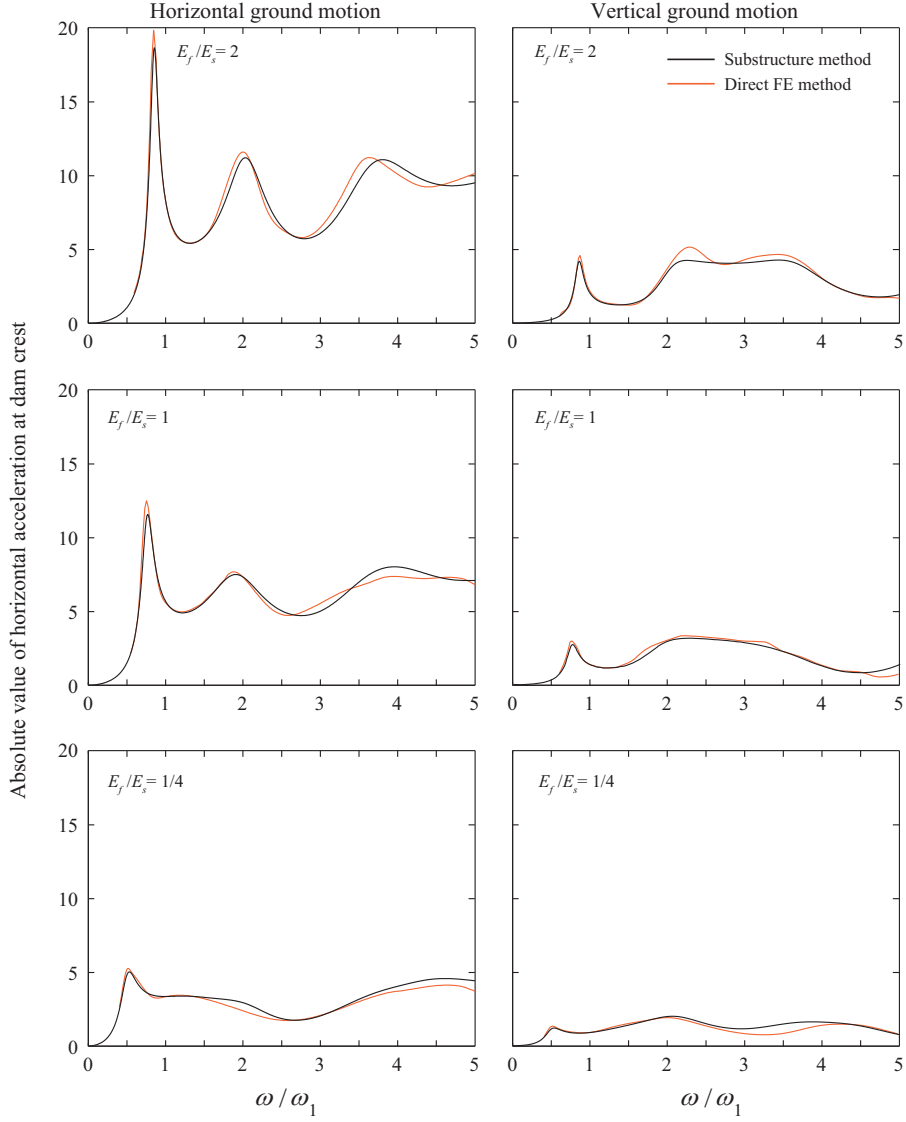


Figure 3.6: Comparison of frequency response functions from direct FE and substructure methods for the amplitude of relative horizontal acceleration at the crest of dam on flexible foundation rock due to horizontal and vertical ground motion. $\zeta_s = \zeta_f = 2\%$; $E_f / E_s = 1$.

3.6.3 Ignoring effective earthquake forces at side boundaries

The dam engineering profession has been using a variation of the rigorous procedure summarized in Boxes 3.1 and 3.2, wherein the effective earthquake forces \mathbf{P}_f^0 are applied

only at the bottom boundary, but ignored at the side boundaries. Initiated by the US Bureau of Reclamation and applied to actual projects [43,44], variations of the method have also been used by other dam engineering professionals [73].

Frequency response functions for the dam on flexible foundation rock obtained using such an analysis procedure – where forces are only applied at the bottom foundation boundary – are presented in Figure 3.7. The significant discrepancies observable in the results for both horizontal and vertical ground motion arise from the inability of this model to reproduce free-field conditions. Attempts have been made to correct for this shortcoming by modifying the amplitude and/or frequency content of the input ground motion [45]. However, it is not clear whether such modifications will lead to acceptable results, and neither version of these approximate methods has been validated against the substructure method.

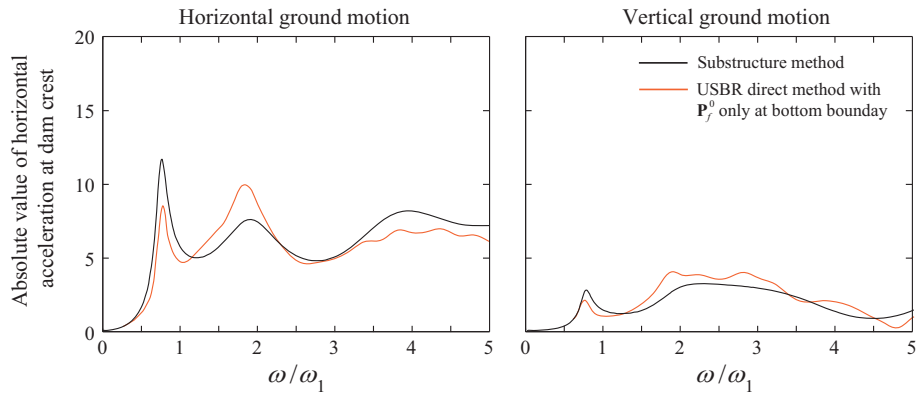


Figure 3.7: Comparison of frequency response functions from the USBR direct method and substructure method for the amplitude of relative horizontal acceleration at the crest of dam on flexible foundation rock due to horizontal and vertical ground motion. $\zeta_s = \zeta_f = 2\%$; $E_f / E_s = 1$.

3.6.4 Can foundation mass be ignored?

The massless foundation model [74] is attractive in its simplicity as it only considers the flexibility of the foundation rock, but neglects the inertia and damping effects. The foundation rock can then be modeled by a small bounded-sized foundation model without absorbing boundaries as part of a standard FE analysis. Despite of its well documented deficiencies [1], the massless foundation model is still being used in dam engineering practice.

Presented in Figure 3.8 are frequency response functions for the dam–foundation rock system computed massless foundation approach and compared to the substructure method including foundation mass. Neglecting the foundation mass – and thereby also radiation damping – greatly overestimates the response of the dam and the results are in significant error. Clearly, such a model is unable to capture the dynamic properties associated with dam–foundation interaction, and should not be used in earthquake analysis of concrete dams.

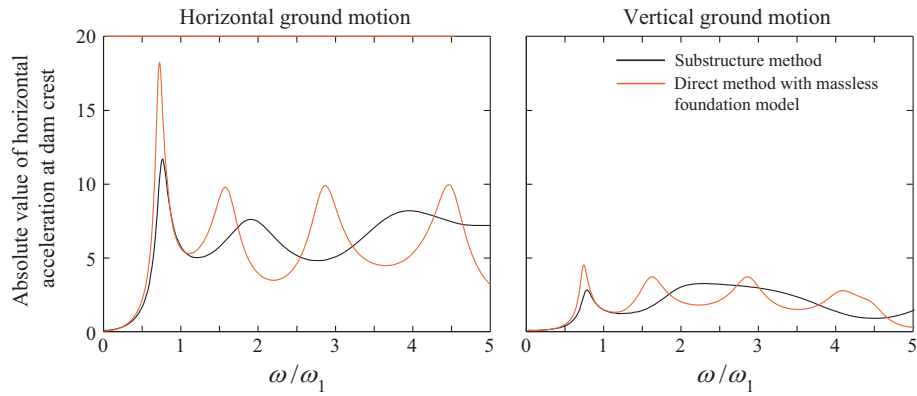


Figure 3.8: Comparison of frequency response functions from the massless foundation model and substructure method for the amplitude of relative horizontal acceleration at the crest of dam on flexible foundation rock due to horizontal and vertical ground motion. $\zeta_s = \zeta_f = 2\%$; $E_f / E_s = 1$.

4 Dam-water system

4.1 Dam-water interaction as a scattering problem

In this chapter, dam-water interaction is again treated as a scattering problem – in which the dam perturbs a "free-field" state of the system – to derive the effective earthquake forces for the fluid domain at the absorbing boundary Γ_r .

Consider the fluid in its "free-field" state, consisting only of the semi-unbounded prismatic channel Ω^+ upstream of the future absorbing boundary Γ_r (Figure 4.1a). This system is not representative of any physical state of the fluid, but it facilitates formulation of the analysis procedure. Because the bottom boundary of the prismatic channel is horizontal, the free-field hydrodynamic pressures \mathbf{p}^0 in Ω^+ will be zero if the ground motion is purely horizontal, but they will be nonzero for vertical ground motion. A procedure for determining these pressures will be presented in Section 4.4.

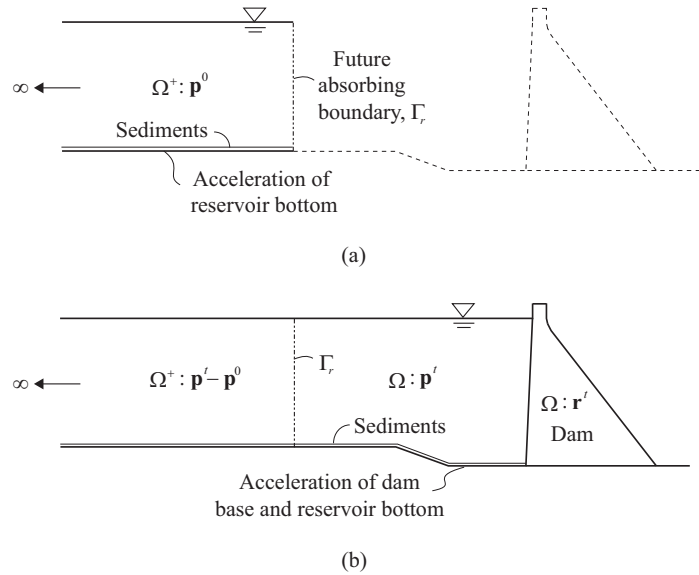


Figure 4.1: Illustration of dam-water interaction as a scattering problem: (a) fluid domain in its "free-field" state with hydrodynamic pressures defined by \mathbf{p}^0 in Ω^+ ; (b) dam-water system with hydrodynamic pressures defined by total pressures \mathbf{p}^f in Ω and scattered pressures $\mathbf{p}^f - \mathbf{p}^0$ in Ω^+ .

The dam-water system is separated into two subdomains: Ω denotes the dam and irregular fluid region between the dam and the absorbing boundary Γ_r , and Ω^+ is the semi-unbounded prismatic channel (Figure 4.1b); the latter is identical to the free-field system.

Following the same approach as for the dam–foundation rock system (Chapter 3), the hydrodynamic pressure field in the dam–water system is defined by the variables

$$\mathbf{p}^t, \quad \text{in the interior region } \Omega \quad (4.1a)$$

$$\mathbf{p}^t - \mathbf{p}^0, \quad \text{in the exterior region } \Omega^+ \quad (4.1b)$$

where \mathbf{p}^t is the vector of total hydrodynamic pressures governed by Equation (2.5), and $\mathbf{p}^t - \mathbf{p}^0$ represents the *scattered hydrodynamic pressures* in the exterior region Ω^+ , i.e., the perturbation of the free-field pressures caused by the existence of the dam and the irregular fluid region. This choice of variables in Ω^+ will subsequently allow formulation of the governing equations for the viscous-damper boundary in a way that the unknown forces \mathbf{H}_r^t associated with the absorbing boundary Γ_r , which first appeared in Equation (2.5), can be determined from the free-field pressures.

4.2 Viscous-damper absorbing boundary

A set of continuously distributed viscous dampers enforces the one-dimensional radiation condition for a fluid [52]. For incident waves perpendicular to the boundary, this condition is

$$\frac{\partial p}{\partial n} + \frac{1}{C} \dot{p} = 0 \quad (4.2)$$

where n denotes the outward normal to the fluid boundary. This boundary condition is also known as the *plane wave approximation*.

The viscous-damper boundary models the unbounded prismatic fluid channel Ω^+ where the scattered pressure $p^t - p^0$ was chosen as the variable to define hydrodynamic pressures (Equation 4.1b). Because the fluid in Ω^+ is assumed linear, Equation (4.2) becomes

$$\frac{\partial(p^t - p^0)}{\partial n} + \frac{1}{C}(\dot{p}^t - \dot{p}^0) = 0 \quad (4.3a)$$

which can be rewritten as

$$\frac{\partial p^t}{\partial n} = \frac{\partial p^0}{\partial n} - \frac{1}{C}(\dot{p}^t - \dot{p}^0) \quad (4.3b)$$

The distributed dampers are lumped to the boundary nodes in the discretized model, resulting in discrete viscous dampers with coefficient:

$$c_r = A / C \quad (4.4)$$

where A is the tributary area (tributary length in a 2D model) for the node. Equation (4.3) written in finite element notation for nodes on the boundary Γ_r is

$$\mathbf{H}_r^t = \mathbf{H}_r^0 - \mathbf{c}_r [\dot{\mathbf{p}}_r^t - \dot{\mathbf{p}}_r^0] \quad (4.5)$$

where \mathbf{H}_r^0 is the vector of nodal forces consistent with the free-field pressure gradient $\partial p^0 / \partial n$, and \mathbf{c}_r is the matrix of damping coefficients c_r . The vectors \mathbf{H}_r^t , \mathbf{H}_r^0 and matrix \mathbf{c}_r have non-zero entries only for nodes on Γ_r .

Working with the scattered pressures in Ω^+ has enabled the derivation of Equation (4.5) for the unknown forces \mathbf{H}_r^t in Equation (2.1) associated with the absorbing boundary Γ_r in terms of the free-field pressures.

4.3 Equations of motion

Equation (2.1) that governs the dam–foundation rock subsystem is specialized for the dam alone:

$$\mathbf{m}\ddot{\mathbf{r}}^t + \mathbf{c}\dot{\mathbf{r}}^t + \mathbf{f}(\mathbf{r}^t) = \mathbf{R}_h^t + \mathbf{R}^{\text{st}} \quad (4.6)$$

where \mathbf{R}^{st} now includes only gravity loads and hydrostatic forces on the dam, and the hydrodynamic forces are $\mathbf{R}_h^t = \mathbf{Q}_h \mathbf{p}^t$, where \mathbf{Q}_h was defined in Equation (2.6). Combining Equation (4.6) with Equation (2.5) for the truncated fluid domain and rearranging terms:

$$\begin{aligned} \begin{bmatrix} \mathbf{m} & \mathbf{0} \\ \rho\mathbf{Q}_h^T & \mathbf{s} \end{bmatrix} \begin{Bmatrix} \ddot{\mathbf{r}}^t \\ \ddot{\mathbf{p}}^t \end{Bmatrix} + \begin{bmatrix} \mathbf{c} & \mathbf{0} \\ \mathbf{0} & \mathbf{b} \end{bmatrix} \begin{Bmatrix} \dot{\mathbf{r}}^t \\ \dot{\mathbf{p}}^t \end{Bmatrix} \\ + \begin{Bmatrix} \mathbf{f}(\mathbf{r}^t) \\ \mathbf{0} \end{Bmatrix} + \begin{bmatrix} \mathbf{0} & -\mathbf{Q}_h \\ \mathbf{0} & \mathbf{h} \end{bmatrix} \begin{Bmatrix} \mathbf{r}^t \\ \mathbf{p}^t \end{Bmatrix} = \begin{Bmatrix} \mathbf{R}^{\text{st}} \\ \mathbf{H}_r^t - \rho\mathbf{Q}_b^T \dot{\mathbf{r}}_b^t \end{Bmatrix} \end{aligned} \quad (4.7)$$

where $\ddot{\mathbf{r}}_b^t$ denotes the prescribed accelerations of the rigid foundation rock at the water–foundation rock interface Γ_b , and the matrix \mathbf{Q}_b is computed similarly to Equation (2.6) but integrated over Γ_b .

Substituting Equation (4.5) for the unknown forces \mathbf{H}_r^t leads to the final equations of motion for the dam–water-system with truncated fluid domain:

$$\begin{aligned} \begin{bmatrix} \mathbf{m} & \mathbf{0} \\ \rho\mathbf{Q}_h^T & \mathbf{s} \end{bmatrix} \begin{Bmatrix} \ddot{\mathbf{r}}^t \\ \ddot{\mathbf{p}}^t \end{Bmatrix} + \begin{bmatrix} \mathbf{c} & \mathbf{0} \\ \mathbf{0} & \mathbf{b} + \mathbf{c}_r \end{bmatrix} \begin{Bmatrix} \dot{\mathbf{r}}^t \\ \dot{\mathbf{p}}^t \end{Bmatrix} \\ + \begin{Bmatrix} \mathbf{f}(\mathbf{r}^t) \\ \mathbf{0} \end{Bmatrix} + \begin{bmatrix} \mathbf{0} & -\mathbf{Q}_h \\ \mathbf{0} & \mathbf{h} \end{bmatrix} \begin{Bmatrix} \mathbf{r}^t \\ \mathbf{p}^t \end{Bmatrix} = \begin{Bmatrix} \mathbf{R}^{\text{st}} \\ \mathbf{P}_r^0 - \rho\mathbf{Q}_b^T \dot{\mathbf{r}}_b^t \end{Bmatrix} \end{aligned} \quad (4.8)$$

where the effective earthquake forces at Γ_r are

$$\mathbf{P}_r^0 = \mathbf{H}_r^0 + \mathbf{c}_r \dot{\mathbf{p}}_r^0 \quad (4.9)$$

The forces \mathbf{H}_r^0 are zero for both horizontal and vertical ground motion because the pressure gradient $\partial p^0 / \partial n$ at Γ_r is zero when the foundation rock is rigid and the reservoir bottom is horizontal. The second term $\mathbf{c}_r \dot{\mathbf{p}}_r^0$ represents the contribution from earthquake-induced pressures in the fluid upstream of Γ_r that has been eliminated.

The earthquake excitation enters in Equation (4.8) through two quantities: (1) the forces $-\rho \mathbf{Q}_b^T \ddot{\mathbf{r}}_b^t$ acting on Γ_b due to the prescribed accelerations $\ddot{\mathbf{r}}_b^t$, and (2) the effective earthquake forces \mathbf{P}_r^0 acting on Γ_r . Because the foundation rock is rigid, $\ddot{\mathbf{r}}_b^t$ is defined directly by the free-field ground accelerations $a_g^k(t)$ (Figure 2.1); these accelerations are also applied to the base of the dam. Thus, the only information required to specify the earthquake excitation is the free-field ground accelerations $a_g^k(t)$ and the free-field pressures \mathbf{p}_r^0 .

Accelerations $\ddot{\mathbf{r}}_h^t$ are coupled with the hydrodynamic pressures \mathbf{p}_h^t at the upstream face of the dam (Γ_h) through the matrix \mathbf{Q}_h defined in Equation (2.6). In some FE programs, these conditions can be enforced by specification of tie constraints at the interfaces [75]. Alternatively, interface elements can be introduced to perform this coupling. These interface element will have three DOFs, two displacements and one pressure, and are defined by the mass and stiffness matrices [41]:

$$\text{DOFs: } \begin{Bmatrix} \mathbf{r}_h^{t(e)} \\ \mathbf{p}_h^{t(e)} \end{Bmatrix} \quad \text{Mass: } \begin{bmatrix} \mathbf{0} & \mathbf{0} \\ \rho \mathbf{Q}_h^{(e)T} & \mathbf{0} \end{bmatrix} \quad \text{Stiffness: } \begin{bmatrix} \mathbf{0} & -\mathbf{Q}_h^{(e)} \\ \mathbf{0} & \mathbf{0} \end{bmatrix} \quad (4.10)$$

Because these matrices are unsymmetric, they lead to an unsymmetric system of global equations in the numerical model. This rarely causes problems in modern FE programs however, because these normally have efficient and robust solvers for sparse, unsymmetric systems of equations.

4.4 Computing effective earthquake forces at Γ_r

The effective earthquake forces \mathbf{P}_r^0 at Γ_r are to be computed by analysis of the free-field fluid system, which is a prismatic channel of uniform depth (Figure 4.1a). Horizontal ground motion will not generate any hydrodynamic pressures because the reservoir bottom is horizontal, hence $\mathbf{P}_r^0 = \mathbf{0}$. Analysis of the prismatic channel for vertical ground motion reduces to a single column of fluid elements of unit width subjected to forces ρa_g^y at its base (Figure 4.2a). This analysis provides the pressures \mathbf{p}_r^0 (and its time derivatives) that are required in Equation (4.9). The procedure is summarized in Box 4.1 and illustrated in Figure 4.2.

Box 4.1: Computing \mathbf{P}_r^0 at upstream fluid boundary.

1. Develop a FE model for the free-field fluid (Figure 4.2a): a single column of elements of unit width with the same mesh density as the fluid adjacent to the boundary Γ_r . Apply a single line element to model reservoir bottom sediments.
2. Calculate $\dot{\mathbf{p}}_r^0$ at every nodal point along the height by analyzing the fluid column subjected to forces ρa_g^y at its base for vertical ground motion; $\dot{\mathbf{p}}_r^0 = \mathbf{0}$ for horizontal ground motion
3. Compute the effective earthquake forces \mathbf{P}_r^0 at the fluid boundary Γ_r from Equation (4.9) using $\dot{\mathbf{p}}_r^0$ from Step 2.

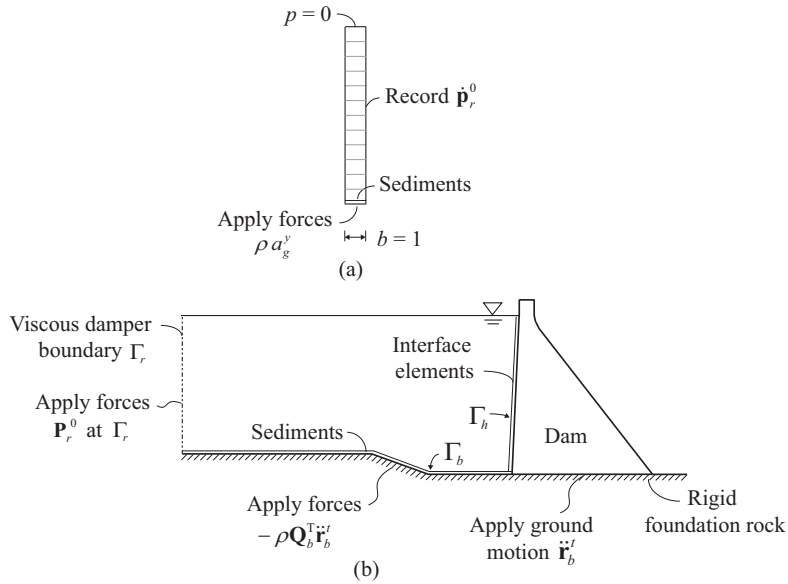


Figure 4.2: Summary of analysis procedure for dam–water subsystem: (a) auxiliary analysis of single column of fluid elements to determine $\dot{\mathbf{p}}_r^0$ for vertical ground motion; (b) application of earthquake excitation and effective earthquake forces to truncated FE model.

4.5 Numerical validation

The analysis procedure developed in the preceding sections is validated by computing the dynamic response of the idealized dam–water system shown in Figure 4.3 subjected to horizontal and vertical ground motion. The idealized dam has the same cross-section, FE discretization and material properties as the ones used in Section 3.6. Standard solid and acoustic elements [68] are used in the dam and fluid, respectively; interface elements are

applied at the dam–water interface; and line elements are applied to model sediments at the reservoir bottom using the approximate 1D sediment model (Equation 2.4). Material damping in the dam is modeled by Rayleigh damping implemented using the procedure described in Section 3.6 specialized for the dam alone, but with $\zeta_s = 5\%$ viscous damping selected for the dam concrete to provide reasonable overall energy dissipation in the system with rigid foundation rock. The impounded water has the same depth as the height of the dam, density $\rho = 1000 \text{ kg/m}^3$, and pressure-wave velocity $C = 1440 \text{ m/s}$. The ground motion is specified by the ground acceleration $a_g^k(t)$ of the rigid foundation at the dam base. Effective earthquake forces at the boundary of the fluid domain are computed from Equation (4.9) using the procedure in Box 4.1.

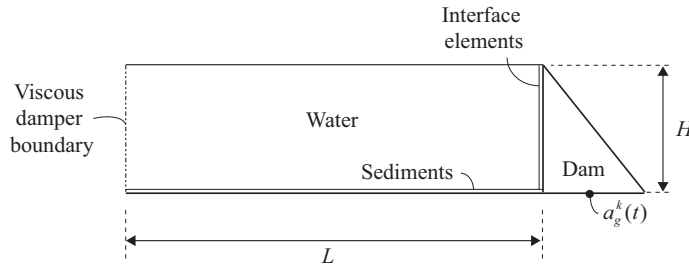


Figure 4.3: Dimensions of FE model for dam–water system with viscous damper boundary to truncate the semi-unbounded fluid domain.

4.5.1 Hydrodynamic forces on rigid dam

To determine the influence of the length of the bounded fluid domain on the accuracy of the results, the hydrodynamic forces on a rigid dam is computed first. The frequency response functions for the hydrodynamic forces $|F_0^x(\omega)|$ and $|F_0^y(\omega)|$ on the upstream face of a rigid dam due to horizontal and vertical ground motion, respectively, are determined by computing the steady-state response of the system at many excitation frequencies. These forces are compared with analytical results for an unbounded fluid domain [17] in Figure 4.4, where the results are normalized with respect to the hydrostatic force $F_{st} = 1/2\rho gH^2$.

For horizontal excitation, the viscous-damper boundary is inadequate when using very small domain lengths ($L = H$), and results are unacceptable for all values of α . Increasing the length to $L = 4H$ significantly improves the accuracy and results are generally acceptable; however, some scatter is still observable for $\alpha=0.90$. This occurs for high values of α because radiation damping is then effectively the only source of energy dissipation in the system, and the response becomes sensitive for even small wave reflections at the viscous-damper boundary. This effect is much less prominent for low α -values because wave absorption at the reservoir bottom then contributes more to the overall energy dissipation.

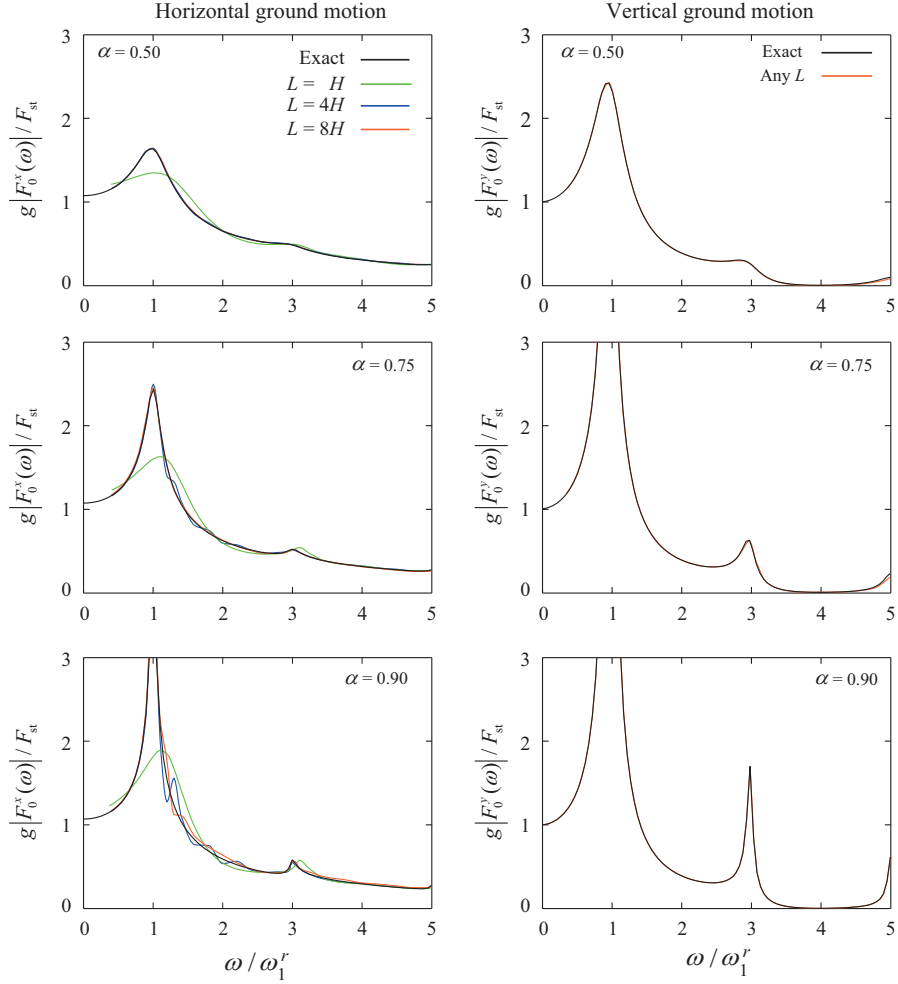


Figure 4.4: Influence of length of bounded fluid domain on hydrodynamic forces on a rigid dam. Results are plotted against the normalized frequency ω / ω_1^r , where $\omega_1^r = \pi C / 2H$ is the fundamental vibration frequency of the fluid domain. "Exact" results are from Ref. [17].

For vertical excitation, the numerical results match the analytical solution for all lengths of the bounded domain, because the simple fluid geometry and uniform excitation at the reservoir bottom leads to a 1D pressure distribution in the fluid. Thus, when the effective earthquake forces \mathbf{P}_r^0 – representing the contribution from earthquake-induced pressures in the part of the fluid that has been eliminated – are applied at Γ_r , these 1D conditions are exactly reproduced in the model. For a flexible dam however, this simple 1D behavior is no longer maintained, and larger domain lengths are required to obtain acceptable results.

4.5.2 Dam–water system

Frequency response functions for the amplitude of the relative horizontal acceleration at the crest of the dam–water system (Figure 4.3) subjected to $a_g^x(t)$ and $a_g^y(t)$ defined by a harmonic function of unit amplitude is computed. These are compared in Figure 4.5 to results obtained directly in the frequency domain by the substructure method [76], that models the reservoir rigorously using semi-analytical solutions. Results are computed for different values of α and length $L=4H$ for the truncated fluid domain.

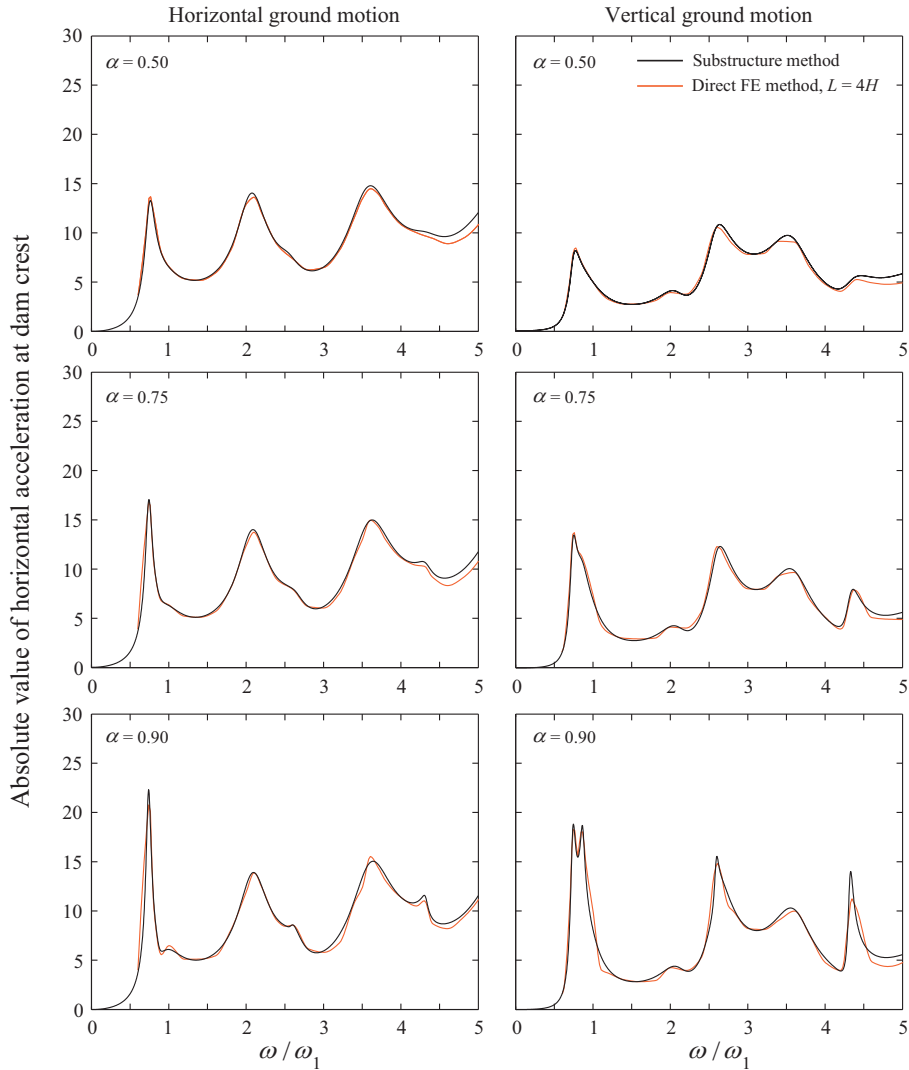


Figure 4.5: Comparison of frequency response functions from direct FE and substructure methods for the amplitude of relative horizontal acceleration at the crest of dam on rigid foundation with full reservoir due to horizontal and vertical ground motion. $\zeta_s = 5\%$.

The results computed by the direct FE method are generally close to the results from the substructure method for both vertical and horizontal ground motion, thus validating its ability to model the semi-unbounded dam–water system even with the moderately sized fluid domain of length $L = 4H$.

4.5.3 Ignoring effective earthquake forces on fluid boundary Γ_r

Implementation of Equation (4.8) may be simplified by ignoring the effective earthquake forces \mathbf{P}_r^0 at Γ_r , which eliminates the need for auxiliary analysis of the 1D fluid column (Section 4.4) for vertical ground motion. This approximation implies that the vertical excitation extends only over the dam and truncated part of the fluid domain, thus neglecting the effect of hydrodynamic pressures caused by excitation of the fluid that has been eliminated upstream of Γ_r .

Presented in Figure 4.6 are frequency response functions for the amplitude of the relative horizontal acceleration at the dam crest due to vertical ground motion for $\alpha=0.50$ and $\alpha=0.75$ and different lengths of the bounded fluid domain. Results are computed by the direct FE method for two cases: including and excluding effective earthquake forces \mathbf{P}_r^0 . Ignoring \mathbf{P}_r^0 leads to considerable differences in the response for higher α -values unless the bounded fluid domain is very long ($L = 8H$) because the excitation is now applied only to the base of the dam and truncated part of the fluid domain, and not to the complete semi-unbounded system. For analysis of an actual dam with a reasonable length for the fluid domain (e.g. $L = 4H$) this discrepancy should be of little concern because uniform ground motion obviously cannot extend to infinity in the upstream direction in a real system.

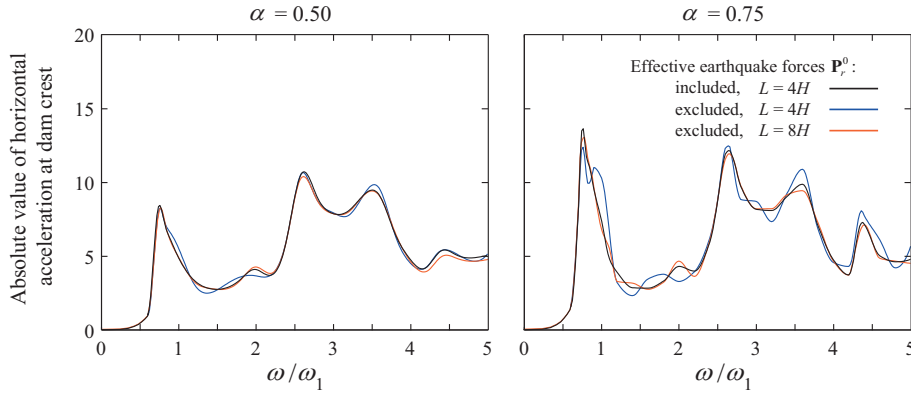


Figure 4.6: Influence of ignoring effective earthquake forces \mathbf{P}_r^0 on the frequency response function for the amplitude of relative horizontal acceleration at the crest of flexible dam with full reservoir due to vertical ground motion. $\zeta_s = 5\%$.

5 Dam–water–foundation rock system

5.1 Dam–water–foundation rock interaction as a scattering problem

Procedures for computing the earthquake response of a dam–foundation rock system (with empty reservoir) or dam–water system (supported on rigid rock) were developed in the previous chapters. Utilizing the same principle of viewing interaction as a scattering problem, wherein the dam perturbs a free-field state, these procedures are combined and extended to the entire dam–water–foundation rock interacting system.

The auxiliary system is now defined as shown in Figure 5.1a as the combination of the two free-field systems introduced in Figures 3.1a and 4.1a. It consists of three subdomains: Ω^a denotes the foundation region interior of the future absorbing boundary Γ_f ; Ω_f^+ is the semi-unbounded foundation region exterior to Γ_f ; and Ω_r^+ is the prismatic fluid channel upstream of the future absorbing boundary Γ_r . This auxiliary system does not correspond to any physical state, but facilitates formulation of the analysis procedure. The displacements and hydrodynamic pressures in the auxiliary system are defined as \mathbf{r}^a and \mathbf{p}^a , respectively.

The dam–water–foundation rock system is also separated into three subdomains (Figure 5.1b): Ω denotes the dam and adjacent foundation and fluid regions interior of Γ_f and Γ_r , and Ω_f^+ and Ω_r^+ are the semi-unbounded foundation and fluid domains exterior to Γ_f and Γ_r ; these are identical to the exterior regions of the auxiliary system. In order to subsequently formulate the governing equations for the absorbing boundaries in terms of free-field quantities – following Chapters 3 and 4 – the displacements and hydrodynamic pressures are defined by the variables

$$\mathbf{r}^t \text{ and } \mathbf{p}^t, \text{ in the interior region } \Omega \quad (5.1a)$$

$$\mathbf{r}^t - \mathbf{r}^a \text{ and } \mathbf{p}^t - \mathbf{p}^a, \text{ in the exterior regions } \Omega_f^+ \text{ and } \Omega_r^+ \quad (5.1b)$$

The variables chosen in Ω_f^+ and Ω_r^+ represent the *scattered motion* and *scattered hydrodynamic pressures*, i.e., the perturbation of the free-field motion (Chapter 2) and pressures (Chapter 3) due to the presence of the dam and the bounded, irregular fluid region. This choice of variables in the exterior domains will subsequently allow reformulation of the governing equations for the absorbing boundaries in a way that the unknown forces \mathbf{R}_f^t and \mathbf{H}_r^t associated with Γ_f and Γ_r (Equation 2.8) can be determined from \mathbf{r}^a and \mathbf{p}^a .

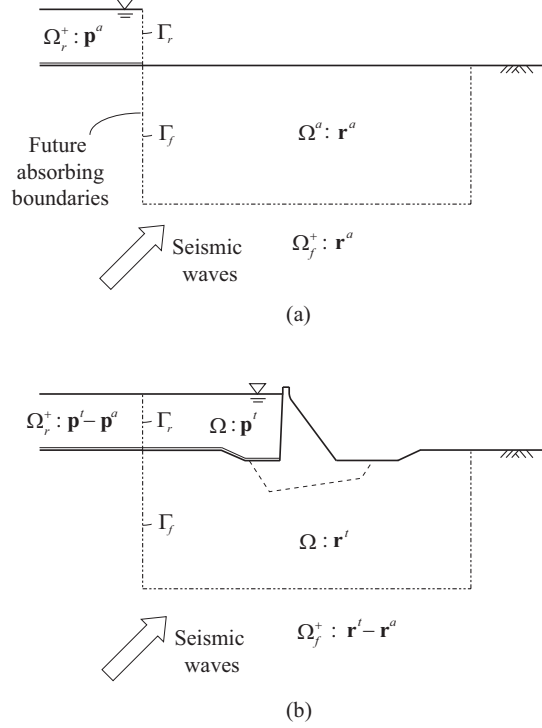


Figure 5.1: Illustration of dam–water–foundation rock interaction as a scattering problem: (a) auxiliary water–foundation rock system in its "free-field" state with variables defined by \mathbf{p}^a in Ω_r^+ and \mathbf{r}^a in $\Omega^a \cup \Omega_f^+$; (b) dam–water–foundation rock system with variables defined by \mathbf{p}^f and \mathbf{r}^f in Ω and the scattered variables $\mathbf{p}^f - \mathbf{p}^a$ in Ω_r^+ and $\mathbf{r}^f - \mathbf{r}^a$ in Ω_f^+ .

5.2 Equations of motion

The equations of motion for the dam–water–foundation rock system contained within the domain Ω are given by Equation (2.8). The unknown forces \mathbf{R}_f^f and \mathbf{H}_r^f associated with the absorbing boundaries Γ_f and Γ_r are given by Equations (3.5) and (4.5), respectively, with an obvious change of notation:

$$\mathbf{R}_f^f = \mathbf{R}_f^a - \mathbf{c}_f [\dot{\mathbf{r}}_f^f - \dot{\mathbf{r}}_f^a] \quad (5.2a)$$

$$\mathbf{H}_r^f = \mathbf{H}_r^a - \mathbf{c}_r [\dot{\mathbf{p}}_r^f - \dot{\mathbf{p}}_r^a] \quad (5.2b)$$

where variables with superscript a are for the auxiliary water–foundation rock system; \mathbf{R}_f^a are the forces consistent with the boundary tractions at Γ_f ; and \mathbf{H}_r^a are the forces consistent with the hydrodynamic pressure gradient at Γ_r .

Included in Equation (2.8) are various interaction effects: dam–foundation rock interaction is included directly in the system matrices, dam–water and water–foundation rock interaction is represented by the coupling matrices \mathbf{Q}_h and \mathbf{Q}_b , respectively, and reservoir bottom absorption is represented through the damping matrix \mathbf{b} . Water–foundation rock interaction is also considered in the exterior domain $\Omega_f^+ \cup \Omega_r^+$ through the variables entering Equation (5.2): (1) the displacements \mathbf{r}_f^a and forces \mathbf{R}_f^a at Γ_f include the effects of hydrodynamic pressures; and (2) the hydrodynamic pressures \mathbf{p}_r^a and forces \mathbf{H}_r^a at Γ_r include the effects of foundation-rock flexibility.

5.2.1 Approximating water–foundation rock interaction

These quantities are to be determined by analysis of the auxiliary water–foundation rock system (Figure 5.1a). This complicated analysis can be avoided by ignoring the effects of water–foundation rock interaction in $\Omega_f^+ \cup \Omega_r^+$:

$$\mathbf{r}_f^a \approx \mathbf{r}_f^0 \text{ and } \mathbf{R}_f^a \approx \mathbf{R}_f^0 \text{ in the foundation domain } \Omega^a \cup \Omega_f^+ \quad (5.3a)$$

$$\mathbf{p}_r^a \approx \mathbf{p}_r^0 \text{ and } \mathbf{H}_r^a \approx \mathbf{H}_r^0 \equiv \mathbf{0}^\dagger \text{ in the fluid domain } \Omega_r^+ \quad (5.3b)$$

where the free-field motion \mathbf{r}_f^0 and forces \mathbf{R}_f^0 at the boundary Γ_f are computed from analysis of the free-field foundation-rock system (Figure 3.1a), thus ignoring the effects of hydrodynamic pressures in Ω_r^+ on the foundation-rock motions; and the free-field hydrodynamic pressures \mathbf{p}_r^0 are computed from analysis of the fluid in its "free-field" state (Figure 4.1a) with rigid foundation rock, thus ignoring the effects of foundation-rock flexibility on the hydrodynamic pressures in Ω_r^+ .

It has been demonstrated through numerical results that the response of gravity dams to horizontal ground motion is essentially unaffected by the above approximation of water–foundation rock interaction, and that the response to vertical ground motion is only noticeably affected for large values of the wave-reflection coefficient α , where the approximate results tends to overestimate the response [41]. These conclusions were based on analyses using very small domain sizes; the errors will be much smaller when using larger domain sizes that are required by the viscous-damper boundaries (Figure 2.2).

Although the secondary effects of water–foundation rock interaction in $\Omega_f^+ \cup \Omega_r^+$ are ignored, the dominant effects within the truncated FE domain Ω are still rigorously represented by the coupling matrix \mathbf{Q}_b . Alternatively, water–foundation rock interaction can be neglected altogether by setting $\mathbf{Q}_b \equiv \mathbf{0}$; however, because this approximation can lead to significant error (Section 5.4.3), it is not introduced here.

[†] Recall from Section 4.3 that the forces \mathbf{H}_r^0 associated with the free-field pressure gradient $\partial p^0 / \partial n$ at Γ_r are zero for both horizontal and vertical ground motion.

5.2.2 Dam–water–foundation rock system

With the preceding approximations in modeling water–foundation rock interaction, the forces \mathbf{R}'_f and \mathbf{H}'_r can be determined independently of each other by considering the free-field systems of Figure 3.1a and Figure 4.1a, respectively. Substituting Equation (3.5) and (4.5) into Equation (2.8), the final equations of motion for the dam–water–foundation rock system are obtained:

$$\begin{aligned} \begin{bmatrix} \mathbf{m} & \mathbf{0} \\ \rho(\mathbf{Q}_h^T + \mathbf{Q}_b^T) & \mathbf{s} \end{bmatrix} \begin{Bmatrix} \ddot{\mathbf{r}}' \\ \ddot{\mathbf{p}}' \end{Bmatrix} + \begin{bmatrix} \mathbf{c} + \mathbf{c}_f & \mathbf{0} \\ \mathbf{0} & \mathbf{b} + \mathbf{c}_r \end{bmatrix} \begin{Bmatrix} \dot{\mathbf{r}}' \\ \dot{\mathbf{p}}' \end{Bmatrix} \\ + \begin{Bmatrix} \mathbf{f}(\mathbf{r}') \\ \mathbf{0} \end{Bmatrix} + \begin{bmatrix} \mathbf{0} & -(\mathbf{Q}_h + \mathbf{Q}_b) \\ \mathbf{0} & \mathbf{h} \end{bmatrix} \begin{Bmatrix} \mathbf{r}' \\ \mathbf{p}' \end{Bmatrix} = \begin{Bmatrix} \mathbf{R}^{\text{st}} \\ \mathbf{0} \end{Bmatrix} + \begin{Bmatrix} \mathbf{P}_f^0 \\ \mathbf{P}_r^0 \end{Bmatrix} \end{aligned} \quad (5.4)$$

The earthquake excitation is specified in Equation (5.4) by the effective earthquake forces \mathbf{P}_f^0 at Γ_f defined by Equations (3.11) and (3.7) for the bottom and side boundaries of the foundation domain, respectively; and the effective earthquake forces \mathbf{P}_r^0 at Γ_r defined by Equation (4.9). These forces are easily obtained using the procedures developed in Sections 3.5 and 4.4.

5.3 Summary of procedure

Analysis of the dam–water–foundation rock system subjected to the free-field ground acceleration $a_g^k(t)$, $k = x, y$, defined at a control point at the surface of the foundation rock (Figure 2.1) is organized in three parts: static analysis, linear analyses of the free-field foundation-rock and fluid systems, and nonlinear dynamic analysis of the dam–water–foundation rock system.

Static analysis:

1. Develop a FE model for static analysis of the dam–foundation rock system with a suitable material model for the dam concrete and a suitable (static) model for the foundation rock.
2. Determine the static response of this system to gravity loads on the dam and hydrostatic forces on the dam and foundation rock.
3. Record the static state of the dam–foundation rock system, including reactions from the foundation rock at the boundary Γ_f .

Linear analysis of free-field foundation-rock system (Figure 5.2a):

4. Obtain the free-field motion at the base of the foundation model by deconvolution of the surface ground motion $a_g^k(t)$.

5. Calculate the effective earthquake forces \mathbf{P}_f^0 at the bottom boundary from Eq. (3.11), with the motion \mathbf{r}_f^0 due to the incident (upward propagating) seismic wave taken as 1/2 the outcrop motion extracted from the deconvolution analysis.
6. Develop a FE model for the free-field foundation-rock system: a single column of elements that has the same mesh density as the main FE model adjacent to the side boundaries, with viscous dampers applied at the base in the x - and y -directions.
7. Compute $\dot{\mathbf{r}}_f^0$ and \mathbf{R}_f^0 at each node along the height by analyzing the foundation-rock column subjected to forces given by Eq. (3.11) at its base.
8. Calculate the effective earthquake forces \mathbf{P}_f^0 at the side boundaries of the foundation domain from Eq. (3.7) using $\dot{\mathbf{r}}_f^0$ and \mathbf{R}_f^0 from Step 7.

Steps 6-8 may be avoided if free-field boundary elements are applied along the side boundaries (Figure 3.3b).

Linear analysis of free-field fluid system (Figure 5.2b):

9. Develop a FE model for the free-field fluid: a single column of elements of unit width with the same mesh density as the fluid adjacent to the boundary Γ_r , add a single line element to model reservoir bottom sediments.
10. Calculate $\dot{\mathbf{p}}_r^0$ at every node along the height by analyzing the fluid column subjected to forces ρa_g^y at its base for vertical ground motion; $\dot{\mathbf{p}}_r^0 = \mathbf{0}$ for horizontal motion.
11. Compute the effective earthquake forces \mathbf{P}_r^0 at the fluid boundary Γ_r from Eq. (4.9) using $\dot{\mathbf{p}}_r^0$ from Step 10.

Nonlinear dynamic analysis of dam–water–foundation rock system (Figure 5.2c):

12. Develop a FE model of the dam–water–foundation rock system with viscous-damper boundaries to truncate the semi-unbounded foundation and fluid domains at Γ_f and Γ_r , respectively. Use standard solid and fluid elements for the dam, foundation rock, and fluid, and apply interface elements (or tie constraints) at the upstream dam face and at the water–foundation rock interface. Reservoir bottom sediments can be approximately modeled using line elements based on the 1D absorption model, or by using one of several more sophisticated methods (Section 2.3.2).
13. Calculate the response of the FE model of the dam–water–foundation rock system subjected to effective earthquake forces \mathbf{P}_f^0 at the boundary Γ_f calculated in Steps 5 and 8, \mathbf{P}_r^0 at the boundary Γ_r calculated in Step 11, plus static loads and foundation reactions at Γ_f . The static state of the dam (Step 3) is taken as the initial state in the nonlinear dynamic analysis.

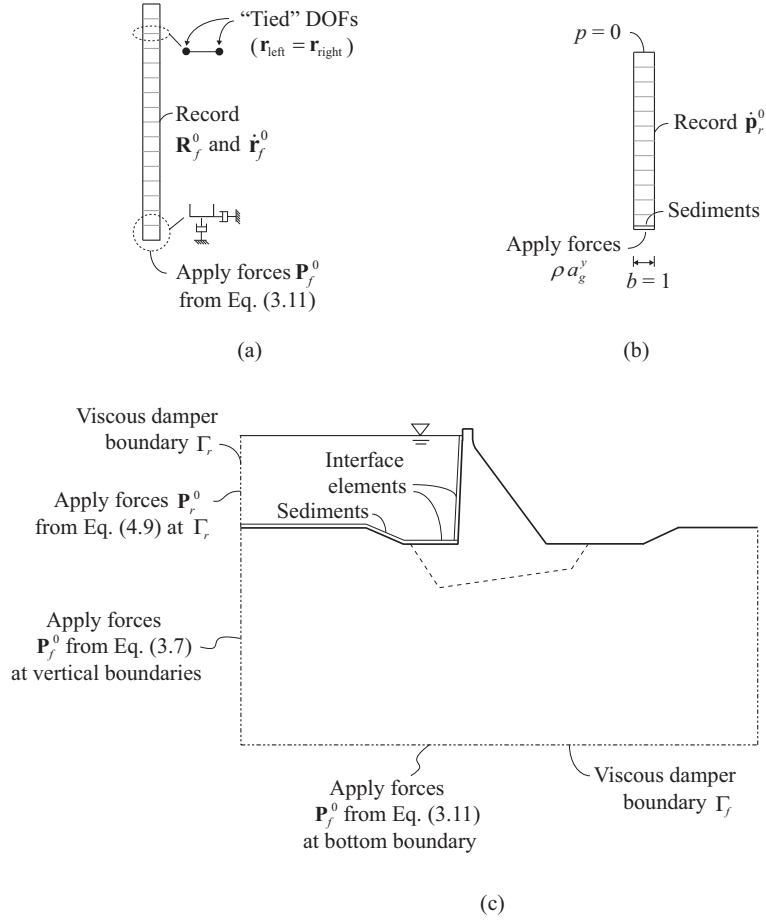


Figure 5.2: Summary of analysis procedure for dam–water–foundation rock system: (a) auxiliary analysis of single column of foundation-rock elements to compute $\dot{\mathbf{r}}_f^0$ and \mathbf{R}_f^0 ; (b) analysis of 1D column of fluid elements to calculate $\dot{\mathbf{p}}_r^0$ for vertical ground motion; (c) application of effective earthquake forces to truncated FE model.

5.4 Numerical validation

The direct FE method developed in the preceding sections is validated by computing the dynamic response of the dam–water–foundation rock system shown in Figure 5.3 to horizontal and vertical ground motion. The idealized dam–water–foundation rock system has the same geometry, FE mesh and material parameters as the systems used in Sections 3.6 and 4.5, but is combined to form the complete dam–water–foundation rock system. Material damping in the dam and foundation rock is modeled by Rayleigh damping with $\zeta_s = 2\%$ and $\zeta_f = 2\%$ viscous damping specified for the dam and foundation rock separately, implemented using the procedure described in Section 3.6.

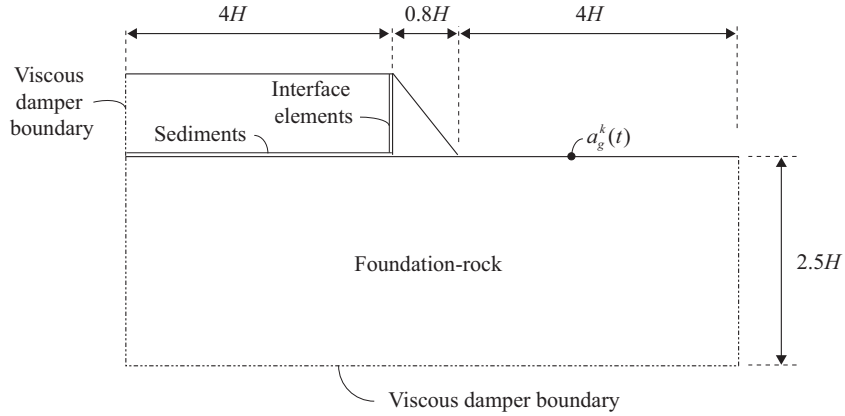


Figure 5.3: Dimensions of FE model for idealized dam–water–foundation rock system with viscous-damper boundaries to truncate semi-unbounded foundation and fluid domains.

The ground motion is specified by the ground acceleration $a_g^k(t)$ at the foundation surface. The free-field motion at depth in the model is obtained by deconvolution of this motion; then effective earthquake forces at the bottom and side boundaries of the foundation rock are then computed from Equations (3.11) and (3.7), respectively. For vertical ground motion, the effective earthquake forces at the fluid boundary Γ_r are computed from Equation (4.9).

5.4.1 Frequency response functions for dam response

Frequency response functions for the amplitude of the relative horizontal acceleration at the crest of the dam is computed and shown in Figure 5.4 for three values of α . The results are compared to results obtained by the substructure method [76] where the foundation rock is modeled as a viscoelastic halfspace, hydrodynamic pressures are modeled by analytical solutions, and the earthquake excitation is specified directly at the dam–foundation interface. Because the computer program EAGD84 – used to compute the substructure results – ignores water–foundation rock interaction, this interaction is also ignored in the direct FE method for these validation analyses.

The results computed by the direct FE method are very close to the results from the substructure analysis for both vertical and horizontal ground motion, thus validating its ability to model the semi-unbounded dam–water–foundation rock system. The slight differences at some frequencies are attributable to the approximate nature of the viscous-damper boundary, which is unable to perfectly absorb all outgoing waves. As previously mentioned, these discrepancies will generally decrease as the sizes of the foundation and fluid domains included in the FE model increases.

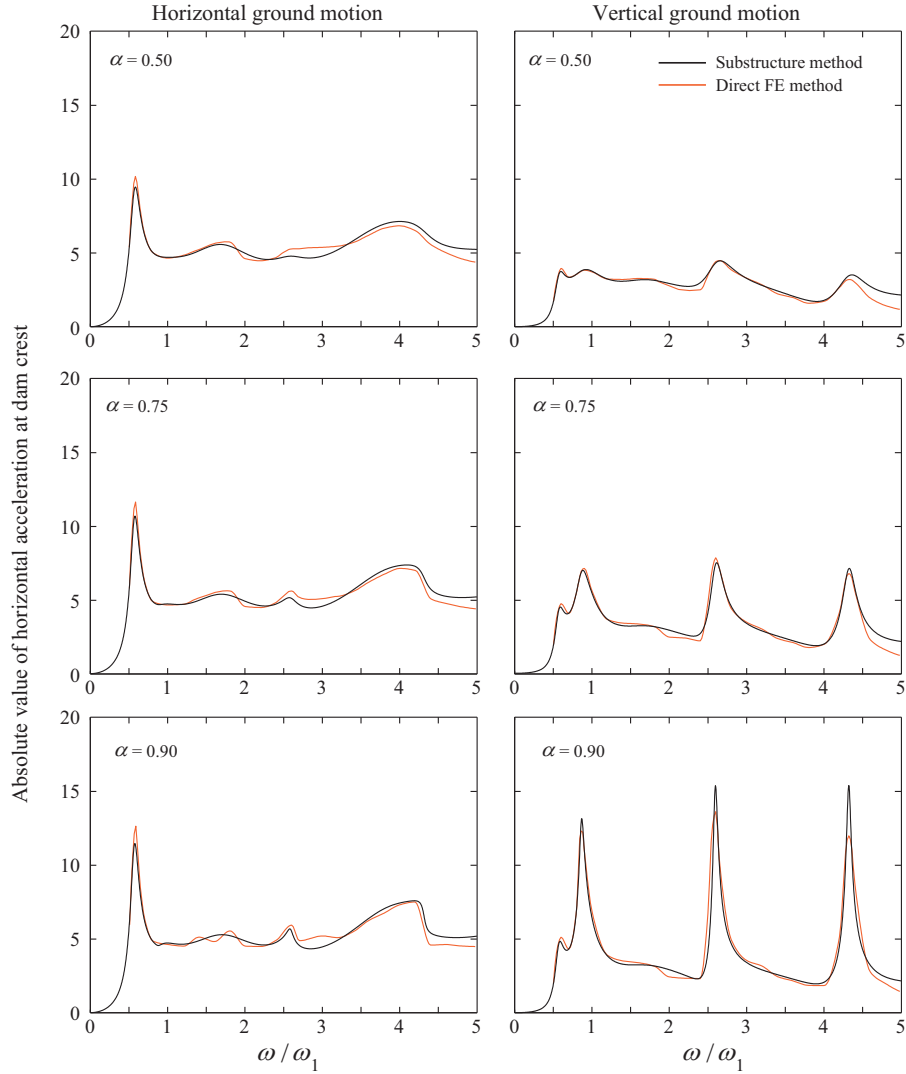


Figure 5.4: Comparison of frequency response functions from direct and substructure methods for the amplitude of relative horizontal acceleration at the crest of dam on flexible foundation rock with full reservoir due to horizontal and vertical ground motion. $\zeta_s = \zeta_f = 2\%$; $E_f / E_s = 1.0$.

5.4.2 Response to transient motion

To demonstrate the ability of the direct FE method to accurately compute the response of the dam–water–foundation rock system to earthquake excitation, the system is analyzed for $a_g^x(t)$ and $a_g^y(t)$ specified as the S69E and vertical components, respectively, of the motion recorded at Taft Lincoln School Tunnel during the 1952 Kern County earthquake. The

response was also computed by the substructure method. The relative horizontal displacements and accelerations at the dam crest are presented in Figure 5.5, and the envelope values of the maximum principal stresses in Figure 5.6. It can be seen that the results from the direct FE method closely match the substructure method results, as expected to by the close agreement observed earlier for the frequency response functions.

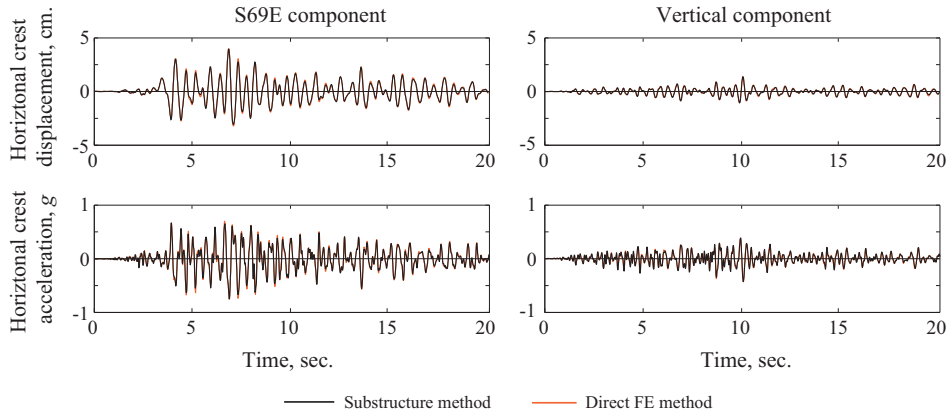


Figure 5.5: Horizontal displacements and accelerations at the crest of the dam on flexible foundation rock with full reservoir due to the S69E and vertical components, separately, of Taft ground motion. $\zeta_s = \zeta_f = 2\%$; $E_f / E_s = 1.0$; $\alpha = 0.75$.

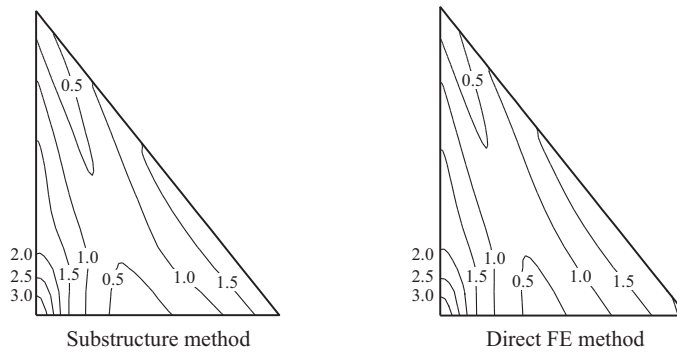


Figure 5.6: Envelope values of maximum principal stresses, in MPa, in dam on flexible foundation rock with full reservoir due to S69E component of Taft ground motion; initial static stresses are excluded. $\zeta_s = \zeta_f = 2\%$; $E_f / E_s = 1.0$; $\alpha = 0.75$.

5.4.3 Influence of water–foundation rock interaction

In the direct FE method, water–foundation rock interaction is directly represented in the equations of motion (Equation 5.4) through the matrix \mathbf{Q}_b that couples accelerations and

hydrodynamic pressures at the reservoir boundaries. In the preceding validation results however, water–foundation rock interaction was excluded in the direct FE method to ensure comparability with the substructure method results used as benchmark, which completely neglects water–foundation rock interaction. The influence of this assumption on dam response is investigated next.

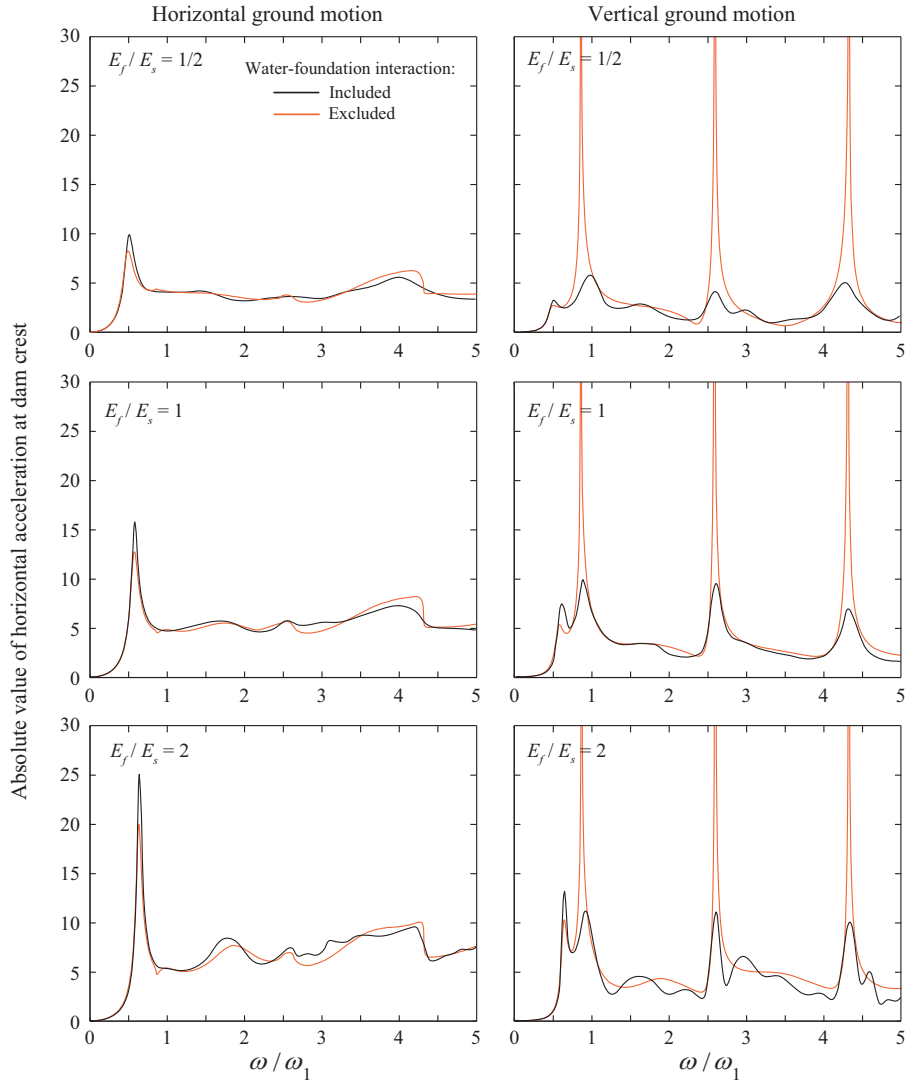


Figure 5.7: Influence of water–foundation rock interaction on frequency response function for dam on flexible foundation rock with full reservoir, without sediments, due to horizontal and vertical ground motion.

$$\zeta_s = \zeta_f = 2\% .$$

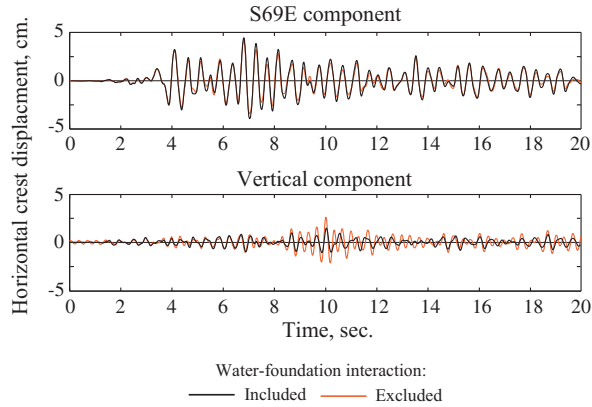


Figure 5.8: Influence of water–foundation rock interaction on earthquake response of dam on flexible foundation rock with full reservoir, without sediments. $\zeta_s = \zeta_f = 2\%$; $E_f / E_s = 1.0$.

Presented in Figures 5.7 and 5.8 are frequency response functions and earthquake response, respectively, for the dam on flexible foundation rock with a full reservoir with no sediments (i.e., $\alpha = 1.0$). Results are computed by the direct FE method for two cases: (1) including water–foundation rock interaction; (2) excluding water–foundation rock interaction. Neglecting water–foundation rock interaction has little influence on the response to horizontal ground motion except near the first resonance peak where the response is underestimated. For vertical ground motion, neglecting water–foundation rock interaction significantly overestimates the response near the resonance frequencies of the reservoir and the resonance peaks become unbounded. The same trends are seen in the response to earthquake excitation. Because water–foundation rock interaction can be significant for the dam response, and the fact that there is no advantage in ignoring it in the direct FE method, it should be included in earthquake analysis of concrete dams.

6 Conclusions

A direct FE method for earthquake analysis of concrete dams interacting with fluid and foundation rock, which may be semi-unbounded domains, has been developed. The analysis procedure uses viscous-damper boundaries to truncate these semi-unbounded domains and specifies the seismic input as effective earthquake forces directly at the model truncations. The analysis procedure is formulated by treating dam–water–foundation rock interaction as a scattering problem [41] where the dam perturbs an assumed "free-field" state of the system. The FE model of the fluid includes water compressibility and reservoir bottom absorption, and the FE model of the foundation rock includes mass, stiffness, and material damping appropriate for rock. Thus, the unrealistic assumptions of massless rock and incompressible water, sometimes used in engineering practice, are eliminated.

The seismic input to the procedure is defined by a ground motion specified at a control point on the foundation surface. The free-field motion at the bottom of the foundation rock is determined by deconvolution of this motion. Effective earthquake forces at the boundaries of the foundation and fluid domains are then computed from analysis of two individual 1D free-field systems. Implementation of these analyses is straightforward, and does not require modification of the source code of a commercial FE program.

The analysis procedure is validated numerically by computing the dynamic response of an idealized dam–water–foundation rock system and comparing against results obtained using the substructure method [17]. The excellent agreement demonstrates that (1) the truncated foundation and fluid models with viscous-damper boundaries are able to model the semi-unbounded domains; (2) the earthquake excitation is properly defined by the effective earthquake forces determined from the free-field variables.

Because the direct FE method is applicable to nonlinear systems, it allows for modeling of concrete cracking, as well as sliding and separation at construction joints, lift joints, and at concrete-rock interfaces. Implementation of the procedure is facilitated by commercial FE software, with their nonlinear material models, that permit modeling of viscous-damper boundaries and specification of effective earthquake forces at these boundaries.

PART II

**Direct finite element method for nonlinear
earthquake analysis of three-dimensional dam–
water–foundation rock system**

1 Introduction

Earthquake analysis of arch dams requires three-dimensional dam–water–foundation rock systems that recognize all factors known to significantly influence their earthquake response [1]: dam–water interaction including water compressibility and wave absorption at the reservoir bottom [4,77]; dam–foundation rock interaction including inertia effects of the rock [3]; radiation damping due to the semi-unbounded sizes of the reservoir and foundation domains [3,7]; spatial variation of ground motion at the dam–canyon interface [78,79]; and nonlinear behavior of the dam and foundation rock [7,8,12].

Most dam engineers prefer to work with the *direct method* of analysis – implemented in commercial FE software with their user-friendly interfaces – that models the entire system using finite elements and analyzes it directly in the time-domain. While these programs are able to model nonlinear mechanisms, they often neglect or use simplistic models for dam–water–foundation rock interaction and the semi-unbounded domains. Furthermore, spatial variation of earthquake motions at the dam–canyon interface is typically ignored in dam engineering practice, even though there is substantial evidence that such variations can significantly influence the response of arch dams [78–81].

Accurate modeling of dam–water–foundation rock systems requires a FE model that includes mass, stiffness, and material damping properties of the foundation rock, the compressibility of water, and the effects of energy dissipation at the reservoir bottom. The semi-unbounded foundation and fluid domains must be reduced to bounded sizes using *absorbing boundaries* [20,23], and the seismic input specified by *effective earthquake forces* applied either directly to these boundaries [20,35], or via a single layer of elements interior of the boundaries [38,40].

Utilizing the former of these approaches, a direct FE method for nonlinear earthquake analysis of 2D dam–water–foundation rock systems was developed in Part I of this thesis. Standard viscous-damper boundaries [18] were selected to model the semi-unbounded domains and the seismic input was specified as tractions directly at these boundaries. These are standard features in FE analyses, thus ensuring that this direct FE method can be implemented with any commercial FE software without modification of the source code.

The objective of the work presented here is to generalize the direct FE method to 3D dam–water–foundation rock systems. After defining the components of the 3D dam–water–foundation rock system in Chapter 2, the analysis procedure is developed in Chapter 3, and step-by-step procedures for computing effective earthquake forces at the foundation and fluid boundaries are outlined in Chapter 4. Several examples are presented in Chapter 5 to validate the accuracy of the direct FE method. First, the method is used to compute the free-field motion at the surface of a flat foundation box and at a semi-cylindrical canyon and compared to classical solutions. The dynamic response of an arch dam system is computed next and

compared against results from the substructure method. To facilitate implementation of the direct FE method for 3D systems, several simplifications of the procedure are proposed in Chapter 6, and their efficacy is evaluated. Finally, in Chapter 7, the analysis procedure is summarized in step-by-step form.

A shortened version of this part of the thesis has been published in the journal *Earthquake Engineering and Structural Dynamics*:

Løkke, A., and Chopra, A.K., (2018). Direct finite element method for nonlinear earthquake analysis of 3-dimensional semi-unbounded dam–water–foundation rock systems. *Earthquake Engineering & Structural Dynamics*, 47(5), 1309-1328.

2 System and ground motion

2.1 Semi-unbounded dam–water–foundation rock system

The idealized, three-dimensional dam–water–foundation rock system considered consists of three subsystems (Figure 2.1): (1) the concrete dam with nonlinear properties; (2) the foundation rock, consisting of a bounded region adjacent to the dam that may be nonlinear, inhomogeneous, and irregular in geometry; and the exterior, semi-unbounded, region with "regular" geometry that has linear constitutive properties and is homogeneous or horizontally layered; and (3) the fluid domain, consisting of a bounded region of arbitrary geometry adjacent to the dam that may be nonlinear; and a uniform channel, unbounded in the upstream direction, that is restricted to be linear.

By "regular" geometry of the semi-unbounded foundation region, it is meant that the canyon upstream of the bounded region has a uniform cross-section, and similarly, the canyon downstream of the bounded region has a uniform cross-section; however, the two cross-sections may be different. The assumption of homogeneous or horizontally layered properties in the exterior foundation region is introduced to permit use of a 1D deconvolution method – based on the assumption of vertically propagating waves – to define the seismic input for the system starting from ground motion specified at the surface of the foundation rock (Section 2.2).

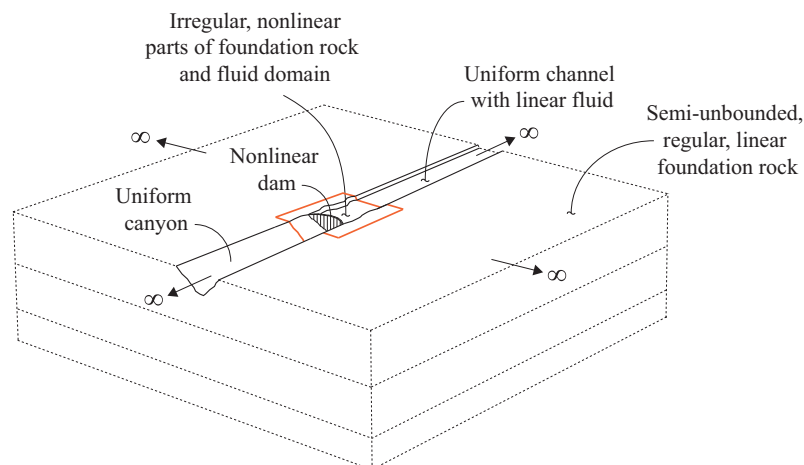


Figure 2.1: Semi-unbounded dam–water–foundation rock system showing main parts: (1) the nonlinear dam; (2) the foundation rock, consisting of an irregular, nonlinear region and a semi-unbounded region that is linear and has regular geometry and homogeneous properties; (3) the fluid domain, consisting of an irregular nonlinear region, and a semi-unbounded uniform channel with linear fluid.

The semi-unbounded system in Figure 2.1 is modeled by a 3D finite-element discretization of a bounded system with viscous-damper boundaries at the bottom and side boundaries of the foundation domain to model its semi-unbounded geometry, and at the upstream end of the fluid domain to model its essentially "unbounded" length (Figure 2.2). Although many absorbing boundaries have been proposed in the literature (e.g. [18–34]), the well-known viscous damper [18] has been chosen herein because of its availability in every commercial FE code, acceptable accuracy, and ease of implementation.

The linear, regular parts of the foundation and fluid domains included in the FE model provide a transition from the irregular geometry and nonlinear behavior adjacent to the dam to the regular geometry and linear behavior required at the absorbing boundaries. The minimum sizes for these domains are determined by the ability of the viscous-damper boundaries to absorb outgoing scattered waves from the system. Because the viscous damper is a "simple" absorbing boundary, larger domain sizes are required than if an "advanced" boundary such as PML was used. However, as will be seen in Section 6, the use of larger domains has the advantage that it enables introduction of two simplifications that significantly reduce the complexity of implementing the analysis method.

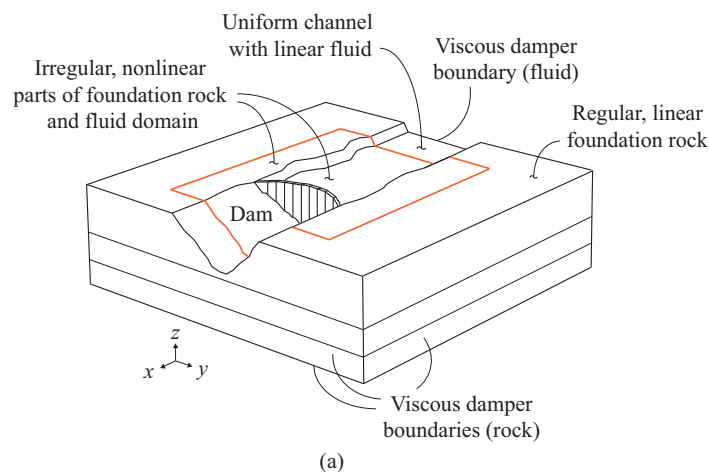


Figure 2.2: Dam–water–foundation rock system with truncated foundation and fluid domains: (a) 3D perspective view.

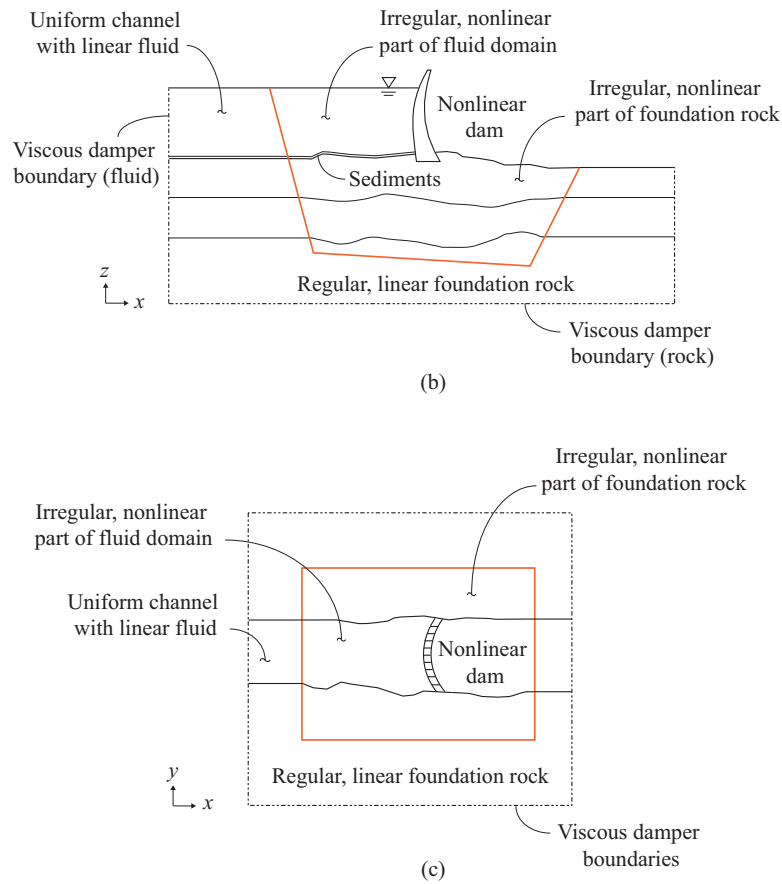


Figure 2.2 (continued): Dam–water–foundation rock system with truncated foundation and fluid domains: (b) section view through center of canyon; (c) plan view.

The use of finite elements for the entire system permits modeling of arbitrary geometry and inhomogeneous material properties of the dam, canyon, foundation and fluid domains adjacent to the dam. Furthermore, it allows for modeling of nonlinear mechanisms (Figure 2.3) such as cracking of the dam concrete [7,8,14,82], sliding and separation at construction joints, lift joints, and at concrete-rock interfaces [7,11,83–85], discontinuities in the rock due to local cracks and fissures [36,86], and cavitation in the fluid [87].

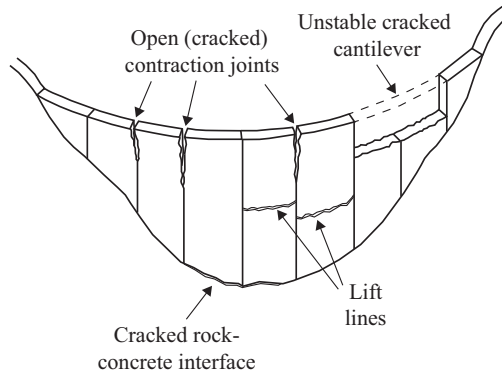


Figure 2.3: Nonlinear mechanisms for concrete arch dams. Figure adapted from Ref. [88].

2.2 Earthquake excitation

Equations governing the motion of the system in Figure 2.2 subjected to earthquake excitation defined by the free-field ground motion – the motion that would occur in the foundation rock without the dam and water present – will be formulated in Chapter 3. These equations require that the spatially varying free-field motions at all future boundaries of the FE model are known. Specifying such motions remains a challenging problem.

The most general approach is to perform large-scale simulation of seismic wave propagation from an earthquake source to the dam site [89–91], shown schematically in Figure 2.4a. Here, physics-based FE or finite difference models of large regions subjected to a fault slip are analyzed. Although such regional simulations have been reported in the research literature, they seem impractical for concrete dam analysis for two reasons: (1) information regarding the details of the earthquake fault rupture and the properties of the geological materials is lacking; and (2) simulation models are currently limited to lower frequencies compared to the vibration properties of concrete dams.

Another approach would be to use boundary element methods (BEM) to compute the free-field motions resulting from incident plane waves propagating from infinity to the dam site at predefined angles, shown schematically in Figure 2.4b. Such methods have been used to compute the free-field motions at the surface of canyons [81,92], and to investigate the influence of assumed incident angles on the dam response [93]. However, due to the obvious difficulty in selecting a combination of wave types and their incidence angles for an actual situation, these methods are rarely applied to solve practical problems.

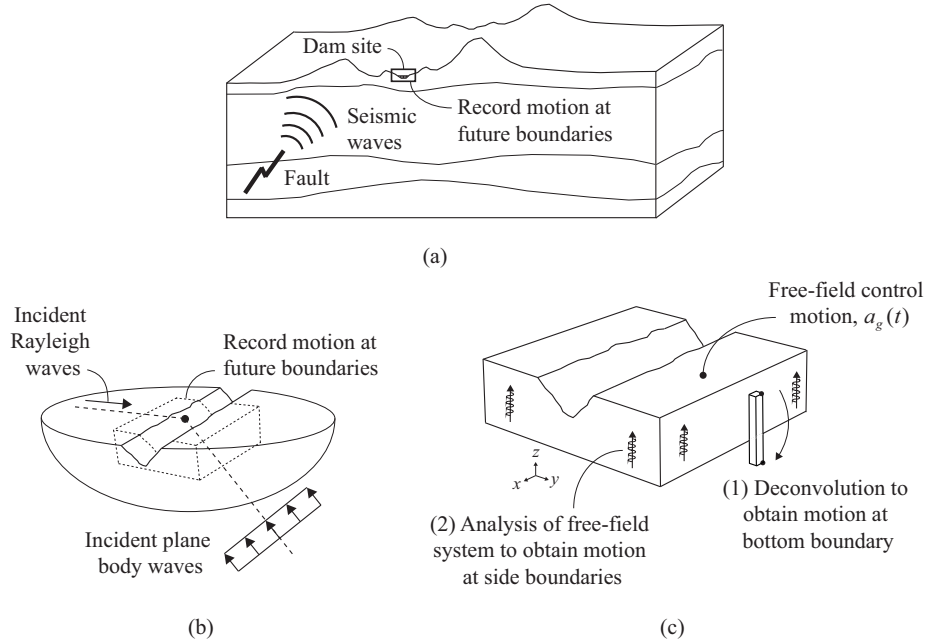


Figure 2.4: Illustration of methods to obtain free-field earthquake motion: (a) large scale fault-rupture simulation; (b) boundary element method with incident plane waves propagating from infinity at predefined angles; (c) deconvolution analysis starting with a free-field surface control motion $a_g^k(t)$.

Presently, the standard approach is to define the earthquake excitation by three components of free-field acceleration specified at a control point on the foundation surface (Figure 2.4c): the stream component, $a_g^x(t)$, the cross-stream component $a_g^y(t)$ and the vertical component $a_g^z(t)$. Because the ground motion cannot be defined uniquely, an ensemble of motions is required. These motions should, in some sense, be consistent with a target design spectrum that represents the seismic hazard at the site, e.g., the uniform hazard spectrum (UHS) or some variation of the conditional mean spectrum (CMS). Several methods have been developed to select and scale ground motion records to "match" a target spectrum [94–96]. The UHS (and CMS) applies to an outcrop location on level ground; this control point is chosen at the elevation of the dam abutments in the linear, regular part of the foundation rock (Figure 2.4c). It could also be at other locations however, for example if the purpose is to perform analysis using earthquake input motions recorded at specific locations near the dam.

The free-field motion at the bottom and side boundaries of the foundation domain can be determined from the surface control motion $a_g^k(t)$ using a deconvolution-type analysis (Figure 2.4c). For this analysis, it will be assumed that the incident wave field consists solely of plane SH-, SV- and P-waves propagating vertically upwards from the underlying semi-

unbounded foundation rock. This is clearly a major simplification but, at the present time, it seems to be a reasonable pragmatic choice.

When specifying the earthquake excitation this way, spatial variation of the ground motion, both amplitude and phase, is automatically considered in the analysis, albeit predominantly in the vertical direction. To demonstrate this, such free-field motions are computed by the direct FE method to be developed in Chapters 3 and 4 applied to analyze the FE model in Figure 2.5 consisting of a canyon without a dam or reservoir. In these analyses, the control motion at the surface of the foundation rock was defined in the stream direction by the S69E component of the motion recorded at Taft Lincoln School Tunnel during the 1952 Kern County earthquake.

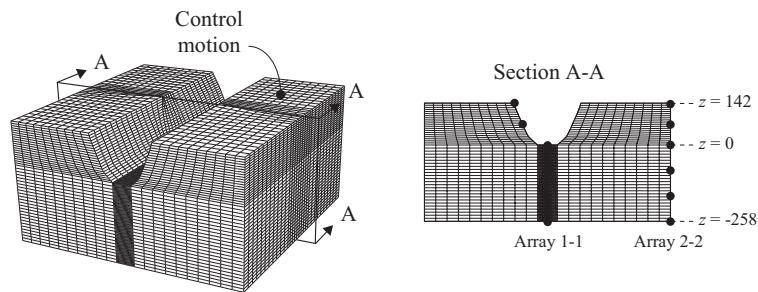


Figure 2.5: FE model of canyon showing location of two vertical node arrays: array 1-1 at the center of the model, and array 2-2 at the side boundary of the model.

Observe from the results in Figure 2.6 that the amplitude and phase of the motion varies greatly with height, and by comparing the motions at two locations at the same elevation (e.g. at $z = 0\text{m}$), it is evident that scattering and diffraction of waves from the canyon cause variation of the motion also in the horizontal direction. Because of the assumption of vertically incident waves however, this spatial variation is significant in the vertical direction, but less so in the horizontal direction.

PART II: SYSTEM AND GROUND MOTION

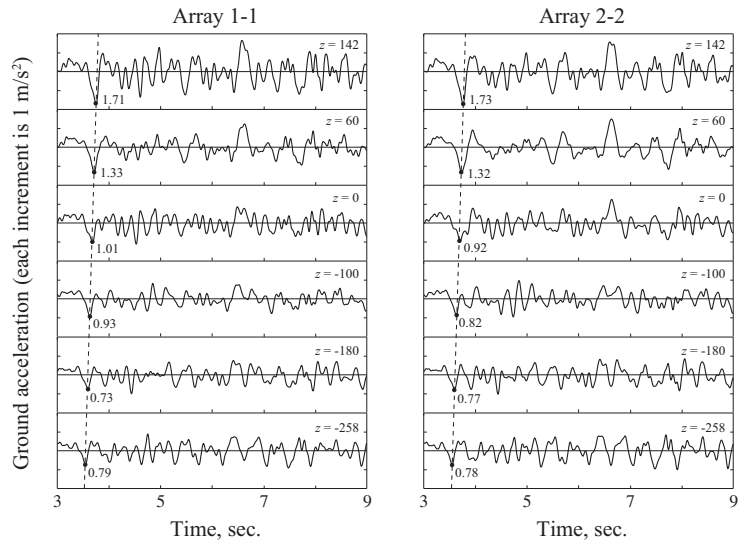


Figure 2.6: Stream component of free-field earthquake motion computed by the direct FE method at six different elevations at the two arrays. A specific peak in the acceleration history is identified and connected by a dashed line to demonstrate the amplitude change and time shift in the motions at higher elevations.

3 Equations of motion

3.1 Governing equations

The governing equations for a 2D gravity dam–water–foundation rock system idealized as an ensemble of finite elements with viscous-damper boundaries were derived in Part II. These equations are repeated here and generalized for 3D dam–water–foundation rock systems (Figure 3.1):

$$\begin{aligned} & \begin{bmatrix} \mathbf{m} & \mathbf{0} \\ \rho(\mathbf{Q}_h^T + \mathbf{Q}_b^T) & \mathbf{s} \end{bmatrix} \begin{Bmatrix} \ddot{\mathbf{r}}^t \\ \ddot{\mathbf{p}}^t \end{Bmatrix} + \begin{bmatrix} \mathbf{c} & \mathbf{0} \\ \mathbf{0} & \mathbf{b} \end{bmatrix} \begin{Bmatrix} \dot{\mathbf{r}}^t \\ \dot{\mathbf{p}}^t \end{Bmatrix} \\ & + \begin{Bmatrix} \mathbf{f}(\mathbf{r}^t) \\ \mathbf{0} \end{Bmatrix} + \begin{bmatrix} \mathbf{0} & -(\mathbf{Q}_h + \mathbf{Q}_b) \\ \mathbf{0} & \mathbf{h} \end{bmatrix} \begin{Bmatrix} \mathbf{r}^t \\ \mathbf{p}^t \end{Bmatrix} = \begin{Bmatrix} \mathbf{R}_f^t + \mathbf{R}^{\text{st}} \\ \mathbf{H}_r^t \end{Bmatrix} \end{aligned} \quad (3.1)$$

where \mathbf{r}^t is the vector of total displacements in the dam and foundation rock; \mathbf{p}^t is the vector of total hydrodynamic pressures in the fluid, idealized as a linear (for convenience of notation), inviscid, irrotational and compressible Eulerian fluid[†] [52]; \mathbf{m} and \mathbf{c} are the standard mass and damping matrices, respectively, for the dam–foundation rock system; $\mathbf{f}(\mathbf{r}^t)$ is the vector of internal forces due to (nonlinear) material response; \mathbf{s} , \mathbf{b} and \mathbf{h} are the "mass", "damping" and "stiffness" matrices, respectively, for the fluid [52]; ρ is the density of water; \mathbf{Q}_h and \mathbf{Q}_b are matrices that couple accelerations to hydrodynamic pressures at the dam–water interface Γ_h and water–foundation rock interface Γ_b , respectively; \mathbf{R}^{st} is the vector of static forces, including self-weight, hydrostatic pressures, and static foundation reactions at Γ_f (see Chapter 7 for details); \mathbf{R}_f^t is the vector of dynamic forces associated with the absorbing foundation boundary Γ_f ; and \mathbf{H}_r^t is the vector of dynamic forces associated with the absorbing fluid boundary Γ_r . Expressions for the unknown forces \mathbf{R}_f^t and \mathbf{H}_r^t will be derived later in this chapter.

Hydrodynamic wave energy is lost at Γ_b – the bottom and side boundaries of the reservoir – by means of two mechanisms. The first is wave absorption in sediments invariably deposited at the reservoir bottom. This mechanism is – for the purpose of comparing against results from the substructure method in Chapter 5 – modeled approximated by the reservoir bottom reflection coefficient α [6], and its effects are included in Equation (3.1) through the damping matrix \mathbf{b} . The second mechanism, associated with water–foundation rock interaction, is explicitly considered in the FE model through the coupling matrix \mathbf{Q}_b . Because this mechanism automatically accounts for some radiation of hydrodynamic waves, care

[†] The analysis procedure is also applicable to a Lagrangian fluid formulation with appropriate modifications of Equation (3.1)

should be taken not to overestimate the total amount of energy lost at these boundaries when also including sediment absorption in the FE model. For example, if the foundation consists of sandstone or granite, including water–foundation rock interaction has approximately the same amount of energy dissipation as a 1D absorption model with $\alpha = 0.50$ or $\alpha = 0.75$, respectively.

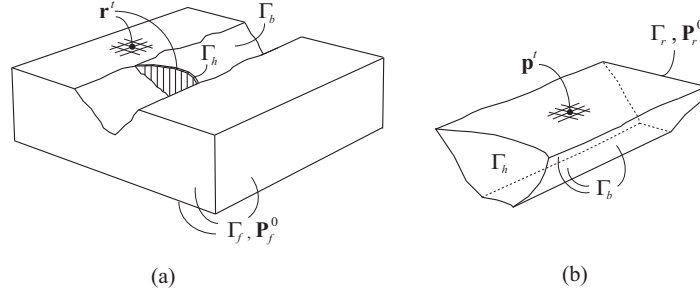


Figure 3.1: Schematic FE model of (a) dam and foundation domain, and (b) fluid domain. Absorbing boundaries Γ_f and Γ_r at the truncation of the foundation and fluid domains, and interfaces Γ_h at the upstream dam face and Γ_b at the reservoir bottom and sides are highlighted.

The wave-absorbing boundaries that enforce the radiation condition at the foundation and fluid boundaries are modeled by viscous dampers (dashpots) lumped at the boundary nodes of the FE model (Figure 3.2). Their governing equations can be written in FE notation as

$$\mathbf{R}_f + \mathbf{c}_f \dot{\mathbf{r}}_f = \mathbf{0}, \quad \text{at the foundation boundaries } \Gamma_f \quad (3.2a)$$

$$\mathbf{H}_r + \mathbf{c}_r \dot{\mathbf{p}}_r = \mathbf{0}, \quad \text{at the upstream fluid boundary } \Gamma_r \quad (3.2b)$$

In Equation (3.2a), \mathbf{c}_f is the matrix of normal and tangential damper coefficients $c_p = A\rho_f V_p$ and $c_s = A\rho_f V_s$, respectively, where A is the tributary area of the node, and ρ_f , V_s and V_p are the density, shear wave velocity and pressure wave velocity, respectively, of the rock. In Equation (3.2b), \mathbf{c}_r is the matrix of damper coefficients $c_r = A/C$, where C is the speed of pressure waves in water. In the next section, these equations will be reformulated in terms of the total variables that enter into Equation (3.1).

3.2 Interaction as a scattering problem

Dam–water–foundation interaction may be interpreted as a scattering problem, in which the dam perturbs a "free-field" state of the system. Utilizing this idea, the procedure developed for 2D gravity dam systems in Part II is extended next for 3D dam–water–foundation rock systems.

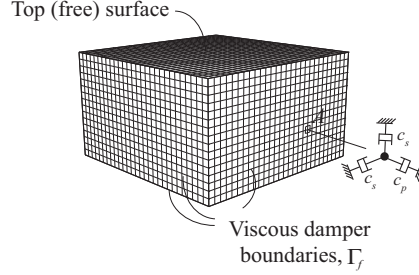


Figure 3.2: Viscous-damper boundary Γ_f for foundation rock.

Consider the auxiliary water–foundation rock system defined in Figure 3.3a, which consists of three subdomains: Ω^a denotes the foundation region with an irregular canyon interior to the future absorbing boundary Γ_f ; Ω_f^+ is the semi-unbounded, regular foundation region exterior to Γ_f ; and Ω_r^+ is the semi-unbounded, uniform fluid channel upstream of the future absorbing boundary Γ_r . The displacements and hydrodynamic pressures in this auxiliary water–foundation rock system are defined as \mathbf{r}^a and \mathbf{p}^a , respectively. This auxiliary system does not correspond to any physical state, but is introduced to facilitate formulation of the analysis procedure.

The dam–water–foundation rock system is also separated into three subdomains (Figure 3.3b): Ω denotes the dam and adjacent parts of the foundation and fluid domains interior to Γ_f and Γ_r ; and Ω_f^+ and Ω_r^+ are the semi-unbounded foundation and fluid domains exterior to Γ_f and Γ_r ; these are identical to the exterior regions of the auxiliary system. In order to formulate the governing equations for the absorbing boundaries in terms of free-field quantities, the displacements and hydrodynamic pressures are defined by the variables

$$\mathbf{r}^f \text{ and } \mathbf{p}^f, \text{ in the interior region } \Omega \quad (3.3a)$$

$$\mathbf{r}^f - \mathbf{r}^a \text{ and } \mathbf{p}^f - \mathbf{p}^a, \text{ in the exterior regions } \Omega_f^+ \text{ and } \Omega_r^+ \quad (3.3b)$$

The variables chosen in the exterior regions Ω_f^+ and Ω_r^+ represent the *scattered motion* and *scattered hydrodynamic pressures*, i.e., the perturbation of the motion and pressures in the auxiliary water–foundation rock system due to the presence of the dam and irregular fluid region. The viscous-damper boundaries Γ_f and Γ_r are intended to simulate these semi-unbounded regions. Because linear material behavior was assumed in these exterior domains, the boundary forces (tractions) corresponding to the scattered variables are $\mathbf{R}_f = \mathbf{R}_f^f - \mathbf{R}_f^a$ at Γ_f and $\mathbf{H}_r = \mathbf{H}_r^f - \mathbf{H}_r^a$ at Γ_r . Substituting these expressions into the radiation conditions for the viscous-damper boundaries (Equation 3.2), one obtains:

$$\mathbf{R}_f^t = \mathbf{R}_f^a - \mathbf{c}_f [\dot{\mathbf{r}}_f^t - \dot{\mathbf{r}}_f^a] \quad \mathbf{H}_r^t = \mathbf{H}_r^a - \mathbf{c}_r [\dot{\mathbf{p}}_r^t - \dot{\mathbf{p}}_r^a] \quad (3.4)$$

The total forces on the viscous-damper boundaries can be seen to consist of two parts: the forces \mathbf{R}_f^a and \mathbf{H}_r^a consistent with the boundary tractions in the auxiliary system at Γ_f and Γ_r , respectively, and the product of damper coefficients and the scattered motion and scattered hydrodynamic pressure.

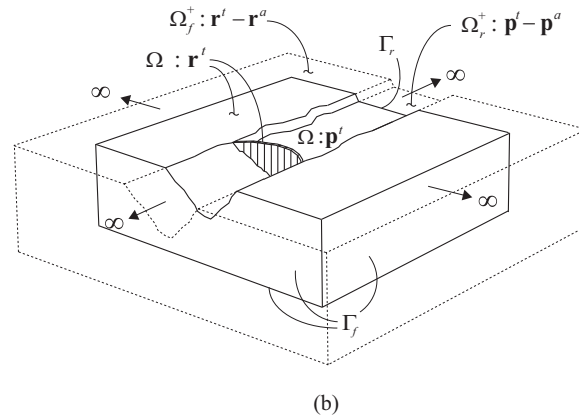
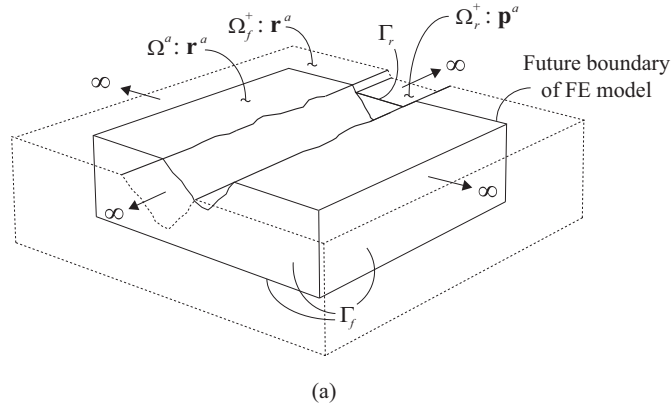


Figure 3.3: Illustration of dam–water–foundation rock interaction as a scattering problem: (a) semi-bounded auxiliary water–foundation rock system in its "free-field" state with variables defined by \mathbf{p}^a in Ω_r^+ and \mathbf{r}^a in $\Omega^a \cup \Omega_f^+$; (b) dam–water–foundation rock system with variables defined by \mathbf{p}^t and \mathbf{r}^t in Ω and the scattered variables $\mathbf{p}^t - \mathbf{p}^a$ in Ω_r^+ and $\mathbf{r}^t - \mathbf{r}^a$ in Ω_f^+ .

where the free-field motion \mathbf{r}_f^0 and forces \mathbf{R}_f^0 at the boundary Γ_f are computed from analysis of the foundation domain alone (Figure 3.5a), thus ignoring the effects of hydrodynamic pressures in Ω_r^+ on the foundation-rock motions; and the free-field hydrodynamic pressures \mathbf{p}_r^0 are computed from analysis of the fluid part alone (Figure 3.5b) with rigid foundation rock, thus ignoring the effects of foundation-rock flexibility on the hydrodynamic pressures in Ω_r^+ .

Although the secondary effects of water–foundation rock interaction in the exterior domain $\Omega_f^+ \cup \Omega_r^+$ distant from the dam are ignored, the dominant effects within the FE domain Ω that contains the dam are still rigorously represented by the coupling matrix \mathbf{Q}_b ,

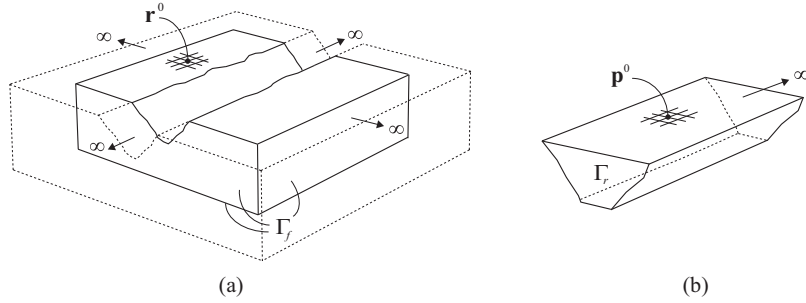


Figure 3.5: (a) Free-field foundation-rock system with displacements defined by \mathbf{r}^0 ,
 (b) "free-field" fluid channel upstream of Γ_r with pressures defined by \mathbf{p}^0 .

3.4 Final equations of motion

Substituting the above expressions for the viscous-damper boundaries (Equation 3.4) with the approximations in Equation (3.5) into Equation (3.1), the final equations of motion for the 3D dam–water–foundation rock system are obtained:

$$\begin{aligned} \begin{bmatrix} \mathbf{m} & \mathbf{0} \\ \rho(\mathbf{Q}_h^T + \mathbf{Q}_b^T) & \mathbf{s} \end{bmatrix} \begin{Bmatrix} \dot{\mathbf{r}}^t \\ \dot{\mathbf{p}}^t \end{Bmatrix} + \begin{bmatrix} \mathbf{c} + \mathbf{c}_f & \mathbf{0} \\ \mathbf{0} & \mathbf{b} + \mathbf{c}_r \end{bmatrix} \begin{Bmatrix} \mathbf{r}^t \\ \mathbf{p}^t \end{Bmatrix} \\ + \begin{Bmatrix} \mathbf{f}(\mathbf{r}^t) \\ \mathbf{0} \end{Bmatrix} + \begin{bmatrix} \mathbf{0} & -(\mathbf{Q}_h + \mathbf{Q}_b) \\ \mathbf{0} & \mathbf{h} \end{bmatrix} \begin{Bmatrix} \mathbf{r}^t \\ \mathbf{p}^t \end{Bmatrix} = \begin{Bmatrix} \mathbf{R}^{\text{st}} \\ \mathbf{0} \end{Bmatrix} + \begin{Bmatrix} \mathbf{P}_f^0 \\ \mathbf{P}_r^0 \end{Bmatrix} \end{aligned} \quad (3.6)$$

where the last term on the right hand side represents the effective earthquake forces:

$$\mathbf{P}_f^0 = \mathbf{R}_f^0 + \mathbf{c}_f \dot{\mathbf{r}}_f^0 \text{ at the foundation boundaries } \Gamma_f \quad (3.7a)$$

$$\mathbf{P}_r^0 = \mathbf{c}_r \dot{\mathbf{p}}_r^0 \text{ at the upstream fluid boundary } \Gamma_r \quad (3.7b)$$

PART II: EQUATIONS OF MOTION

Working with the scattered variables in Ω_f^+ and Ω_r^+ , and approximating water–foundation rock interaction, has enabled Equation (3.7) to be derived for the effective earthquake forces in terms of free-field variables only. These free-field variables represent the minimal set of seismic input data required for determining the response of the dam–water–foundation rock system to earthquake excitation.

4 Computing effective earthquake forces

4.1 Forces at bottom boundary

Similarly as for the 2D system in Part I, the equation for the effective earthquake forces at the bottom boundary (Equation 3.7a) is reformulated as:

$$\mathbf{P}_f^0 = 2\mathbf{c}_f \dot{\mathbf{r}}_f^0 \quad (4.1)$$

where \mathbf{r}_f^0 is the motion at the bottom boundary due to the incident (upward propagating) seismic waves. The incident motion \mathbf{r}_f^0 is obtained by 1D deconvolution of the surface motion $a_g(t)$ assuming vertically propagating seismic waves and homogeneous (or horizontally layered) rock. Deconvolution is an inverse procedure to determine the amplitude and frequency content of an input signal to be consistent with the observed output signal. It is most conveniently implemented in the frequency domain, either directly by computing the inverse of the transfer function for a 1D halfspace [57], or by utilizing available 1D wave propagation software such as SHAKE [55] or DEEPSOIL [59].

Although rather straightforward, deconvolution is often subject to considerable confusion because 1D wave propagation software typically operate with two possible motions at every depth [97]: an *outcrop motion* and a *within motion*. By definition, the within motion is the superposition of the incident and reflected waves, i.e., it is the total (or "actual") motion at any given depth in the halfspace. In contrast, the outcrop motion is the motion that would occur at a theoretical outcrop location at the same depth; this is equal to twice the amplitude of the incident motion. Thus, the incident motion \mathbf{r}_f^0 needed in Equation (4.1) is one-half the outcrop motion at the bottom boundary determined in the deconvolution analysis. The procedure to compute effective earthquake forces \mathbf{P}_f^0 from Equation (4.1) is summarized in Box 4.1.

Box 4.1: Computing \mathbf{P}_f^0 at bottom boundary of foundation rock.

1. Determine the outcrop motion at the bottom foundation-rock boundary by 1D deconvolution of each component of the surface control motion $a_g^k(t)$, $k = x, y, z$.
2. Compute the incident motion \mathbf{r}_f^0 as 1/2 the outcrop motion at the bottom boundary determined in Step 1 and obtain $\dot{\mathbf{r}}_f^0$ as the time derivative of \mathbf{r}_f^0 .
3. Calculate the effective earthquake forces \mathbf{P}_f^0 at the bottom boundary from Eq. (4.1) using $\dot{\mathbf{r}}_f^0$ from Step 2.

Some researchers have avoided deconvolution of the surface motion by idealizing the foundation rock as a homogeneous, undamped halfspace [7,98]. While this simplification may be appropriate for the simple case of a homogeneous, undamped halfspace, it can cause significant error in dam response for foundations with damping and for layered foundations, as will be demonstrated later in Section 6.3.

4.2 Forces at side boundaries

The computation and application of effective earthquake forces at the four side boundaries of the foundation domain (Equation 3.7a) can be done automatically within the FE code using a special class of so-called free-field boundary elements [35,99]. Such elements solve the radiation condition for 1D wave propagation and apply a form of effective earthquake forces at the boundaries at every time step as the analysis progresses in time.

However, because very few commercial FE programs have such elements available, an alternative procedure will be presented wherein the effective earthquake forces are computed in a separate auxiliary analysis of the free-field system before the actual dam–water–foundation rock system is analyzed. This approach has the advantage that it does not require modification of the FE source code, but has the disadvantage that it requires major data transfer.

4.2.1 Computing forces at side boundaries: uniform canyon

The free-field motion \mathbf{r}_f^0 and boundary forces \mathbf{R}_f^0 required to compute the effective earthquake forces \mathbf{P}_f^0 at the four side boundaries (Equation 3.7a) are determined from dynamic analysis of the foundation rock in its free-field state (Figure 3.4a). Before presenting the general procedure, a special case is considered where two additional geometric restrictions are imposed: (1) the canyon cross-section is assumed to be uniform in the stream direction, and (2) the surface of the foundation rock is horizontal. Under these assumptions, the free-field foundation-rock system is an infinitely long canyon of arbitrary, but uniform cross-section cut in a homogeneous or horizontally layered halfspace (Figure 4.1a). Analysis of this 3D system subjected to vertically propagating seismic waves reduces to a 2D analysis (Figure 4.1b) where incident SH-waves cause the stream (out-of-plane) component of ground motion, and incident SV- and P-waves cause the cross-stream and vertical components.

For this special system, the quantities \mathbf{r}_f^0 and \mathbf{R}_f^0 that enter into Equation (3.7a) can be determined by two simpler analyses: (1) analysis of a single column of foundation-rock elements subjected to forces of Equation (4.1) at the base (Figure 4.1c) suffices for the two boundaries oriented in the stream direction; and (2) analysis of the 2D system of Figure 4.1d subjected to forces of Equation (4.1) at the base and forces \mathbf{P}_f^0 on the sides determined from the first analysis (these latter forces are required because the domain has been truncated) provides the desired results for the boundaries oriented in the cross-canyon direction at the

upstream and downstream ends of the foundation domain. The procedure is summarized in Box 4.2.

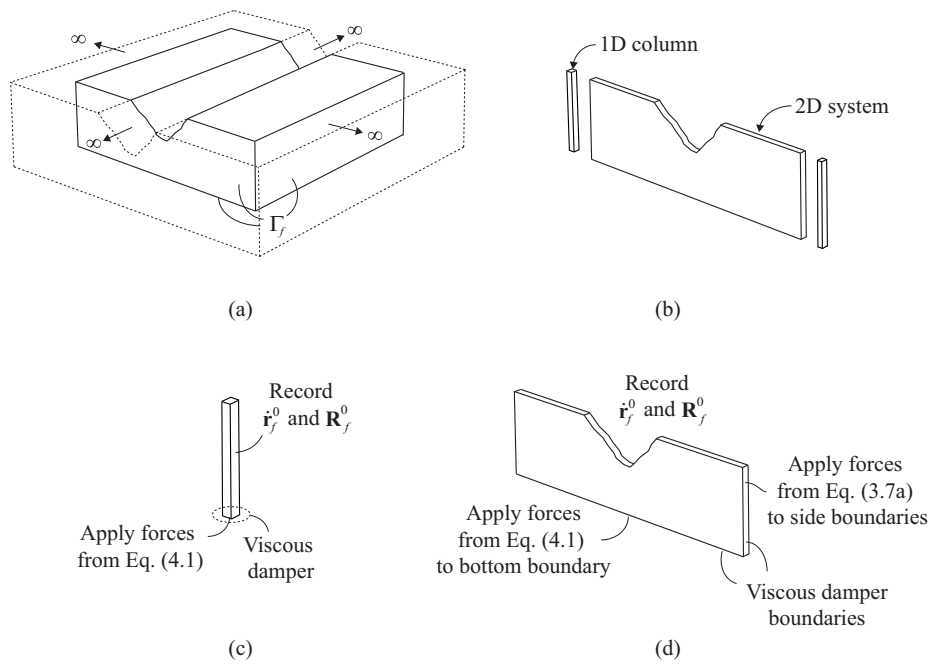


Figure 4.1: Computing \mathbf{P}_f^0 for uniform canyon: (a) 3D free-field system with uniform canyon cut in foundation-rock halfspace; (b) "two-dimensional" free-field system with corresponding 1D corner columns; (c) analysis of 1D foundation-rock column to compute $\dot{\mathbf{r}}_f^0$ and \mathbf{R}_f^0 at side boundaries, (c) analysis of 2D system to compute $\dot{\mathbf{r}}_f^0$ and \mathbf{R}_f^0 at upstream and downstream boundaries.

Box 4.2: Computing \mathbf{P}_f^0 at side boundaries of foundation domain: uniform canyon.

Analysis of 1D column

1. Develop a FE model for the 1D foundation-rock column that has the same mesh density as the boundary of the 2D system.
2. For each component of ground motion, $k = x, y, z$, add a viscous damper at the base in the k -direction and constrain DOFs in other directions to permit only shear ($k = x, y$) or axial ($k = z$) deformation of the 1D column.
3. Apply effective earthquake forces (Eq. 4.1) to the base in k -direction and compute $\dot{\mathbf{r}}_f^0$ and \mathbf{R}_f^0 at every node along the height.

Analysis of 2D system

4. Develop a FE model for the 2D foundation-rock system, with the same mesh density as the main FE model at the upstream/downstream boundary.
5. For each component of ground motion, $k = x, y, z$, add viscous dampers at the bottom and side boundaries and constrain the DOFs at the faces to model the "infinite length" in the direction normal to the model boundary (e.g., if the x -axis is parallel to the upstream direction, two nodes with the same y -, and z -coordinates should be constrained to move identically).
6. Apply effective earthquake forces from Eq. (4.1) to the bottom boundary and from Eq. (3.7a) to the side boundaries using $\dot{\mathbf{r}}_f^0$ and \mathbf{R}_f^0 from the 1D analysis, and compute $\dot{\mathbf{r}}_f^0$ and \mathbf{R}_f^0 at every node in the 2D system.

Computing effective earthquake forces for main model

7. Compute the effective earthquake forces \mathbf{P}_f^0 at every node along the side boundaries of the foundation domain from Eq. (3.7a) using $\dot{\mathbf{r}}_f^0$ and \mathbf{R}_f^0 from Step 3 at the along-canyon boundaries and from Step 6 at the cross-canyon boundaries at the upstream and downstream ends of the domain.

4.2.2 Computing forces at side boundaries: arbitrary canyon geometry

Next, the geometric restrictions of a uniform canyon and horizontal foundation surface that were introduced in the preceding section are removed, implying that the free-field system becomes much more complicated. Although a system with arbitrary canyon geometry (Figure 4.2a) is not amenable to 2D analyses, the same type of analysis methodology can be extended to the system provided that it satisfies the general constraints described in Section 2.1.

For such a system, the quantities $\dot{\mathbf{r}}_f^0$ and \mathbf{R}_f^0 that enter in Equation (3.7a) can be determined by two sets of four simpler analyses: (1) analysis of four 1D corner columns of

foundation-rock elements subjected to forces of Equation (4.1) at the base; and (2) analyses of the four 2D systems in Figure 4.2b subjected to forces of Equation (4.1) at the base and forces \mathbf{P}_f^0 on the sides determined from the first set of 1D analyses. The latter set of analyses provide $\dot{\mathbf{r}}_f^0$ and \mathbf{R}_f^0 for nodes on all four side boundaries. The procedure is illustrated in Figure 4.2 and summarized in Box 4.3.

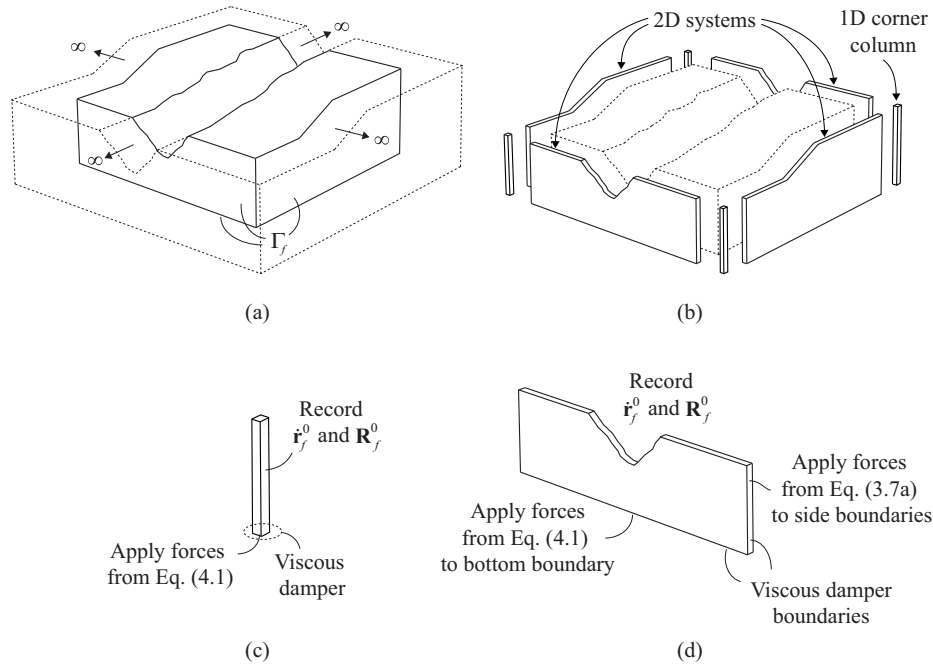


Figure 4.2: Computing \mathbf{P}_f^0 for arbitrary canyon geometry: (a) 3D free-field system with canyon of arbitrary geometry cut in foundation-rock halfspace; (b) free-field system with corresponding 1D corner columns and 2D systems; (c) analysis of 1D corner columns to compute $\dot{\mathbf{r}}_f^0$ and \mathbf{R}_f^0 at corners, (d) analysis of 2D systems to compute $\dot{\mathbf{r}}_f^0$ and \mathbf{R}_f^0 at the four side boundaries.

This procedure for computing \mathbf{P}_f^0 at the boundaries of a system with arbitrary geometry is based on the assumption that the motion in each of the four 2D systems (Figure 4.2b) can be determined independently of the other 2D systems. This assumption seems reasonable as long as the foundation domain is large enough, which is normally the case in the direct FE method because viscous-damper boundaries generally require large domains to ensure acceptable modeling of the semi-unbounded domains.

Implementation of the procedure in Box 4.3 means that eight auxiliary analyses are required for each of the three components of ground motion. The computational effort required for each of these linear dynamic analyses is minimal, and the procedure can be automated in a pre-processing script that is set up and executed before the nonlinear dynamic

analysis of the dam–water–foundation rock system takes place. For example, in this work MATLAB [71] is used to compute and store effective earthquake forces that are used with the FE code OPENSEES [65] to analyze the complete system; a similar method has been implemented by Saouma [37] in the FE code MERLIN [100].

The disadvantage of this approach is that substantial amounts of data management and transfers are required for analyzing 3D models, which may easily have tens of thousands of boundary nodes. In Section 6.1, it will be demonstrated that that – under certain conditions – it is possible to drastically reduce these requirements by replace the actual 3D free-field system by a much simpler system.

Box 4.3: Computing \mathbf{P}_f^0 at side boundaries of foundation domain: arbitrary canyon geometry.

Analysis of four 1D corner columns

1. Develop FE models for each of the four 1D corner columns of the foundation rock that have the same mesh density as the corners of the main FE model.
2. For each component of ground motion, $k = x, y, z$, add a viscous damper at the base in the k -direction and constrain DOFs in other directions to permit only shear ($k = x, y$) or axial ($k = z$) deformation of the 1D column.
3. Apply effective earthquake forces (Eq. 4.1) to the base in k -direction and compute $\dot{\mathbf{r}}_f^0$ and \mathbf{R}_f^0 at every node along the height.

Analysis of four 2D systems

4. Develop FE models for each of the four 2D systems of the foundation rock, with the same mesh density as the main FE model at the boundaries.
5. For each component of ground motion, $k = x, y, z$, add viscous dampers at the bottom and side boundaries and constrain DOFs at the faces to model the "infinite length" conditions in the direction normal to the boundary.
6. Apply effective earthquake forces from Eq. (4.1) to the bottom boundary and from Eq. (3.7a) to the side boundaries using $\dot{\mathbf{r}}_f^0$ and \mathbf{R}_f^0 from the 1D analyses, and compute $\dot{\mathbf{r}}_f^0$ and \mathbf{R}_f^0 at every node in the 2D system.

Computing effective earthquake forces for main model

7. Compute effective earthquake forces \mathbf{P}_f^0 at every node at the four sides of the foundation domain from Eq. (3.7a) using $\dot{\mathbf{r}}_f^0$ and \mathbf{R}_f^0 from Step 6.

4.3 Forces at upstream fluid boundary

The free-field pressures \mathbf{p}_r^0 required to compute \mathbf{P}_r^0 at Γ_r are to be determined by dynamic analysis of the fluid in its free-field state (Figure 4.3a): a fluid channel of uniform cross-

section unbounded in the upstream direction. Because this system is uniform in the upstream direction, the analysis reduces to two dimensions. For cross-stream and vertical components of ground motion, the free-field pressures \mathbf{p}_r^0 on the boundary Γ_r can be computed from an analysis of the 2D fluid domain cross-section with rigid foundation rock (Figure 4.3b). The stream component of ground motion will not generate any hydrodynamic pressures, thus implying $\mathbf{P}_r^0 = \mathbf{0}$. The procedure is summarized in Box 4.4.

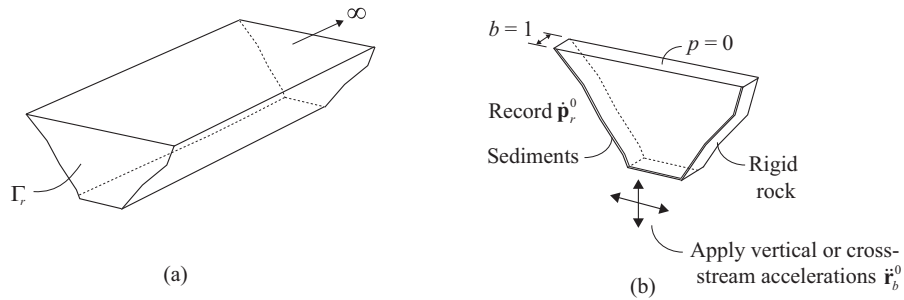


Figure 4.3: Computing \mathbf{P}_r^0 at upstream fluid boundary: (a) 3D "free-field" fluid channel upstream of Γ_r ; (b) analysis of 2D cross section subjected to vertical and cross-stream excitation to compute $\dot{\mathbf{p}}_r^0$.

Box 4.4: Computing \mathbf{P}_r^0 at upstream fluid boundary.

Analysis of 2D fluid section

1. Develop a FE model of the 2D fluid cross-section with the same mesh density as the main model at the upstream fluid boundary Γ_r , add surface elements at the reservoir bottom and sides to model sediments.
2. For cross-stream and vertical components of ground motion, $k = y, z$, calculate $\dot{\mathbf{p}}_r^0$ at every node by analyzing the 2D model subjected to accelerations $\ddot{\mathbf{r}}_b^0$ at the base, where $\ddot{\mathbf{r}}_b^0$ is the foundation-rock accelerations at the interface $\Gamma_b \cap \Gamma_r$ (Figure 3.1b); these can be extracted from the relevant 2D analysis described in Section 4.2.

Computing effective earthquake forces

3. Compute the effective earthquake forces \mathbf{P}_r^0 for every node at the fluid boundary from Eq. (3.7b) using $\dot{\mathbf{p}}_r^0$ from Step 2.

PART II: COMPUTING EFFECTIVE EARTHQUAKE FORCES

The forces \mathbf{P}_r^0 are associated with earthquake-induced pressures due to vertical and cross-stream excitation of the part of the fluid domain that has been eliminated upstream of Γ_r . These forces are required because of the system idealization (Figure 2.1), where the excitation is implicitly assumed to extend along the entire length of the unbounded fluid channel. Later in Section 6.4, it will be demonstrate that these forces are inconsequential to the dam response and may therefore be dropped from the analysis.

5 Numerical validation of the direct FE method

In this chapter several examples are documented to validate the accuracy of the direct FE method that was developed in Chapters 3 and 4 and implemented with the FE program OPENSEES [65]. First, the ability of the method to reproduce free-field motions at the surface of a flat foundation box is documented. The free-field response of a uniform, semicylindrical canyon cut in a foundation halfspace is determined next and compared with classical solutions. Lastly, the dynamic response of Morrow Point Dam is computed for a wide range of conditions and compared with results obtained from the substructure method.

5.1 Reproducing free-field motion in foundation rock

5.1.1 Free-field motion at flat box surface (the flat box test)

The flat box model shown in Figure 5.1 has a domain size and mesh density that is representative of an actual dam–water–foundation rock system with viscous dampers employed at the bottom and side boundaries. The free-field control motion $a_g^k(t)$ is defined at the surface in the two horizontal and vertical directions by the S69E, S21W and vertical components of the Taft ground motion, respectively. Each component of ground motion is deconvolved, effective earthquake forces \mathbf{P}_f^0 are computed from the procedures summarized in Box 4.1 and Box 4.3 and applied to the bottom and side boundaries of the foundation box, respectively, and the response of the system is computed.

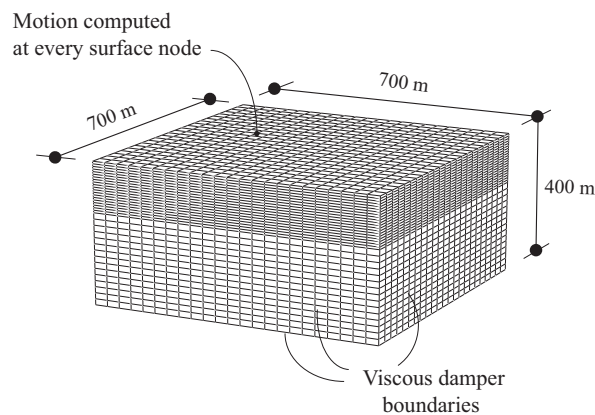


Figure 5.1: FE model of flat foundation box.

The results presented in Figure 5.2 show a near perfect match between the specified free-field control motion and the computed surface motions at every node on the surface of

the flat box, thus demonstrating that the direct FE method is able to exactly reproduce free-field conditions for this simple system to within FE discretization error. This is achieved without iterative procedures to adjust the amplitude and/or frequency content of the input motion, which is sometimes used to overcome deficiencies in FE models [45,101].

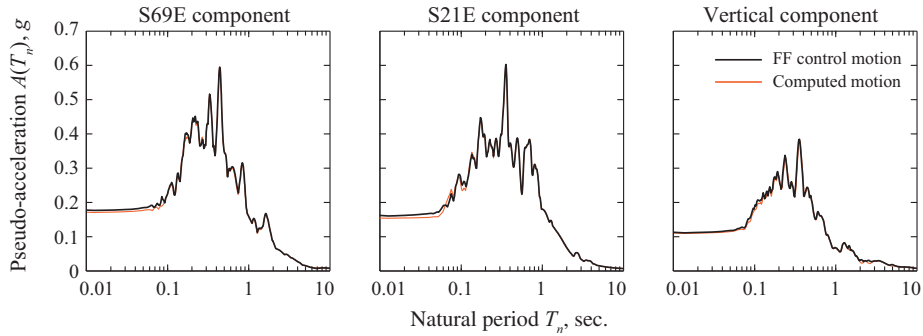


Figure 5.2: Comparison of 5% damped pseudo-acceleration response spectra for control motion and computed motion at nodes on flax box surface.

5.1.2 Free-field motion at canyon surface

Next, the ability of the direct FE method to accurately compute the free-field earthquake motion at the surface of a semicylindrical canyon is evaluated; this is the motion that in turn will excite a dam supported in the canyon. Available analytical and numerical solutions for this classical problem [102,103] serve as the benchmark for the evaluation.

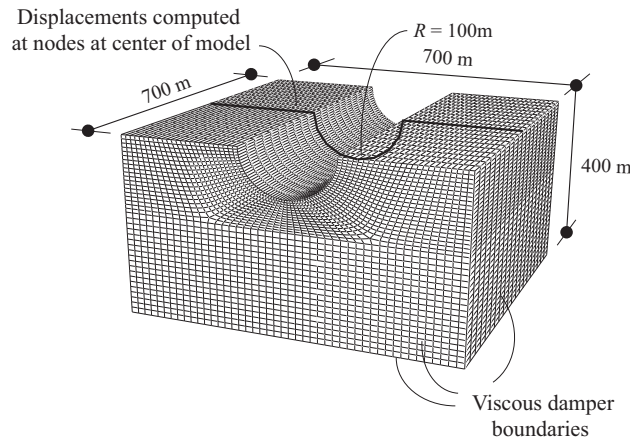


Figure 5.3: FE model of semi-cylindrical canyon cut in halfspace.

The semi-cylindrical canyon with radius R discretized as a FE system with viscous-damper boundaries (Figure 5.3) is subjected to effective earthquake forces \mathbf{P}_f^0 computed from

the procedures summarized in Boxes 4.1 and 4.3 with the vertically incident seismic motion \mathbf{r}_f^0 specified as a plane wave of unit amplitude and frequency f . The forces \mathbf{P}_f^0 are applied to the bottom and side boundaries of the FE model, and the displacement response along the canyon and top surface of the foundation is computed. Results are presented for Poisson's ratio $\nu_s = 1/3$ and different values of $\eta = 2fR/V_s$, where V_s is the shear wave velocity of the foundation medium. The dimensionless frequency η may be interpreted as the ratio of the canyon width to the wavelength of the incident waves. When plotted in this form, results are independent of the actual material properties as long as the ratio R/V_s is maintained.

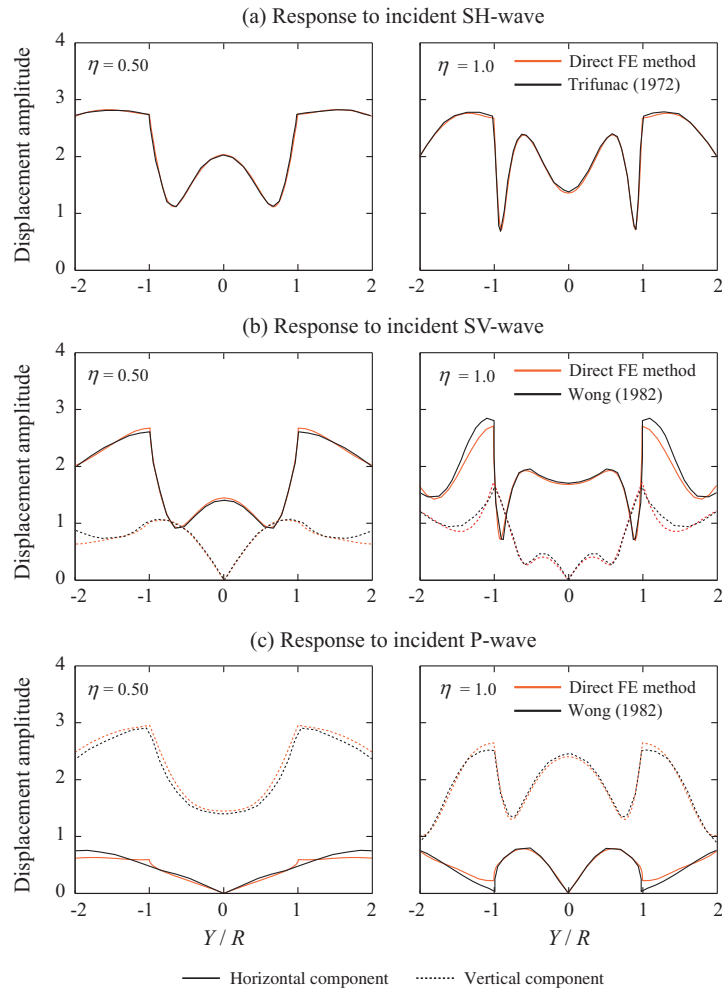


Figure 5.4: Displacement amplitudes at canyon surface computed by the direct FE method and compared with results by Trifunac [102] and Wong [103]. Responses to incident SH-, SV-, and P-waves are plotted against dimensionless distance Y/R , where Y is the transverse distance from the center and R the radius.

The displacement amplitude, defined as the ratio of the Fourier transform of the computed displacements to the unit amplitude input motion, are presented in Figure 5.4 for incident SH-, SV- and P-waves; these correspond to excitation in the canyon, cross-canyon and vertical directions, respectively. The results obtained by the direct FE method closely match the analytical results by Trifunac [102] for incident SH-waves, and the numerical results by Wong [103] using boundary integral methods for incident SV-waves and P-waves. The small discrepancies are due to the inability of viscous-damper boundaries to perfectly absorb all scattered and diffracted waves from the canyon. This is most prominent in the response to incident SV-waves and P-waves because these excitations generate surface waves that are not effectively absorbed by the viscous dampers; but even for these excitations, the discrepancies are small. The excellent agreement demonstrates the ability of the direct FE method to accurately predict free-field motions at the surface of a canyon.

5.2 Dynamic response of Morrow Point Dam

5.2.1 System analyzed

The ability of the direct FE method to accurately compute the dynamic response of concrete dams is validated numerically by analyzing Morrow Point Dam, a 142 m high, approximately symmetric, single centered arch dam located on the Gunnison River in Colorado. The linear material properties and damping values selected for the dam concrete and foundation rock are based on the results from forced vibration tests of the dam and subsequent numerical studies performed to match the experimental results [104,105]. The concrete and foundation rock is assumed to be homogeneous, isotropic and linearly elastic. The concrete has a modulus of elasticity $E_s = 34.5$ GPa, density $\rho_s = 2403$ kg/m³, and Poisson's ratio $\nu_s = 0.20$. The foundation rock has a modulus of elasticity $E_f = 24.1$ GPa (i.e. $E_f / E_s = 0.70$), density $\rho_f = 2723$ kg/m³ and Poisson's ratio $\nu_f = 0.20$. The impounded water has the same depth as the height of the dam, density $\rho = 1000$ kg/m³, and pressure-wave velocity $C = 1440$ m/s. The reservoir-bottom reflection coefficient is selected as $\alpha = 0.80$.

Material damping in the dam and foundation rock is modeled in the direct FE method by Rayleigh damping with $\zeta_s = 1\%$ and $\zeta_f = 2\%$ viscous damping specified for the dam concrete and foundation rock, respectively, at two frequencies: $f_1 = 5$ Hz, the fundamental resonance frequency of the dam alone on rigid rock, and at three times this frequency. The damping matrix for the complete system is then constructed using standard procedures for assembling damping matrices for two subdomains [67]. Determined by the half-power bandwidth method applied to the resonance curve, the overall damping in the dam–water–foundation rock system is 3-5% for the first few modes of vibration, which is consistent with the range of measured damping values at the dam [104].

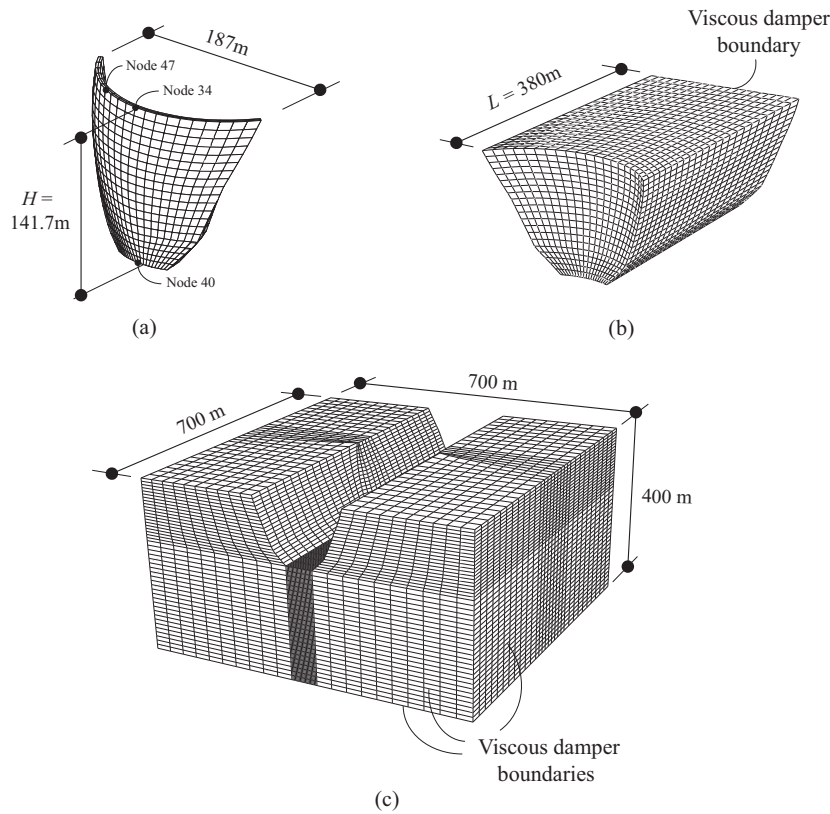


Figure 5.5: FE model of Morrow Point Dam: (a) dam; (b) fluid domain; (c) foundation domain.

The FE mesh shown in Figure 5.5 is assembled using standard 8-node brick elements, with 800 solid elements for the dam, 42,000 solid elements for the foundation rock, and 9,200 acoustic fluid elements for the water in the reservoir. Interface elements couple accelerations with hydrodynamic pressures at the fluid–solid interfaces, surface elements at the bottom and sides of the reservoir model the 1D wave absorption due to sediments, and viscous dampers (dashpots) at the foundation domain boundaries and at the upstream end of the fluid domain model the semi-unbounded domains. The combined FE model consists of approx. 63,000 elements and 150,000 DOFs, and the overall dimensions are $700\text{m} \times 700\text{m} \times 400\text{m}$, corresponding to approx. $5H \times 5H \times 3H$, where H is the height of the dam. These dimensions are sufficiently large to minimize reflections from the viscous-damper boundaries, and were selected based on an initial study of the influence of domain size on the arch dam response (not included here). Interestingly, the response of the 3D arch dam system was found to be less sensitive to the size of the foundation domain than was the case for 2D gravity dam systems, which may be explained by the observation that dam–foundation interaction generally has less influence on arch dam response than on gravity dam response [106].

5.2.2 EACD3D-08 model for substructure method

The dynamic response of this FE model – computed by the direct FE method – will be compared against independent results obtained using the substructure method [107]. Analyzed using the computer program EACD3D-08 [108], wherein the foundation rock is treated as a semi-unbounded halfspace, the fluid domain as unbounded in the upstream direction, and the earthquake excitation is specified directly at the dam–canyon interface, this method avoids artificial model truncations and absorbing boundaries.

In order to effectively work with this computer program – which does not have a user interface or any pre- or post-processing capabilities – a set of MATLAB modules were developed to perform pre-processing of the input and post-processing the analysis output. These modules significantly increase the accessibility of EACD3D-08 by providing the user with a rational way to set up the analysis model, run the analysis, and gain easy access to the output data in the user-friendly MATLAB interface. The resulting EACD3D-08 model, shown in Figure. 5.6, includes 800 solid elements for the dam, the FE mesh for the irregular part of the fluid domain, and the boundary element mesh at the dam–foundation rock interface.

Material damping in the substructure method is modeled by rate-independent, constant hysteretic damping [67] defined by the damping factors $\eta_s = 0.02$ and $\eta_f = 0.04$ specified for the dam and foundation rock separately; these correspond to viscous damping ratios of $\zeta_s = 1\%$ and $\zeta_f = 2\%$ at all frequencies. A numerical investigation confirmed that the damping in the direct FE method, as defined earlier, is adequately consistent with this rate-independent damping over the frequency range of interest. Because EACD3D-08 does not consider water–foundation rock interaction, this is also excluded in the direct FE method for these validation analyses to allow for a meaningful comparison.

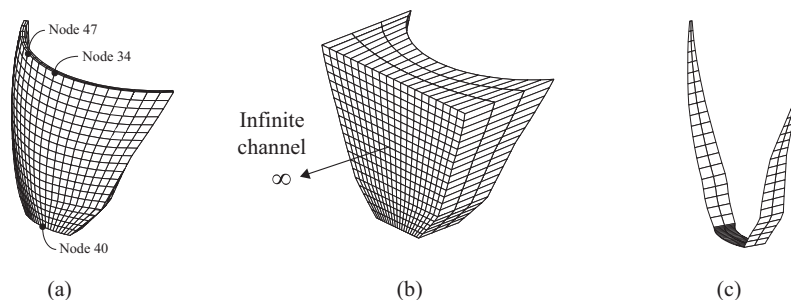


Figure 5.6: EACD3D-08 model for Morrow Point Dam: (a) FE model for dam, (b) FE model for semi-unbounded fluid domain, (c) boundary element mesh for foundation rock at dam–canyon interface.

5.2.3 Frequency response functions for dam response

Results for the dam response are presented in the form of dimensionless frequency response functions that represent the amplitude of radial acceleration at the crest of the dam due to unit harmonic, free-field motion; the actual location at the dam crest is selected at node 34 – the

center node – for upstream and vertical ground motions, and at node 47 for cross-stream motion. These frequency response functions are determined in the direct FE method from time-domain analysis of the FE model (Figure 5.5) subjected to effective earthquake forces \mathbf{P}_f^0 and \mathbf{P}_r^0 computed from the procedures summarized in Boxes 4.1 and 4.3 at the bottom and side boundaries of the foundation rock and Box 4.4 at the upstream fluid boundary, respectively. The free-field control motion, $a_g^k(t)$, is specified at the control point at the foundation surface as a long sequence of unit harmonics with gradually increasing frequency. Details of this procedure are provided in Appendix C.

Implemented in the frequency domain, the substructure method directly provides frequency response functions. The earthquake excitation is here defined by the free-field motion at the dam–canyon interface. To determine this motion consistent with the specified control motion $a_g^k(t)$, a direct FE analysis is implemented of the foundation domain without the dam or impounded water (Figure 5.7) subjected to the same boundary forces \mathbf{P}_f^0 as described in the preceding paragraph. The motion recorded at the dam–canyon interface is then used as the spatially varying input excitation to the EACD3D-08 analysis.

Frequency response functions obtained by the direct FE and substructure methods for the dam on flexible foundation rock are compared for two cases: empty reservoir and full reservoir in Figures 5.8 and 5.9, respectively. Results for a full reservoir (Figure 5.9) are presented here only for the upstream component of ground motion, because limitations in the EACD3D-08 computer program do not allow for a meaningful comparison with the direct FE method for cross-stream and vertical ground motions[†].

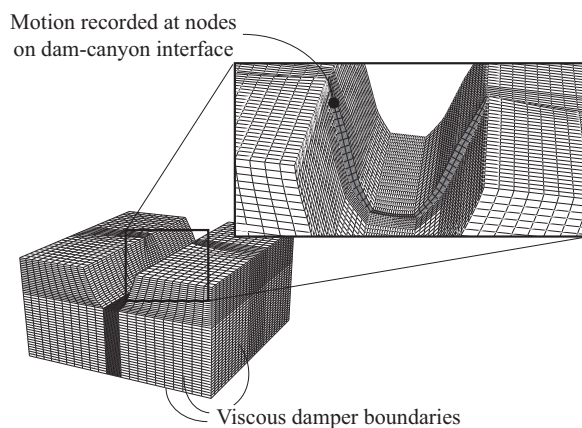


Figure 5.7: FE model of foundation domain to compute free-field motion at dam–canyon interface used as input to EACD3D-08 analysis.

[†] EACD3D-08 requires the user to specify the earthquake excitation to the fluid domain directly at the reservoir boundaries, but restricts this motion to be uniform in the upstream direction [108]. These assumptions cannot be reproduced exactly in the direct FE method. For stream ground motion however, the issue is avoided when the reservoir boundaries are uniform in the upstream direction (Figure 5.5b), thus implying that no hydrodynamic pressures are generated at these boundaries by the stream component of ground motion.

The response results obtained by the direct FE method are very close to those from the substructure method. The small discrepancies near some of the resonant peaks (Figure 5.8), and at frequencies higher than approx. 15 Hz (Figure 5.9), are primarily caused by reflections from the viscous-damper boundaries, which are incapable of perfectly absorbing all scattered waves. Such errors will generally decrease with larger domain sizes.

The good agreement demonstrates the ability of the direct FE method to model the factors important for earthquake analysis of arch dams: dam–water–foundation rock interaction including water compressibility and wave absorption at the reservoir boundaries, radiation damping in the semi-unbounded foundation and fluid domains, and the earthquake excitation defined by the control motion at the surface of the foundation rock.

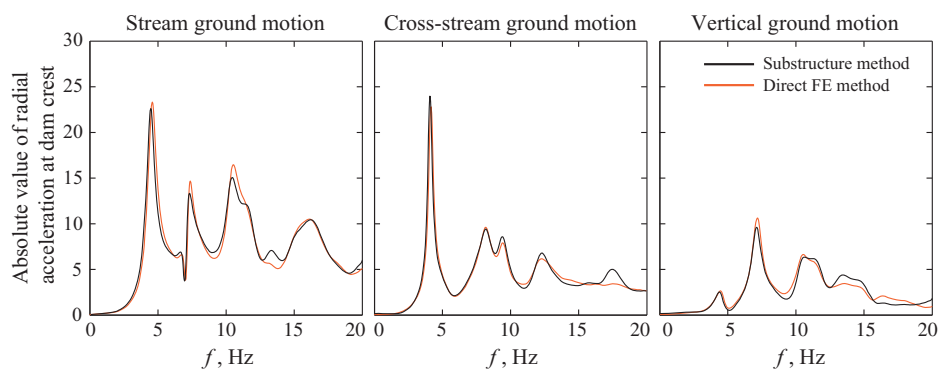


Figure 5.8: Frequency response functions for the amplitude of radial acceleration at the crest of Morrow Point dam including dam–foundation rock interaction (empty reservoir) due to stream, cross-stream and vertical ground motions. Results are computed by direct FE method and substructure method.

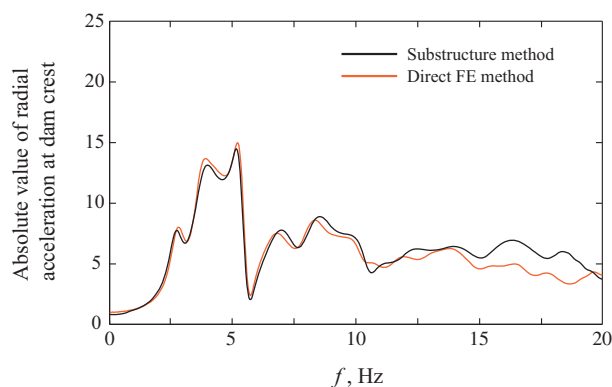


Figure 5.9: Frequency response functions for the amplitude of radial acceleration at the crest of Morrow Point dam including dam–water–foundation rock interaction (full reservoir) due to stream ground motion. Results are computed by direct FE method and substructure method.

5.2.4 Response to transient motion

To demonstrate the ability of the direct FE method to accurately compute the response of the arch dam–water–foundation rock system to earthquake excitation, the system is analyzed with the free-field control motion in the stream direction, $a_g^x(t)$, defined by the S69E component of the Taft ground motion. The radial displacements and accelerations at the crest of the dam relative to the base of the dam (node 40) are presented in Figure 5.10, and envelope values of maximum tensile arch and cantilever stresses on the upstream face of the dam in Figure 5.11. The results from the direct FE method closely match those from the substructure method: the displacements and accelerations at the crest show a near perfect match, and the envelope stress values are also close. The small discrepancies in the stress contour plots were found to be caused by differences in the FE stress recovery algorithms in the two computer programs.

The effectiveness of the direct FE method is apparent from the fact that these excellent results (Figures 5.8–5.11) are achieved even with relatively moderate domain sizes: the overall dimensions of the FE model are approx. $5H \times 5H \times 3H$, where H is the height of the dam. It is noted that larger domains were required to ensure similar levels of accuracy for 2D analysis of gravity dams (Appendix A).

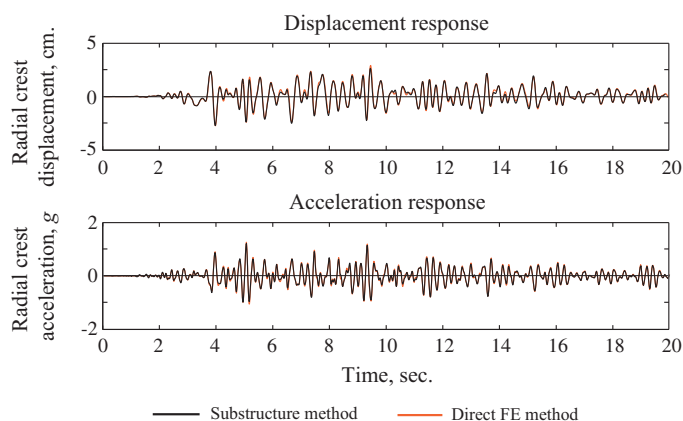


Figure 5.10: Relative radial displacement and acceleration histories at crest of Morrow Point Dam including dam–water–foundation rock interaction due to S69E component of Taft ground motion applied in the stream direction; static displacements are excluded. Results are computed by direct FE and substructure methods.

The direct FE analyses were implemented in OPENSEES on a local workstation (without parallel processing capabilities) using a set of MATLAB script to perform the data management for computing and applying effective earthquake forces. The CPU time required to determine the dynamic response of the FE model in Figure 5.5 with roughly 150 000 DOFs was 68 minutes; approximately 13 minutes were required for the auxiliary analyses to set up the effective earthquake forces and 55 minutes for the (linear) dynamic analysis of the dam–water–foundation rock system. The computational effort required to determine the effective

earthquake forces for the system is small compared to the time required for dynamic analysis of the overall system. Clearly, it is negligible compared to the time required to perform a more sophisticated nonlinear dynamic analysis of such systems.

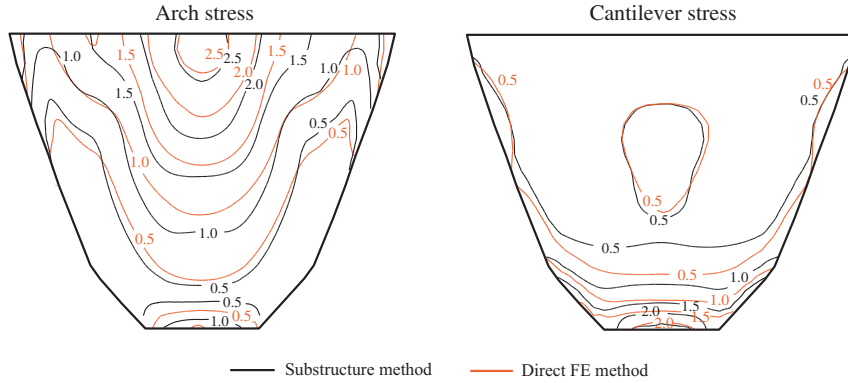


Figure 5.11: Envelope values of maximum tensile stresses, in MPa, on upstream face of Morrow Point Dam including dam–water–foundation rock interaction due to S69E component of Taft ground motion applied in the stream direction; static stresses are excluded. Results are computed by direct FE and substructure methods.

5.3 Frequency response functions for spatially uniform motion

Now that the direct FE method has been validated for the "actual" Morrow Point dam model, it is tested over a wide range of parameters that characterize the properties of the dam, foundation rock and reservoir bottom materials: E_s , E_f / E_s and α . For each of the analysis cases in Table 5.1, frequency response functions for the radial acceleration at the crest of the dam (relative to the base of the dam) are computed under the assumption that the free-field

Table 5.1: Cases of dam–water–foundation rock system analyzed.

Case	Dam concrete		Foundation rock			Impounded water	
	E_s (GPa)	ζ_s	Condition	E_f / E_s	ζ_f	Condition	α
1	any [†]	3%	rigid	∞	-	empty	-
2	34.5	1%	flexible	1/2	2%	empty	-
3	34.5	1%	flexible	1	2%	empty	-
4	34.5	1%	flexible	2	2%	empty	-
5	any [*]	3%	rigid	∞	-	full	0.50
6	any [*]	3%	rigid	∞	-	full	0.80
7	34.5	1%	flexible	1	2%	full	0.50
8	34.5	1%	flexible	1	2%	full	0.80

[†] When plotted against the normalized frequency ω / ω_1 , these results are valid for all values of E_s

earthquake motion is spatially uniform at the dam–foundation and water–foundation interfaces. This assumption is introduced for two reasons: (1) it facilitates a focused evaluation of the ability of the viscous-damper boundaries to model the semi-unbounded domains, and (2) it circumvents the aforementioned limitation in EACD3D-08 when specifying spatially varying motion in the substructure method (see footnote in Section 5.2.3).

The spatially uniform ground motion at the dam–foundation and water–foundation interfaces is directly input in the substructure method. In the direct FE method, an alternative procedure for seismic input is implemented to achieve such uniform ground motion wherein a different set of effective earthquake forces are computed directly from the uniform ground motion and applied to the dam nodes and to the dam–water and water–foundation interfaces (see Appendix D for details).

5.3.1 Dam on rigid foundation rock

Computed by the two methods, frequency response functions for the dam supported on rigid foundation with empty reservoir (Case 1 in Table 5.1) are presented in Figure 5.12. Results are plotted against the dimensionless frequency ω/ω_1 , where ω_1 is the fundamental frequency of the dam alone on rigid foundation. The close agreement between the two set of results demonstrates that the computational models employed in the direct FE (OPENSEES) and substructure (EACD3D-08) methods are equivalent, and validates the time-domain procedure for computing frequency response functions in the direct FE method.

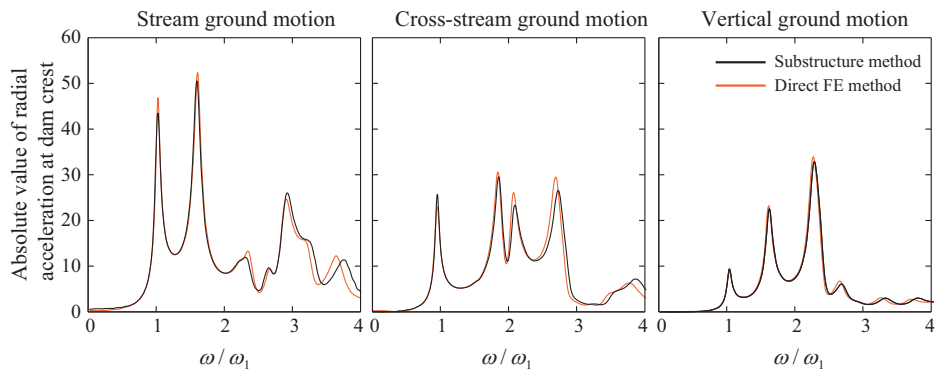


Figure 5.12: Frequency response functions for the amplitude of relative radial acceleration at the crest of Morrow Point Dam supported on rigid foundation with empty reservoir due to uniform stream, cross-stream and vertical ground motions (Case 1 in Table 5.1). Results are computed by direct FE and substructure methods.

5.3.2 Dam–foundation rock system

The frequency response functions for the dam on flexible foundation rock with empty reservoir obtained by the direct FE and substructure methods are compared in Figure 5.13 for

several values of E_f / E_s (Cases 2 to 4 in Table 5.1). The close agreement between the two set of results demonstrates the ability of the direct FE method to model the semi-unbounded foundation domain including radiation damping.

The discrepancies observable near some of the resonance peaks are caused by reflections from the viscous-damper boundaries, which are unable to perfectly absorb all scattered waves. Because the accuracy of these boundaries generally improves for higher values of the ratio r / λ , where r is the distance from the dam to the boundary and λ the wavelength of the scattered waves [20], such errors are more prominent for stiff foundations (longer wavelengths) than for soft foundations.

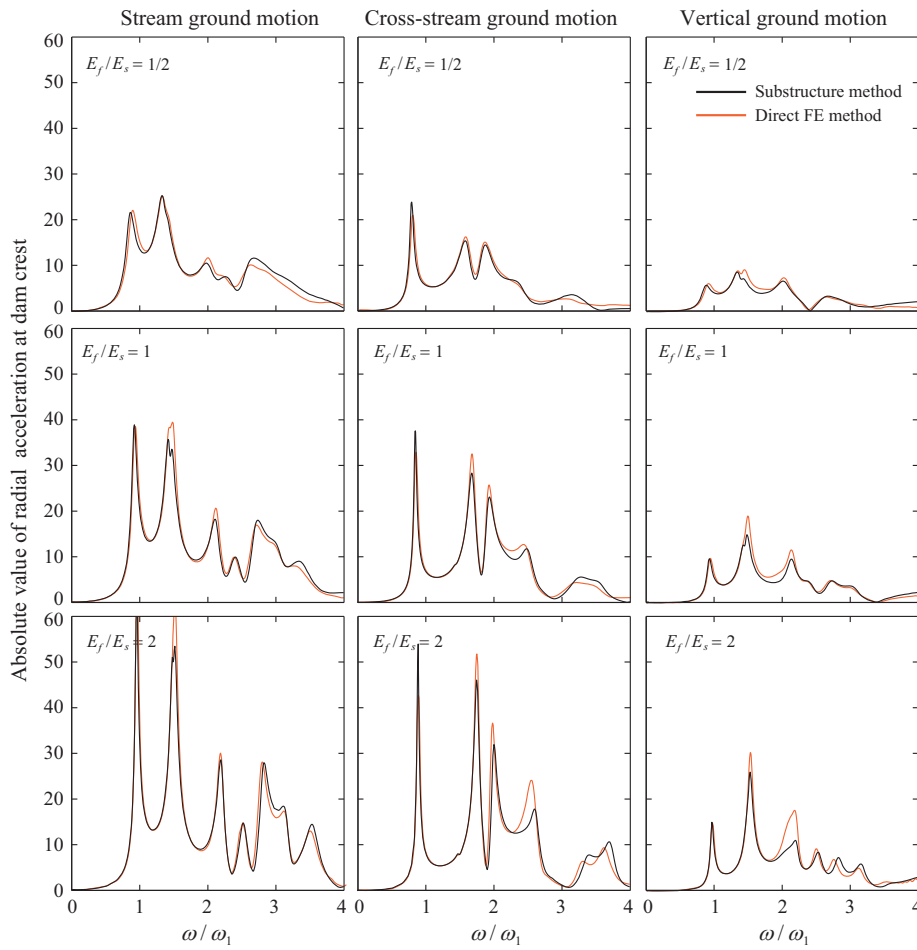


Figure 5.13: Frequency response functions for the amplitude of relative radial acceleration at the crest of Morrow Point Dam supported on flexible foundation rock with empty reservoir due to uniform stream, cross-stream and vertical ground motions. Results computed by direct FE and substructure methods are presented for three values of the moduli ratio E_f / E_s (Cases 2 to 4 in Table 5.1).

5.3.3 Dam–water system

The frequency response functions for the dam on rigid foundation with full reservoir obtained by the two methods are presented in Figure 5.14 for two values of the wave-reflection coefficient α (Cases 5 and 6 in Table 5.1). In the direct FE method, effective earthquake forces \mathbf{P}_r^0 are computed by the procedure summarized in Box 4.4 and applied to the fluid boundary Γ_r .

The results from the direct FE method closely match those from the substructure method for both values of α , thus validating the ability of the direct FE method to model the semi-unbounded fluid domain and water compressibility, reservoir bottom absorption, and radiation damping in the fluid.

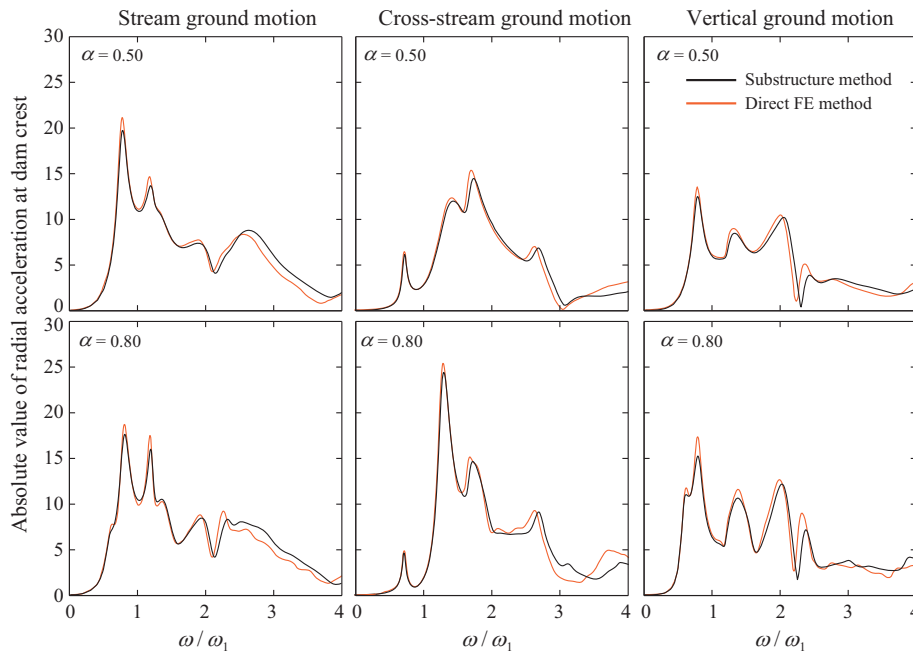


Figure 5.14: Frequency response functions for the amplitude of relative radial acceleration at the crest of Morrow Point Dam supported on rigid foundation with full reservoir due to uniform stream, cross-stream and vertical ground motions. Results computed by direct FE and substructure methods are presented for two values of the wave-reflection coefficient α (Cases 5 and 6 in Table 5.1).

5.3.4 Dam–water–foundation rock system

The frequency response functions for the dam on flexible foundation rock with full reservoir obtained by the two methods are compared in Figure 5.15 for two values of the wave-reflection coefficient α (Cases 7 and 8 in Table 5.1). The close agreement demonstrates that

the direct FE method with viscous-damper boundaries is able to accurately model the dam–water–foundation rock system with semi-unbounded subdomains and all its interaction effects. The small discrepancies are – as mentioned previously – due to the approximate nature of the viscous dampers, and will generally decrease with larger domain sizes.

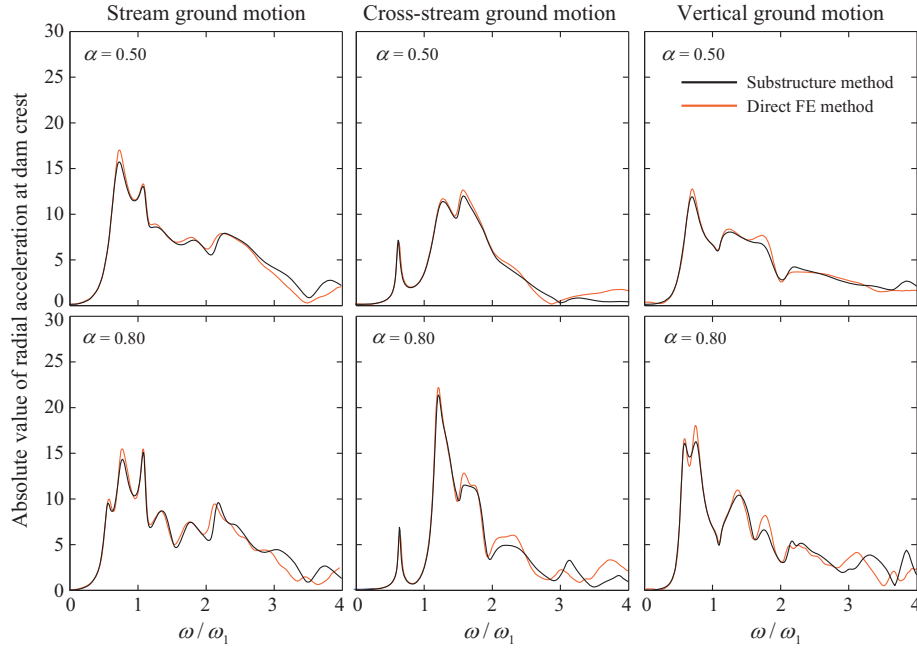


Figure 5.15: Frequency response functions for the amplitude of relative radial acceleration at the crest of Morrow Point Dam supported on flexible foundation rock with full reservoir due to uniform stream, cross-stream and vertical ground motions. Results computed by direct FE and substructure methods are presented for two values of the wave-reflection coefficient α (Cases 7 and 8 in Table 5.1).

6 Simplifications of the direct FE method

The procedures summarized in Boxes 4.1–4.4 for computing effective earthquake forces are conceptually straightforward, however, they require up to 24 auxiliary analyses for the foundation rock (8 analyses for each component of ground motion), and 2 auxiliary analyses for the fluid domain (1 analysis each for vertical and cross stream components). Substantial amounts of data management and "book-keeping" is required when using these procedures to analyze 3D models, which may have tens of thousands of boundary nodes. The next section presents simplifications to the direct FE method that drastically reduces these requirements, with the goal of simplifying the practical implementation of the analysis procedure.

6.1 Using 1D analysis to compute effective earthquake forces at side foundation boundaries

The use of a combination of 1D and 2D analyses to compute effective earthquake forces \mathbf{P}_f^0 at the side boundaries of the foundation domain is necessary to satisfy the general requirement in soil–structure interaction analyses that any admissible free-field system must be identical to the actual system in the region exterior to the absorbing boundaries [20,40]. However, it is reasonable to expect that even a much simpler system that technically violates this requirement could give accurate results provided the foundation domain is sufficiently large. This is normally the situation in the direct FE method with viscous-damper boundaries, because these always require large domain sizes to ensure acceptable modeling of the semi-unbounded foundation rock.

To test this hypothesis, the actual free-field foundation-rock system (Figure 4.2a) is replaced by a much simpler system (Figure 6.1a): a flat foundation box with homogeneous (or horizontally layered) material properties, implying that the effects of the canyon are ignored in the free-field analysis. This simplification is especially attractive because analysis of this 3D flat box to vertically propagating seismic waves reduces to analysis of the simple 1D column of foundation-rock elements shown in Figure 6.1b.

Analysis of the 1D system of Figure 6.1b, discretized to match the elevations of the boundary nodes in the main model, subjected to the forces of Equation (4.1) at the base provides the motion \mathbf{r}_f^0 at every node along the height. Alternatively, \mathbf{r}_f^0 may be extracted at every elevation directly from the deconvolution analysis. Boundary tractions are computed from \mathbf{r}_f^0 using stress-strain relationships for a 1D system (see Appendix E) and converted to nodal forces for the FE model by multiplying by the tributary area of each node. The analysis is repeated for each component of ground motion (x, y, z) considered in the analysis. Step-by-step instructions for implementation of the procedure are presented in Box 6.1.

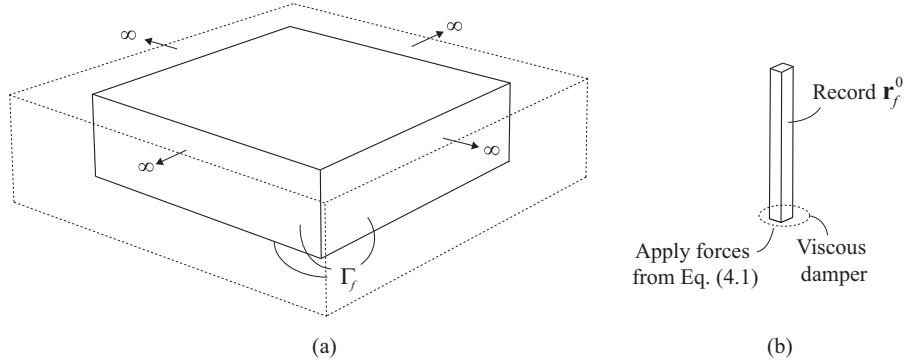


Figure 6.1: (a) Free-field foundation-rock system without canyon; (b) analysis of single column of foundation-rock elements to compute \mathbf{r}_f^0 .

Box 6.1: Computing effective earthquake forces \mathbf{P}_f^0 at side boundaries by 1D free-field analysis

Determining \mathbf{r}_f^0 by analysis of single foundation-rock column

1. Develop a FE model of the simplified free-field foundation-rock system: a single column of foundation-rock elements with discretization to match the elevations of the boundary nodes in the main model (Figure 6.1b).
2. For each direction of ground motion, $k = x, y, z$ add a viscous damper at the base in the k -direction and constrain DOFs in the other directions to allow only shear ($k = x, y$) or axial ($k = z$) deformation of the column.
3. Apply effective earthquake forces from Eq. (4.1) to the base in the k -direction, and compute the motion \mathbf{r}_f^0 at each node along the height.

As an alternative to Steps 1-3, the motion \mathbf{r}_f^0 may be extracted at every elevation directly from a 1D deconvolution analysis.

Compute effective earthquake forces \mathbf{P}_f^0

4. Compute $\dot{\mathbf{r}}_f^0$ as the time derivative of \mathbf{r}_f^0 .
5. Compute boundary tractions from \mathbf{r}_f^0 using 1D stress-strain relations (Appendix E) and multiply them by the tributary area of each node to determine \mathbf{R}_f^0 .
6. Calculate effective earthquake forces \mathbf{P}_f^0 at the side foundation boundaries from Eq. (3.7a) using $\dot{\mathbf{r}}_f^0$ from Step 4 and \mathbf{R}_f^0 from Step 5.

Such a single, 1D free-field analysis is drastically simpler compared to the rigorous procedure developed in Section 4.2.2 that required 24 auxiliary analyses and extensive data transfer. However, because the assumed system in Figure 6.1a is not identical to the actual system in the region exterior to the absorbing boundary, it will introduce errors in the

solution. The resulting errors in the free-field response at the center of the semi-cylindrical canyon (Figure 5.3) are shown in Figure 6.2, where results obtained by the direct FE method using 1D and 3D free-field analyses to compute effective earthquake at the side boundaries are compared.

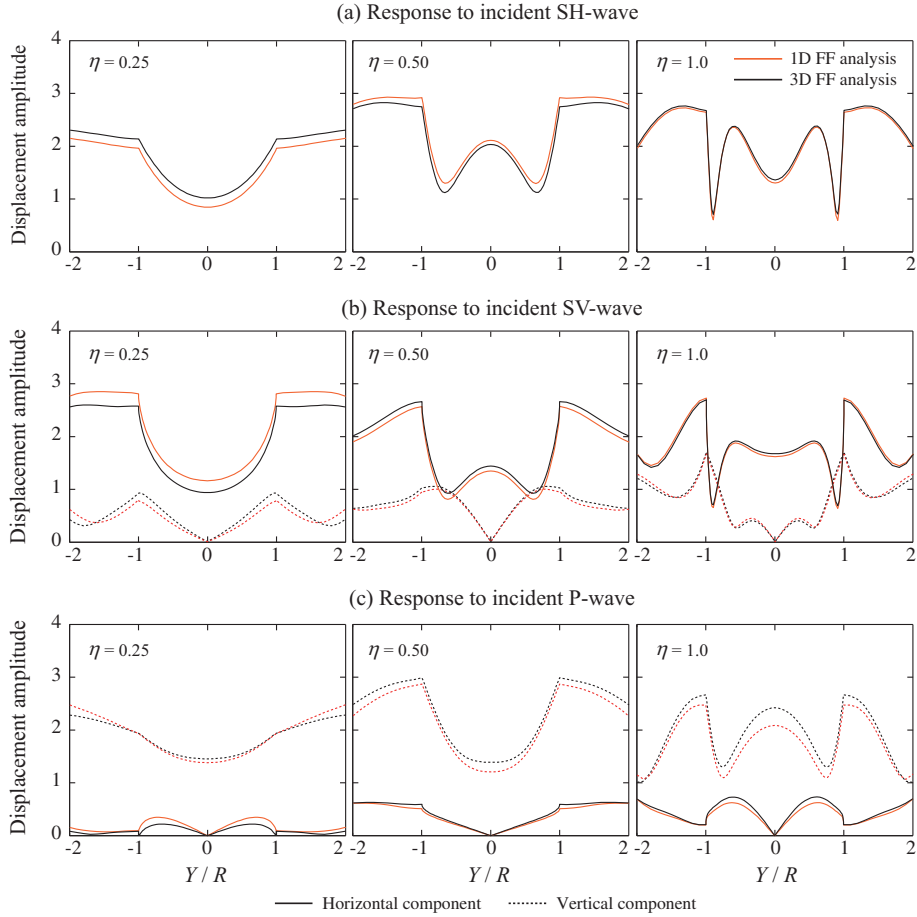


Figure 6.2: Displacement amplitudes at semi-cylindrical canyon subjected to incident SH-, SV-, and P-waves. Results are computed by the direct FE method with effective earthquake forces \mathbf{P}_f^0 on the side boundaries determined from 1D and 3D free-field analyses.

The displacements at the canyon surface computed by the two methods (Figure 6.2) are reasonably close for all types of incident waves and for a wide range of dimensionless frequencies η , thus suggesting that using 1D analysis to compute effective earthquake forces may be an acceptable approximation for this system. Later in this section, this approximation will be examined in the context of dam response.

The good agreement in Figure 6.2 is achieved – in part – because the foundation domain is sufficiently large: typical dimensions for a dam model (700m x 700m x 400m) was used relative to a canyon radius of $R = 100\text{m}$, thus ensuring sufficient distance from the center of the model to the side boundaries where the effective earthquake forces are applied. For a much smaller domain (200m x 400m x 400m), the resulting errors are considerably larger, as demonstrated in Figure 6.3.

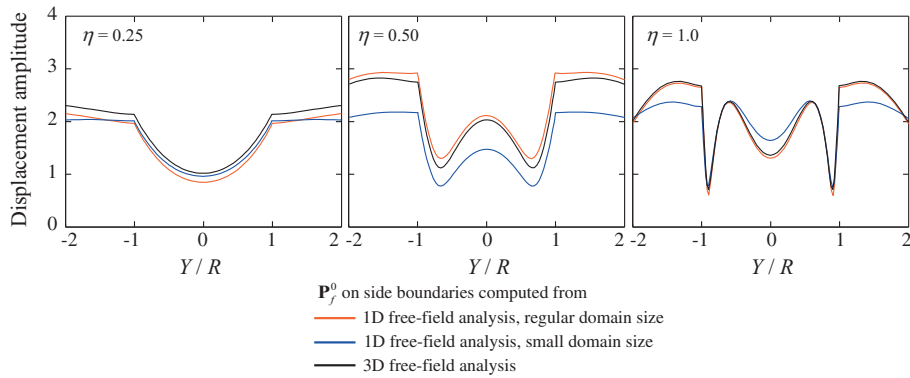


Figure 6.3: Influence of domain size on the errors in displacement amplitudes at semi-cylindrical canyon subjected to incident SH-waves when using 1D free-field analysis to compute effective earthquake forces \mathbf{P}_f^0 on the side boundaries.

The accuracy of using the simplified 1D free-field analysis when determining the dynamic response of concrete dams by the direct FE method is investigated by analyzing Morrow Point Dam (Figure 5.5). Frequency response functions for the amplitude of radial acceleration at the crest of the dam supported on flexible rock with empty reservoir are presented in Figure 6.4, where results obtained using 1D and 3D free-field analysis to compute effective earthquake forces are compared. The closeness of the two sets of results justifies the use of 1D free-field analysis to compute effective earthquake forces for this system.

These results demonstrate that the loss of accuracy from using 1D free-field analysis is insignificant as long as the foundation domain is sufficiently large. As previously mentioned, this requirement is normally satisfied in the direct FE method when employing viscous-damper boundaries because these always require large domain sizes to ensure acceptable modeling of the semi-unbounded foundation domain. Thus, the use of 1D free-field analysis is appropriate for practical analyses in the direct FE method.

This conclusion puts the direct FE method at a significant advantage over previous analysis procedures [41] where high performing PML boundaries were used together with DRM to apply the seismic input. Because the attractiveness of such advanced methods lies in their ability to use very small domain sizes, they are not amenable for using such simplified

1D free-field analysis, and therefore require analysis of complicated 3D systems and extensive data transfer to determine the seismic input.

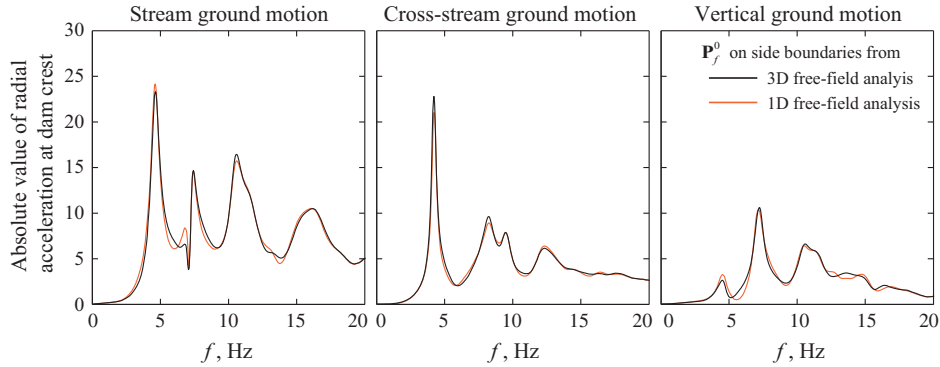


Figure 6.4: Influence of using 1D free-field analysis to determine effective earthquake forces \mathbf{P}_f^0 on the side boundaries on the response of Morrow Point dam on flexible foundation rock with empty reservoir.

6.2 Ignoring effective earthquake forces at side foundation boundaries

The dam engineering profession has been using a variation of the direct FE method wherein effective earthquake forces \mathbf{P}_f^0 are applied only to the bottom boundary, and not to the side boundaries [45,73,101]. This approximation is attractive because it eliminates the need for analysis of the free-field foundation-rock system altogether, but as will be demonstrated, the resulting errors in the dam response can be large.

First observed are the large errors in the free-field motion at the surface of the semi-cylindrical canyon of Figure 5.3 computed by the direct FE method with and without effective earthquake forces applied to the side boundaries. The results are unacceptable for all three types of excitation over a wide range of η -values (Figure 6.5) because, without effective earthquake forces applied to the side boundaries, the viscous dampers boundaries attenuate seismic waves as they propagate up through the model. Some researchers have referred to this effect as *leakage* [99]. Because this leakage is frequency dependent, it affects the motion at some frequencies (η -values) more than others.

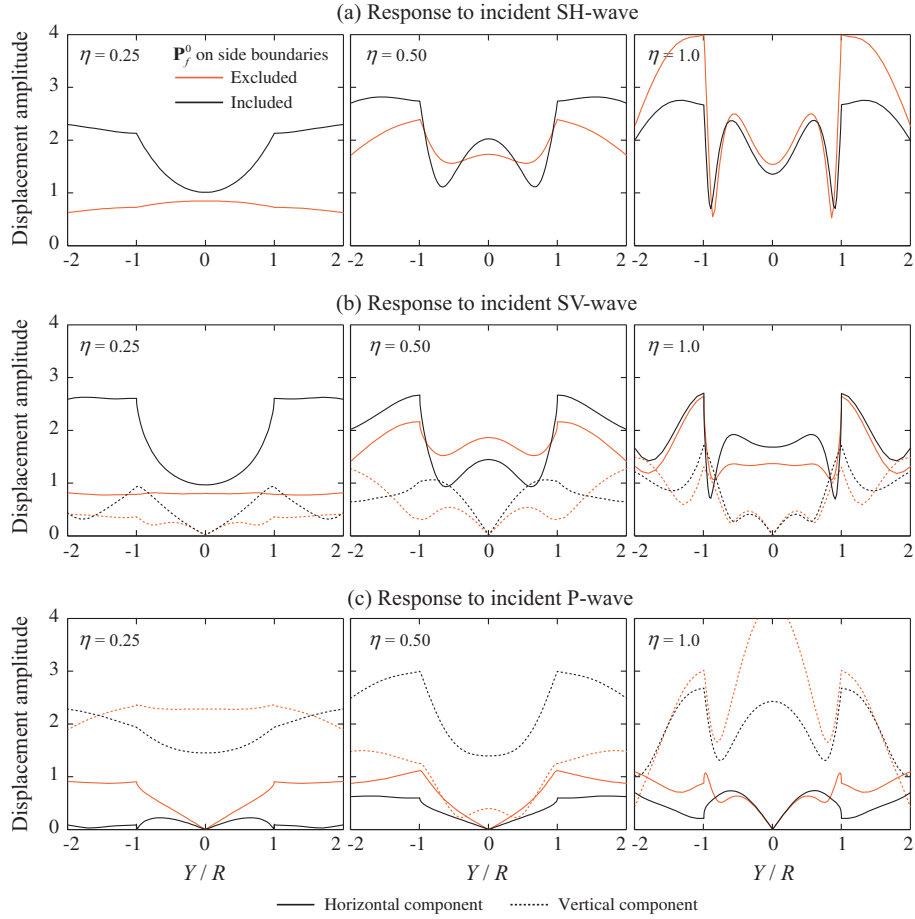


Figure 6.5: Displacement amplitudes at semi-cylindrical canyon subjected to incident SH-, SV-, and P-waves. Results are computed from two analyses: excluding and including effective earthquake forces \mathbf{P}_f^0 on the side boundaries.

The errors can be reduced by increasing the domain size, i.e., by moving the absorbing boundaries further away from the center of the model. This is demonstrated in Figure 6.6, where results are presented for two domain sizes: the "regular" domain size (700m x 700m x 400m) used in the preceding analyses, and a large domain size, 1400m x 1400m x 400m. Increasing the horizontal dimensions of the foundation domain improves the results, but the errors remain significant even for this large domain.

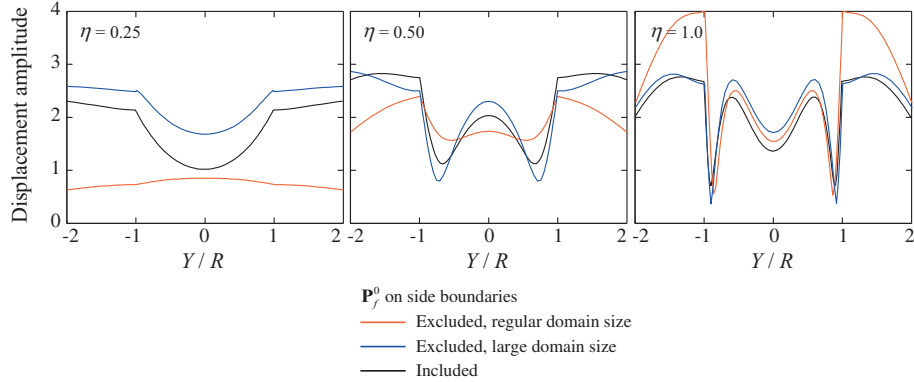


Figure 6.6: Influence of domain size on the errors in displacement amplitudes at semi-cylindrical canyon subjected to incident SH -waves when excluding effective earthquake forces \mathbf{P}_f^0 on the side boundaries.

Frequency response functions for the amplitude of radial acceleration at the crest of Morrow Point Dam supported on flexible foundation rock with empty reservoir are shown in Figure 6.7. Results are computed by the direct FE method with and without effective earthquake forces applied to the side boundaries. As anticipated by the poor agreement in the free-field response at the canyon surface, excluding \mathbf{P}_f^0 at the side boundaries cause significant error in the dam response to all components of ground motion.

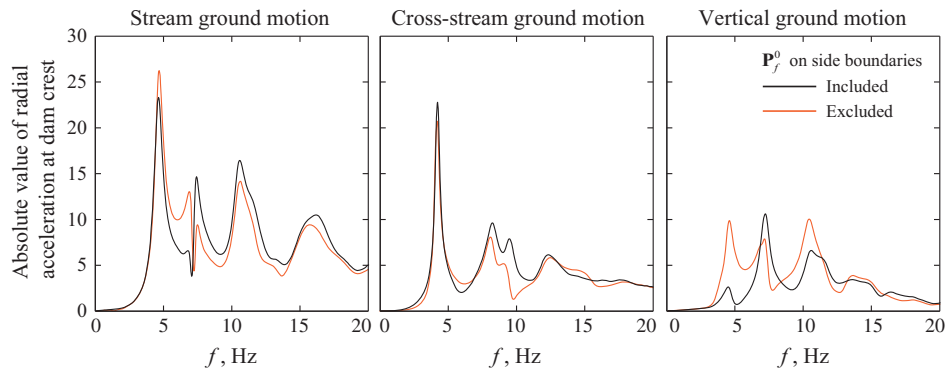


Figure 6.7: Influence of excluding effective earthquake forces \mathbf{P}_f^0 on the side boundaries on the response of Morrow Point dam on flexible foundation rock with empty reservoir.

In light of these results, there seems to be no justification in ignoring the effective earthquake forces on the side boundaries. Computing these forces using the simple 1D free-field analysis (Box 6.1) requires very little effort, with minimal loss of accuracy compared to the more rigorous 3D free-field analysis summarized in Box 4.3.

6.3 Avoiding deconvolution of the surface control motion

Some researchers have avoided deconvolution of the specified surface control motion $a_g^k(t)$ by idealizing the foundation as a homogeneous, undamped, halfspace [7,98]. In this special case, a vertically propagating plane wave does not attenuate, implying that the incident earthquake motion at the bottom boundary, \mathbf{r}_l^0 , is equal to one-half the specified surface motion, except for a time shift. The validity of this assumption for different foundation idealizations is investigated next.

A flat foundation box (Figure 5.1) is first analyzed by the direct FE method and the computed surface motions are compared against the specified control motion. Effective earthquake forces at the bottom and side boundaries are computed using two methods for obtaining the incident motion \mathbf{r}_l^0 at the bottom boundary: "rigorous" deconvolution of the surface control motion, and $1/2$ the surface control motion. Such comparison is presented in Figure 6.8 for three different foundation idealizations[†]: (a) homogeneous foundation with zero material damping, (b) homogeneous foundation with 4% material damping, and (c) horizontally layered foundation with zero material damping. For all three cases, the free-field control motion $a_g^k(t)$ is defined at the surface in the two horizontal and vertical directions by the S69E, S21W and vertical component of the Taft ground motion, respectively.

Observe from the results in Figure 6.8 that when the incident motion \mathbf{r}_l^0 is determined by deconvolution of the surface control motion, the computed surface motion is essentially identical (to within FE discretization error) to the specified control motion for all three foundation idealizations. In contrast, specifying \mathbf{r}_l^0 as $1/2$ the surface control motion gives essentially the exact results if the foundation is homogeneous and undamped (Figure 6.8a), but leads to significant underestimation of the surface motion for a damped foundation (Figure 6.8b) and overestimation for a layered foundation (Figure 6.8c). These results suggests that dam response would be accurately computed with \mathbf{r}_l^0 taken as $1/2$ the surface control motion only if the foundation domain is homogeneous and undamped, but that errors will be introduced for other cases.

Frequency response functions for the amplitude of radial acceleration at the crest of Morrow Point Dam including dam–foundation interaction (empty reservoir) are presented in Figure 6.9 for two cases: (a) homogeneous foundation with zero material damping, and (b) homogeneous foundation with 4% material damping. For both cases, results obtained with \mathbf{r}_l^0 computed by deconvolution and as $1/2$ the surface control motion are compared. As expected by the results in Figure 6.8, specifying \mathbf{r}_l^0 as $1/2$ the surface control motion does not introduce error in dam response when the foundation is undamped (Figure 6.9a), but causes significant underestimation of the response for foundations with damping (Figure 6.9b).

[†] The material properties for the foundation are: density = 2723 kg/m³ and Poisson's ratio = 0.20. The homogeneous foundation (Cases a and b) has shear wave velocity $V_s = 2000$ m/s. The layered foundation (Case c) consists of three layers of equal thickness 133m on top of homogenous bedrock, with shear wave velocities that increase with depth: $V_{s,1} = 1500$ m/s, $V_{s,2} = 2000$ m/s, $V_{s,3} = 2500$ m/s, and $V_{s,bedrock} = 3000$ m/s;

To eliminate such errors, the incident motion \mathbf{r}_i^0 at the bottom foundation boundary should be computed by 1D deconvolution analysis. There is little justification in bypassing such analysis, especially because it is a straightforward and requires very little computational effort compared to 3D analysis of the dam–water–foundation system.

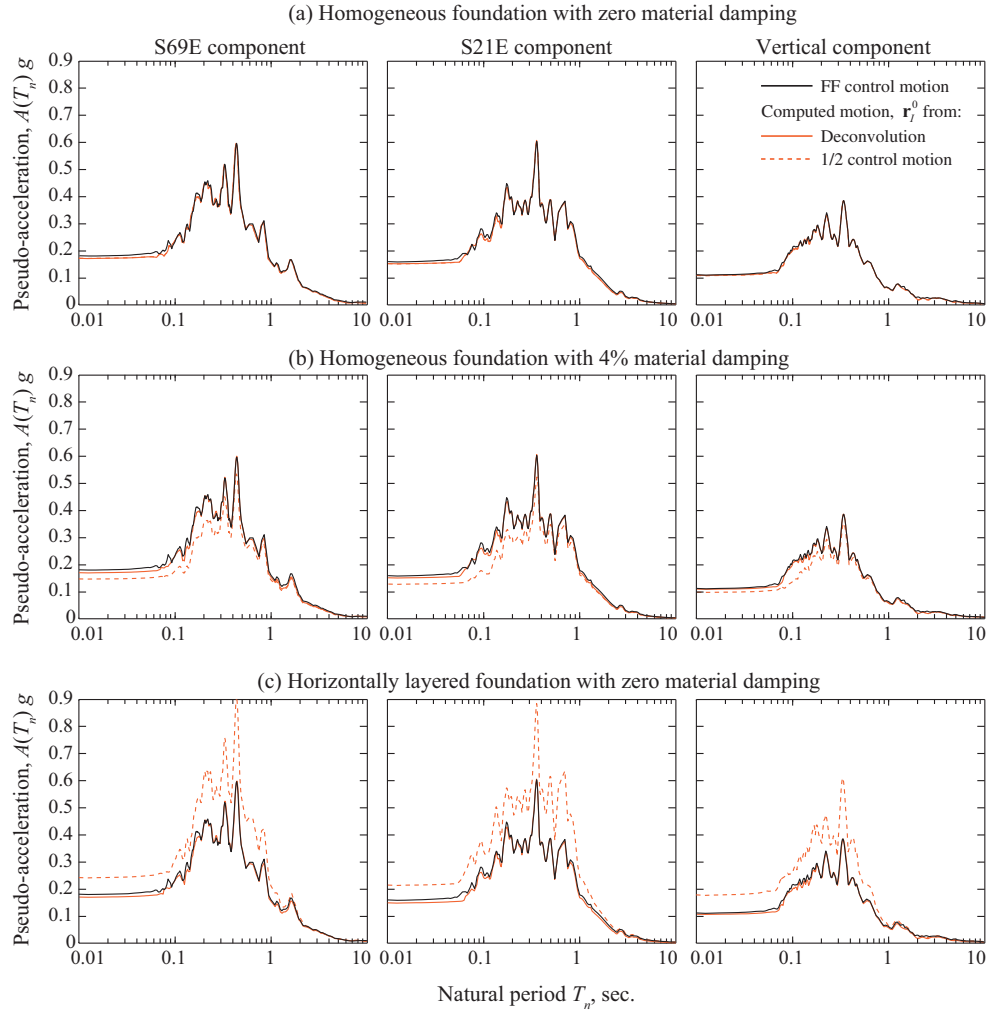


Figure 6.8: Comparison of 5% damped pseudo-acceleration response spectra for specified free-field control motion and motion computed at the surface of flat foundation box for three foundation idealizations. Results obtained with \mathbf{r}_i^0 computed from deconvolution and as $\frac{1}{2}$ the surface control motion are compared.

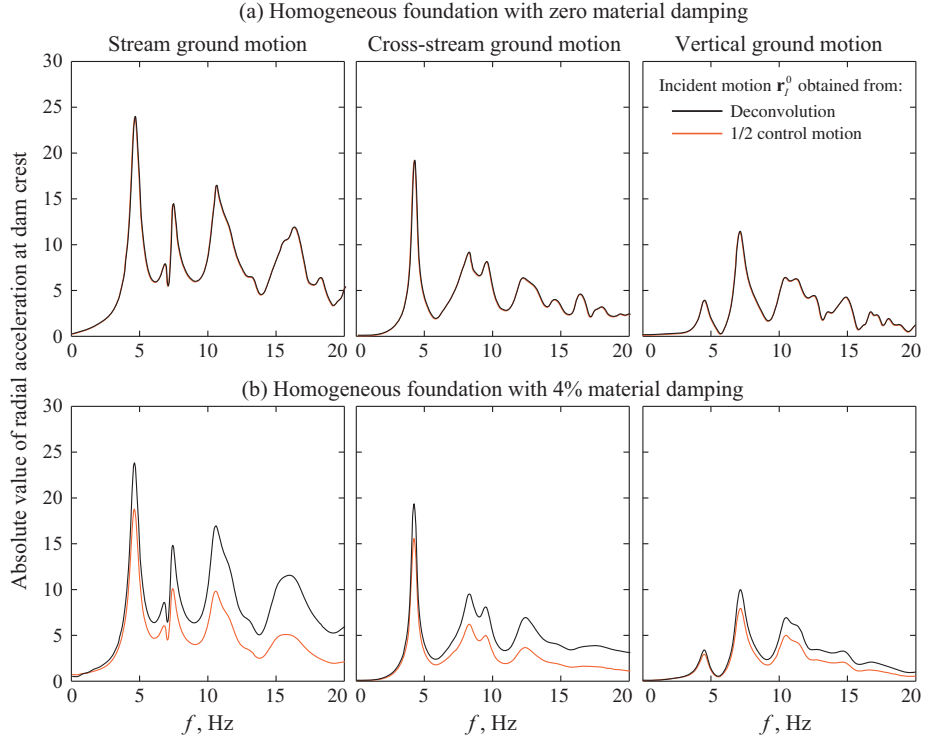


Figure 6.9: Discrepancies introduced by approximating \mathbf{r}_i^0 as $\frac{1}{2}$ the surface control motion on the response of Morrow Point Dam including dam–foundation interaction (reservoir is empty) for two foundation idealizations.

6.4 Ignoring effective earthquake forces on upstream boundary of fluid domain

Implementation of the direct FE method may be simplified by excluding effective earthquake forces \mathbf{P}_r^0 at the upstream fluid boundary Γ_r , which are the forces associated with earthquake-induced hydrodynamic pressures in the semi-unbounded fluid channel upstream of Γ_r . This is attractive because it eliminates the need for the 2D auxiliary analysis of the fluid cross-section (Section 4.3) for vertical and cross-stream components of ground motion

Presented in Figure 6.10 are frequency response functions for the radial acceleration at the crest of Morrow Point Dam on rigid foundation with full reservoir subjected to ground motions that are uniform at the dam–foundation and water–foundation interfaces for two values of the wave reflection coefficient characterizing sediment absorption[†]: $\alpha = 0.50$ and $\alpha = 0.80$. Results from three analyses are presented for each α -value: (1) fluid domain

[†] Sediments are included herein only for the purpose of introducing some energy absorption at the reservoir boundaries in the absence of dam–foundation and water–foundation interaction mechanisms in this system with rigid foundation.

length of $L = 2.5H$ including \mathbf{P}_r^0 on the upstream fluid boundary, (2) $L = 2.5H$ excluding \mathbf{P}_r^0 , and (3) $L = 5H$ excluding \mathbf{P}_r^0 . Excluding \mathbf{P}_r^0 for cross-stream and vertical ground motions has little influence on the response for $\alpha = 0.50$, but leads to errors for higher α -values ($\alpha = 0.80$) and short fluid domains ($L = 2.5H$). For the stream component of ground motion, $\mathbf{P}_r^0 = \mathbf{0}$ (Section 4.3), so all three cases give essentially identical results.

These discrepancies occur because of the idealization of the system analyzed (Figure 2.1): the uniform fluid channel is unbounded in the upstream direction and the excitation is implicitly assumed to extend along the entire length of this channel. In reality, neither the uniform fluid channel nor the ground motion could extend to infinity in the upstream direction, so excluding \mathbf{P}_r^0 from the analysis – implying that the excitation stops at the boundary Γ_r – seems to be a more appropriate idealization. Thus, it can be concluded that the errors observed in Figure 6.10 are inconsequential for analysis of actual dams, and that \mathbf{P}_r^0 can be left out of the analysis without loss of accuracy as long as the fluid domain is large enough to accurately model dam–water interaction and radiation damping using the viscous-damper boundaries (Section 5.3.3).

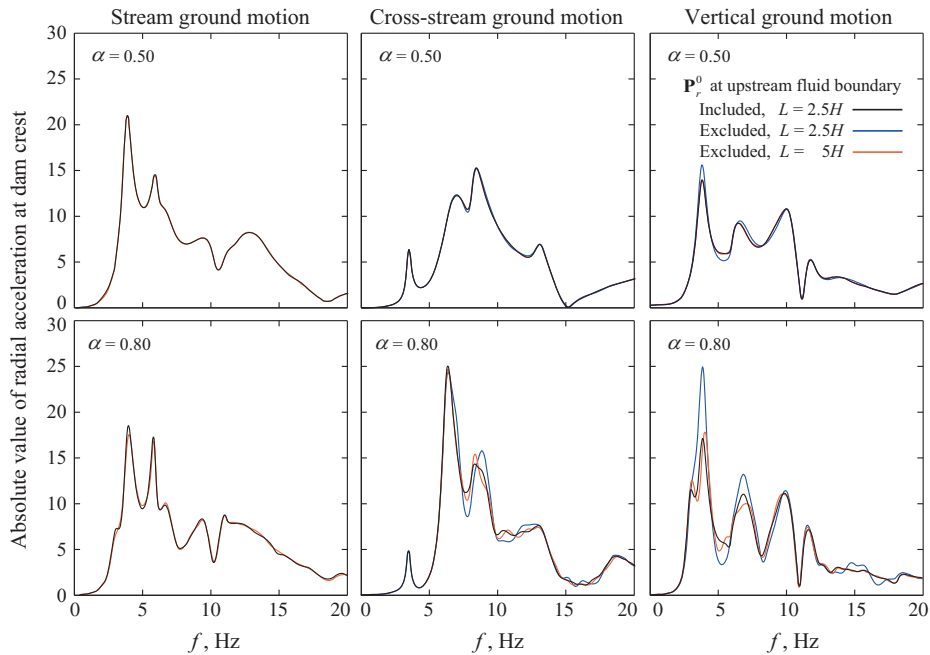


Figure 6.10: Influence of excluding effective earthquake forces \mathbf{P}_r^0 on the upstream fluid boundary on the response of Morrow Point dam on rigid foundation with full reservoir. Results are presented for two values of the wave-reflection coefficient: $\alpha = 0.50$ and $\alpha = 0.80$. $\zeta_s = 3\%$ damping is specified for the dam alone.

7 Summary of procedure

The earthquake input for the three-dimensional dam–water–foundation rock system is defined by the free-field ground acceleration $a_g^k(t)$, $k = x, y, z$, specified at a control point on the foundation surface at the level of the dam abutments (Figure 2.4c). This motion may for example be from an ensemble of recorded ground motions selected and scaled to "match" a target spectrum, or synthetic motions developed for an earthquake scenario.

Analysis of 3D dam–water–foundation rock systems by the direct FE method – making use of the recommended simplifications presented in Sections 6.1 and 6.4 – is organized in three parts: static analysis, linear analyses of the free-field foundation-rock system, and nonlinear dynamic analysis of the dam–water–foundation rock system.

Static analysis:

1. Develop a FE model for static analysis of the dam–foundation rock system with an appropriate material model for the dam concrete and an appropriate (static) model for the semi-unbounded foundation rock.
2. Compute the response of this system to self-weight and hydrostatic forces; for arch dams this may include effects of a staged construction sequence.
3. Record the static state of the dam and foundation rock, including reactions from the foundation rock at the boundary Γ_f .

Linear analysis of the free-field foundation-rock system (using 1D free-field analysis):

4. Obtain the outcrop motion at the base of the foundation-rock model by deconvolution of the surface control motion $a_g^k(t)$.
5. Calculate the effective earthquake forces \mathbf{P}_f^0 at the bottom boundary of the foundation domain from the procedure in Box 4.1.
6. Compute the effective earthquake forces \mathbf{P}_f^0 at the side boundaries of the foundation domain from the procedure in Box 6.1.

Step 6 may be avoided if free-field boundary elements [99] are employed at the side boundaries of the truncated foundation domain.

Nonlinear dynamic analysis of dam–water–foundation rock system:

7. Develop a FE model of the dam–water–foundation rock system with viscous-damper boundaries to truncate the semi-unbounded foundation and fluid domains at Γ_f and Γ_r , respectively. Use solid elements for the dam and foundation rock, fluid elements for the water, and interface elements (or tie constraints) at the dam–water and water–foundation rock interfaces. Sediments at the reservoir bottom can be modelled

PART II: SUMMARY OF PROCEDURE

approximately by surface elements based on the one-dimensional absorption model, or by using more sophisticated viscoelastic or poroelastic material models.

8. Calculate the response of this FE model subjected to effective earthquake forces \mathbf{P}_f^0 computed in Step 5 at the bottom foundation boundary and in Step 6 at the side boundaries, as well as self-weight, hydrostatic forces and static foundation reactions at Γ_f . The static state of the dam (Step 3) is taken as the initial state in the nonlinear dynamic analysis.

8 Conclusions

The direct FE method developed in Part I of this thesis for nonlinear earthquake analysis of two-dimensional dam–water–foundation rock systems has been generalized for three-dimensional systems. Formulated by interpreting dam–water–foundation rock interaction as a scattering problem where the dam perturbs a free-field state of the system, the direct FE method considers all the factors important in the earthquake response of arch dams: dam–water interaction including water compressibility and wave absorption at the reservoir boundaries; dam–foundation rock interaction including mass, stiffness and damping in the rock; radiation damping due to the semi-unbounded sizes of the foundation rock and reservoir domains; spatial variation of the ground motions around the dam–canyon interface; and nonlinear behavior in the dam and adjacent parts of the foundation and fluid domains.

The seismic input to the procedure is specified by a ground motion at a control point on the foundation surface. The free-field motion at depth in the foundation rock is determined by deconvolution of this control motion. Then, effective earthquake forces are computed from a set of 1D and 2D analysis and applied to the boundaries of the FE model. Each of these analyses requires very little computational effort and can be implemented without modifying the FE source code, the main challenge is management and transfer of large amounts of data.

Several examples are presented to validate the accuracy of the direct FE method applied to 3D problems. One of these examples compares the dynamic response of Morrow Point Dam computed by the direct FE method with independent benchmark solutions obtained by the substructure method. The excellent agreement achieved for a wide range of analysis cases demonstrates that (1) the effects of dam–water–foundation rock interaction are accurately modeled, (2) the bounded foundation and fluid models with viscous-damper boundaries are able to simulate the semi-unbounded extent of these domains, and (3) the earthquake excitation is properly defined by specifying – at the boundaries of the FE model – effective earthquake forces determined from a surface control motion.

To facilitate implementation of the direct FE method, several simplifications of the analysis procedure are proposed and their efficacy evaluated. The presented results led to the following conclusions:

1. Using 1D free-field analysis to compute effective earthquake forces \mathbf{P}_f^0 at the side boundaries of the foundation rock, which drastically reduces the amount of data transfer and data management, is an appropriate approximation provided that the foundation domain is sufficiently large. This is normally the case when using viscous-damper boundaries because these already require large domain sizes to model the semi-unbounded foundation domain.
2. In contrast, ignoring the effective earthquake forces \mathbf{P}_f^0 at the side boundaries – a popular simplification in the dam engineering profession – can lead to large errors in

PART II: CONCLUSIONS

the dam response. There seems to be no justification in ignoring these forces when they can be included with minimal effort using the simplified 1D free-field analysis.

3. Specifying the incident motion \mathbf{r}_f^0 at the bottom foundation boundary as $\frac{1}{2}$ the surface motion – thereby avoiding 1D deconvolution analysis – can cause significant error in dam response for foundations with damping and for layered foundations. To eliminate such errors, the incident motion at the bottom foundation boundary should be computed by 1D deconvolution of the surface control motion.
4. Ignoring the effective earthquake forces \mathbf{P}_f^0 at the upstream fluid boundary – implying that the earthquake excitation stops at the fluid boundary – is appropriate for practical analysis as long as the fluid domain is long enough. This is normally the case in the direct FE method because large domains are already required to accurately model dam–water interaction.

The direct FE method is applicable to nonlinear systems, thus allowing for modeling of concrete cracking, as well as sliding and separation at construction joints, lift joints, and at concrete-rock interfaces. The procedure can be implemented with any commercial FE program that permits modeling of viscous-damper boundaries and specification of effective earthquake forces at these boundaries.

PART III

**Modeling and practical implementation of the direct
finite element method for performance based
earthquake engineering of concrete dams**

1 Introduction

Much research has been devoted to developing the framework for seismic design and safety assessments of structures called Performance Based Earthquake Engineering (PBEE), which is routinely applied to evaluate structures such as buildings, nuclear power plants and bridges [109–112]. However, much less work has been done on PBEE in the context of concrete dams (with a few notable exceptions, e.g. [113]), and most of the conducted research have been focused investigations on developing seismic fragility curves for 2D gravity dam systems [114–116].

One obstacle for the adaption of PBEE by the dam engineering community is the lack of accurate and efficient analysis procedures for conducting the large number of nonlinear response history analyses (RHA) required to quantify the uncertainties in earthquake ground motions and material properties of the system. For years, nonlinear RHA of concrete dams were limited by major deficiencies: overly simplistic models for dam–water–foundation rock interaction, not accounting for radiation damping in the semi-unbounded foundation and fluid domains, and ignoring spatial variation of ground motions along the dam–canyon interface. These limitations were overcome in the direct FE method developed in Parts I and II of this thesis. Because this direct FE method was developed in a form that can be implemented with any commercial FE program, it is readily available for researchers and engineers who may be committed to using a particular program.

Presented in this part of the thesis is an introduction to modeling and practical implementation of the direct FE method within the framework of PBEE of concrete dams. In Chapter 2, an introduction to PBEE of concrete dams is presented. The basic principles of PBEE are described, key equations are explained, and the current state of knowledge for PBEE of concrete dams is contrasted to that for buildings. Chapter 3 presents a discussion on nonlinear modeling of concrete dams by the direct FE method. First, the most significant nonlinear mechanisms that can develop in concrete dams are reviewed, and suitable modeling alternatives presented. In the second part of Chapter 3, the discussion focuses on the various types of linear energy dissipation (damping) that takes place within dam–water–foundation rock systems. Practical suggestions on how to model energy dissipation at the reservoir boundaries are presented, and recommendations are given for how to ensure consistency between damping in the numerical model and the damping measured at actual dams. Finally, in Chapter 4, the capabilities of the direct FE method when implemented with a commercial FE code is demonstrated by performing a nonlinear earthquake analysis of an actual arch dam using the commercial FE program ABAQUS [75].

A condensed version of this part of the thesis has been submitted for publication in *Earthquake Engineering and Structural Dynamics*.

2 Performance based earthquake engineering of dams

Performance Based Earthquake Engineering (PBEE) is a probabilistic framework for seismic design and safety assessments of structures that considers all the inherent uncertainties in earthquake performance assessments. In contrast to traditional load-and-resistance-factor design procedures which typically result in a "binary" fail or safe conclusion, PBEE offers a complete framework for performance evaluations that considers and quantifies the various sources of uncertainty along the way. PBEE is well developed and frequently used for performance evaluations of buildings, bridges and nuclear power plants; but has yet to be adapted to a meaningful degree by the dam engineering community.

2.1 The Pacific Earthquake Engineering Research Center PBEE framework

Several variations of PBEE have been proposed after the introduction of the first generation performance based earthquake engineering and design procedures for buildings in the United States [117,118]. Today, the most commonly used "version" of PBEE is the framework developed by the Pacific Earthquake Engineering Research Center (PEER). First proposed by Cornell and Krawinkler [119], The PEER PBEE framework provides a general tool to determine the probability distribution and rate of exceedance for various system-level performance measures for a given structure at a given site. From this information, and the information obtained in intermediate steps, a wide range of useful performance metrics (e.g. risk of collapse, annualized repair costs, expected number of casualties, etc.) can be extracted and used to make risk-informed decisions regarding the design of new dams or safety evaluations of an existing dam.

The PEER framework can be summarized in the following equation [119]:

$$\lambda(DV) = \int_{IM} \int_{EDP} \int_{DM} G(DV | DM) |dG(DM | EDP)| |dG(EDP | IM)| |d\lambda(IM)| \quad (2.1)$$

where $G(X | Y)$ is the probability that X exceeds a specified value given Y (also known as the complimentary cumulative distribution function); $\lambda(X)$ is the mean annual rate of exceedance of X ; and DV = decision variable, DM = damage measure, EDP = engineering demand parameter and IM = intensity measure.

Recognizing the complexity and multi-disciplinary nature of problem, the PEER framework can be separated into four phases that each can be solved using appropriate techniques and tools (Figure 2.1): (1) seismic hazard analysis, (2) structural analysis, (3) damage analysis, and (4) loss analysis. The output from each phase is quantified using the four variables IM , EDP , DM and DV . This convenient decomposition is based on the

assumption that, conditioned on EDP, DM is independent of IM, and, conditioned on DM, DV is independent of EDP and IM [120]. Through this decomposition, each of the four phases provides valuable information about the seismic hazard, structural response, and uncertainties in the analysis.

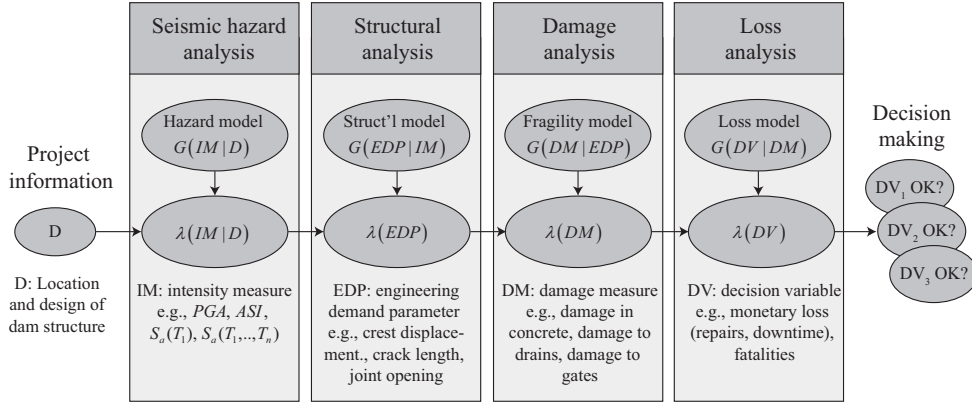


Figure 2.1: Pacific Earthquake Engineering Research Center PBEE framework applied to concrete dams. Figure adapted from [109].

From Equation (2.1), several analogous formulas can be written out for intermediate measures. For example, the annual rate of exceedance of a given DM is

$$\lambda(DM) = \int \int_{IM \ EDP} G(DM | EDP) |dG(EDP | IM)| |d\lambda(IM)| \quad (2.2)$$

and the annual rate of exceedance of a given EDP is given by

$$\lambda(EDP) = \int_{IM} G(EDP | IM) |d\lambda(IM)| \quad (2.3)$$

Equation (2.3) is often referred to as the *seismic demand hazard curve* (SDHC) [94]. Evaluation of the SDHCs directly provides the rate of exceedance for a given structural capacity, or the seismic demand associated with a specified return period.

Another metric, the so-called *fragility function* or *fragility curve*[†] is obtained by isolating the integrand in Equation (2.2):

[†] The "fragility function" is here defined as the probability of exceeding a DM given an IM, $G(DM | IM)$. The same terminology is sometimes used to describe other metrics such as the probability of exceeding an EDP given an IM, $G(EDP | IM)$, or the probability of exceeding a DM given an EDP, $G(DM | EDP)$.

$$G(DM | IM) = \int_{EDP} G(DM | EDP) |dG(EDP | IM)| \quad (2.4)$$

The fragility function describes the probability of exceeding a certain damage state (or limit state) in the structure at different levels of intensity, for example the probability of exceeding a certain crest displacement at different levels of peak ground acceleration (PGA).

In the following sections, each phase of the PBEE framework is described in more detail and put into context of concrete dam analysis.

2.2 Seismic hazard analysis

The goal of this phase is to perform a probabilistic seismic hazard analysis (PSHA) [53,54] of the dam site to obtain the intensity measure hazard curve (IMHC), $\lambda(IM | D)$. The IMHC quantifies the annual rate of exceedance for an IM given the site characteristics D by using ground motion prediction models that consider the seismic environment such as nearby faults, recurrence rates, site conditions, etc. Several online tools and open source computer programs are available for this purpose [121,122].

The IM in the PSHA may be defined as a scalar or a vector. Most often, the spectral acceleration $S_a(T_1)$ at the fundamental period T_1 of the dam–water–foundation rock system is chosen. Several other IMs are also possible, for example peak ground acceleration (PGA), acceleration spectrum intensity (ASI), or multiple-period intensity $S_a(T_1, T_2, \dots, T_N)$. However, recent research have demonstrated that $S_a(T_1)$ is a very good choice of IM for concrete dam analysis [123].

From the IMHC, the next step is to develop a target spectrum for a given hazard level (or return period). This can for example be the uniform hazard spectrum (UHS) or some variation of the conditional mean spectrum (CMS) [54]; both are commonly used in PSHA. Finally, an ensemble of ground motions whose IM matches the target spectrum at T_1 , or closely matches the target spectrum over a period range of interest, is selected for the structural analysis. Because it is unlikely to find a sufficient number of unscaled records that matches the target spectrum, this process requires scaling and modification of existing ground motions [95]; or alternatively, development of synthetic motions [124].

Tools for probabilistic seismic hazard analysis for one or two components of horizontal ground motion conditioned on a single vibration period are well developed. These tools must be extended to consider three simultaneous components of ground motion (two horizontal and one vertical) over multiple vibration periods before they are fully applicable to concrete dam analysis. Such work is in progress [125,126], but as of now, these issues remain largely unresolved.

2.3 Structural analysis

In the structural analysis phase, a large number of nonlinear response history analyses (RHA) of the dam are conducted to determine $G(EDP|IM)$, the response of an EDP given an IM. Relevant EDPs for concrete dams can be maximum displacements or accelerations at the dam crest (for operability of appurtenant structures); maximum opening at contraction joints or sliding at lift joints; extent of tensile cracking in the dam concrete; or relative movement of rock wedges and dam abutments. Common for these (nonlinear) EDPs is that they usually show a high degree of sensitivity to the choice of modeling assumptions and selection of material parameters in the analysis. Thus, the sensitivity of the results to the choice of modeling assumptions should be checked as part of the analysis.

The results of the nonlinear RHA can be integrated with the IMHC $\lambda(IM)$ from the seismic hazard analysis to form the SDHC (Equation 2.3). Construction of the seismic demand hazard curve is illustrated in Figure 2.2. First, the IMHC is discretized at different intensity levels (Figure 2.2a) and ground motions are selected and scaled to match the IM (Figure 2.2b) at a given intensity level im_0 . Using the selected ensemble of ground motions, nonlinear RHA are conducted and the output used to determine the probability distribution $G(EDP|IM)$, often by fitting a lognormal distribution to the individual data points (Figure 2.2c). Numerical evaluation of Equation (2.3) at discrete levels gives the data point for edp_0 in Figure 2.2d, and repeating the process at multiple intensity levels im_0 provides the complete SDHC. This curve can be used to determine the rate of exceedance for a specific structural capacity (e.g. the exceedance rate of a certain crest displacement value), or to determine the structural demand for a given return period (e.g. the maximum joint opening expected for a 10,000 year return period).

Implementation of these nonlinear RHA requires accurate and efficient analysis procedures. Accuracy is obviously needed to ensure meaningful results. Efficiency is also essential, for two reasons: (1) nonlinear RHA of the large FE models required to model dam–water–foundation rock systems is computationally demanding, even by modern standards; and (2) a large number of nonlinear RHAs are required to quantify the uncertainties in earthquake ground motions and material properties of the system. The direct FE method developed in Parts I and II of this thesis meets both of these criteria.

Significant resources have been spent developing and validating (through experimental programs) nonlinear models for the behavior of the various structural components that make up multi-story buildings. The state of research for concrete dams is much less mature because it is difficult and expensive to perform meaningful experimental tests on dams, and there is little field evidence to go by since few concrete dams have been damaged during earthquakes. Without more research on this topic, it will be difficult to reduce the substantial uncertainties involved in estimating nonlinear dam response.

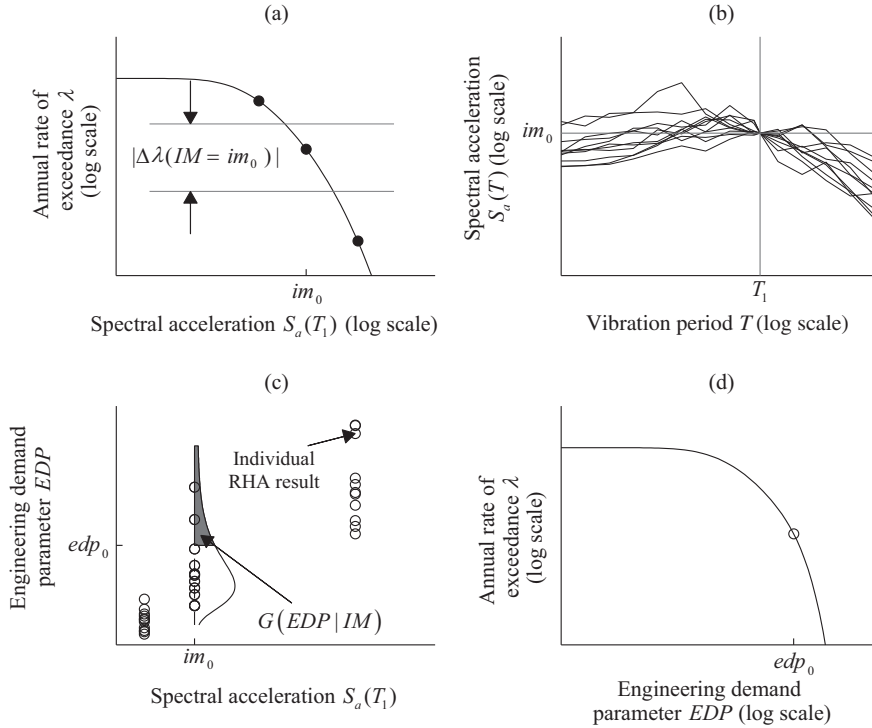


Figure 2.2: Construction of the SDHC when $IM = S_a(T_1)$: (a) discretization of the IMHC, $\lambda(IM)$; (b) selection and scaling of ground motions so that $IM = im_0$; (c) Nonlinear RHA of the dam to estimate $G(EDP | IM)$; (d) resulting SDHC, $\lambda(EDP)$. Figure adapted from [94].

2.4 Damage analysis

The damage analysis seeks to determine the level of physical damage DM given an EDP, $G(DM | EDP)$. For buildings, this damage analysis is usually performed on a component level using available data on the expected damage given various deformations, force levels, etc., compiled from laboratory experiments and field experience. As previously mentioned, such data is not available for concrete dams. Thus, it is often more useful to define damage states (or limit states) for the dam directly on the structural level, and use damage measures to quantify the damage in each of these states. Defining such meaningful damage states requires identification and evaluation of the potential failure modes of the dam [127].

The resulting output can be visualized in the form of fragility curves for the dam, $G(DM | IM)$, defined by Equation (2.4). Construction of the fragility curve is illustrated in Figure 2.3a: first, outputs from a large number of nonlinear RHA at several intensity levels are used to determine the fraction of analyses exceeding a certain damage threshold. A fragility function is then fitted to the data set, usually in the form of a lognormal cumulative

distribution [128]. Examples of fragility curves for relevant damage states in concrete dams are shown in Figure 2.3b. If an important objective for the dam is to ensure operability of flood gates at the crest, a useful damage measure can for example be the maximum crest displacement. Such curves should be computed not only for extreme damage states (e.g. uncontrolled release of the reservoir), but rather at multiple intermediate stages to give a complete description of the gate performance at different hazard levels.

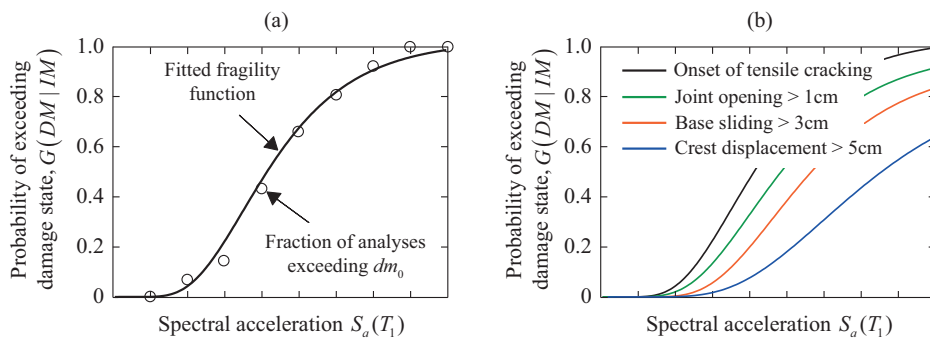


Figure 2.3: Illustration of fragility curve: (a) fitting of fragility curve to output from nonlinear RHA; (b) examples of fragility curves relevant for concrete dams.

Researchers have successfully applied the concepts of seismic fragility analysis to study the influence of modeling assumptions on the seismic performance of gravity dams at different intensity levels [114–116]. However, routine use of such methods in professional practice does not seem practical at present time.

2.5 Loss analysis

The last phase in the PBEE framework is loss analysis, which seeks to determine $\lambda(DV)$, the rate of exceedance of a certain decision variable. For concrete dams, these can be system-level measures such as repair costs, loss of power generation or loss of life downstream of the dam, or "component" measures such as gate operability.

Information about the rate of exceedance of these DVs – as well as other performance metrics derivable from $\lambda(DV)$ [110] – is useful for making risk-informed decisions for a broad range of problems. Example application can be to determine whether the expected future earthquake repair cost of a new dam is acceptable, or to assess the effectiveness of a planned dam retrofit in reducing the expected loss of power generation due to earthquakes.

Detailed loss models have been developed and made available to researchers and engineers to systematically estimate repair costs, downtime, number of casualties, etc. in buildings at different damage levels [109]. Such models are currently not available for concrete dams because of the very limited experience with earthquake damage in these

structures. As for the damage analysis phase, more research on this topic is needed before PBEE can become a routine part of dam safety assessments.

2.6 Modeling of uncertainty

Uncertainty is present at every step of the analysis process. The integration of conditional probabilities in Equation (2.1) ensures that this uncertainty is allowed to propagate from one step of the analysis to the next in the PBEE framework, thus achieving in the end a probabilistic overall prediction of the dam performance.

The resulting total uncertainty can be separated into two categories: aleatory and epistemic. The aleatory uncertainty is associated with the inherent randomness of processes, such as future earthquake events, and cannot (at least as of now) be completely eliminated. This form of uncertainty is accounted for in the PSHA, which considers a range of earthquake events and aggregates their contribution to the overall seismic risk, and in the structural analysis by considering an ensemble of different ground motions. In contrast, epistemic uncertainty is that caused by lack of knowledge about modeling assumptions, material parameters, etc., which can be reduced or completely eliminated by gathering more information.

The epistemic uncertainty in the analysis can be quantified by treating each input parameter as a basic random variable and applying statistical sampling techniques (e.g. Monte Carlo Simulations or Latin Hypercube Sampling) to estimate the variance of the analysis outputs (EDP, DM, DV) to changes in the input. However, because conducting a very large number of nonlinear RHAs of 3D dam–water–foundation rock systems is challenging, these methods are not commonly used for concrete dam analyses.

A more practical alternative is to quantify the influence of epistemic uncertainty using a so-called tornado-diagram-analysis [129,130], wherein the change in output is measured for each uncertain input by varying it from a lower limit to an upper limit while keeping all other parameters constant. From the results, a tornado diagram (Figure 2.4) is developed, and the influence of individual uncertainties on the overall response can be evaluated. Similarly, parameters that have insignificant influence on the results can be identified and treated as deterministic in subsequent analyses.

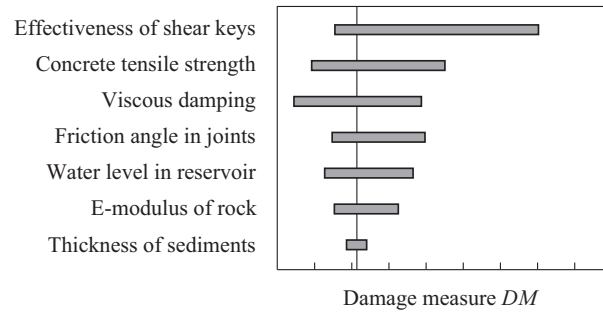


Figure 2.4: Illustration of tornado diagram. Figure adapted from [109].

3 Modeling of concrete dams by the direct FE method

Having accurate and reliable analysis procedures for predicting the nonlinear earthquake response of concrete dams is essential for successful application of the PBEE framework. To avoid introducing unnecessary error in the results, the nonlinear FE model must consider all the significant factors in the earthquake response of concrete dams (see Part II). However, implementation of the large number of RHA required for PBEE also requires that the analysis procedure is efficient, robust, and for practical reasons, possible to implement with the various commercial FE programs preferred by dam engineers. The direct FE method developed in Parts I and II of this thesis meets all these requirements. In this chapter, recommendations for practical modeling of concrete dams by the direct FE method, emphasizing modeling of nonlinear mechanisms and energy dissipation (damping), are presented.

3.1 Modeling of nonlinear mechanisms

Linear analyses cannot predict the performance of concrete dams during ground motions that are intense enough to cause extensive cracking in concrete or initiate other mechanisms of nonlinear behavior. Examples of such nonlinear mechanisms are: cracking in the dam concrete [8,82,131]; opening, closing and sliding of vertical contraction joints [83,85,132]; sliding and separation at lift joints and at concrete–rock interfaces [84,133,134]; relative movement of discontinuous rock wedges in the foundation [36,86]; and possibly, separation of water from the upstream face of the dam causing cavitation [87].

The study of these mechanisms and their influence on dam response is a vast field with extensive literature. In this section, the discussion is limited to a brief introduction to how the most influential mechanisms can be practically modeled in the direct FE method using commercial FE programs. These findings will then be utilized in the example nonlinear analysis of an actual arch dam presented in Chapter 4.

3.1.1 Cracking of concrete

Concrete dams are designed to resist static loads primarily through compressive stress fields that are much below the compressive strength of concrete, and with little or no tensile stresses. However, intense ground motions are likely to induce tensile stresses in the dam that exceed the low tensile resistance of the unreinforced mass concrete used in dam construction, typically around 10% of the compressive strength. Thus, cracking of concrete is an important mechanism to consider when evaluating the seismic safety of concrete dams.

The two most common methods for modeling crack propagation in concrete dams are the *discrete crack model* and the *smearred crack model* (Figure 3.1). Each of these are briefly

presented below; the reader is referred to the review by Bhattacharjee and Léger [135] for a more comprehensive discussion.

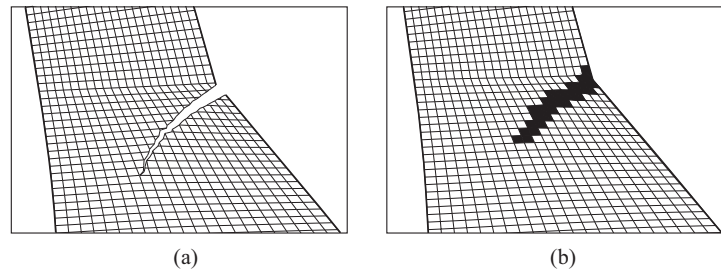


Figure 3.1: Two approaches to modeling crack propagation in FE models of concrete dams: (a) discrete crack model based on the Extended Finite Element Method (XFEM), (b) smeared crack model.

3.1.1.1 The discrete crack model

Early studies of cracking in concrete dams employed linear fracture mechanics theory and the *discrete crack model* [136] applied to 2D gravity dam models [137,138]. Modeling of discrete cracks would appear to be a physically realistic approach that can explicitly consider penetration of water in the crack, uplift pressure on crack-open surfaces, aggregate interlock at rough-crack surfaces, opening and closing of cracks, and impact and sliding of sections of the dam after extensive cracking. However, the approach is computationally challenging because the finite element mesh is redefined at each time step, and the crack propagation is strongly dependent on the size, shape, orientation and order of finite elements in the mesh; thus the results are not unique.

The preferred way to model discrete crack propagation today is the Extended Finite Element Method (XFEM) [139] that allows cracks to propagate through the finite elements, and hence does not require modification of the FE mesh. This is achieved by adding enrichment functions to the finite element approximation to account for the presence of a crack that can propagate arbitrarily through the elements. The XFEM has been employed to study the nonlinear earthquake response of both gravity dams and arch dams [131,140,141]; however, most current implementations of XFEM do not allow for multiple cracks to form within any single region, which is a significant limitation for practical analysis of concrete dams where the crack pattern is not known prior to the analysis.

3.1.1.2 The smeared crack model

To overcome the aforementioned difficulties encountered in the discrete crack model, the fracture can instead be idealized as "smeared" over the finite elements or over a certain bandwidth of the element. The *smeared crack model* [142] employs a suitable constitutive model to describe the crack initiation and the softening response of concrete during crack

propagation. After initiation of the fracture, the constitutive relation is changed from the original pre-crack relation to an updated damage relation, usually based on nonlinear fracture mechanics theory [143]. This eliminates the need for remeshing as the only factor requiring updating is the constitutive relationship, thus making it computationally attractive, but with the disadvantage that it can cause diffuse crack patterns and is unable to provide information about the physical dimensions of the crack. Various implementations of the smeared crack model have been used to study crack propagation in both 2D gravity dam systems [8,12,82,140] and 3D arch dam systems [131,144]. Most commercial FE programs have one or more variations of the smeared crack model available.

The plastic damage model for cyclic loading of concrete proposed by Lee and Fenves [82] is a variation of the smeared crack model. Several features of this model have made it attractive for earthquake analysis of concrete dams. By keeping track of tensile damage and compressive damage through two damage variables d_t and d_c , the complex stiffness change in concrete during cycling loading (Figure 3.2a) – where the stiffness in compression is recovered when a crack closes, but the stiffness in tension is not – can be simulated. The model also allows for the conceptual separation of the behavior in tension into two parts: linear stress–strain relation before the tensile strength, f_t , is exceeded (Figure 3.2b); and softening behavior after crack initiation described by fracture mechanics theory relating stresses to crack opening displacements u_{cr} (Figure 3.2c). This approach to defining the behavior after crack initiation offers two important advantages. First, the dissipated fracture energy per unit length of crack remains independent of the FE mesh, thus ensuring that the results are less sensitive to mesh size [82,143]. Second, it introduces the concept of the *specific fracture energy* for concrete, G_F , defined as the area under the stress–crack opening displacement curve (Figure 3.2c). The two significant material parameters for this model, the tensile strength f_t and specific fracture energy G_F , can both be determined experimentally: f_t from a direct tensile test or splitting tensile test [145], and G_F from a wedge splitting test [146,147].

Experimental tests have shown that the strength of mass concrete increases at higher strain rates, which can be modeled by increasing the static fracture parameters [145,147]. However, there is no clear consensus in the literature on what is an appropriate value for such dynamic magnification. Because of the high uncertainty in specifying material parameters for cracking models, the sensitivity of the results to the selected values should always be checked.

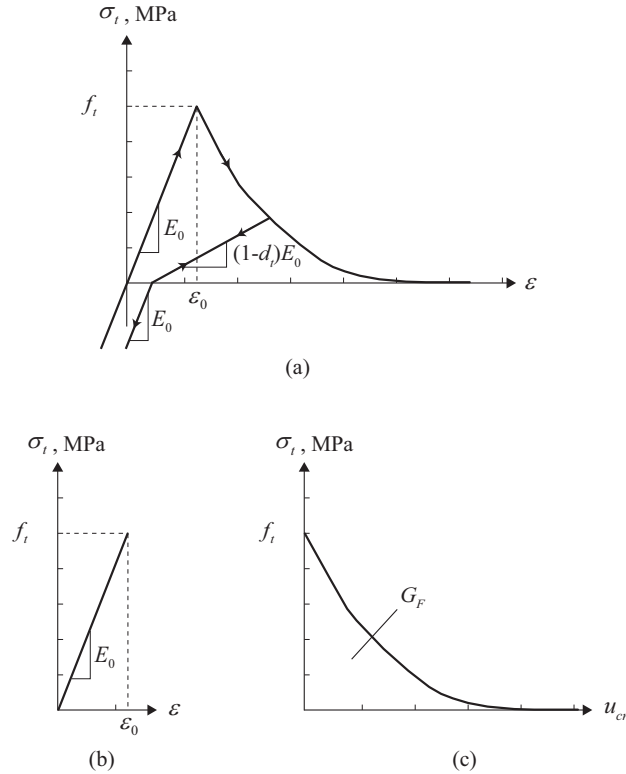


Figure 3.2: (a) Softening response of concrete under uniaxial cyclic loading; (b) linear stress–strain curve for pre-failure response; (c) post-failure stress–crack opening displacement curve, where the area under the curve is the fracture energy G_F . Figure adapted from [147].

3.1.2 Opening and closing of vertical contraction joints

Vertical contraction joints between cantilevers, which are grouted possibly with shear keys, are unable to resist any significant net tension in the arch direction, and are therefore likely to open and close during intense ground motions. This nonlinear response mechanism affects the dam response in two ways: (1) opening of a joint temporarily reduces the resistance in the arch direction, causing an increase in flexural stress and possibly horizontal cracking of cantilevers, (2) repeated opening-closing may cause compression failure of the joint. Model tests have demonstrated that these effects can have significant influence on the dynamic response of arch dams [83].

Several numerical formulations are available to model contraction joints; frequently used are discrete joint elements [10,11,85], or a contact formulation at the surfaces between cantilevers [7,141,148]. Opening and closing of the joint in the normal direction may be specified by a zero-tensile strength master-slave contact relation with a pressure-overclosure

relationship (Figure 3.3a) to prevent node penetration to prevent node penetration [75]. Alternatively, the joint failure under combined normal and shear forces can be modeled by a traction separation law based on nonlinear fracture mechanics theory. In the tangential directions, shear keys can be modeled by very stiff linear springs; if shear keys are not present, frictional sliding can be modeled by the Mohr-Coulomb friction criterion (Figure 3.3b): $\tau = \sigma \tan \phi + c$, where τ is the shear stress, σ the normal stress, and the material parameters ϕ and c represents the friction angle and cohesion of the joint, respectively.

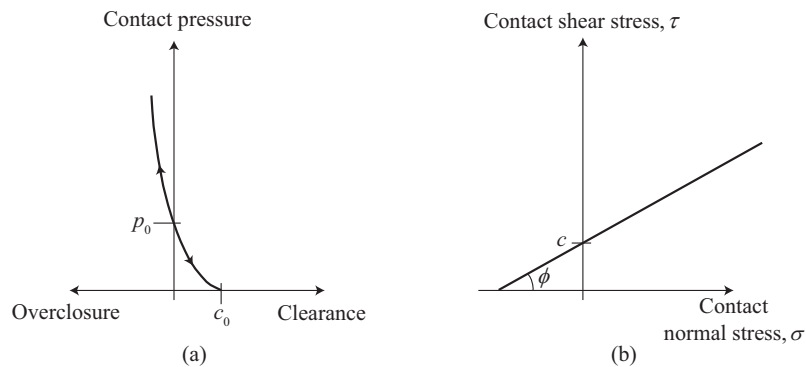


Figure 3.3: (a) Exponential pressure-overclosure relation for normal contact in contraction joint, where c_0 is the clearance at zero pressure and p_0 the pressure at zero opening. (b) Mohr-Coulomb friction criterion.

Figure adapted from [75].

3.1.3 Sliding and separation at lift joints and concrete-rock interfaces

The properties of lift joints and concrete–rock interfaces are greatly influenced by how the surface was prepared before pouring the next concrete lift. Even with good preparation, the strength and fracture properties at these joints are usually much lower than values for mass concrete [133,149,150]. Thus, cracks are likely to form along these joints rather than through the mass concrete.

Lift joints and concrete–rock interfaces can be modeled by joint interface elements [84,151] or by a contact formulation. The failure of the joint can be defined by a traction-separation law, with the residual strength described by the Mohr-Coulomb friction criterion. However, the high degree of uncertainty regarding the properties of lift joints and concrete–rock interfaces – such as tensile strength, fracture energy and roughness – makes it difficult to specify material parameters for these models with confidence. Thus, sensitivity analyses should always be conducted.

3.1.4 Discontinuities in the foundation rock

The foundation near a dam behaves nonlinearly because it is often fractured and discontinuous, with weak planes permitting sliding and separation of rock masses at these surfaces. During an earthquake, the increase in forces transmitted to the foundation from the dam may initiate shear failure along these weak planes.

Planes of weakness in the foundation rock can be modeled using nonlinear joint elements [84,151], or assemblages of individual rock wedges can be modeled using the discrete element method (DEM) [86]. Such modeling is a very challenging problem, particularly because detailed information about subsurface rock conditions at dam sites is usually limited. Consequently, such detailed modeling is often excluded from the dynamic analysis of the dam–water–foundation system. However, given that experience shows that most major concrete dam failures have been initiated in the foundation [152], the potential for instabilities in the foundation should always be evaluated by supplemental analyses.

3.2 Modeling of energy dissipating mechanisms

The FE model of the dam–water–foundation rock system includes three main sources of energy dissipation that combine to form the total (linear) damping in the system: (1) material damping in the concrete and rock, (2) radiation damping in the semi-unbounded foundation and fluid domains, and (3) dissipation of hydrodynamic wave energy at the reservoir boundaries.

3.2.1 Material damping

Modeling of material damping in dam concrete and foundation rock is highly uncertain, even when restricted to the linear range of behavior. Phenomenological modeling of these mechanisms is not practical due to the lack of experimental data on the energy dissipating behavior of mass concrete and rock under seismic loading conditions [8]. As a substitute, highly idealized linear viscous damping models, such as modal damping or Rayleigh damping, are almost invariably used. It is widely accepted that these models do not represent any actual physical mechanism, but are instead used for their mathematical convenience.

3.2.1.1 *Modification of Rayleigh damping for nonlinear modeling*

In most commercial FE codes, the linear damping matrix \mathbf{c} is constructed by assembling damping submatrices \mathbf{c}_c and \mathbf{c}_r for the dam concrete and foundation rock, respectively, using mass- and stiffness proportional Rayleigh damping in the form $\mathbf{c} = a_0\mathbf{m} + a_1\mathbf{k}$, where the Rayleigh coefficients a_0 and a_1 are determined from a viscous damping ratio specified for the dam concrete and foundation rock, separately, at a selected frequency. Usually, this frequency is chosen as the fundamental natural frequency of the dam–foundation rock or dam–water–foundation rock system.

Although Rayleigh damping is commonly used for several classes of structures including buildings and bridges, it does not seem to be appropriate for continua of mass concrete and rock. Mass-proportional damping is inappropriate in the presence of sliding of the dam along the dam–foundation rock interface or cracks that extends through the dam thickness because it causes spurious damping forces that prohibit sliding and overturning of sections above an open crack [12,153,154]. Stiffness proportional damping is intuitively more appealing because the element damping forces are proportional to deformation rates in the element (specifically, the relative velocity between nodes). Stiffness proportional damping matrices for the dam concrete and foundation rock, respectively, are defined as: $\mathbf{c}_c = a_{1c}\mathbf{k}_c$ and $\mathbf{c}_r = a_{1r}\mathbf{k}_r$.

In nonlinear RHA, this damping matrix should not be constructed using the initial stiffness matrix, \mathbf{k}^0 , because this can lead to transfer of tensile damping forces across open cracks that can falsely prohibit crack growth and cause diffuse crack patterns [8,154]. To overcome this issue, several solutions have been proposed: (1) setting the element damping to zero upon initial cracking of an element [12]; (2) using the tangent stiffness matrix instead of the initial stiffness matrix [8]; (3) capping the damping forces at a maximum value for each element [154]; or (4) using the degraded elastic stiffness matrix $\mathbf{k}^{el}(t)$ [82] that is a function of the damage variables d_t and d_c (Section 3.1.1.2). The latter of these approaches has the advantage that it eliminates transfer of tensile damping forces when a crack is open ($d = 1$), but allows for recovery of compressive damping forces upon closing of the crack ($d < 1$). Most commercial FE software has one or several of these options available; however, they are not always activated in the default settings.

3.2.2 Radiation damping

Seismic waves reflected from the dam to propagate outwards in the semi-unbounded foundation domain will not be reflected back unless there is a sharp impedance difference, which generally do not exist at dam sites. This mechanism for energy dissipation, called radiation damping, can be significant for seismic waves in the foundation domain, but less so for hydrodynamic waves in the fluid domain, except at high frequencies [2].

Presented in Figure 3.4 is the added damping due to dam–foundation rock interaction – which is primarily attributable to radiation damping – for 2D gravity dams and 3D arch dams supported on homogeneous foundations. Observe that radiation damping is a major source of energy dissipation for 2D gravity dam models unless the rock is much stiffer than concrete; however, for arch dams the effect is much less significant. The large added damping in the 2D system is caused by the assumption of homogeneous rock, which implies no wave reflections in the foundation domain. For other foundation idealizations (e.g. a layered halfspace) the radiation damping effects will be smaller due to multiple reflections and refractions of waves in the layered system.

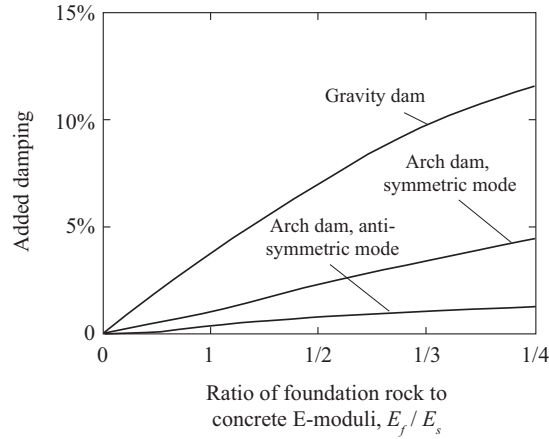


Figure 3.4: Additional damping in the fundamental mode of vibration due to dam–foundation interaction for 2D gravity dams and 3D arch dams supported on foundation modeled as a homogeneous halfspace. Data for gravity dams are from Ref. [76] and arch dams from Ref. [106].

3.2.3 Energy dissipation at the reservoir boundaries

The bottom of a reservoir upstream of the dam may consist of highly variable layers of exposed bedrock, alluvium, silt, and other sedimentary materials. Hydrodynamic wave energy is dissipated at these boundaries by two mechanisms: (1) water–foundation rock interaction causing radiation of wave energy to the underlying semi-unbounded foundation domain; and (2) energy absorption in the sediments deposited at the reservoir boundaries.

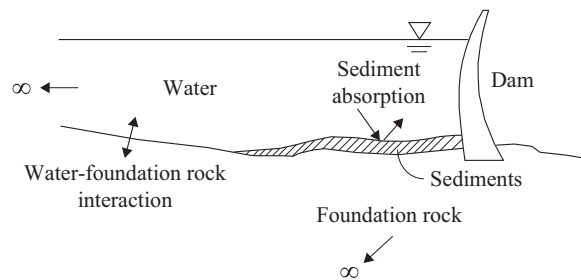


Figure 3.5: Conceptual overview of two mechanisms for energy dissipation at reservoir boundaries: (1) water–foundation rock interaction, (2) absorption in sediments deposited at the reservoir bottom.

Most of the past investigations of the effects of sediments deposited at reservoir boundaries have been based on results from the substructure method, wherein water–foundation rock interaction is ignored and sediments modeled implicitly by the one-

dimensional wave reflection coefficient, α [2,155]. The effects of sediments on dam response are re-investigated here by the direct FE method, where water–foundation interaction is rigorously included, and the sediments – with their thickness and extent – can be explicitly modeled by finite elements.

Researchers have primarily investigated two types of material models for sediments: a two-phase fluid saturated poroelastic model, and a viscoelastic model. The most sophisticated of these is the two-phase fluid-saturated poroelastic material [49,50]. It has been demonstrated that sediments modeled in this manner have little influence on the response of concrete dams if the sediments are fully saturated, but show great influence if they are partially saturated, even for very small variations in the degree of saturation [50,156]. This two-phase poroelastic model is presently not ready for practical application, for two reasons: (1) the dam response is extremely sensitive to the degree to which sediments are saturated, a quantity that cannot be determined precisely; and (2) the model requires detailed information on sediment properties such as grain size, porosity and hydraulic conductivity, for which data is not available for reservoirs impounded behind dams.

A simpler model for sediments is a viscoelastic material [47,48], characterized by familiar parameters: modulus of elasticity E_{sed} , Poisson's ratio ν_{sed} , material density ρ_{sed} , and material damping ratio. These properties have rarely been measured at dam sites, but data exists in the literature for river delta deposits and marine underwater sediments (e.g. [157]). Thus, the viscoelastic material model seems to be a pragmatic choice for modeling sediments in the direct FE method. However, it will be demonstrated next that sediments modeled in this manner may have very little influence on dam response.

3.2.3.1 Gravity dams

The effect of sediments on the dynamic response of a gravity dam is investigated first. Determined by the direct FE method, frequency response functions for the idealized 2D gravity dam on flexible foundation with full reservoir used in Section 5.4 of Part I are presented in Figure 3.6 for three values of the moduli ratio E_f / E_s . For each moduli ratio, two cases are compared: (1) no sediments at the reservoir bottom, and (2) sediment layer modeled as a viscoelastic material. The viscoelastic sediments have uniform thickness $H_{sed} = 0.1H$, where $H = 120$ m is the height of the dam, $\rho_{sed} = 1600$ kg/m³, $\nu_{sed} = 0.46$, viscous damping = 10% and pressure wave velocity = 1700 m/s ($E_{sed} = 1.0$ GPa); these properties are based on typical values for saturated underwater sediments [157].

The results in Figure 3.6 demonstrate that sediments have little influence on gravity dam response to horizontal ground motion; the first resonant peak – which is the most significant in earthquake response of dams – is unaffected, but the response at higher frequencies is more noticeably affected. Relatively speaking, sediments have more influence on the frequency response functions for vertical ground motion. The discrepancy in response at the first two resonant frequencies is noticeable, although it is small, and the response at

higher resonant frequencies is greatly influenced by sediments with the resonance peaks almost completely eliminated.

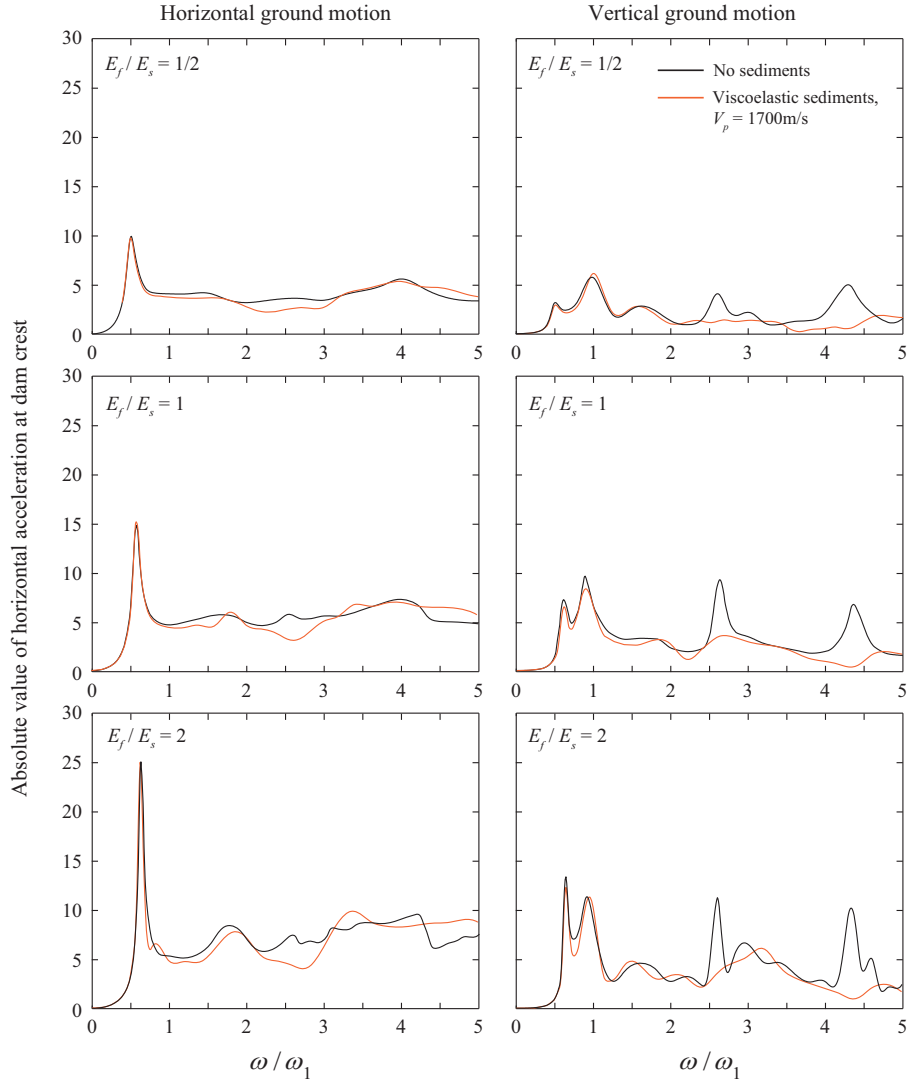


Figure 3.6: Influence of sediments on the response of idealized gravity dam on flexible foundation rock with full reservoir due to horizontal and vertical ground motion. Results are plotted against normalized frequency ω/ω_1 where ω_1 is the fundamental frequency of the dam on rigid foundation.

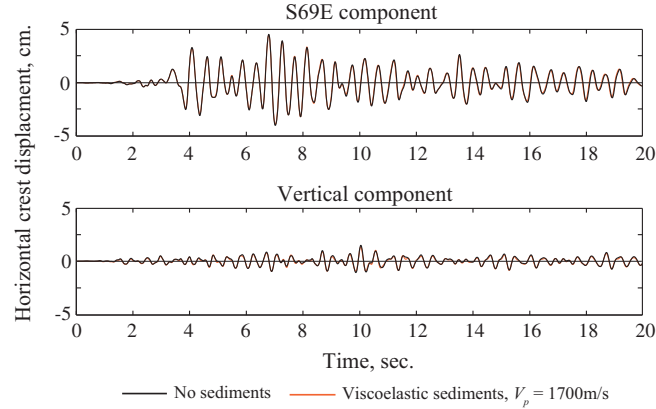


Figure 3.7: Influence of sediments on the displacement response of idealized gravity dam on flexible foundation rock with full reservoir due to the S69E and vertical components, separately, of the Taft ground motion; $E_f / E_s = 1.0$.

The influence of sediments on the earthquake response of the gravity dam is not significant however, as confirmed by the two sets of response histories presented in Figure 3.7, which are essentially identical. Similar results have been reported by other researchers [48,158,159].

3.2.3.2 Arch dams

The effect of sediments on arch dam response is investigated next. Determined by the direct FE method, frequency response functions for Morrow Point Dam (properties described in Section 5.2.1 of Part II) are presented in Figure 3.8 for two cases: (1) no sediments at the reservoir boundaries, (2) sediment layer modeled as a viscoelastic material. The sediments have uniform thickness $H_{sed} = 0.1H$, where $H = 142\text{m}$ is the dam height, $\rho_{sed} = 1600 \text{ kg/m}^3$, $\nu_{sed} = 0.46$ and viscous damping = 10%; two values for the pressure-wave velocity are considered, 1400 m/s ($E_{sed} = 0.68 \text{ GPa}$) and 1800 m/s ($E_{sed} = 1.12 \text{ GPa}$). The results demonstrate that, just as in the case of gravity dams, sediments have small influence on the dam response: the first two resonant peaks due to ground motions in the stream and cross-stream directions, and the first resonant peak due to vertical ground motion, are essentially unaffected, but responses at higher resonant frequencies are more noticeably affected. Where differences are noticeable, ignoring sediments tends to be a conservative assumption.

The overall influence of sediments on earthquake response of the arch dam is not significant however, as demonstrated by the two sets of displacement and acceleration response histories presented in Figure 3.9, which are nearly identical.

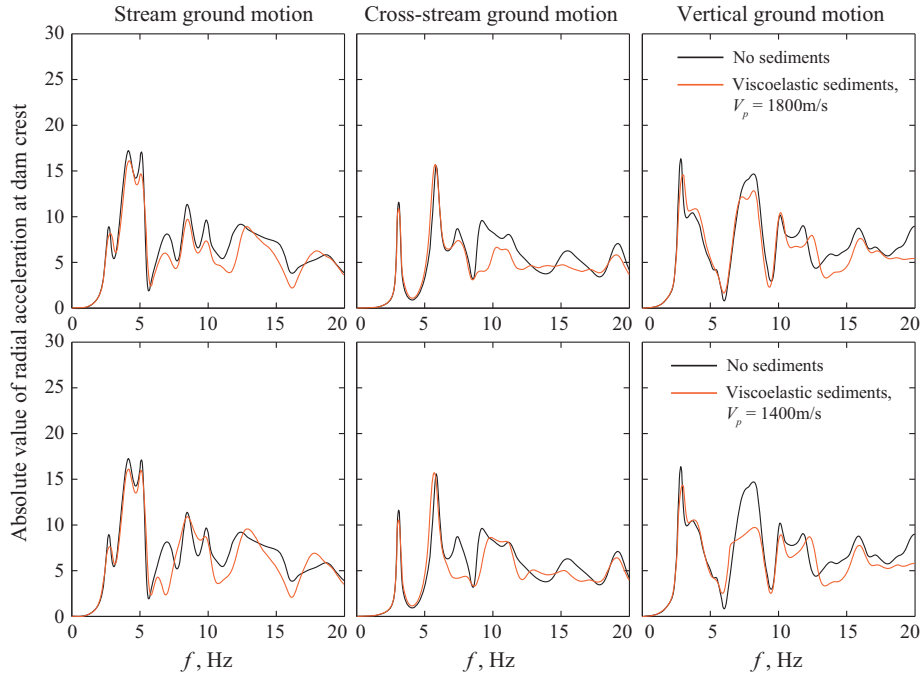


Figure 3.8: Influence of sediments on the response of Morrow Point Dam on flexible foundation rock with full reservoir subjected to stream, cross-stream and vertical ground motions.

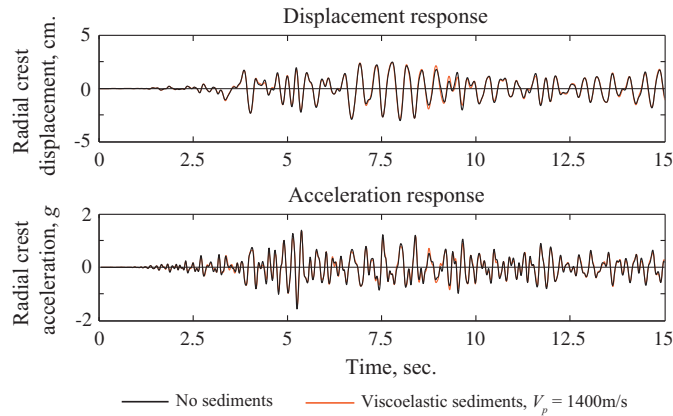


Figure 3.9: Influence of sediments on the earthquake response of Morrow Point Dam on flexible foundation rock with full reservoir subjected to the S69E, S21W and vertical components, applied simultaneously, of the Taft ground motion.

3.2.3.3 *Can sediments be ignored?*

The preceding results indicate that the influence of sediments at the reservoir boundaries – modeled as a viscoelastic material – has negligible influence on the response of gravity dams as well as arch dams. Because water–foundation interaction and the associated radiation damping is included in the analysis, the additional loss of vibration energy due to sediments is apparently of little consequence. Thus, at the present time, it seems reasonable to ignore sediments in analysis of dam–water–foundation systems by the direct FE method.

This conclusion may seem to contradict earlier results obtained by the substructure method, which found that sediments may influence dam response significantly [2,155]. Because water–foundation interaction (and the associated radiation damping) is ignored in the substructure method, the loss of vibration energy associated with wave absorption in the α -model apparently becomes significant.

3.2.4 Calibration of damping values

Damping in the numerical model for the dam–water–foundation system should be consistent with measured values at the dam determined from low-amplitude motions – within the linear range of response – recorded during forced vibration tests, ambient vibrations or small earthquakes. Obviously, these measured values represent the *overall* damping in the system, including material damping, radiation damping, and energy loss at the reservoir boundaries; experimental data on the contributions of individual sources is generally not available.

Summarized in Figure 3.10 are data for damping "measured" at 32 concrete dams determined by forced vibration tests and ambient vibration measurements [80,160,161]. Both gravity dams and arch dams covering a wide range of system parameters are included. The overall damping values measured at these dams are all in the range of approximately 1–5%. These comprehensive data lead to an important conclusion: overall damping in the numerical model should generally not exceed 5% unless a larger value was "measured" at the particular dam. In contrast, the current practice of specifying a viscous damping ratio of 5% for the concrete dam and a similar value for the foundation domain will lead to damping in the range of 10–15% in the overall dam–water–foundation system [76,106]. Thus, this current practice of choosing damping values should be abandoned because it will underestimate the earthquake response of dams.

Material damping in the numerical model is usually specified separately for the two substructures, dam and foundation; however the contributions from energy loss at the reservoir boundaries and radiation damping are not known prior to the earthquake analysis of the dam. It is therefore not possible to know in advance the damping values that should be specified for the two substructures to achieve a target value of, say, 5% overall damping. Thus, material damping in the two substructures should be determined by trial and error to achieve an overall damping consistent with the target value. The overall damping in the

numerical model can be determined from frequency response functions or system identification techniques applied to the response histories.

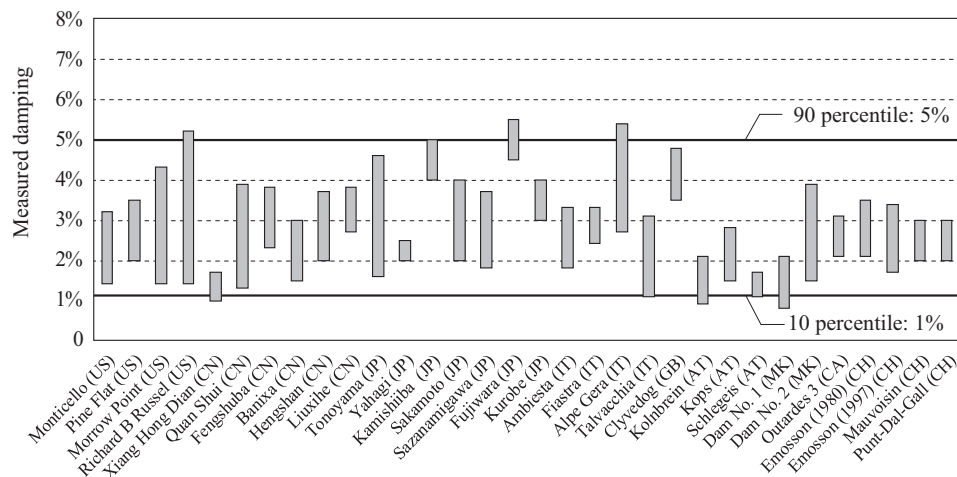


Figure 3.10: Measured damping at 32[†] concrete dams during forced vibration field tests and ambient vibration measurements, compiled from Refs. [80,160,161]. The range for each dam shows the minimum and maximum damping values measured at the first few (1-5) resonant frequencies.

Based on a sensitivity study conducted during this thesis (not included here) and reported cases in the literature, it is found that specifying damping in the range of 1–2% for the dam concrete and 1–4% for the foundation rock is likely to lead to overall damping in 3D analysis models is consistent with the range of measured values in Figure 3.10. For example, viscous damping ratios of 1% and 3% for the dam and foundation, respectively, in the case of Mauvoisin Dam; 2% and 4%, respectively, for Pacoima Dam; and 1% and 2%, respectively, for Morrow Point Dam, combined to provide damping in the overall dam–water–foundation system that was consistent with measured damping for these dams: 2–3% for Mauvoisin Dam, 6–7% for Pacoima Dam and 1.5–4% for Morrow Point Dam. Responses computed from the numerical models for Mauvoisin Dam and Pacoima Dam were in good agreement with motions recorded during small earthquakes at these two dams [79]. More recent examples include analyses of Tagokura gravity dam (1% in dam, 0% in foundation) and Kurobe arch dam (1% in dam, 0% in foundation) [98].

Limiting the overall damping to less than 5% in 2D numerical models is very difficult because of the large amount of radiation damping associated with 2D homogeneous, semi-unbounded foundation models (Figure 3.4). Presented in Table 3.1 are examples of total

[†] Four data points that were deemed inaccurate in Ref. [160] due to excessive modal interference in the dam response are excluded from the data set.

damping in a 2D model of Pine Flat Dam computed by the substructure method [17] for several values of the parameters that characterize energy loss in the system: material damping in the dam, ζ_s ; material damping in the foundation, ζ_f ; the moduli ratio of the foundation to the dam concrete, E_f / E_s ; and the reservoir bottom reflection coefficient α , which is computed based on rock properties alone. For example, specifying 2% damping in the dam and 2% for the foundation domain (Case 2 in Table 3.1) leads to overall damping of approximately 10% in the 2D numerical model, which is much higher than the 2–4% damping "measured" at the dam during forced vibration tests [162].

Observe from Table 3.1 that it is not possible to achieve consistency with the measured damping for Pine Flat Dam unless the foundation is much stiffer than concrete and essentially zero material damping is specified in the dam as well as the foundation. Thus, for final design analysis, 2D numerical models may have to be abandoned in favor of 3D models, which also permit realistic modeling of the 3D geometries of gravity dams.

Table 3.1: Overall damping resulting in a 2D numerical model of Pine Flat Dam computed by the substructure method for several values of the parameters that characterize energy loss in the system.

Case	Dam	Foundation rock		Reservoir bottom	Overall damping
	ζ_s	E_f / E_s	ζ_f	α	
1	5%	1	5%	0.68	13%
2	2%	1	2%	0.68	10%
3	0%	1	0.5%	0.68	8.5%
4	0%	2	0.5%	0.77	5.0%
5	0%	3	0.5%	0.80	3.7%

4 Nonlinear earthquake analysis of Morrow Point Dam

The direct FE method developed in Parts I and II of this thesis has been proposed as a tool for conducting the large number of RHAs required for PBEE of concrete dams. In this chapter, the capabilities of the direct FE method to conduct such analyses are demonstrated by performing a nonlinear earthquake analysis of an actual arch dam using the commercial FE code ABAQUS [75]. A step-by-step procedure for how to use the direct FE method with any FE program is presented, example outputs from the nonlinear RHA of engineering interest are shown, and use of the direct FE method as a tool for PBEE of concrete dams is discussed.

4.1 System and ground motion

4.1.1 FE model of dam–water–foundation rock system

Chosen for the example analysis is the 142m high Morrow Point Dam. The FE mesh of the dam, foundation rock and fluid shown in Figure 4.1 includes 4,196 solid elements for the dam (with four elements through the dam thickness), 14,175 solid elements for the foundation domain, and 9,200 acoustic elements for the fluid domain. A tie constraint couples accelerations with hydrodynamic pressures at the dam–water and water–foundation rock interfaces, and standard viscous dampers are included at all outer boundaries to model the semi-unbounded extent of the foundation and fluid domains. The overall dimensions of the FE model are 700m x 700m x 400m, corresponding to approx. $5H \times 5H \times 3H$, where H is the height of the dam.

The elastic material properties for the dam–water–foundation rock system are the same as those in Section 5.2.1 of Part II of this thesis, but for two exceptions: (1) sediments at the reservoir bottom and sides are not included because their effects on the dynamic response of arch dams are negligible (Sec. 3.2.3); (2) material damping in the dam and foundation is modeled by stiffness proportional damping using the degraded elastic stiffness matrix instead of the initial stiffness (Sec. 3.2.1.1). The damping coefficients $a_{1c} = 1.1 \times 10^{-4}$ and $a_{1r} = 2.2 \times 10^{-4}$ were chosen to give 1% damping in the dam and 2% in the foundation at the fundamental vibration period of the dam–water–foundation system. With these values, the overall damping in the system is within the range of 1.5–4% damping measured at the first few resonant frequencies during forced vibration tests in the 1980s [104].

4.1.2 Nonlinear modeling parameters

Included in the numerical model are several nonlinear mechanisms based on the review in Section 3.1. Opening and closing of contraction joints (Figure 4.1a) is modeled using the "general contact" model in ABAQUS, with properties in the normal direction is specified by a zero-tensile-strength contact constraint with an exponential pressure-overclosure relationship given the following properties: initial clearance $c_0 = 0.1$ mm and contact pressure at zero opening $p_0 = 5$ MPa. Morrow Point Dam was constructed with large and frequent shear keys that limit relative tangential movements between cantilevers unless the joint opens more than approximately 150 mm (6 inches) [163]. These are modeled by linear springs given very high stiffness to effectively prevent tangential slip at the joint.

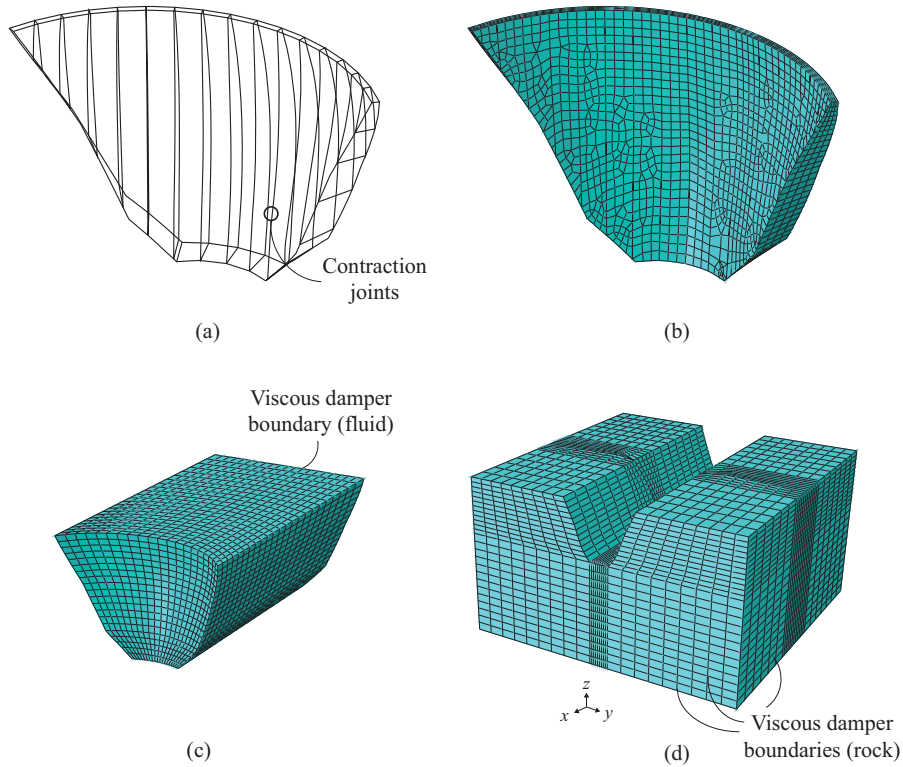


Figure 4.1: (a) Morrow Point Dam showing location of contraction joints; (b) FE model of dam; (c) FE model of water in reservoir; (d) FE model of foundation rock.

The dam–foundation rock interface is approximately modeled using a zero-tensile-strength contact constraint to allow opening and closing of this joint, but relative tangential sliding is prevented using linear springs with high stiffness. For simplicity, the effects of weaker planes along lift lines in the dam are not modeled.

Cracking of the dam concrete is modeled by the Lee–Fenves concrete damage model [82], but excluding the possibility of compression failure after an initial analysis confirmed that the maximum compressive stresses are much lower than the compressive strength of concrete. The tensile fracture properties for this model (Figure 4.2) are based on typical values for dam concrete [135,164]: tensile strength, $f_t = 2.5$ MPa and specific fracture energy $G_F = 250$ N/m. These static values are increased by a dynamic magnification factor of 1.20 to represent the effects of higher strain-rates in the dynamic analysis; thus $f_{t,dyn} = 3.0$ MPa and $G_{F,dyn} = 300$ N/m.

The nonlinear dynamic analysis is conducted in ABAQUS/Standard using the implicit HHT-alpha [66] time integration scheme and an automatic time step control that changes the time increment depending on the convergence rate of the solution. Convergence is checked at the end of each time step as the analysis progresses, and in addition, the energy balance error [8] is controlled at the end of the analysis to ensure that the overall solution remained stable.

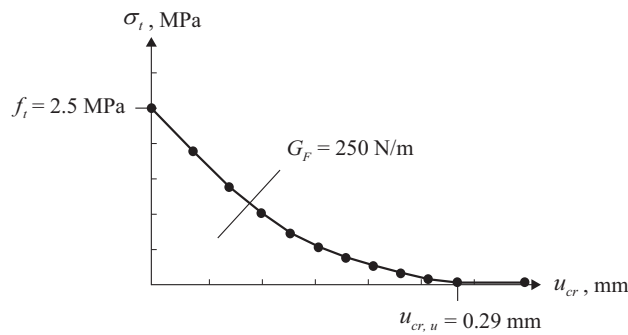


Figure 4.2: Stress-displacement curve for concrete in tension (static values).

4.1.3 Static and dynamic loads

An initial static analysis is conducted using a model with outer boundaries of the foundation domain fixed. Gravity loads are applied to the dam cantilevers first, then the reservoir is filled, and hydrostatic pressures applied; uplift pressures at the dam–foundation interface are not modeled. The state of the dam and foundation domain at the end of this static analysis is recorded to define the initial state for the nonlinear dynamic analysis.

The free-field control motion, $a_g^k(t)$, specified at the surface of the foundation domain (at the level of the dam abutments) is defined in the stream, cross-stream and vertical directions by the S69E, S21W and vertical components, respectively, of the Taft ground motion. Each component of ground motion is amplitude-scaled by a factor of 2.0,

corresponding to a PGA of approximately $0.35g$ for the S69E component[†]. From the specified control motions, effective earthquake forces at the bottom and side foundation boundaries are determined by the method described in Section 6.1 of Part II.

4.2 Implementation of the direct FE method with ABAQUS

The direct FE method has been developed in a form that can be implemented with any commercial FE code. Here, ABAQUS was chosen and used with a simple pre-processing script in MATLAB developed to interact with the input file to compute and store the effective earthquake forces. This procedure is organized in three phases: (1) an initial static analysis simulates the sequence of construction of the dam and filling of the reservoir; (2) deconvolution of the free-field control motion followed by analysis of a 1D foundation column determines the effective earthquake forces at the bottom and side boundaries of the foundation domain; and (3) nonlinear dynamic analysis of the FE model subjected to effective earthquake forces from Step 2, where the results from Step 1 provide the initial state of the system.

Thus, the only addition to a "standard" dynamic analysis in ABAQUS is the use of the MATLAB script in Step 2, which conducts the following tasks (Figure 4.3): first, the mesh and material properties of the foundation domain are extracted from the ABAQUS input file. The earthquake ground motion is deconvolved, and effective earthquake forces are computed at the bottom boundary using the procedure in Box 4.1 of Part II. Then, following the procedure in Box 6.1 of Part II, a 1D foundation column is analyzed to determine free-field displacements over the height of the foundation that are used with 1D stress-strain relations to compute effective earthquake forces at the side boundaries at various elevations. Finally, these computed forces are mapped to each node on the four sides of the actual foundation domain mesh and stored for later use.

This process for setting up the model for nonlinear dynamic analysis is general and can be implemented with any FE code. The process is entirely automated, and requires less than a few minutes to produce an updated input file that – together with the static state of the system – contains all information required for dynamic analysis. Thus, the analysis can easily be set up to run repeatedly for a large number of ground motions, or for the same ground motion for a range of input parameters, both of which are required to quantify uncertainty within the PBEE framework (Chapter 2). The resulting set of input files can then be deployed in batches to a high performance computing (HPC) service locally or in the cloud to save significantly on computational time.

[†] No attempt has been made to select ground motions consistent with the seismic hazard at the site of Morrow Point Dam; thus, the results presented in Section 4.3 are merely illustrative

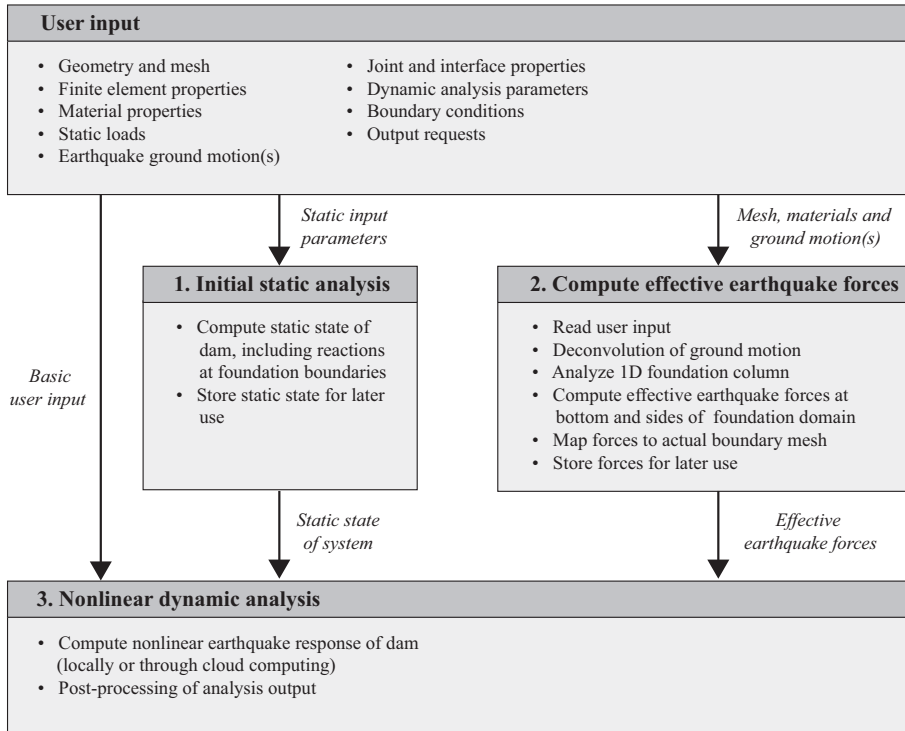


Figure 4.3: Implementation of the direct FE method with a commercial FE program.

4.3 Results from nonlinear dynamic analysis

Commercial FE codes can provide results for any response quantity of engineering interest; examples of such output are presented in Figures 4.4–4.8. Displacement response histories in the stream, cross-stream and vertical directions at the midpoint on the dam crest are shown in Figure 4.4, and envelope values of the stream displacements over the length of the crest in Figure 4.5. Such results are of interest in evaluating the operability of appurtenant structures, such as mechanical equipment, gates and roadway bridges, over any spillway.

To illustrate the nonlinear contraction joint response, two types of output are presented: response histories for the opening of two contraction joints at the crest level are plotted as a function of time in Figure 4.6, and envelope values of the maximum (over time) opening of all joints at the crest level is presented in Figure 4.7. The maximum opening of any contraction joint is approximately 25 mm (near the right abutment), which is much less than the 150 mm "depth" of the shear keys, implying that the shear keys remain interlocked during the selected ground motion. Interestingly, the maximum joint opening occurs near the right abutment, and not at the center of the dam (Figure 4.7), which illustrates the significance

of the cross-stream component of ground motion for this particular system. Had the dam been excited only in the stream and vertical directions, it would have responded much more symmetrically due to its (almost) symmetric design.

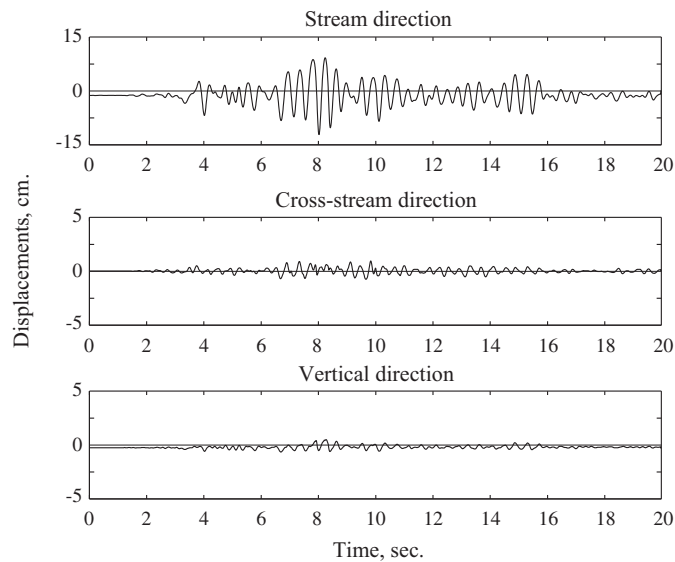


Figure 4.4: Displacements histories at center of dam crest in the stream, cross-stream and vertical directions, caused by simultaneous application of the S69E, S21W and vertical components of the Taft ground motion.

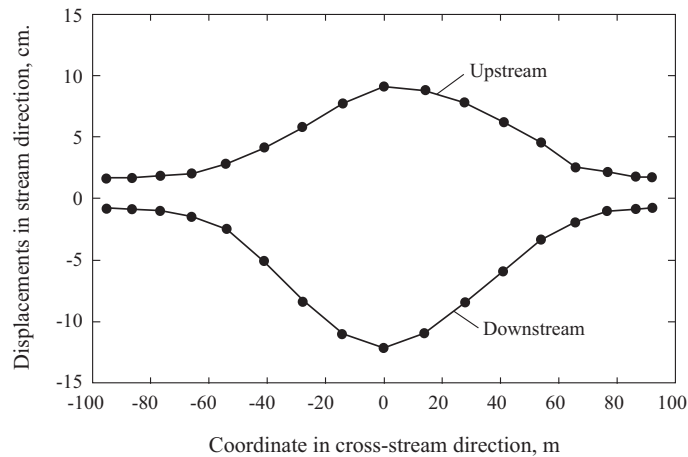


Figure 4.5: Envelope values of maximum and minimum displacements along dam crest.

The distribution of tensile damage over the two faces of the dam is presented in Figure 4.8. While this is not a direct measurement of cracking in the concrete, it gives an indication

of areas to expect cracks in the dam. The tensile damage is greater on the downstream face of the dam and along one side of the dam–foundation interface (Figures 4.8a and b). The dam is beginning to show signs of a semi-circular crack pattern in the upper, central part of the dam, which has been observed as a potential failure mode during model studies of arch dams [165]. However, no single crack has yet formed through thickness of the dam (Figure 4.8c) to fully develop such a mechanism.

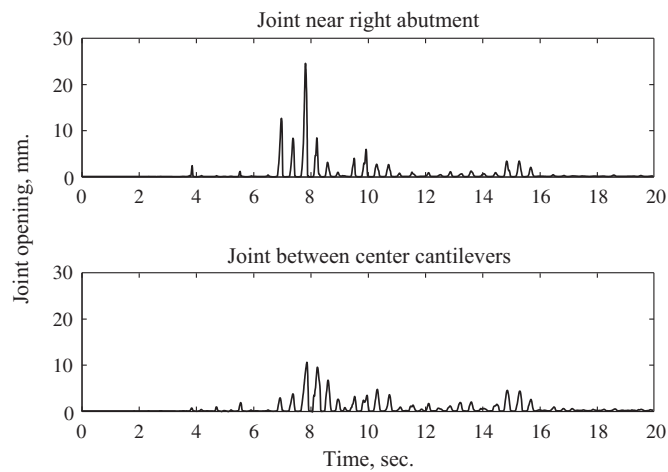


Figure 4.6: Opening of contraction joints at two locations: at the joint near the right abutment where maximum joint opening occurs, and at the joint between the center cantilevers.

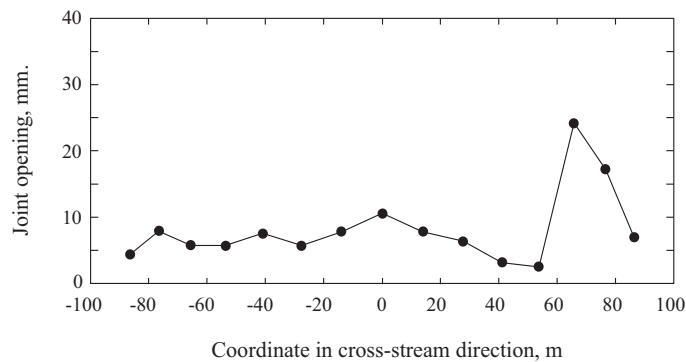


Figure 4.7: Envelope values of maximum contraction joint opening along the dam crest.

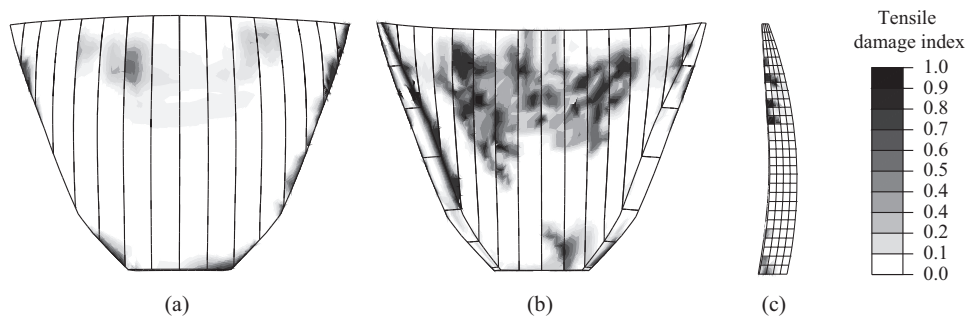


Figure 4.8: Distribution of tensile damage on (a) upstream face, (b) downstream face, (c) section through center (crown) cantilever.

Engineering demand parameters obtained from nonlinear RHA (such as the ones presented in Figures 4.4–4.8) can be systemized to quantify the performance of concrete dams over a wide range of possible scenarios. For example, by doing repeated nonlinear RHA for an ensemble of ground motions scaled to different intensity levels, the SDHC and fragility curves (Sections 2.3–2.4) for the structure can be computed for any EDP or DM of interest. The effects of uncertainty in input parameters can be estimated by repeated analysis of the system in a tornado-diagram analysis. As previously mentioned, such information is essential for making risk-informed decisions regarding the performance of dams.

The total runtime for the analysis was approximately 15 hours on a local workstation, of which only a few minutes were required for setting up the effective earthquake forces. This runtime can be reduced significantly by deploying the analysis to a HPC service locally or in the cloud. Utilizing such services to run analyses with the direct FE method is especially attractive for conducting the large number of nonlinear RHAs required to consider the inherent uncertainties in ground motions and the material properties of the system.

5 Conclusions

Using the direct FE method for conducting the large number of nonlinear RHAs required for PBEE of concrete dams has been proposed. The discussion and results presented in this part of the thesis can be summarized as follows:

- The state-of-research for Performance Based Earthquake Engineering (PBEE) of concrete dams is behind that for other classes of structures such as buildings and nuclear power plants. Two factors that have contributed to this situation are: (1) the deficiencies in commonly used procedures for RHA of concrete dams; (2) the lack of knowledge about the nonlinear behavior and failure mechanisms of concrete dams during earthquakes. Development of the direct FE method addresses the first of these.
- Sediments at the reservoir boundaries – modeled as a viscoelastic material – have negligible influence on the response of gravity dams as well as arch dams when water–foundation rock interaction and the associated radiation damping is included in the analysis. Thus, at the present time, it seems reasonable to ignore sediments in analysis of dam–water–foundation systems by the direct FE method.
- Based on "measured" data at 32 concrete dams, the overall damping in the numerical model of the dam–water–foundation system should not exceed 5% unless a larger value was "measured" at the dam to be analyzed. Specifying viscous damping ratios in the range of 1–2% for the dam alone and 1–4% for the foundation domain is likely to lead to overall damping that is consistent with the measure values. Consequently, the common practice of specifying 5% viscous damping for the dam and a similar value for the foundation should be abandoned because it would significantly underestimate the earthquake response of dams.
- The direct FE method has been developed in a form that can be implemented in any commercial FE code; an example analysis implemented in ABAQUS has been presented. The procedure is entirely automated, and requires less than a few minutes of computation to produce an updated input file that – together with the static state of the system – contains all information required for dynamic analysis. The effectiveness of the procedure makes it attractive for conducting the large number of nonlinear RHAs required to recognize the uncertainties in ground motions and the material properties of the system.

Evaluating the seismic performance of concrete dams subjected to ground motions intense enough to cause damage is a very challenging problem. Although commercial FE programs contain models and material libraries capable of modeling a wide range of nonlinear mechanisms, experience in their application is limited. Quantitative measures for the extent of

PART III: CONCLUSIONS

damage – cracking in concrete, sliding at lift joints or at cracked interfaces, and opening of contraction joints – that dams can sustain while still retaining the impounded water are lacking. A great deal of innovative experimental, modeling, and analytical research must yet be done to accurately model the nonlinear behavior of mass concrete, rock, and joints; and extensive numerical parameter studies must be performed to better understand the factors that control the seismic safety of concrete dams.

CONCLUSIONS AND FUTURE WORK

Summary and conclusions

The work presented in this thesis has developed a direct FE method for nonlinear earthquake analysis of two- or three-dimensional dam–water–foundation rock systems. The analysis procedure considers all the factors important in the earthquake response of dams: dam–water interaction including water compressibility and absorption of hydrodynamic waves energy at the reservoir boundaries; dam–foundation rock interaction including mass, stiffness and damping in the rock; radiation damping due to the semi-unbounded sizes of the foundation and fluid domains; spatial variation of the ground motions around the dam–canyon interface; and nonlinear behavior in the dam and adjacent parts of the foundation and fluid domains. The key contributions of each part of the work are summarized in the following.

Part I presented the analytical framework underlying the direct FE method: treating dam–foundation rock interaction, dam–water interaction, and ultimately dam–water–foundation rock interaction as different scattering problems wherein the dam perturbs assumed "free-field" states of the system. Applying these concepts to a bounded FE model with viscous-damper absorbing boundaries to model the semi-unbounded domains, the equations of motions for the direct FE method for earthquake analysis of 2D gravity dam systems were derived. A free-field control motion specified at the foundation surface defines the earthquake input to the procedure; such motions are standard output from PSHA. The motion at the bottom of the foundation rock is determined by deconvolution of this motion. Then, effective earthquake forces at the boundaries of the foundation and fluid domains are determined from analysis of two 1D free-field systems. Several examples were presented to validate the accuracy of the direct FE method for 2D systems covering a wide range of system parameters. The excellent agreement demonstrates that (1) the effects of dam–water–foundation rock interaction are accurately modeled in the direct FE method, (2) the bounded foundation and fluid models with viscous-damper boundaries are able to simulate the semi-unbounded extent of these domains, and (3) the earthquake excitation is properly defined by specifying – at the boundaries of the FE model – effective earthquake forces determined from a surface control motion.

Part II generalized the direct FE method to 3D systems. While the fundamental concepts of treating dam–water–foundation rock interaction as a scattering problem are similar for 2D and 3D systems, the derivation of the method – but more significantly, its implementation – is more involved for 3D systems. Effective earthquake forces must now be

computed by analyzing a set of different 1D and 2D systems derived from the free-field foundation and fluid systems and applied to the boundaries of the main FE model. A wide range of numerical examples demonstrated the accuracy of the direct FE method when applied to analyze 3D problems. Even though the aforementioned sets of 1D and 2D analyses each require little computational effort and can be implemented without modifying the FE source code, the management and transfer of large amounts of data is challenging for large 3D models. To ease implementation of the direct FE method for such systems, several possible simplifications were evaluated, of which two were recommended: (1) using 1D free-field analysis to compute effective earthquake forces at the side boundaries of the foundation rock, and (2) ignoring the effective earthquake forces at the upstream fluid boundary. Through several numerical examples it was demonstrated that these approximations are appropriate as long as the sizes of the foundation and fluid domains are sufficiently large. This is normally the case when using viscous-damper boundaries because these always require large domain sizes to accurately model the semi-unbounded domains.

Part III of the thesis proposed using the direct FE method for conducting the large number of nonlinear RHAs required for PBEE of concrete dams. Even though the state of research for PBEE of concrete dams is lagging behind that for other classes of structures, interest in the topic for concrete dams is increasing. Practical implementation of two of the most uncertain aspects of nonlinear RHA of dams, modeling of nonlinear mechanisms and modeling of damping, were reviewed. It was found that (1) most commercial FE codes have ways of modeling the nonlinear mechanisms in concrete dams, the main challenge is the selection of parameters for these models; (2) viscoelastic sediments have little influence on dam response when water–foundation rock interaction is included in the FE model. As a practical simplification, the effects of sediments can therefore be ignored in the direct FE method; (3) measured damping compiled from 32 concrete dams suggests limiting the overall damping in the numerical model to no more than 5% unless there is measured data to justify higher values. Specifying material damping in the range of 1–2% in the dam concrete and 1–4% in the foundation rock is likely to achieve damping consistency for 3D models.

At the end of Part III, the direct FE method was implemented with the commercial FE program ABAQUS and used to compute the nonlinear response of an actual arch dam. The results demonstrate the capabilities of the direct FE method to compute the types of nonlinear engineering demand parameters required for PBEE of concrete dams. Utilizing cloud computing services – which are becoming increasingly available – to run analyses with the direct FE method is an attractive alternative for conducting the large number of nonlinear RHA required for PBEE of dams.

Future work

During the work with this thesis, several topics for future work were identified. Following is a summary of some of these topics.

-
- PBEE of concrete dams is still in its early days, and most of the work conducted has been focused investigations on a narrow subset of the overall framework. While such studies are useful, there is also a need for research applying all four phases of the framework in the same study. Such studies would be useful to evaluate the feasibility for adaption of the PBEE framework on an overall level, and identify subsets in each phase where focused investigations would provide the most benefit for developing the overall state-of-research.
 - The direct FE method developed in this thesis presents one solution for accurate and efficient earthquake analysis of concrete dams; obviously there are several others. An interesting project would be to develop a common set of standardized numerical examples that can be used by researchers and engineers for validation and verification of different parts of their own analysis procedures (e.g. examples to validate foundation modeling, hydrodynamic modeling, simple nonlinear examples, etc.). Once such a framework is available, different methods and models can be compared and a common understanding established in the dam engineering community as to how these methods work and what are their relative strengths and weaknesses.
 - Even though the numerical models for predicting earthquake response of concrete dams are becoming increasingly sophisticated, there remains a significant mismatch between the nonlinear behavior predicted by numerical models and the actual performance of concrete dams subjected to intense earthquakes. To explain this gap and give confidence in the output from numerical models, the numerical models must be validated against observed motions and performance of actual dams that have experienced strong earthquakes. Numerical benchmark workshops, such as those hosted by the United States Society on Dams, US Bureau of Reclamation and the ICOLD Committee on Computational Aspects of Dam Analysis and Design are great tools in this regard, and more of these should be conducted.
 - Development of ground motion selection and modification procedures is a broad field where extensive research has been conducted mostly in the context of multi-story buildings and nuclear power plants. These procedures must be extended for concrete dam analysis to account for: (1) three components of ground motion (two horizontal plus one vertical) acting simultaneously; (2) multiple vibration periods of interest; and (3) the fact that concrete dams are typically supported on firm bedrock, and not soft soils on which most of the available ground motions were recorded.
 - In the direct FE method, the ground motion at depth in the model was determined by deconvolution of a ground motion specified at a control point on the foundation surface; deconvolution assumes vertically propagating seismic waves. Overcoming this assumption requires research on how to develop realistic ground motions without making the inherent assumptions in deconvolution. Progress in this arena would be of significance not only in dam engineering, but also for other critical or expensive

facilities where soil–structure interaction is significant, such as offshore platforms and nuclear power plants.

- Researchers and practicing engineers have investigated isolated aspects of the nonlinear behavior of concrete dams; however, much research is yet to be done on studying the overall nonlinear behavior of these structures under a variety of earthquake scenarios. Performing extensive numerical parameter studies of concrete dams – considering all factors that may significantly influence dam response – will be an important step in understanding the factors that control the nonlinear seismic behavior dams.
- In addition to these numerical research objectives, there is a need for a major experimental research program for (1) investigating the nonlinear properties of mass concrete used in dam construction and its failure mechanisms under cyclic deformations at strain rates expected during seismic loading of the dam; and (2) performing shaking table tests and/or hybrid tests to verify the developed analysis models on a macro (i.e., dam level) scale.

REFERENCES

1. Chopra AK. Earthquake analysis of arch dams: Factors to be considered. *Journal of Structural Engineering* 2012; **138**(2): 205–214. DOI: 10.1061/(ASCE)ST.1943-541X.0000431.
2. Fenves G, Chopra AK. Effects of reservoir bottom absorption and dam-water-foundation rock interaction on frequency response functions for concrete gravity dams. *Earthquake Engineering & Structural Dynamics* 1985; **13**(1): 13–31. DOI: 10.1002/eqe.4290130104.
3. Tan H, Chopra AK. Dam-foundation rock interaction effects in earthquake response of arch dams. *Journal of Structural Engineering* 1996; **122**(5): 528–538. DOI: 10.1061/(ASCE)0733-9445(1996)122:5(528).
4. Hall JF, Chopra AK. Hydrodynamic effects in the dynamic response of concrete gravity dams. *Earthquake Engineering & Structural Dynamics* 1982; **10**(2): 333–345. DOI: 10.1002/eqe.4290100212.
5. Hall JF, Chopra AK. Dynamic analysis of arch dams including hydrodynamic effects. *Journal of Engineering Mechanics* 1983; **109**(1): 149–167.
6. Fenves G, Chopra AK. Effects of reservoir bottom absorption on earthquake response of concrete gravity dams. *Earthquake Engineering & Structural Dynamics* 1983; **11**(6): 809–829. DOI: 10.1002/eqe.4290110607.
7. Zhang CH, Pan JW, Wang JT. Influence of seismic input mechanisms and radiation damping on arch dam response. *Soil Dynamics and Earthquake Engineering* 2009; **29**(9): 1282–1293. DOI: 10.1016/j.soildyn.2009.03.003.
8. Bhattacharjee SS, Léger P. Seismic cracking and energy dissipation in concrete gravity dams. *Earthquake Engineering & Structural Dynamics* 1993; **22**(11): 991–1007. DOI: 10.1002/eqe.4290221106.
9. Cervera M, Oliver J, Faria R. Seismic evaluation of concrete dams via continuum damage models. *Earthquake Engineering & Structural Dynamics* 1995; **24**(9): 1225–1245. DOI: 10.1002/eqe.4290240905.
10. Dowling MJ, Hall JF. Nonlinear seismic analysis of arch dams. *Journal of Engineering Mechanics* 1989; **115**(4): 768–789.
11. Fenves G, Mojtahedi S, Reimer RB. Effect of contraction joints on earthquake response of an arch dam. *Journal of Structural Engineering* 1992; **118**(4): 1039–1055. DOI: 10.1061/(ASCE)0733-9445(1992)118:4(1039).
12. El-Aidi B, Hall JF. Non-linear earthquake response of concrete gravity dams part 1: modelling. *Earthquake Engineering & Structural Dynamics* 1989; **18**(6): 837–851. DOI: 10.1002/eqe.4290180607.
13. Mlakar PF. Nonlinear response of concrete gravity dams to strong earthquake-induced ground motion. *Computers & Structures* 1987; **26**(1–2): 165–173.
14. Vargas-Loli LM, Fenves G. Effects of concrete cracking on the earthquake response of gravity dams. *Earthquake Engineering & Structural Dynamics* 1989; **18**(4): 575–592.
15. Chávez JW, Fenves G. Earthquake response of concrete gravity dams including base sliding. *Journal of Structural Engineering* 1995; **121**(5): 865–875. DOI: 10.1061/(ASCE)0733-9445(1995)121:5(865).
16. Chopra AK, Zhang L. Earthquake-induced base sliding of concrete gravity dams. *Journal of Structural Engineering* 1991; **117**(12): 3698–3719.
17. Fenves G, Chopra AK. Earthquake analysis of concrete gravity dams including reservoir bottom absorption and dam-water-foundation rock interaction. *Earthquake Engineering & Structural Dynamics* 1984; **12**(5): 663–680. DOI: 10.1002/eqe.4290120507.
18. Lysmer J, Kuhlemeyer RL. Finite dynamic model for infinite media. *Journal of the Engineering Mechanics Division* 1969; **95**(4): 859–878.
19. Smith WD. A nonreflecting plane boundary for wave propagation problems. *Journal of Computational Physics* 1974; **15**(4): 492–503. DOI: 10.1016/0021-9991(74)90075-8.
20. Wolf JP. *Soil-Structure Interaction in Time Domain*. Englewood Cliffs, NJ: Prentice Hall; 1988.
21. Wolf JP, Song C. Doubly asymptotic multi-directional transmitting boundary for dynamic unbounded medium-structure-interaction analysis. *Earthquake Engineering & Structural Dynamics* 1995; **24**(2):

-
- 175–188.
22. Wolf JP, Song C. *Finite-element modelling of unbounded media*. Chichester: Wiley; 1996.
 23. Kellezi L. Local transmitting boundaries for transient elastic analysis. *Soil Dynamics and Earthquake Engineering* 2000; **19**(7): 533–547. DOI: 10.1016/S0267-7261(00)00029-4.
 24. Basu U, Chopra AK. Perfectly matched layers for time-harmonic elastodynamics of unbounded domains: Theory and finite-element implementation. *Computer Methods in Applied Mechanics and Engineering* 2003; **192**(11–12): 1337–1375. DOI: 10.1016/S0045-7825(02)00642-4.
 25. Basu U, Chopra AK. Perfectly matched layers for transient elastodynamics of unbounded domains. *International Journal for Numerical Methods in Engineering* 2004; **59**(8): 1039–1074. DOI: 10.1002/nme.896.
 26. Basu U. Explicit finite element perfectly matched layer for transient three-dimensional elastic waves. *International Journal for Numerical Methods in Engineering* 2009; **77**(2): 151–176. DOI: 10.1002/nme.2397.
 27. White W, Lee IK, Valliappan S. Unified boundary for finite dynamic models. *Journal of the Engineering Mechanics Division* 1977; **103**(5): 949–964.
 28. Engquist B, Majda A. Absorbing boundary conditions for numerical simulation of waves. *Proc of the National Academy of Sciences* 1977; **74**(5): 1765–1766.
 29. Clayton R, Engquist B. Absorbing boundary conditions for acoustic and elastic wave equations. *Bulletin of the Seismological Society of America* 1977; **67**(6): 1529–1540.
 30. Underwood P, Geers TL. Doubly asymptotic, boundary-element analysis of dynamic soil-structure interaction. *International Journal of Solids and Structures* 1981; **17**(7): 687–697. DOI: 10.1016/0020-7683(81)90005-6.
 31. Kausel E, Tassoulas JL. Transmitting boundaries: A closed-form comparison. *Bulletin of the Seismological Society of America* 1981; **71**(1): 143–159.
 32. Liao ZP, Wong HL. A transmitting boundary for the numerical simulation of elastic wave propagation. *International Journal of Soil Dynamics and Earthquake Engineering* 1984; **3**(4): 174–183. DOI: 10.1016/0261-7277(84)90033-0.
 33. Higdon RL. Absorbing boundary conditions for difference approximations to the multi-dimensional wave equation. *Mathematics of Computation* 1986; **47**(176): 437–459. DOI: 10.1090/S0025-5718-1986-0856696-4.
 34. Higdon RL. Numerical absorbing boundary conditions for the wave equation. *Mathematics of Computation* 1987; **49**(179): 65–90. DOI: 10.1090/S0025-5718-1987-0890254-1.
 35. Zienkiewicz OC, Bicanic N, Shen FQ. Earthquake input definition and the transmitting boundary conditions. *Advances in Computational Nonlinear Mechanics*, Springer; 1989.
 36. Lemos J V. Discrete element analysis of dam foundations. *Distinct Element Modelling in Geomechanics*, Rotterdam: Balkema; 1999.
 37. Saouma V, Miura F, Lebon G, Yagome Y. A simplified 3D model for soil-structure interaction with radiation damping and free field input. *Bulletin of Earthquake Engineering* 2011; **9**(5): 1387–1402. DOI: 10.1007/s10518-011-9261-7.
 38. Bielak J, Christiano P. On the effective seismic input for non-linear soil-structure interaction systems. *Earthquake Engineering & Structural Dynamics* 1984; **12**(3): 107–119. DOI: 10.1002/eqe.4290120108.
 39. Aydinoglu MN. Consistent formulation of direct and substructure methods in nonlinear soil-structure interaction. *Soil Dynamics and Earthquake Engineering* 1993; **12**(7): 403–410. DOI: 10.1016/0267-7261(93)90003-A.
 40. Bielak J, Loukakis K, Hisada Y, Yoshimura C. Domain reduction method for three-dimensional earthquake modeling in localized regions, Part I: Theory. *Bulletin of the Seismological Society of America* 2003; **93**(2): 817–824. DOI: 10.1785/0120010251.
 41. Basu U. Perfectly matched layers for acoustic and elastic waves: Theory, finite-element implementation and application to earthquake analysis of dam-water-foundation rock systems. PhD thesis, University of California, Berkeley, 2004.
 42. Hallquist JO. LS-DYNA keyword user’s manual, Livermore Software Technology Corporation 2016.
 43. Noble CR, Nuss L. Implicit and explicit nonlinear dynamic analysis of a large thin-arch dam using massively parallel computing. *Proc. for 13th World Conference on Earthquake Engineering*, Vancouver, Canada: 2004.
-

-
44. Mills-Bria B, Nuss L, Chopra AK. Current methodology at the Bureau of Reclamation for the nonlinear analyses of arch dams using explicit finite element techniques. *Proc. for 14th World Conference on Earthquake Engineering*, Beijing, China: 2008.
 45. US Bureau of Reclamation. *State-of-Practice for the Nonlinear Analysis of Concrete Dams 2013*. Denver, CO: 2013.
 46. Herrera I, Bielak J. Soil-structure interaction as a diffraction problem. *Proc. for 6th World Conference on Earthquake Engineering*, vol. 2, New Delhi, India: 1977.
 47. Lotfi V, Roesset JM, Tassoulas JL. A technique for the analysis of the response of dams to earthquakes. *Earthquake Engineering & Structural Dynamics* 1987; **15**(4): 463–489. DOI: 10.1002/eqe.4290150405.
 48. Medina F, Dominguez J, Tassoulas JL. Response of dams to earthquakes including effects of sediments. *Journal of Structural Engineering* 1990; **116**(11): 3108–3121. DOI: 10.1061/(ASCE)0733-9445(1990)116:11(3108).
 49. Bougacha S, Tassoulas JL. Seismic analysis of gravity dams. I: Modeling of sediments. *Journal of Engineering Mechanics* 1991; **117**(8): 1826–1837. DOI: 10.1061/(ASCE)0733-9399(1991)117:8(1826).
 50. Domínguez J, Gallego R, Japón BR. Effects of porous sediments on seismic response of concrete gravity dams. *Journal of Engineering Mechanics* 1997; **123**(4): 302–311. DOI: 10.1061/(ASCE)0733-9399(1997)123:4(302).
 51. Chopra AK. Hydrodynamic pressures on dams during earthquakes. *Journal of the Engineering Mechanics Division* 1967; **93**(6): 205–224.
 52. Zienkiewicz OC, Bettess P. Fluid-structure dynamic interaction and wave forces. An introduction to numerical treatment. *International Journal for Numerical Methods in Engineering* 1978; **13**(1): 1–16. DOI: 10.1002/nme.1620130102.
 53. McGuire RK. *Seismic Hazard and Risk Analysis*. Earthquake Engineering Research Institute; 2004.
 54. Baker JW. Conditional mean spectrum: Tool for ground motion selection. *Journal of Structural Engineering* 2011; **137**(3): 322–331. DOI: 10.1061/(ASCE)ST.1943-541X.0000215.
 55. Schnabel PB, Lysmer J, Seed HB. SHAKE: A computer program for earthquake response analysis of horizontally layered sites. *Report No. UCB/EERC-72/12*, Earthquake Engineering Research Center, Univ. of California, Berkeley: 1972.
 56. Wolf JP. *Dynamic Soil-Structure Interaction*. Englewood Cliffs, NJ: Prentice Hall; 1985.
 57. Kramer SL. *Geotechnical Earthquake Engineering*. vol. 6. 1st ed. Upper Saddle River, NJ: Prentice Hall; 1996. DOI: 10.1007/978-3-540-35783-4.
 58. Ordóñez GA. SHAKE2000: A computer program for the 1D analysis of geotechnical earthquake engineering problems 2000.
 59. Hashash YMA, Groholski DR, Phillips CA, Park D, Musgrove M. DEEPSOIL user manual and tutorial. Version 5.0, University of Illinois, Urbana, IL, USA 2011.
 60. Joyner WB, Chen ATF. Calculation of nonlinear ground response in earthquakes. *Bulletin of the Seismological Society of America* 1975; **65**(5): 1315–1336.
 61. Nielsen AH. Absorbing boundary conditions for seismic analysis in ABAQUS. *Proc. of the 2006 ABAQUS Users' Conference*, Boston, MA, USA: 2006.
 62. Itasca Consulting Group Inc. FLAC3D - Fast Lagrangian Analysis of Continua in Three-Dimensions, Ver. 5.0., Minneapolis, USA 2012.
 63. Brinkgreve RBJ, Engin E, Swolfs WM. Plaxis Reference Manual 2016. *Plaxis BV, The Netherlands*.
 64. Kontoe S, Zdravkovic L, Potts DM. An assessment of the domain reduction method as an advanced boundary condition and some pitfalls in the use of conventional absorbing boundaries. *International Journal for Numerical and Analytical Methods in Geomechanics* 2009; **33**(3): 309–330.
 65. McKenna F. OpenSees: A framework for earthquake engineering simulation. *Computing in Science and Engineering* 2011; **13**(4): 58–66. DOI: 10.1109/MCSE.2011.66.
 66. Hilber HM, Hughes TJR, Taylor RL. Improved numerical dissipation for time integration algorithms in structural dynamics. *Earthquake Engineering & Structural Dynamics* 1977; **5**(3): 283–292. DOI: 10.1002/eqe.4290050306.
 67. Chopra AK. *Dynamics of Structures: Theory and Applications to Earthquake Engineering*. Upper Saddle River, NJ: Prentice Hall; 2012.
 68. Cook RD, Malkus DS, Plesha ME, Witt RJ. *Concepts and applications of finite element analysis*. 4th ed. New York: John Wiley & Sons; 2007.
-

-
69. Lysmer J, Waas G. Shear waves in plane infinite structures. *Journal of the Engineering Mechanics Division* 1972.
 70. Fenves G, Chopra AK. EAGD-84: A computer program for earthquake analysis of concrete gravity dams. *Report No. UCB/EERC-84/11*, Earthquake Engineering Research Center, Univ. of California, Berkeley: 1984.
 71. The MathWorks Inc. MATLAB user's guide (R2012a). Natick, MA, USA 2012.
 72. Løkke A. User Manual: Pre- and post-processing modules to facilitate analysis with EAGD-84. Published by the Earthquake Engineering Research Center, Univ. of California, Berkeley 2013.
 73. Curtis DD, Sooch G, Brewer T, Schildmeyer A. Explicit seismic analysis of Mossyrock Dam. *Proc. for the 33rd Annual USSD Conference*, Phenix, AZ, USA: 2013.
 74. Clough RW. Nonlinear mechanisms in the seismic response of arch dams. *Proc. for International Reserach Conference on Earthquake Engineering*, Skopje, Yugoslavia: 1980.
 75. Dassault Systems. Abaqus/Standard user's manual, version 6.13.
 76. Fenves G, Chopra AK. Earthquake analysis and response of concrete gravity dams. *Report No. UCB/EERC-84/10*, Earthquake Engineering Research Center, Univ. of California, Berkeley: 1984.
 77. Fok KL, Chopra AK. Hydrodynamic and foundation flexibility effects in earthquake response of arch dams. *Journal of Structural Engineering* 1986; **112**(8): 1810–1828. DOI: 10.1061/(ASCE)0733-9445(1986)112:8(1810).
 78. Alves SW, Hall JF. Generation of spatially nonuniform ground motion for nonlinear analysis of a concrete arch dam. *Earthquake Engineering & Structural Dynamics* 2006; **35**(11): 1339–1357. DOI: 10.1002/eqe.576.
 79. Chopra AK, Wang JT. Earthquake response of arch dams to spatially varying ground motion. *Earthquake Engineering & Structural Dynamics* 2009; **39**(8): 887–906. DOI: 10.1002/eqe.974.
 80. Proulx J, Darbre GR, Kamileris N. Analytical and experimental investigation of damping in arch dams based on recorded earthquakes. *Proc. for 13th World Conference on Earthquake Engineering*, Vancouver, Canada: 2004.
 81. Maeso O, Aznárez JJ, Domínguez J. Effects of space distribution of excitation on seismic response of arch dams. *Journal of Engineering Mechanics* 2002; **128**(7): 759–768. DOI: 10.1061/(ASCE)0733-9399(2002)128:7(759).
 82. Lee J, Fenves G. A plastic-damage concrete model for earthquake analysis of dams. *Earthquake Engineering & Structural Dynamics* 1998; **27**(9): 937–956. DOI: 10.1002/(SICI)1096-9845(199809)27:9<937::AID-EQE764>3.0.CO;2-5.
 83. Niwa A, Clough RW. Non-linear seismic response of arch dams. *Earthquake Engineering & Structural Dynamics* 1982; **10**(2): 267–281. DOI: 10.1002/eqe.4290100208.
 84. Léger P, Katsouli M. Seismic stability of concrete gravity dams. *Earthquake Engineering & Structural Dynamics* 1989; **18**(6): 889–902. DOI: 10.1002/eqe.4290180611.
 85. Lau DT, Noruziaan B, Razaqpur AG. Modelling of contraction joint and shear sliding effects on earthquake response of arch dams. *Earthquake Engineering & Structural Dynamics* 1998; **27**(10): 1013–1029. DOI: 10.1002/(SICI)1096-9845(199810)27:10<1013::AID-EQE765>3.0.CO;2-0.
 86. Lemos J V. Block modelling of rock masses: concepts and application to dam foundations. *European Journal of Environmental and Civil Engineering* 2008; **12**(7–8): 915–949. DOI: 10.1080/19648189.2008.9693054.
 87. Zienkiewicz OC, Paul DK, Hinton E. Cavitation in fluid-structure response (with particular reference to dams under earthquake loading). *Earthquake Engineering & Structural Dynamics* 1983; **11**(4): 463–481. DOI: 10.1002/eqe.4290110403.
 88. Priscu R, Popovici A, Stematiu D, Stere C. *Earthquake Engineering for Large Dams*. 2nd ed. New York, NY: John Wiley and Sons, Inc.; 1985.
 89. Bao H, Bielak J, Ghattas O, Kallivokas LF, O'Hallaron DR, Shewchuk JR, *et al.* Large-scale simulation of elastic wave propagation in heterogeneous media on parallel computers. *Computer Methods in Applied Mechanics and Engineering* 1998; **152**(1–2): 85–102. DOI: 10.1016/S0045-7825(97)00183-7.
 90. Graves RW. Simulating seismic wave propagation in 3D elastic media using staggered-grid finite differences. *Bulletin of the Seismological Society of America* 1996; **86**(4): 1091–1106.
 91. Moczo P, Kristek J, Galis M, Pazak P, Balazovjeh M. The finite-difference and finite-element modeling of seismic wave propagation and earthquake motion. *Acta Physica Slovaca* 2007; **57**(2): 177–406.
-

-
92. Zhang L, Chopra AK. Impedance functions for three-dimensional foundations supported on an infinitely-long canyon of uniform cross-section in a homogeneous half-space. *Earthquake Engineering & Structural Dynamics* 1991; **20**(11): 1011–1027. DOI: 10.1002/eqe.4290201104.
 93. García F, Aznárez JJ, Padrón LA, Maeso O. Relevance of the incidence angle of the seismic waves on the dynamic response of arch dams. *Soil Dynamics and Earthquake Engineering* 2016; **90**: 442–453. DOI: 10.1002/eqe.4290201104.
 94. Kwong NS, Chopra AK, McGuire RK. A framework for the evaluation of ground motion selection and modification procedures. *Earthquake Engineering & Structural Dynamics* 2015; **44**(5): 795–815. DOI: 10.1002/eqe.2502.
 95. Haselton CB. Evaluation of ground motion selection and modification methods: predicting median interstory drift response of buildings. *Report No. PEER 2009/01*, Pacific Earthquake Engineering Research Center, Univ. of California, Berkeley: 2009.
 96. Katsanos EI, Sextos AG, Manolis GD. Selection of earthquake ground motion records: A state-of-the-art review from a structural engineering perspective. *Soil Dynamics and Earthquake Engineering* 2010; **30**(4): 157–169. DOI: 10.1016/j.soildyn.2009.10.005.
 97. Mejia LH, Dawson EM. Earthquake deconvolution for FLAC. *Proc. of the 4th International FLAC Symposium on Numerical Modeling in Geomechanics*, 2006.
 98. Robbe E, Kashiwayanagi M, Yamane Y. Seismic analyses of concrete dam, comparison between finite-element analyses and seismic records. *Proc. for 16th World Conference on Earthquake Engineering*, Santiago, Chile: 2017.
 99. Nielsen AH. Towards a complete framework for seismic analysis in Abaqus. *Proceedings of the Institution of Civil Engineers - Engineering and Computational Mechanics* 2014; **167**(1): 3–12. DOI: 10.1680/eacm.12.00004.
 100. Saouma V, Cervenka J, Reich R. Merlin finite element user's manual, Univ. of Colorado, Boulder 2013.
 101. Cvijanovic V, Schultz M, Armstrong R. Application of nonlinear analysis methods to hydraulic structures subject to extreme loading conditions. *Proc. for 34th Annual USSD Conference*, San Francisco, CA, USA: 2014.
 102. Trifunac MD. Scattering of plane SH waves by a semi-cylindrical canyon. *Earthquake Engineering & Structural Dynamics* 1972; **1**(3): 267–281. DOI: 10.1002/eqe.4290010307.
 103. Wong HL. Effect of surface topography on the diffraction of P, SV, and Rayleigh waves. *Bulletin of the Seismological Society of America* 1982; **72**(4): 1167–1183.
 104. Duron ZH, Hall JF. Experimental and finite element studies of the forced vibration response of Morrow Point Dam. *Earthquake Engineering & Structural Dynamics* 1988; **16**(7): 1021–1039.
 105. Nuss L. Comparison of EACD3D96 computed response to shaker tests on Morrow Point Dam. *Technical Memorandum No. MP-D8110-IE-2001-2*, Denver, CO: US Bureau of Reclamation; 2001.
 106. Tan H, Chopra AK. Earthquake analysis and response of concrete arch dams. *Report No. UCB/ERC-95/07*, Earthquake Engineering Research Center, Univ. of California, Berkeley: 1995.
 107. Wang JT, Chopra AK. Linear analysis of concrete arch dams including dam-water-foundation rock interaction considering spatially varying ground motions. *Earthquake Engineering & Structural Dynamics* 2010; **39**(7): 731–750. DOI: 10.1002/eqe.968.
 108. Wang JT, Chopra AK. EACD-3D-2008: A computer program for three-dimensional earthquake analysis of concrete dams considering spatially-varying ground motion. *Report No. UCB/ERC-2008/04*, Earthquake Engineering Research Center, Univ. of California, Berkeley: 2008.
 109. Porter KA. An overview of PEER's performance-based earthquake engineering methodology. *Proc. of 9th International Conference on Applications of Statistics and Probability in Civil Engineering*, San Francisco, CA, USA: 2003.
 110. Moehle J, Deierlein GG. A framework methodology for performance-based earthquake engineering. *Proc. for 13th World Conference on Earthquake Engineering*, vol. 679, Vancouver, Canada: 2004.
 111. Goulet CA, Haselton CB, Mitrani-Reiser J, Beck JL, Deierlein GG, Porter KA, *et al.* Evaluation of the seismic performance of a code-conforming reinforced-concrete frame building—from seismic hazard to collapse safety and economic losses. *Earthquake Engineering & Structural Dynamics* 2007; **36**(13): 1973–1997. DOI: 10.1002/eqe.694.
 112. Zhang Y, Conte JP, Yang Z, Elgamal A, Bielak J, Acero G. Two-dimensional nonlinear earthquake response analysis of a bridge-foundation-ground system. *Earthquake Spectra* 2008; **24**(2): 343–386.
-

-
- DOI: 10.1193/1.2923925.
113. Hariri-Ardebili MA. Performance based earthquake engineering of concrete dams. University of Colorado at Boulder, 2015.
 114. Ghanaat Y, Patev R, Chudgar A. Seismic fragility analysis of concrete gravity dams. *Proc. for 15th World Conference on Earthquake Engineering*, Lisbon, Portugal: 2012.
 115. Tekie PB, Ellingwood BR. Seismic fragility assessment of concrete gravity dams. *Earthquake Engineering & Structural Dynamics* 2003; **32**(14): 2221–2240. DOI: 10.1002/eqe.325.
 116. Hariri-Ardebili MA, Saouma VE. Collapse fragility curves for concrete dams: comprehensive study. *Journal of Structural Engineering* 2016; **142**(10): 04016075. DOI: 10.1061/(ASCE)ST.1943-541X.0001541.
 117. ATC. Seismic evaluation and retrofit of concrete buildings. *Report No. ATC-40*, Applied Technology Council, Redwood City, CA: 1996.
 118. FEMA. NEHRP guidelines for the seismic rehabilitation of buildings. *Report No. FEMA-273*, Federal Emergency Management Agency, Washington, D.C.: 1997.
 119. Cornell CA, Krawinkler H. Progress and challenges in seismic performance assessment. *PEER Center News* 2000; **3**(2): 1–3.
 120. Der Kiureghian A. Non-ergodicity and PEER’s framework formula. *Earthquake Engineering & Structural Dynamics* 2005; **34**(13): 1643–1652.
 121. Field EH, Jordan TH, Cornell CA. OpenSHA: a developing community-modeling environment for seismic hazard analysis. *Seismological Research Letters* 2003; **74**(4): 406–419. DOI: 10.1785/gssrl.74.4.406.
 122. U.S. Geological Survey. Unified Hazard Tool. <https://earthquake.usgs.gov/hazards/interactive/>, 2018.
 123. Hariri-Ardebili MA, Saouma VE. Probabilistic seismic demand model and optimal intensity measure for concrete dams. *Structural Safety* 2016; **59**: 67–85. DOI: 10.1016/j.strusafe.2015.12.001.
 124. Douglas J, Aochi H. A survey of techniques for predicting earthquake ground motions for engineering purposes. *Surveys in Geophysics* 2008; **29**(3): 187–220. DOI: 10.1007/s10712-008-9046-y.
 125. Kwong NS, Chopra AK. A generalized conditional mean spectrum and its application for intensity-based assessments of seismic demands. *Earthquake Spectra* 2017; **33**(1): 123–143. DOI: 10.1193/040416EQS050M.
 126. Kwong NS, Chopra AK. Determining bi-directional ground motions for nonlinear response history analysis of buildings at far-field sites. *Earthquake Spectra* 2018: 052217EQS093M. DOI: 10.1193/052217EQS093M.
 127. Hariri-Ardebili MA, Saouma VE, Porter KA. Quantification of seismic potential failure modes in concrete dams. *Earthquake Engineering & Structural Dynamics* 2016; **45**(6): 979–997. DOI: 10.1002/eqe.2697.
 128. Baker JW. Efficient analytical fragility function fitting using dynamic structural analysis. *Earthquake Spectra* 2015; **31**(1): 579–599. DOI: 10.1193/021113EQS025M.
 129. Porter KA, Beck JL, Shaikhutdinov R V. Sensitivity of building loss estimates to major uncertain variables. *Earthquake Spectra* 2002; **18**(4): 719–743. DOI: 10.1193/1.1516201.
 130. Hariri-Ardebili MA, Saouma VE. Sensitivity and uncertainty quantification of the cohesive crack model. *Engineering Fracture Mechanics* 2016; **155**: 18–35. DOI: 10.1016/j.engfracmech.2016.01.008.
 131. Pan JW, Zhang CH, Xu Y, Jin F. A comparative study of the different procedures for seismic cracking analysis of concrete dams. *Soil Dynamics and Earthquake Engineering* 2011; **31**(11): 1594–1606. DOI: 10.1016/j.soildyn.2011.06.011.
 132. He C, Wang JT, Zhang CH. Nonlinear spectral-element method for 3D seismic-wave propagation. *Bulletin of the Seismological Society of America* 2016; **106**(3): 1074–1087. DOI: 10.1785/0120150341.
 133. Fronteddu L, Léger P, Tinawi R. Static and dynamic behavior of concrete lift joint interfaces. *Journal of Structural Engineering* 1998; **124**(12): 1418–1430. DOI: 10.1061/(ASCE)0733-9445(1998)124:12(1418).
 134. Chávez JW, Fenves G. Earthquake analysis of concrete gravity dams including base sliding. *Earthquake Engineering & Structural Dynamics* 1995; **24**(5): 673–686. DOI: 10.1002/eqe.4290240505.
 135. Bhattacharjee SS, Léger P. Concrete constitutive models for nonlinear seismic analysis of gravity dams - state-of-the-art. *Canadian Journal of Civil Engineering* 1992; **19**(3): 492–509. DOI: 10.1139/92-059.
 136. Ngo D, Scordelis AC. Finite element analysis of reinforced concrete beams. *Journal Proceedings*, vol.
-

-
- 64, 1967.
137. Ayari ML, Saouma V. A fracture mechanics based seismic analysis of concrete gravity dams using discrete cracks. *Engineering Fracture Mechanics* 1990; **35**(1–3): 587–598. DOI: 10.1016/0013-7944(90)90233-7.
138. Pekau OA, Chuhan Z, Lingmin F. Seismic fracture analysis of concrete gravity dams. *Earthquake Engineering & Structural Dynamics* 1991; **20**(4): 335–354. DOI: 10.1002/eqe.4290200404.
139. Belytschko T, Black T. Elastic crack growth in finite elements with minimal remeshing. *International Journal for Numerical Methods in Engineering* 1999; **45**(5): 601–620. DOI: 10.1002/(SICI)1097-0207(19990620)45:5<601::AID-NME598>3.0.CO;2-S.
140. Zhang S, Wang G, Yu X. Seismic cracking analysis of concrete gravity dams with initial cracks using the extended finite element method. *Engineering Structures* 2013; **56**: 528–543. DOI: 10.1016/j.engstruct.2013.05.037.
141. Goldgruber M. Nonlinear seismic modelling of concrete dams. Technical University, Graz, 2015. DOI: 10.13140/RG.2.1.3001.6485.
142. Rashid YR. Ultimate strength analysis of prestressed concrete pressure vessels. *Nuclear Engineering and Design* 1968; **7**(4): 334–344.
143. Hillerborg A, Mod er M, Petersson PE. Analysis of crack formation and crack growth in concrete by means of fracture mechanics and finite elements. *Cement and Concrete Research* 1976; **6**(6): 773–781. DOI: 10.1016/0008-8846(76)90007-7.
144. Wang JT, Lv DD, Jin F, Zhang CH. Earthquake damage analysis of arch dams considering dam–water–foundation interaction. *Soil Dynamics and Earthquake Engineering* 2013; **49**: 64–74. DOI: 10.1016/j.soildyn.2013.02.006.
145. Raphael JM. Tensile strength of concrete. *Journal Proceedings*, vol. 81, 1984.
146. Br uhwiler E, Wittmann FH. The wedge splitting test, a new method of performing stable fracture mechanics tests. *Engineering Fracture Mechanics* 1990; **35**(1–3): 117–125. DOI: 10.1016/0013-7944(90)90189-N.
147. Br uhwiler E. Fracture of mass concrete under simulated seismic action. *Dam Engineering* 1990; **1**(EPFL-ARTICLE-181083): 153–176.
148. Wang JT, Zhang CH, Jin F. Nonlinear earthquake analysis of high arch dam-water-foundation rock systems. *Earthquake Engineering & Structural Dynamics* 2012; **41**(7): 1157–1176. DOI: 10.1002/eqe.1178.
149. Saouma VE, Broz JJ, Br uhwiler E, Boggs HL. Effect of aggregate and specimen size on fracture properties of dam concrete. *Journal of Materials in Civil Engineering* 1991; **3**(3): 204–218. DOI: 10.1061/(ASCE)0899-1561(1991)3:3(204).
150. Tinawi R, L eger P, Ghrib F, Bhattacharjee SS, Leclerc M. *Structural safety of existing concrete dams: influence of construction joints*. Report to the Canadian Electrical Association, Montreal, Canada: 1998.
151. Goodman RE, Taylor RL, Brekke TL. A model for the mechanics of jointed rock. *Journal of Soil Mechanics & Foundations Div* 1968.
152. National Research Council. *Earthquake Engineering for Concrete Dams: Design, Performance and Research Needs*. Washington, D.C.: The National Academies Press; 1990. DOI: 10.17226/1742.
153. El-Aidi B, Hall JF. Non-linear earthquake response of concrete gravity dams part 2: behaviour. *Earthquake Engineering & Structural Dynamics* 1989; **18**(6): 853–865. DOI: 10.1002/eqe.4290180608.
154. Hall JF. Problems encountered from the use (or misuse) of Rayleigh damping. *Earthquake Engineering & Structural Dynamics* 2006; **35**(5): 525–545. DOI: 10.1002/eqe.541.
155. Tan H, Chopra AK. Dam-foundation rock interaction effects in frequency-response functions of arch dams. *Earthquake Engineering & Structural Dynamics* 1995; **24**(11): 1475–1489. DOI: 10.1002/eqe.4290241105.
156. Maeso O, Azn arez JJ, Dom nguez J. Three-dimensional models of reservoir sediment and effects on the seismic response of arch dams. *Earthquake Engineering & Structural Dynamics* 2004; **33**(10): 1103–1123. DOI: 10.1002/eqe.392.
157. Hamilton EL. Elastic properties of marine sediments. *Journal of Geophysical Research* 1971; **76**(2): 579–604. DOI: 10.1029/JB076i002p00579.
158. Hatami K. Effect of reservoir bottom on earthquake response of concrete dams. *Soil Dynamics and Earthquake Engineering* 1997; **16**(7–8): 407–415. DOI: 10.1016/S0267-7261(97)00023-7.
-

-
159. Zhang C, Yan C, Wang G. Numerical simulation of reservoir sediment and effects on hydro-dynamic response of arch dams. *Earthquake Engineering & Structural Dynamics* 2001; **30**(12): 1817–1837. DOI: 10.1002/eqe.96.
 160. Hall JF. The dynamic and earthquake behaviour of concrete dams: review of experimental behaviour and observational evidence. *Soil Dynamics and Earthquake Engineering* 1988; **7**(2): 58–121. DOI: 10.1016/S0267-7261(88)80001-0.
 161. Proulx J, Paultre P. Experimental and numerical investigation of dam-reservoir-foundation interaction for a large gravity dam. *Canadian Journal of Civil Engineering* 1997; **24**(1): 90–105. DOI: 10.1139/I96-086.
 162. Rea D, Liaw CY, Chopra AK. Mathematical models for the dynamic analysis of concrete gravity dams. *Earthquake Engineering & Structural Dynamics* 1974; **3**(3): 249–258. DOI: 10.1002/eqe.4290030304.
 163. Noble CR, Nuss L. Nonlinear seismic analysis of Morrow Point Dam. *Proc. for 13th World Conference on Earthquake Engineering*, Vancouver, Canada: 2004.
 164. Brühwiler E, Wittmann FH. Failure of dam concrete subjected to seismic loading conditions. *Engineering Fracture Mechanics* 1990; **35**(1–3): 565–571. DOI: 10.1016/0013-7944(90)90231-5.
 165. US Bureau of Reclamation. Investigation of the failure modes of concrete dams - physical model tests. *Report No. DSO-02-02*, Denver, CO: 2002.
 166. Luco JE, Westmann RA. Dynamic response of a rigid footing bonded to an elastic half space. *Journal of Applied Mechanics* 1972; **39**(2): 527–534.
 167. Gazetas G. Dynamic compliance matrix of rigid strip footing bonded to a viscoelastic cross anisotropic halfspace. *International Journal of Mechanical Sciences* 1981; **23**(9): 547–559. DOI: 10.1016/0020-7403(81)90060-6.
 168. Dasgupta G, Chopra AK. Dynamic stiffness matrices for viscoelastic half planes. *Journal of the Engineering Mechanics Division* 1979; **105**(5): 729–745.
 169. Meek JW, Wolf JP. Why cone models can represent the elastic half-space. *Earthquake Engineering & Structural Dynamics* 1993; **22**(9): 759–771. DOI: 10.1002/eqe.4290220903.
 170. Kuhlemeyer RL, Lysmer J. Finite element method accuracy for wave propagation problems. *Journal of the Soil Mechanics and Foundations Division* 1973; **99**(5): 421–427.
 171. Wilson EL. *Three-Dimensional Static and Dynamic Analysis of Structures: A Physical Approach With Emphasis on Earthquake Engineering*. 3rd ed. Computers and Structures Inc.; 2002.

NOTATION

Roman symbols

A	tributary area of node on absorbing boundary
a_g^k	k -component of free-field ground acceleration at the foundation surface
b	"damping" matrix of FE model of fluid
c	damping matrix of FE model of dam and foundation rock
c_p, c_s	$= A\rho_f V_p$ or $A\rho_f V_s$, coefficient for viscous damper at foundation boundary in the normal or tangential direction, respectively
c_r	$= A/C$, coefficient for viscous damper at fluid boundary
$\mathbf{c}_f, \mathbf{c}_r$	matrix of damper coefficients for nodes on absorbing boundaries Γ_f and Γ_r , respectively
C	speed of pressure waves in water
d_c, d_t	damage index for concrete in compression and tension, respectively
E_f, E_s	Young's modulus of elasticity for foundation rock and dam concrete, respectively
f	excitation frequency, in Hz
f_t	tensile strength of concrete
$\mathbf{f}(\mathbf{r}^t)$	vector of (nonlinear) internal forces in dam and foundation rock
$G(X Y)$	probability that X exceeds a specified value given Y
G_F	specific fracture energy for concrete
g	acceleration due to gravity
h	"stiffness" matrix of FE model of fluid
\mathbf{H}_r	vector of dynamic forces associated with absorbing boundary Γ_r
H	height of arch dam
k	stiffness matrix of linear part of FE model of dam and foundation rock
\mathbf{k}^0	initial (linear) stiffness matrix
$\mathbf{k}^{el}(t)$	$= [1 - d(t)]\mathbf{k}^0$, the degraded elastic stiffness matrix
L	length of bounded fluid domain
m	mass matrix of FE model of dam and foundation rock
n	outward normal vector to fluid domain
\mathbf{p}^f	vector of (total) hydrodynamic pressures at FE nodes in fluid
\mathbf{P}_f^0	effective earthquake forces on foundation boundary Γ_f
\mathbf{P}_r^0	effective earthquake forces on fluid boundary Γ_r
Q	fluid-solid coupling matrix
\mathbf{r}^t	vector of total displacements at FE nodes in dam and foundation rock
\mathbf{r}_i^0	vector of displacements for incident seismic wave
\mathbf{R}_f	vector of dynamic forces associated with absorbing boundary Γ_f
R	radius of semi-cylindrical canyon
s	"mass" matrix of FE model of fluid

$S_a(T_1)$	spectral acceleration at the fundamental vibration period T_1
u_{cr}	crack opening displacement in concrete cracking model
V_p, V_s	velocity of pressure waves and shear waves, respectively, in foundation rock

Nodal subscripts on matrices and vectors

b	nodes on water–foundation rock interface, i.e., the reservoir bottom and sides
f	nodes on absorbing boundary in foundation domain, Γ_f
h	nodes on dam–water interface, i.e., the upstream face of the dam
r	nodes on absorbing boundary in fluid domain, Γ_r

Superscripts on matrices and vectors

0	quantities in free-field foundation rock or free-field fluid systems
a	quantities in auxiliary water–foundation rock system
st	static forces
t	total displacements, pressures or forces

Greek symbols

α	wave reflection coefficient for reservoir bottom materials
Γ_b	water–foundation rock interface
Γ_f, Γ_r	absorbing boundaries in foundation and fluid domains, respectively
Γ_h	dam–water interface
ζ_f, ζ_s	viscous damping ratio of foundation rock and dam concrete, respectively
η_f, η_s	hysteretic (rate-independent) damping factors of foundation rock and dam concrete, respectively
η	$= 2fR/V_s$, dimensionless frequency (in Chapters 5 and 6)
λ	wavelength of scattered waves
$\lambda(X)$	mean annual rate of exceedance of X
ν_f, ν_s	Poisson's ratio of foundation rock and dam concrete, respectively
ρ_f, ρ_s, ρ	density of foundation rock, dam concrete and water, respectively
σ	normal tractions on foundation boundary
τ	tangential tractions on foundation boundary
ω_1	natural angular frequency of dam with empty reservoir on rigid foundation rock
Ω	region interior of absorbing boundaries, i.e., the truncated FE model
Ω^0	region interior of Γ_f for free-field foundation-rock system
Ω^a	region interior of Γ_f and Γ_r for auxiliary water–foundation rock system
Ω^+	regions exterior of absorbing boundaries Γ_f and Γ_r

Abbreviations

BEM	Boundary Element Method
-----	-------------------------

CMS	Conditional Mean Spectrum
DRM	Domain Reduction Method
DM	Damage measure
DV	Decision Variable
EDP	Engineering Demand Parameter
ESI	Effective Seismic Input Method
FEM	Finite Element Method
IM	Intensity Measure
IMHC	Intensity Measure Hazard Curve
UHS	Uniform Hazard Spectrum
PBEE	Performance Based Earthquake Engineering
PEER	Pacific Earthquake Engineering Research Center
PSHA	Probabilistic Seismic Hazard Analysis
PML	Perfectly Matched Layer
RHA	Response History Analysis
SDHC	Seismic Demand Hazard Curve

APPENDIX A

Selection of domain size for two-dimensional dam–water–foundation rock systems

A.1 Introduction

An important requirement to ensure accurate results when using the direct FE method for earthquake analysis of concrete dams is that the viscous-dampers boundaries at the truncations of the foundation domain absorb the outgoing (scattered) waves caused by dam–foundation rock interaction. The primary factor determining the effectiveness of these boundaries is the size of foundation domain included in the FE model. In this appendix, guidelines for selecting appropriate domain sizes for 2D gravity dam systems are presented. First, the dynamic response of a rigid footing on a viscoelastic halfspace is analyzed, and then the response of a concrete gravity dam is investigated.

A.2 Dynamic response of rigid footing on a viscoelastic halfspace

Much research has been devoted to the developing generalized dynamic force-displacement relationships for rigid footings of various shapes bonded to a viscoelastic halfspace, as these play an important role in the study of vibrating machinery and soil–structure interaction [166–168]. For long and relatively uniform structures, the footing can best be idealized as an infinitely long strip. If the dynamic loading is uniform in the longitudinal direction, a plain-strain condition is appropriate, and the steady-state harmonic response is fully described by a set of dynamic flexibility (or compliance) coefficients.

In this section, these dynamic flexibility coefficients are used to evaluate the performance of the viscous-damper absorbing boundary for different sized foundation domains. These results will subsequently be used to recommend an appropriate size of the foundation domain to be used for dam–water–foundation interaction analyses.

A.2.1 Formulation of the problem

The infinitely long rigid strip footing of width $2b$ perfectly bonded to a semi-unbounded homogeneous viscoelastic halfspace (Figure A.1a) is analyzed. The rigid footing has three degrees-of-freedom: horizontal translation (H), vertical translation (V) and rocking (M). The properties of the halfspace is defined by its shear modulus μ , Poisson's ratio ν , density ρ , and damping ratio ζ . If \bar{P}_i and $\bar{\Delta}_i$, $i=V,H,M$ denotes the amplitudes of a unit harmonic

force and harmonic displacement, respectively, along the i -th DOF, the dynamic force-displacement relationship can be written as:

$$\begin{Bmatrix} \bar{\Delta}_V \\ \bar{\Delta}_H \\ b\bar{\Delta}_R \end{Bmatrix} = \frac{1}{\pi\mu} \begin{bmatrix} F_{VV}(a_0) & 0 & 0 \\ 0 & F_{HH}(a_0) & F_{HM}(a_0) \\ 0 & F_{MH}(a_0) & F_{MM}(a_0) \end{bmatrix} \begin{Bmatrix} \bar{P}_V \\ \bar{P}_H \\ \bar{P}_M / b \end{Bmatrix} \quad (\text{A.1})$$

The coefficients of the dynamic flexibility matrix are complex-valued quantities with real and imaginary components $F_{ij}(a_0) = f_{ij}(a_0) + ig_{ij}(a_0)$ that are function of the dimensionless frequency parameter

$$a_0 = \omega b / v_s \quad (\text{A.2})$$

The real and imaginary parts of these dynamic flexibility coefficients can be interpreted as measures of flexibility (i.e. inverse of the stiffness) and damping of the underlying halfspace, respectively.

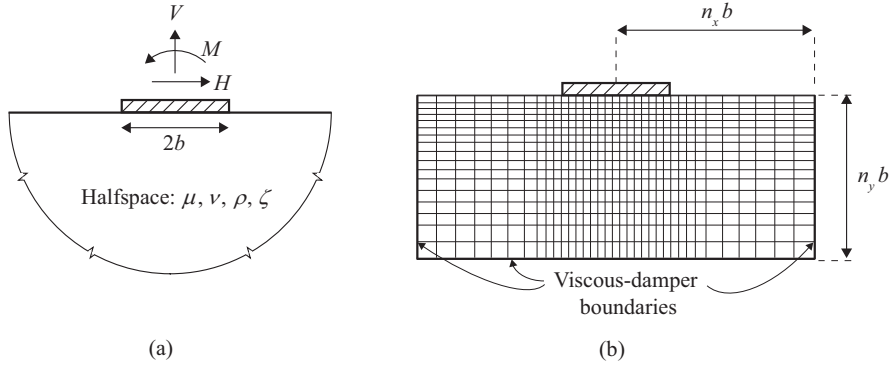


Figure A.1: (a) Cross section of rigid footing on viscoelastic halfspace;
(b) FE model with characteristic width and height.

The system is implemented in the FE program OPENSEES using a mesh with 15 elements under the rigid strip footing, and gradually increasing element size towards the outer boundaries of the model (Figure A.1b). This mesh provides sufficient density to adequately model the range of frequencies considered in the analysis. Material damping is modeled by specifying $\zeta = 2\%$ Raleigh damping at every given excitation frequency; this unconventional choice was implemented to match the constant hysteretic damping model in the benchmark solution. Viscous dampers are applied on the bottom and side boundaries of the foundation domain, with the distance from the center of the footing to the boundaries ($n_x b$ and $n_y b$) varied in the analyses.

APPENDIX A

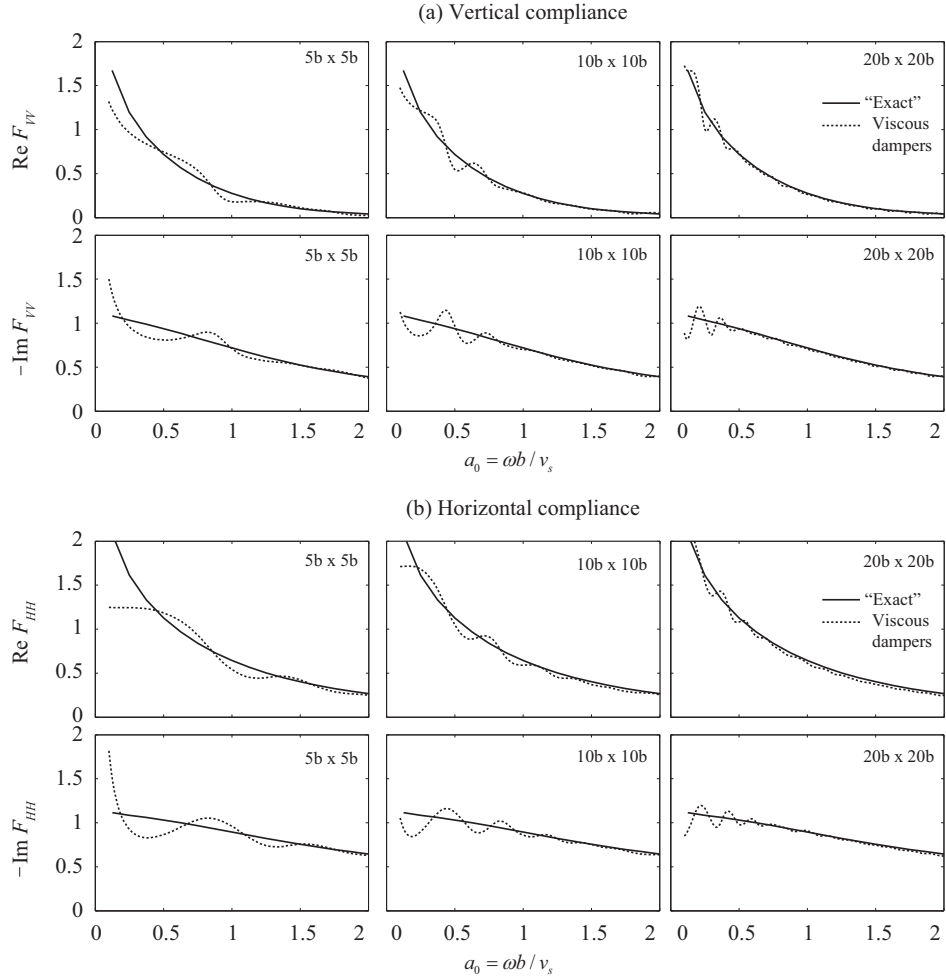


Figure A.2: Dynamic flexibility coefficients for rigid strip footing on viscoelastic homogeneous halfspace due to (a) vertical excitation, (b) horizontal excitation. $\nu = 1/3$; $\zeta = 2\%$.

The steady-state displacement response of the footing due to unit harmonic excitation is determined for vertical, horizontal and rocking vibration modes, and the procedure is repeated at every excitation frequency considered. From the displacement response, components that are in-phase (real) and 90 degrees out-of-phase (imaginary) with the input harmonic force are determined, and the results are compared with available semi-analytical benchmark solutions [168]. These benchmark results are denoted "exact" in Figures A.2– A.4.

A.2.2 Influence of domain size

Results for the horizontal, vertical and rocking compliance are presented in Figures A.2 and A.3, for three domain sizes: $5b \times 5b$, $10b \times 10b$ and $20b \times 20b$. The viscous-damper boundary generally performs well, with increasing accuracy at higher excitation frequencies and for larger domain sizes. This is consistent with results reported elsewhere [20]. The convergence towards the exact solution at higher frequencies is prominent for vertical and horizontal excitation of the footing (Figure A.2), but less so for rocking (Figure A.3). For rocking motion, the wave field is shallower and more of the energy is radiated through surface waves, even at high frequencies [169]. Because the viscous dampers are less effective in absorbing these waves, noticeable oscillations are seen in the results for all domain sizes and at all frequencies. These oscillations are caused by "standing waves" in the model, i.e., small resonance patterns that occur when the ratio of the horizontal distance to the excitation wave length approaches certain values. Such oscillations will be less of a concern for a transient-type excitation.

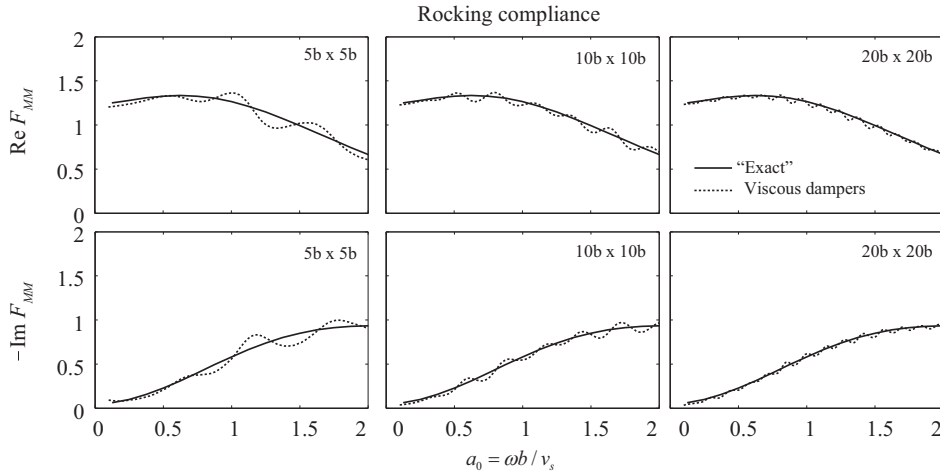


Figure A.3: Dynamic flexibility coefficients for rigid strip footing on viscoelastic homogeneous halfspace due to harmonic rocking motion. $\nu = 1/3$; $\zeta = 2\%$.

Table A.1, shows the mean relative error between the computed results and the benchmark solution for several domain sizes, computed as $\sum_{j=1}^N e_j = |(y_j - \hat{y}_j) / \hat{y}_j|$ where y_j is the computed value, \hat{y}_j is the benchmark value at frequency ω_j , and N is the total number of sampling points. The accuracy of the viscous-damper boundary improves for all modes of vibration when the domain size is increased. "Acceptable" accuracy is obtained at most frequencies with a foundation size of approx. $10b \times 10b$ or higher, with mean relative error around 5-8% for all modes.

APPENDIX A

Table A.1: Mean relative error compared to exact analytical solution, in %, for different domain sizes; error computed between $a_0 = 0.25$ and 2.0 . $\nu = 1/3$, $\zeta = 2\%$.

Distance to boundary	$\text{Re}(F_{VV})$	$-\text{Im}(F_{VV})$	$\text{Re}(F_{HH})$	$-\text{Im}(F_{HH})$	$\text{Re}(F_{MM})$	$-\text{Im}(F_{MM})$
2.5b	23.6	7	16.3	10.8	6.8	19.2
5.0b	16.2	6.1	9.4	7.5	5.1	9.2
7.5b	9.6	5.2	7.4	5.4	3.2	7.3
10b	8.3	4.1	6.5	4	3.1	6.8
15b	5.5	3.2	5.9	2.9	2.2	4.4
20b	5.2	2.1	5.7	2.3	1.7	3.8

A.2.3 Influence of aspect ratio on rocking compliance

Rocking motion is a significant part of the overall dynamic response of stiff and heavy structures such as concrete gravity dams. Because rocking generally causes shallower wave fields than horizontal or vertical excitation, it is interesting to investigate whether acceptable accuracy can be obtained for a shallow domain.

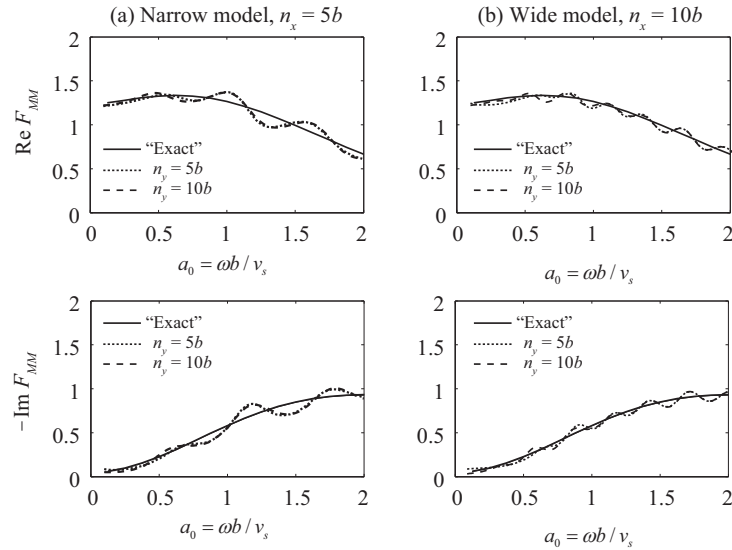


Figure A.4: Dynamic flexibility coefficients for rigid strip footing on viscoelastic homogeneous halfspace due to harmonic rocking motion; (a) $n_x = 5b$; (b) $n_x = 10b$. For both sizes, $\nu = 1/3$, $\zeta = 2\%$.

Figure A.4 compares the results for rocking compliance for two horizontal domain sizes: narrow ($n_x = 5b$) and wide ($n_x = 10b$), and two vertical domain sizes: shallow ($n_y = 5b$) and deep ($n_y = 10b$). The accuracy is generally much better for the wide model than for the narrow model; however, there seems to be no benefit of increasing the vertical

dimension beyond the shallow domain size. This indicates that a shallow and wide model will be the ideal aspect ratio for concrete gravity dam analyses, where rocking is important.

A.3 Dynamic response of Pine Flat Dam

The required size of the foundation domain to be used with the direct FE method developed in Part II of this thesis is investigated by analyzing the dam–foundation rock system shown in Figure A.5. The dam cross section is chosen to be that of Pine Flat Dam (Figure A.5a), which has a geometry representative of many concrete gravity dams. The concrete in the dam is assumed to be homogeneous, isotropic and linear elastic, in a state of plain strain, with modulus of elasticity $E_s = 22.4$ GPa, density $\rho_s = 2483$ kg/m³ and Poisson's ratio $\nu_s = 0.20$. The foundation rock is assumed to be homogeneous, isotropic and linear elastic, in a state of plain strain, with modulus of elasticity $E_f = E_s$, $\rho_f = 2643$ kg/m³, and $\nu_f = 0.33$. The dam is assumed to be supported on the surface of the halfspace. Material damping in the dam and foundation is modeled in the direct FE method analyses by Rayleigh damping with $\zeta_s = \zeta_f = 2\%$ damping specified in the two first periods of vibration for the dam–foundation rock system. For the substructure method analyses used as benchmark, material damping is modeled by constant hysteretic damping with equivalent hysteretic damping factor $\eta = 2\zeta$.

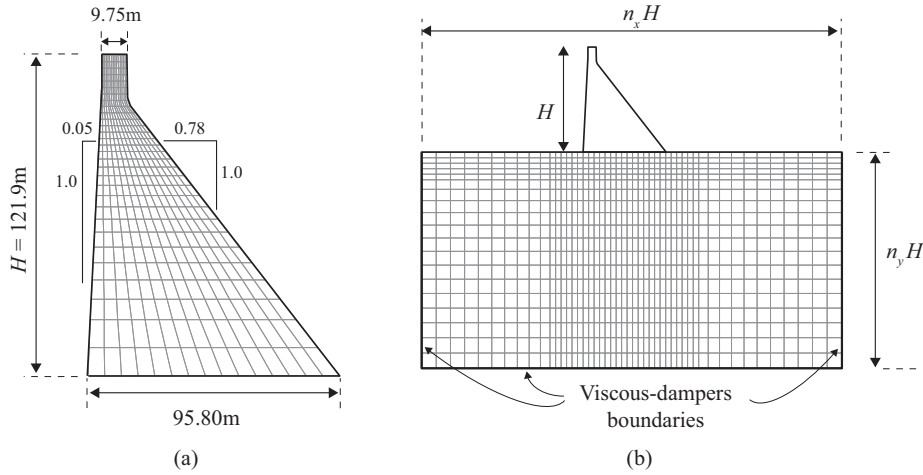


Figure A.5: (a) FE model of dam cross section (Pine Flat Dam); (b) dam–foundation rock system with viscous-damper boundaries to simulate the semi-unbounded foundation domain.

The FE model for the dam cross section consists of four-node solid elements and has 15 elements along the base and 30 elements along the height. The FE model for the foundation rock also consists of four-node solid elements and has a maximum element size chosen to be less than one-tenth of the shortest wavelength considered in the analysis [170]. Viscous-damper boundaries are applied at the bottom and sides of the model. The overall size

of the foundation domain in the horizontal and vertical directions are defined by $n_x H$ and $n_y H$ (Figure A.5b), where H is the dam height.

Frequency response functions are computed by defining a unit-amplitude harmonic surface ground motion, computing effective earthquake forces following the procedure summarized in Boxes 3.1 and 3.2 of Part I, and analyzing the system for long enough time to determine the steady-state response. Results obtained using the substructure method – wherein the foundation rock is modeled rigorously as a semi-infinite halfspace – provide the benchmark for comparison.

A.3.1 Influence of foundation domain size

Frequency response function for the dam–foundation rock system subjected to horizontal and vertical ground motion are shown in Figure A.6. Results are computed for three different of foundation domain sizes: $4H \times 2H$, $8H \times 4H$ and $16H \times 8H$. For all three foundation sizes, the direct FE method is able to closely represent the effects of dam–foundation rock interaction. The shape and amplitude of the response function is close to the benchmark solution for both horizontal and vertical excitation. The peak at the first resonance frequencies is overestimated for the smallest sized foundation domain, but the agreement increases for larger domain sizes. This is consistent with the results observed in Section A.2, where "standing waves" caused oscillations in the compliance coefficients when the ratio of the distance to the boundary to the excitation wave length approached certain values. Choosing a domain size of $8H \times 4H$ seems sufficient to ensure that these oscillations have minimal influence on the dam response, and there is little additional benefit of further increasing the domain size to $16H \times 8H$.

A.3.2 Influence of foundation domain aspect ratio

Figure A.7 compares the accuracy of the direct FE method with viscous-damper boundaries for different aspect ratios of the foundation domain. The aspect ratio of the foundation domain clearly influences the results: there is little improvement by increasing the domain size from $4H \times 2H$ to $4H \times 4H$, and correspondingly, the results for $8H \times 4H$ are almost identical to those for $8H \times 8H$. This lack of improvement in accuracy when increasing the vertical dimension occurs because the scattered wave field from the dam is largely caused by rocking motion, which generates a shallow wave field primarily propagating in the horizontal directions. Additional increase of the vertical dimension will therefore not provide much additional absorption from the viscous dampers. These results indicate that a vertical dimension between $2H$ and $4H$ will likely provide sufficient accuracy for practical analyses.

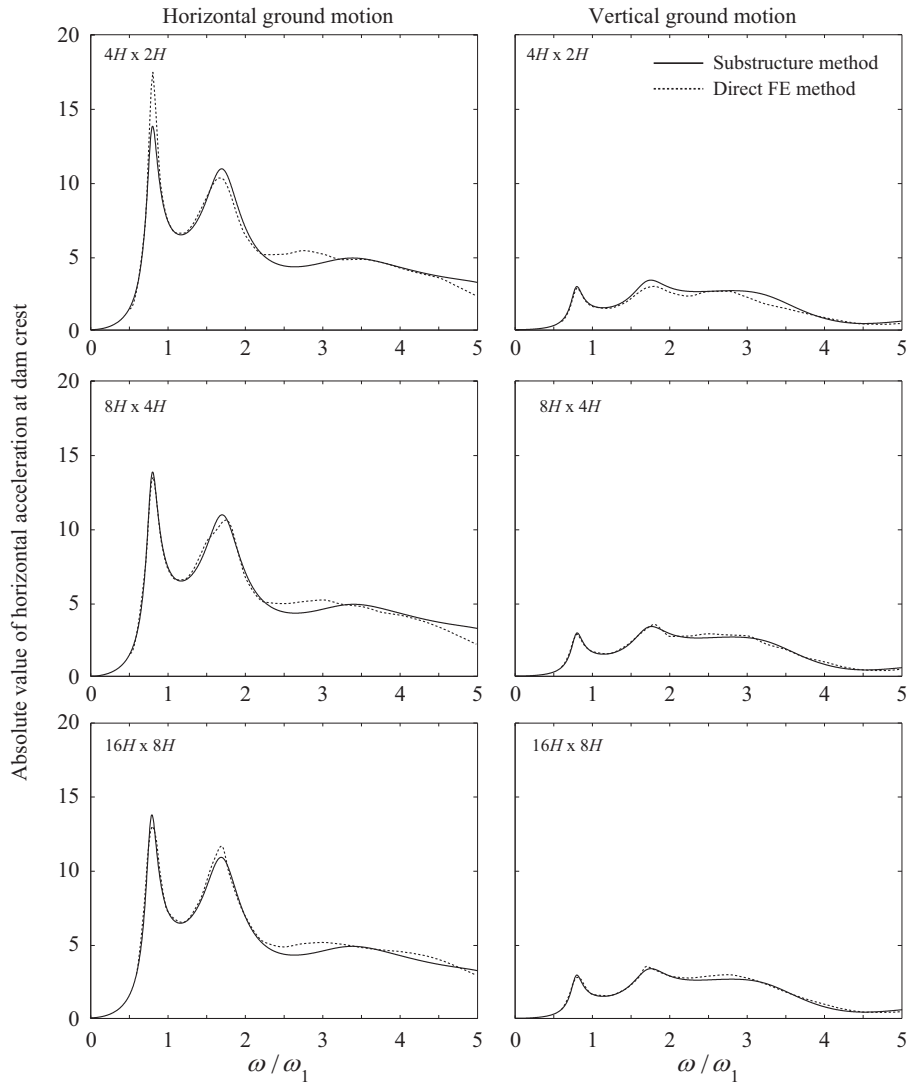


Figure A.6: Influence of foundation domain size on the accuracy of direct FE method in computing the response of dam on flexible foundation due to harmonic horizontal and vertical ground motion.

$$\zeta_s = \zeta_f = 2\%; E_f / E_s = 1.0.$$

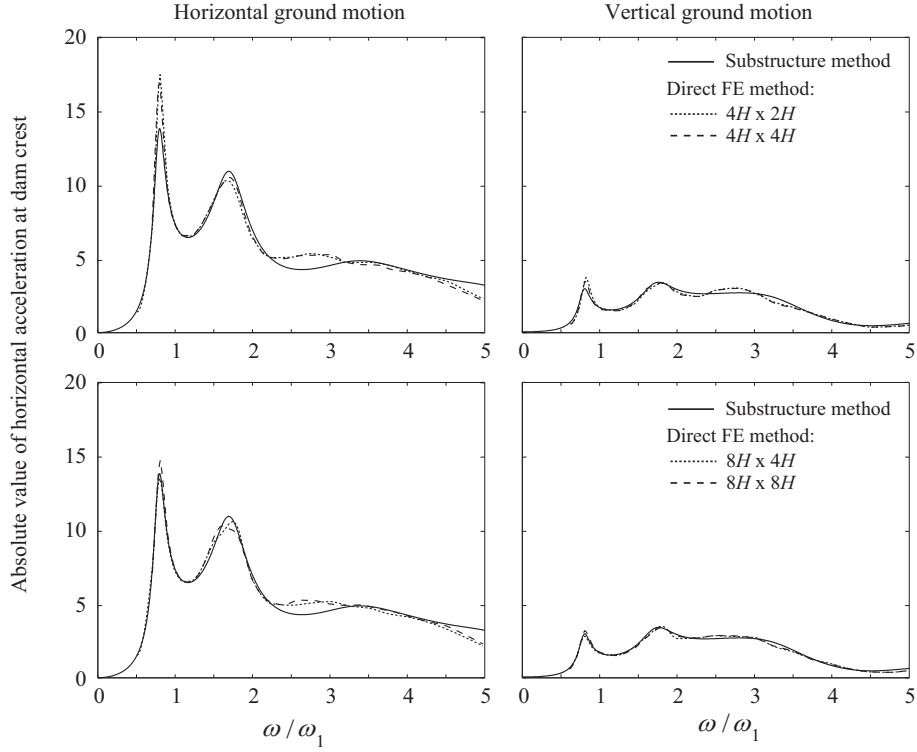


Figure A.7: Influence of foundation domain aspect ratio on the accuracy of direct FE method in computing the response of dam on flexible foundation due to harmonic horizontal and vertical ground motion.

$$\zeta_s = \zeta_f = 2\%; E_f / E_s = 1.0.$$

A.3.3 Influence of foundation stiffness

To investigate how the accuracy of the direct FE method is influenced by changes in the stiffness of the foundation rock, results are presented in Figure A.8 for $E_f / E_s = 2, 1$ and $1/4$. The accuracy generally increases as the moduli ratio E_f / E_s decreases, which for a fixed value of E_s implies increasingly flexible foundation rock. This is a somewhat counter-intuitive result, as one might have expected the accuracy to worsen for a more flexible foundation because the effects of dam–foundation interaction are more prominent. However, the opposite occurs because the ability of the viscous dampers to absorb body waves improves when the ratio of distance to excitation wave length increases [20], and this ratio will decrease with increasing foundation stiffness E_f . The same trend was observed in Figures A.2 and A.3, where the accuracy was seen to increase for higher values of a_0 , which for a fixed frequency implies a more flexible foundation.

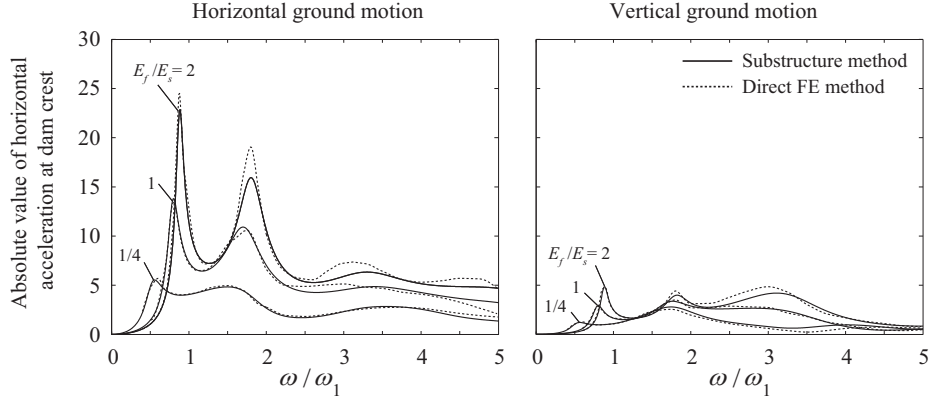


Figure A.8: Influence of foundation stiffness on the accuracy of direct FE method in computing the response of dam on flexible foundation due to harmonic horizontal and vertical ground motion. Size of foundation domain = $8H \times 4H$; $\zeta_s = \zeta_f = 2\%$.

A.3.4 Influence of material damping

Figure A.9 presents the response of the system for two values of material damping in the dam and foundation rock: $\zeta_s = \zeta_f = 2\%$ and $\zeta_s = \zeta_f = 5\%$. Increasing the amount of material damping slightly improves the accuracy of the results from the truncated model because (1) the amplitude of the outward propagating wave is reduced before it hits the boundary leading to less energy for the viscous dampers to absorb; and (2) the wave reflected from the boundary is further damped before it reaches the structure. However, the trend is modest, so increasing the amount of material damping is clearly not a substitute for accurate modeling of the semi-unbounded foundation domain.

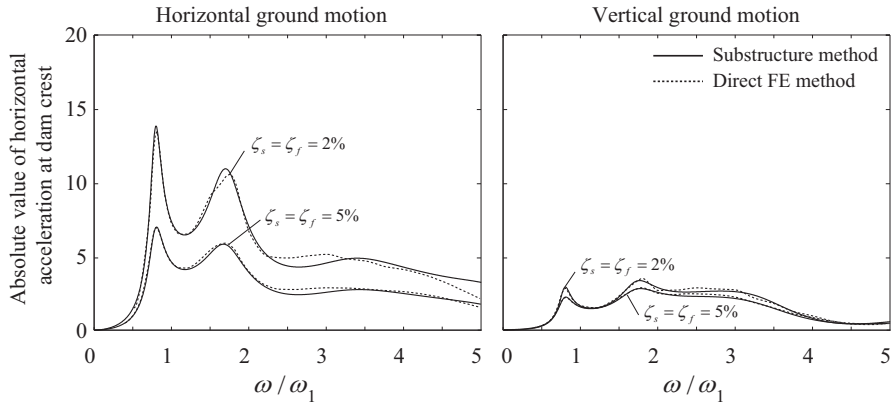


Figure A.9: Influence of material damping on the accuracy of direct FE method in computing the response of dam on flexible foundation due to harmonic horizontal and vertical ground motion. Size of foundation domain = $8H \times 4H$; $E_f / E_s = 1.0$.

A.3.5 Recommendations for domain size

Based on the preceding results, the following conclusions can be stated:

- An overall foundation-domain size of $8H \times 4H$ is sufficient to ensure accurate results in the direct FE method when using viscous-damper boundaries to model the semi-unbounded foundation domain. Further increase in the domain size does not improve the accuracy.
- Increasing the vertical size of the foundation domain beyond a certain minimum value does not improve the results. These presented results indicate that a vertical dimension between $2H$ and $4H$ will likely suffice for practical analyses.
- The accuracy is generally better for more flexible foundations because the performance of the viscous-damper boundary is inversely proportional to the foundation stiffness. For stiff foundations, the dimensions recommended above may have to be increased.
- Increasing the amount of material damping in the foundation slightly improves the accuracy of the results, but the trend is only modest.

APPENDIX B

The Domain Reduction Method for seismic input in soil–structure-interaction analyses



B.1 Introduction

The Domain Reduction Method, or DRM, [40] is a modular, two-step finite-element methodology developed for modeling response to earthquake ground motion in situations where large contrasts exist between the physical scale of the background model and a smaller localized feature. The method overcomes the problem of multiple physical scales by subdividing the original problem into two simpler ones. The first is an auxiliary problem that simulates the earthquake source and propagation path effects by using a model that encompasses the source and a simpler background structure where the localized feature has been removed. The second problem models the local site effects by using a set of equivalent localized forces derived from the first step as the effective seismic input.

Although primarily developed for large scale geological simulations, the DRM is also directly applicable for soil–structure interaction (SSI) problems. SSI problems under external excitation such as earthquake motion may be viewed as a scattering problem, where a local feature perturbs the free-field motion in a larger soil domain. This concept was utilized to formulate the direct FE method in Parts I and II of this thesis. The local feature could in this context be any type of structure or local geological feature, either supported on, or embedded in the soil domain. The DRM then only requires that the free-field motion is known in a single continuous layer of elements interior of an absorbing boundary.

For SSI analysis, the large-scale simulation approach has the advantage that the 3D wave field is directly available from the motions recorded in the first step. It is therefore not necessary to make simplifying assumptions restricting the shape of the wave field, such as the assumption of vertically propagating waves. However, the DRM can also be used for seismic input under more restrictive assumption, where the free-field motion is obtained from a simpler auxiliary problem.

B.2 Formulation of method

Consider the large, but finite, seismic region Ω^+ that contains a seismic source P_e (Figure B.1a). Within the larger region Ω^+ is a smaller region Ω that contains a local feature such as a structure or a geological feature for which the seismic response is to be computed. The

material in the following derivation is for simplicity assumed to be linear elastic in both Ω^+ and Ω , however this assumption can be partly removed later.

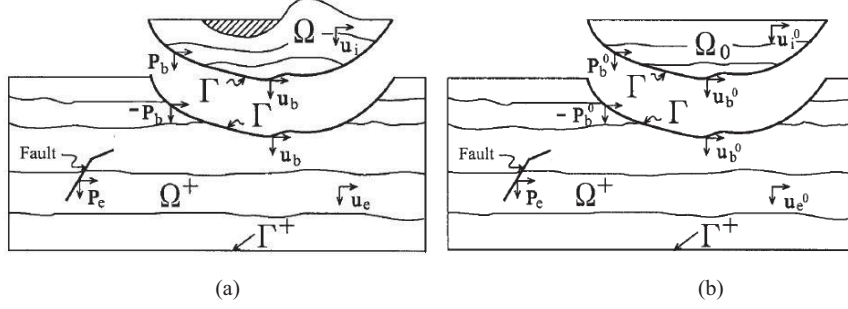


Figure B.1: (a) Original seismic regions partitioned into two substructures Ω and Ω^+ by a fictitious divide Γ ; (b) auxiliary free-field problem where localized features of the actual problem in Ω have been replaced by a simpler background model over domain Ω_0 . Figure from Ref. [40].

Presented herein in its original notation [40], the equations of motion for this system are governed by Navier's equations of elastodynamics, which when discretized spatially by finite elements can be expressed in partitioned form as

$$\begin{bmatrix} M_{ii}^{\Omega} & M_{ib}^{\Omega} \\ M_{bi}^{\Omega} & M_{bb}^{\Omega} \end{bmatrix} \begin{Bmatrix} \ddot{u}_i \\ \ddot{u}_b \end{Bmatrix} + \begin{bmatrix} C_{ii}^{\Omega} & C_{ib}^{\Omega} \\ C_{bi}^{\Omega} & C_{bb}^{\Omega} \end{bmatrix} \begin{Bmatrix} \dot{u}_i \\ \dot{u}_b \end{Bmatrix} + \begin{bmatrix} K_{ii}^{\Omega} & K_{ib}^{\Omega} \\ K_{bi}^{\Omega} & K_{bb}^{\Omega} \end{bmatrix} \begin{Bmatrix} u_i \\ u_b \end{Bmatrix} = \begin{Bmatrix} 0 \\ P_b \end{Bmatrix}, \text{ in } \Omega \quad (\text{B.1a})$$

$$\begin{bmatrix} M_{bb}^{\Omega^+} & M_{be}^{\Omega^+} \\ M_{eb}^{\Omega^+} & M_{ee}^{\Omega^+} \end{bmatrix} \begin{Bmatrix} \ddot{u}_b \\ \ddot{u}_e \end{Bmatrix} + \begin{bmatrix} C_{bb}^{\Omega^+} & C_{be}^{\Omega^+} \\ C_{eb}^{\Omega^+} & C_{ee}^{\Omega^+} \end{bmatrix} \begin{Bmatrix} \dot{u}_b \\ \dot{u}_e \end{Bmatrix} + \begin{bmatrix} K_{bb}^{\Omega^+} & K_{be}^{\Omega^+} \\ K_{eb}^{\Omega^+} & K_{ee}^{\Omega^+} \end{bmatrix} \begin{Bmatrix} u_b \\ u_e \end{Bmatrix} = \begin{Bmatrix} -P_b \\ P_e \end{Bmatrix}, \text{ in } \Omega^+ \quad (\text{B.1b})$$

where the matrices M , C and K are the mass, damping and stiffness matrices, respectively, and the subscripts i , e , b refer to nodes in the interior, exterior and on the boundary between them (Figure B.1a), respectively. To obtain the traditional form of the equations of motion, these equations are added to obtain

$$\begin{bmatrix} M_{ii}^{\Omega} & M_{ib}^{\Omega} & 0 \\ M_{bb}^{\Omega} + M_{bb}^{\Omega^+} & M_{be}^{\Omega^+} & M_{be}^{\Omega^+} \\ \text{sym} & M_{ee}^{\Omega^+} & \end{bmatrix} \begin{Bmatrix} \ddot{u}_i \\ \ddot{u}_b \\ \ddot{u}_e \end{Bmatrix} + \begin{bmatrix} C_{ii}^{\Omega} & C_{ib}^{\Omega} & 0 \\ \text{sym} & C_{bb}^{\Omega} + C_{bb}^{\Omega^+} & C_{be}^{\Omega^+} \\ \text{sym} & C_{ee}^{\Omega^+} & \end{bmatrix} \begin{Bmatrix} \dot{u}_i \\ \dot{u}_b \\ \dot{u}_e \end{Bmatrix} + \begin{bmatrix} K_{ii}^{\Omega} & K_{ib}^{\Omega} & 0 \\ \text{sym} & K_{bb}^{\Omega} + K_{bb}^{\Omega^+} & K_{be}^{\Omega^+} \\ \text{sym} & K_{ee}^{\Omega^+} & \end{bmatrix} \begin{Bmatrix} u_i \\ u_b \\ u_e \end{Bmatrix} = \begin{Bmatrix} 0 \\ 0 \\ P_e \end{Bmatrix} \quad (\text{B.2})$$

To transfer the seismic excitation to the interior region Ω , an auxiliary free-field problem is considered, in which the region Ω is replaced by the simpler background region Ω_0 that does not include the local feature (Figure B.1b). The outer region Ω^+ remains identical. All variables in the auxiliary free-field problem will be denoted using the superscript 0.

With the replacement of the interior region, the equations of motion for the auxiliary "free-field" problem in the outer region Ω^+ can now be written as

$$\begin{bmatrix} M_{bb}^{\Omega^+} & M_{be}^{\Omega^+} \\ M_{eb}^{\Omega^+} & M_{ee}^{\Omega^+} \end{bmatrix} \begin{Bmatrix} \dot{u}_b^0 \\ \dot{u}_e^0 \end{Bmatrix} + \begin{bmatrix} C_{bb}^{\Omega^+} & C_{be}^{\Omega^+} \\ C_{eb}^{\Omega^+} & C_{ee}^{\Omega^+} \end{bmatrix} \begin{Bmatrix} \dot{u}_b^0 \\ \dot{u}_e^0 \end{Bmatrix} + \begin{bmatrix} K_{bb}^{\Omega^+} & K_{be}^{\Omega^+} \\ K_{eb}^{\Omega^+} & K_{ee}^{\Omega^+} \end{bmatrix} \begin{Bmatrix} u_b^0 \\ u_e^0 \end{Bmatrix} = \begin{Bmatrix} -P_b^0 \\ P_e \end{Bmatrix} \quad (\text{B.3})$$

where P_b^0 are the interface forces at the boundary Γ . Since there is no change in the exterior region Ω^+ , the mass, stiffness and damping matrices M , C and K , and force vector P_e , remains the same.

From the second of these equations, the force vector P_e can be expressed as

$$P_e = M_{eb}^{\Omega^+} \ddot{u}_b^0 + M_{ee}^{\Omega^+} \ddot{u}_e^0 + C_{eb}^{\Omega^+} \dot{u}_b^0 + C_{ee}^{\Omega^+} \dot{u}_e^0 + K_{eb}^{\Omega^+} u_b^0 + K_{ee}^{\Omega^+} u_e^0 \quad (\text{B.4})$$

One can solve for the displacement field for the complete domain by substituting Equation (B.4) into Equation (B.2). This is not a very practical approach however, as it requires that the free field motion u_e^0 to be computed and stored in the entire domain Ω^+ .

To simplify, a substitution of variables is introduced to express the total variables u_e as the sum of the free-field u_e^0 and the scattered field w_e due to the local feature:

$$u_e = u_e^0 + w_e \quad (\text{B.5})$$

Substituting Equation (B.5) into Equation (B.2), and then substituting for P_e from Equation (B.4), the desired equation is obtained as

$$\begin{bmatrix} M_{ii}^{\Omega} & M_{ib}^{\Omega} & 0 \\ & M_{bb}^{\Omega} + M_{bb}^{\Omega^+} & M_{be}^{\Omega^+} \\ \text{sym} & & M_{ee}^{\Omega^+} \end{bmatrix} \begin{Bmatrix} \ddot{u}_i \\ \ddot{u}_b \\ \ddot{w}_e \end{Bmatrix} + \begin{bmatrix} C_{ii}^{\Omega} & C_{ib}^{\Omega} & 0 \\ & C_{bb}^{\Omega} + C_{bb}^{\Omega^+} & C_{be}^{\Omega^+} \\ \text{sym} & & C_{ee}^{\Omega^+} \end{bmatrix} \begin{Bmatrix} \dot{u}_i \\ \dot{u}_b \\ \dot{w}_e \end{Bmatrix} + \begin{bmatrix} K_{ii}^{\Omega} & K_{ib}^{\Omega} & 0 \\ & K_{bb}^{\Omega} + K_{bb}^{\Omega^+} & K_{be}^{\Omega^+} \\ \text{sym} & & K_{ee}^{\Omega^+} \end{bmatrix} \begin{Bmatrix} u_i \\ u_b \\ w_e \end{Bmatrix} = \begin{Bmatrix} 0 \\ -M_{be}^{\Omega^+} \ddot{u}_e^0 - C_{be}^{\Omega^+} \dot{u}_e^0 - K_{be}^{\Omega^+} u_e^0 \\ M_{eb}^{\Omega^+} \ddot{u}_b^0 + C_{eb}^{\Omega^+} \dot{u}_b^0 + K_{eb}^{\Omega^+} u_b^0 \end{Bmatrix} \quad (\text{B.6})$$

seismic input in SSI analyses when the wave field is known beforehand at a predefined layer of elements encompassing a local region of interest. This is e.g., the case if the seismic input motion is obtained directly using large scale earthquake simulations, or if certain restrictions are imposed to simplify the shape of the wave field.

When the exterior region is truncated by $\hat{\Gamma}^+$ in Step II, the accuracy is determined by the adequacy of the absorbing boundaries applied at $\hat{\Gamma}^+$ to absorb the scattered wave field w_e . Since the wave field in the exterior region $\hat{\Omega}^+$ in Step II consists only of outgoing waves, the wave field can be monitored to provide information about the dynamic characteristics of the local feature, and the performance of the absorbing boundaries.

B.3 DRM for seismic input in SSI models

Assume that the DRM is used to model the same dam–foundation rock problem from Appendix A (Figure A.5), where viscous dampers are used to model the unbounded extend of the foundation domain. The equations of motion for this system are given by Equation (B.6), The effective seismic input forces are given in terms of the free-field motion by Equation (B.7) and applied to a single layer of elements somewhere interior of the absorbing boundary between Γ and Γ_e (Figure B.3).

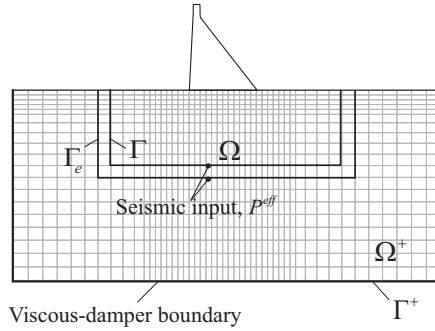


Figure B.3: DRM for seismic input to dam–foundation rock system.

Viscous dampers are applied at the outer boundary of the exterior region Ω^+ . At this boundary, the viscous dampers must absorb the motion relative to the free-field motion, which by definition in the DRM formulation (Equation B.5) is equal to $w_e = u_e - u_e^0$. This means viscous dampers with coefficients ρAV_k can be applied at the truncation boundary without further modification.

Even though the formulation for the DRM seems very different from the direct FE method formulated in Part I, they are in fact quite similar when used for soil–structure interacting models: both formulations provide a method to apply effective earthquake forces to the model, and both allow for the outgoing (scattered) motion to be absorbed at the absorbing boundary. The advantage of the DRM is that it decouples the location of the absorbing boundary from application of earthquake forces, thus allowing advanced boundary

conditions to be used and the domain sizes to be reduced accordingly. However, two significant disadvantages are (1) implementation of DRM requires modification of the FE source code effectively limiting its application to users of LS-DYNA, the only FE code routinely used in dam engineering where DRM is available; and (2) specifying the seismic input for a combined dam–water–foundation rock system with small domain sizes is impractical because it requires auxiliary analysis of a complex water–foundation rock system and extensive book-keeping. For these reasons, the DRM was not chosen as the method for applying seismic input in the direct FE method developed in Part I and II of the thesis.

B.4 Comparison of direct FE method to DRM

To compare the DRM and the direct FE method, the dynamic response of Pine Flat Dam is computed by both methods. The FE mesh and material properties of this system are described in Section A.3 of Appendix A. The seismic input for the DRM is computed from Equation (B.7) with the free-field motions obtained from the same auxiliary analysis that is used for the direct FE method (described in Box 3.2 of Part I). This way, both methods are based on the same set of assumptions regarding the seismic wave field (vertically propagating waves).

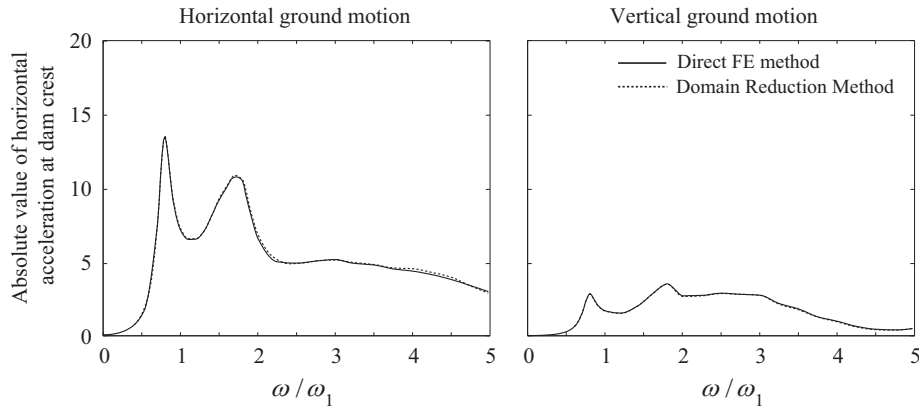


Figure B.4: Comparison of frequency response functions computed by the direct FE method and DRM for dam on flexible foundation rock due to horizontal and vertical ground motion. $\zeta_s = \zeta_f = 2\%$.

Frequency response functions for the dam computed by the two methods are compared in Figure B.4. The response computed by the direct FE method is essentially identical to that when using the DRM, only some insignificant differences exist because of the numerical discretization. This demonstrates the equivalency of the two methods when used to specify seismic inputs: the DRM will give identical results as the direct FE method when used to analyze the same dam–foundation rock system with the same boundary condition and free-field motions based on the same assumptions.

APPENDIX C

Computing frequency response functions in the time domain

The frequency response functions for the dam response that are computed and compared to results from the substructure method in Parts I and II are dimensionless response factors that represent the radial acceleration at the crest of the dam to unit harmonic, free-field acceleration. The details of two procedures for computing these frequency response functions in the direct FE method are presented in this appendix, and both procedures are verified individually by comparing against independent solutions obtained using the substructure method.

C.1 Frequency response functions by repeated steady-state analysis

The first method to determine the frequency response function $H(\omega)$ for the system is to perform repeated steady-state analysis (Figure C.1): (1) first, the steady-state response u_n of the system to a single excitation frequency f_n is computed by solving the by equations of motion for long enough for steady-state to occur; (2) this analysis is repeated at a sufficient number of frequencies to generate a smooth frequency response function.

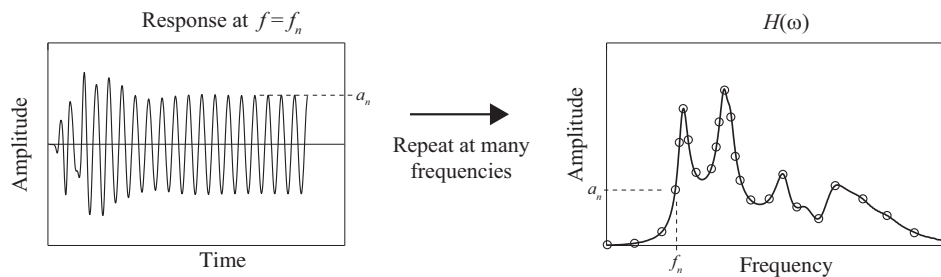


Figure C.1: Schematic overview of procedure for computing frequency response functions by repeated steady-state analysis.

This approach is straightforward, but because it requires repeated steady-state analyses of the system at a high number of frequencies, it becomes excessively time consuming for 3D dam–water–foundation rock systems that may easily have several hundreds of thousands of

finite elements. An alternative procedure that is much more computationally effective is presented next.

C.2 Frequency response functions by Fourier analysis

The dynamic response $u(t)$ of a system can be expressed in the frequency domain as the product of the frequency response function for the system and the Fourier transfer of the applied excitation [67]:

$$U(\omega) = H(\omega) A(\omega) \tag{C.1}$$

where $U(\omega)$ is the Fourier transform of the dynamic response $u(t)$, $H(\omega)$ is the frequency response function (FRF), and $A(\omega)$ is the Fourier transform of the applied excitation $a_g(t)$. Rearranging Equation (C.1), an expression for the FRF for the system is obtained as

$$H(\omega) = U(\omega) / A(\omega) \tag{C.2}$$

If the input and outputs signals were described by analytical expressions valid for all frequencies it would be possible to obtain the exact FRF from Equation (C.2). Such analytical expressions are rarely available except for very simple systems; thus, the above equation will normally provide a *numerical estimate* of the FRF which is valid only within a given range of frequencies. Such an estimate is obtained for the arch dam–water–foundation rock system using the following procedure (Figure C.2):

1. The free-field control motion $a_g(t)$ is defined as a long series of continuous unit harmonic sine waves that has gradually increasing frequency. A sufficient number of frequencies are included in $a_g(t)$ to ensure that the system is excited adequately over the frequency range of interest between approx. 2 – 20 Hz.
2. The dynamic response $u(t)$, here selected as the radial acceleration at the crest of the dam, is computed by time-domain analysis of the FE model by the direct FE method.
3. The Fourier transforms $A(\omega)$ and $U(\omega)$ of the input and output signals, respectively, are computed using the Fast Fourier Transform (FFT).
4. The FRF for the dam response is computed from Equation (C.2).

The advantage of this approach is that it requires only a single dynamic analysis, thus significantly reducing the computational effort compared to doing a repeated number of steady-state analyses. For example, it takes just under 3 hours to accurately compute the FRF for the arch dam–water–foundation rock system analyzed in Part II of this thesis between 2 – 20 Hz using the Fourier analysis approach. In contrast, obtaining the same FRF using repeated steady-state analysis takes in excess of 12 hours.

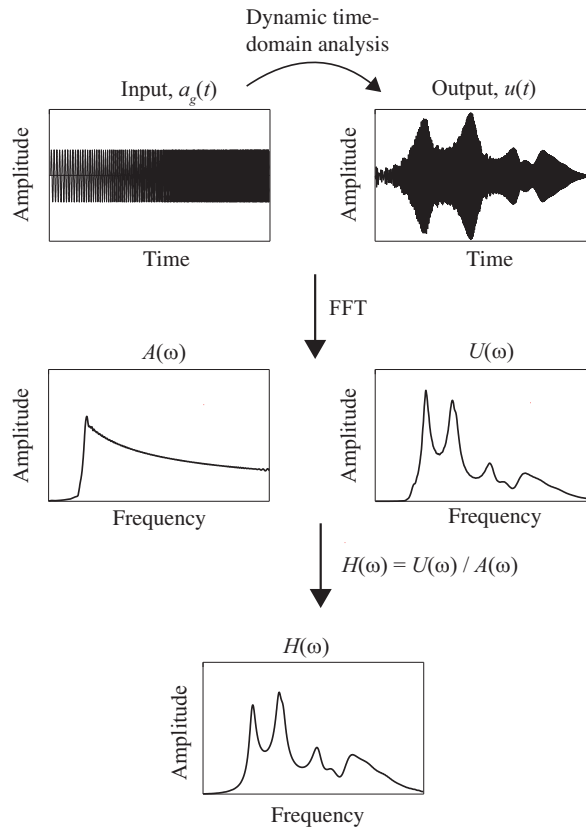


Figure C.2: Schematic overview of procedure for computing frequency response functions using Fourier analysis.

C.3 Verification of implementation

Implementation of the two procedures for obtaining FRFs in the time domain is verified by computing the response of Morrow Point Dam alone on rigid foundation with empty reservoir and comparing against results obtained using the substructure method. The mesh and material properties for the dam are the same as those described in Section 5.2.1 of Part II.

The results presented in Figure C.3 demonstrates that the two procedures for obtaining FRFs give near identical results, and that these results are very close to those obtained using the substructure method.

APPENDIX C

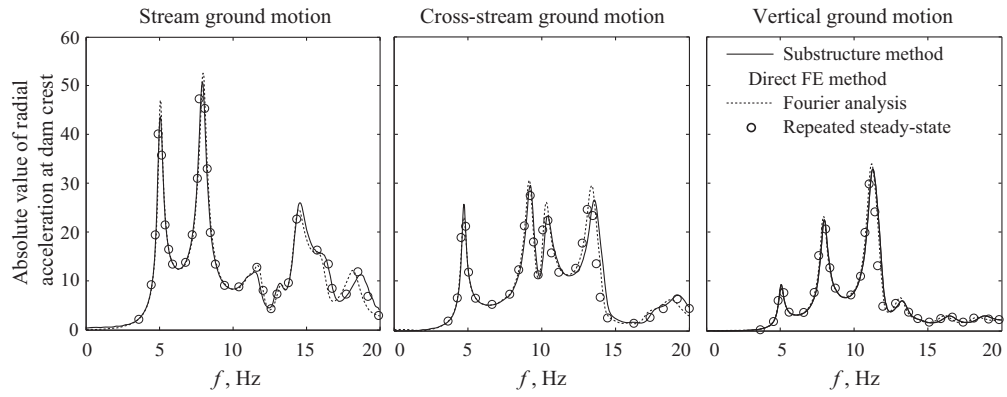


Figure C.3: Comparison of frequency response functions for the amplitude of relative radial acceleration at the crest of dam on rigid foundation with empty reservoir due to uniform stream, cross-stream and vertical ground motions. $\zeta_s = 3\%$.

APPENDIX D

Applying uniform ground motion in the direct FE method

The response results presented in Section 5.3 of Part II for several dam–water–foundation rock systems were computed under the assumption that the ground motion $a_g(t)$ was uniform at the dam–foundation interface and water–foundation interface. For these analyses, the seismic input method proposed by Wilson [171] was extended and implemented to apply the earthquake excitation to the FE model. This method is derived below for the dam–water–foundation rock system

D.1 Equations of motion

Consider the dam–water–foundation rock system (Figure 3.1 of Part II) whose equations of motion were given by Equation (3.1) in Part II. For convenience of notation in the subsequent derivation it is here assumed that the system is linear elastic with no material damping, thus reducing the governing equation for the dam–water–foundation rock system to:

$$\begin{bmatrix} \mathbf{m} & \mathbf{0} \\ \rho(\mathbf{Q}_h^T + \mathbf{Q}_b^T) & \mathbf{s} \end{bmatrix} \begin{Bmatrix} \ddot{\mathbf{r}}^t \\ \ddot{\mathbf{p}}^t \end{Bmatrix} + \begin{bmatrix} \mathbf{k} & -(\mathbf{Q}_h + \mathbf{Q}_b) \\ \mathbf{0} & \mathbf{h} \end{bmatrix} \begin{Bmatrix} \mathbf{r}^t \\ \mathbf{p}^t \end{Bmatrix} = \begin{Bmatrix} \mathbf{R}_f^t \\ \mathbf{H}_r^t \end{Bmatrix} \quad (\text{D.1})$$

If water–foundation rock is ignored upstream of the absorbing boundary Γ_r and the free-field foundation-rock motion \mathbf{r}^0 is known, we can express the total motion \mathbf{r}^t in terms of the displacements \mathbf{r} relative to the free-field motion \mathbf{r}^0 , i.e., $\mathbf{r}^t = \mathbf{r} + \mathbf{r}^0$. Rewriting Equation (D.1) and collecting terms that involve \mathbf{r}^0 on the right hand side, the following equation is obtained:

$$\begin{bmatrix} \mathbf{m} & \mathbf{0} \\ \rho(\mathbf{Q}_h^T + \mathbf{Q}_b^T) & \mathbf{s} \end{bmatrix} \begin{Bmatrix} \ddot{\mathbf{r}} \\ \ddot{\mathbf{p}} \end{Bmatrix} + \begin{bmatrix} \mathbf{k} & -(\mathbf{Q}_h + \mathbf{Q}_b) \\ \mathbf{0} & \mathbf{h} \end{bmatrix} \begin{Bmatrix} \mathbf{r} \\ \mathbf{p} \end{Bmatrix} = \begin{Bmatrix} \mathbf{R}_f \\ \mathbf{H}_r \end{Bmatrix} - \begin{Bmatrix} \mathbf{m}\ddot{\mathbf{r}}^0 + \mathbf{k}\mathbf{r}^0 - \mathbf{R}_f^0 \\ \rho(\mathbf{Q}_h^T + \mathbf{Q}_b^T)\ddot{\mathbf{r}}^0 \end{Bmatrix} \quad (\text{D.2})$$

This equation can be simplified when the free-field displacements \mathbf{r}_b^0 at the dam–foundation interface are uniform. Under this assumption, the static rigid body motion of the dam is:

$$\mathbf{k}_d \mathbf{r}_b^0 = \mathbf{0} \quad (\text{D.3})$$

where \mathbf{k}_d is the stiffness matrix for the dam alone. Furthermore, the equation governing displacements in the free-field foundation-rock system are

$$\mathbf{m}_0 \ddot{\mathbf{r}}^0 + \mathbf{k}_0 \mathbf{r}^0 = \mathbf{R}_f^0 \quad (\text{D.4})$$

where \mathbf{m}_0 and \mathbf{k}_0 are the mass and stiffness matrices, respectively, for the foundation rock alone. Using Equations (D.3) and (D.4) and cancelling terms, Equation (D.2) becomes

$$\begin{bmatrix} \mathbf{m} & \mathbf{0} \\ \rho(\mathbf{Q}_h^T + \mathbf{Q}_b^T) & \mathbf{s} \end{bmatrix} \begin{Bmatrix} \ddot{\mathbf{r}} \\ \ddot{\mathbf{p}}' \end{Bmatrix} + \begin{bmatrix} \mathbf{k} & -(\mathbf{Q}_h + \mathbf{Q}_b) \\ \mathbf{0} & \mathbf{h} \end{bmatrix} \begin{Bmatrix} \mathbf{r} \\ \mathbf{p}' \end{Bmatrix} = \begin{Bmatrix} \mathbf{R}_f \\ \mathbf{H}_r' \end{Bmatrix} + \begin{Bmatrix} \mathbf{P}_d^0 \\ -\rho(\mathbf{Q}_h^T + \mathbf{Q}_b^T) \ddot{\mathbf{r}}_b^0 \end{Bmatrix} \quad (\text{D.5})$$

where the effective earthquake forces \mathbf{P}_d^0 applied to the dam nodes are

$$\mathbf{P}_d^0 = -\mathbf{m}_d \ddot{\mathbf{r}}_b^0 = -\mathbf{m}_d \mathbf{u}_g(t) \quad (\text{D.6})$$

where \mathbf{u} is the influence vector [67], and $a_g(t)$ is the free-field ground motion assumed at the dam–foundation interface.

Substituting Equations (3.2a) and (3.4b) of Part II for \mathbf{R}_f and \mathbf{H}_r' , respectively, in Equation (D.6), and adding material damping and static forces to the formulation, gives the final equations of motion for the dam–water–foundation rock system with uniform excitation:

$$\begin{bmatrix} \mathbf{m} & \mathbf{0} \\ \rho(\mathbf{Q}_h^T + \mathbf{Q}_b^T) & \mathbf{s} \end{bmatrix} \begin{Bmatrix} \ddot{\mathbf{r}} \\ \ddot{\mathbf{p}}' \end{Bmatrix} + \begin{bmatrix} \mathbf{c} + \mathbf{c}_f & \mathbf{0} \\ \mathbf{0} & \mathbf{b} + \mathbf{c}_r \end{bmatrix} \begin{Bmatrix} \dot{\mathbf{r}} \\ \dot{\mathbf{p}}' \end{Bmatrix} + \begin{bmatrix} \mathbf{k} & -(\mathbf{Q}_h + \mathbf{Q}_b) \\ \mathbf{0} & \mathbf{h} \end{bmatrix} \begin{Bmatrix} \mathbf{r} \\ \mathbf{p}' \end{Bmatrix} = \begin{Bmatrix} \mathbf{R}^{\text{st}} \\ \mathbf{0} \end{Bmatrix} + \begin{Bmatrix} \mathbf{P}_d^0 \\ \mathbf{P}_r^0 - \rho(\mathbf{Q}_h^T + \mathbf{Q}_b^T) \ddot{\mathbf{r}}_b^0 \end{Bmatrix} \quad (\text{D.7})$$

Comparing Equation (D.7) to Equation (3.6) it is seen that the change of variable $\mathbf{r}' = \mathbf{r} + \mathbf{r}^0$ in the dam and foundation rock has led to two changes: (1) the effective earthquake forces \mathbf{P}_f^0 at the foundation boundaries have been replaced by the effective earthquake forces \mathbf{P}_d^0 applied to the dam only; and (2) the effective earthquake forces \mathbf{P}_r^0 at the fluid boundary have been supplemented by forces $-\rho(\mathbf{Q}_h^T + \mathbf{Q}_b^T) \ddot{\mathbf{r}}_b^0$ applied to the dam–water and water–foundation interfaces. These modifications allow for application of effective earthquake forces that is consistent with the assumption of uniform ground motion at the dam–foundation and water–foundation interfaces.

D.2 Verification of implementation

Implementation of the method is verified by computing the response of Morrow Point Dam on rigid foundation with full reservoir, with mesh and material properties chosen as the same as those described in Section 5.2.1 of Part II. The results obtained using the method derived in Section D.1 are compared with independent results obtained by directly prescribing the free-field displacements at the dam–foundation and water–foundation interfaces.

The frequency response functions for the amplitude of relative radial acceleration at the crest of the dam obtained by the two methods are presented in Figure D.1. The results obtained using Equation (D.7) leads to results that are essentially identical to those obtained by directly prescribing the free-field displacements for the system. The small differences in the results are due to the slight numerical differences associated with applying forces based on accelerations vs. directly prescribing base displacements.

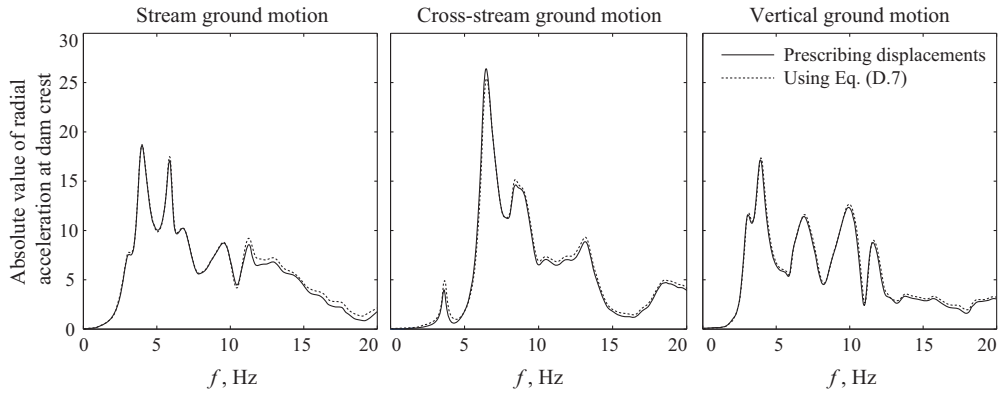


Figure D.1: Comparison of frequency response functions for the amplitude of relative radial acceleration at the crest of dam on rigid foundation with full reservoir due to uniform stream, cross-stream and vertical ground motions. $\zeta_s = 3\%$; $\alpha = 0.80$.

APPENDIX E

Computing boundary tractions from 1D stress-strain relations

E.1 One-dimensional stress-strain relations

The simplified 1D free-field analysis presented in Section 6.1 of Part II replaced the actual free-field foundation-rock system by a much simpler system (Figure 6.1b): a homogeneous or horizontally layered halfspace without the canyon topography. Under the assumption of vertically propagating seismic waves, this system reduces to a single column of foundation-rock elements that only allows for shear and axial deformation (Figure E.1a). The boundary tractions for this system can be computed using standard 1D stress-strain relationships:

$$\tau_{xz} = \mu \frac{du}{dz} n_x, \quad \text{for } x\text{-component of ground motion} \quad (\text{E.1a})$$

$$\tau_{yz} = \mu \frac{dv}{dz} n_y, \quad \text{for } y\text{-component of ground motion} \quad (\text{E.1b})$$

$$\sigma_x = \lambda \frac{dw}{dz} n_x, \quad \sigma_y = \lambda \frac{dw}{dz} n_y, \quad \text{for } z\text{-component of ground motion} \quad (\text{E.1c})$$

where σ_k and τ_{kz} , $k = x, y$ are the normal and tangential boundary tractions (Figure E.1b); u, v, w are the displacements in the x, y and z -direction, respectively; λ and μ are the first and second Lamé parameters for the foundation rock; and $n_k = +1$ or -1 if an outward normal points in the positive or negative k -direction, respectively.

Horizontal excitation will only produce tangential tractions because $dw/dz = 0$, and vertical motion will only produce normal tractions because $du/dz = 0$ and $dv/dz = 0$ (Figure E.1a). From the boundary tractions σ_k and τ_{kz} , nodal forces are computed by multiplying by the tributary area of each node.

E.2 Verification of implementation

Implementation of the method is verified by computing the surface response of the flat foundation domain of Figure 5.1 of Part II with the free-field control motion $a_g^k(t)$ defined at the surface by the S69E, S21W and vertical components of the Taft ground motion. Effective earthquake forces \mathbf{P}_f^0 are computed from the procedures summarized in Box 4.1 of Part II at

the bottom boundary and from a 1D free-field analysis (Box 6.1) with boundary tractions computed from Equation (E.1) at the side boundaries, and the motion at the surface of the flat foundation domain is determined.

The results presented in Figure E.2 shows a near perfect match between the assumed free-field control motion and the computed motion at the surface of the flat foundation domain, thus verifying the implementation of the procedure.

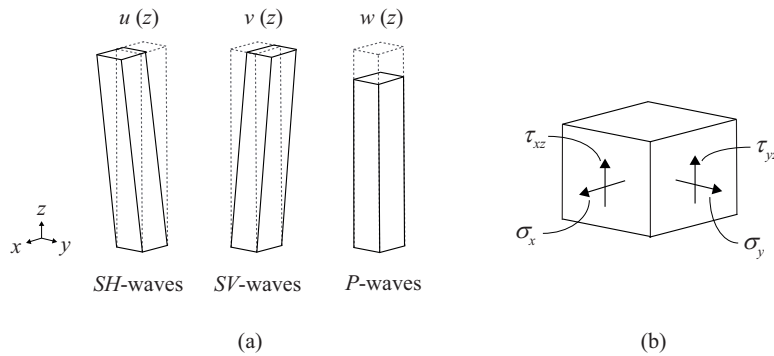


Figure E.1: (a) Deformation of foundation rock column due to vertically propagating SH - , SV - and P -waves; (b) normal and tangential boundary tractions for foundation-rock element.

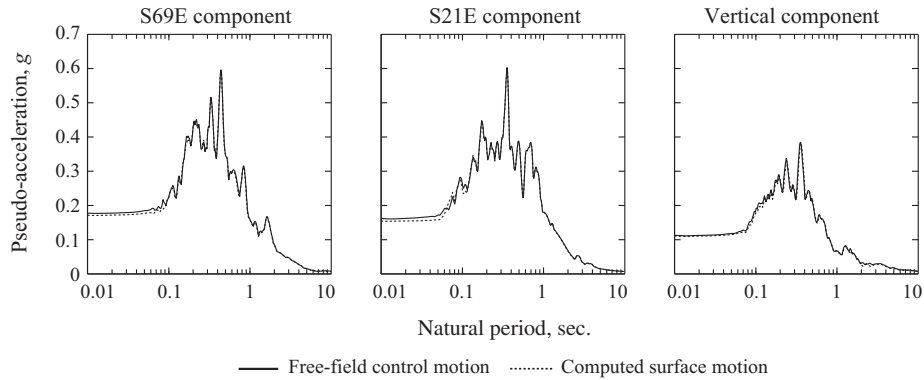


Figure E.2: Results from Flat Box Test: comparison of 5% damped pseudo-acceleration response spectra of free-field control motion and motion computed at nodes on the flat box surface.

**DEPARTMENT OF STRUCTURAL ENGINEERING
NORWEGIAN UNIVERSITY OF SCIENCE AND TECHNOLOGY**

N-7491 TRONDHEIM, NORWAY
Telephone: +47 73 59 47 00 Telefax: +47 73 59 47 01

"Reliability Analysis of Structural Systems using Nonlinear Finite Element Methods",
C. A. Holm, 1990:23, ISBN 82-7119-178-0.

"Uniform Stratified Flow Interaction with a Submerged Horizontal Cylinder",
Ø. Arntsen, 1990:32, ISBN 82-7119-188-8.

"Large Displacement Analysis of Flexible and Rigid Systems Considering Displacement-
Dependent Loads and Nonlinear Constraints",
K. M. Mathisen, 1990:33, ISBN 82-7119-189-6.

"Solid Mechanics and Material Models including Large Deformations",
E. Levold, 1990:56, ISBN 82-7119-214-0, ISSN 0802-3271.

"Inelastic Deformation Capacity of Flexurally-Loaded Aluminium Alloy Structures",
T. Welø, 1990:62, ISBN 82-7119-220-5, ISSN 0802-3271.

"Visualization of Results from Mechanical Engineering Analysis",
K. Aamnes, 1990:63, ISBN 82-7119-221-3, ISSN 0802-3271.

"Object-Oriented Product Modeling for Structural Design",
S. I. Dale, 1991:6, ISBN 82-7119-258-2, ISSN 0802-3271.

"Parallel Techniques for Solving Finite Element Problems on Transputer Networks",
T. H. Hansen, 1991:19, ISBN 82-7119-273-6, ISSN 0802-3271.

"Statistical Description and Estimation of Ocean Drift Ice Environments",
R. Korsnes, 1991:24, ISBN 82-7119-278-7, ISSN 0802-3271.

"Properties of concrete related to fatigue damage: with emphasis on high strength concrete",
G. Petkovic, 1991:35, ISBN 82-7119-290-6, ISSN 0802-3271.

"Turbidity Current Modelling",
B. Brørs, 1991:38, ISBN 82-7119-293-0, ISSN 0802-3271.

"Zero-Slump Concrete: Rheology, Degree of Compaction and Strength. Effects of Fillers as
Part Cement-Replacement",
C. Sørensen, 1992:8, ISBN 82-7119-357-0, ISSN 0802-3271.

"Nonlinear Analysis of Reinforced Concrete Structures Exposed to Transient Loading",
K. V. Høiseth, 1992:15, ISBN 82-7119-364-3, ISSN 0802-3271.

"Finite Element Formulations and Solution Algorithms for Buckling and Collapse Analysis of Thin Shells",
R. O. Bjærum, 1992:30, ISBN 82-7119-380-5, ISSN 0802-3271.

"Response Statistics of Nonlinear Dynamic Systems",
J. M. Johnsen, 1992:42, ISBN 82-7119-393-7, ISSN 0802-3271.

"Digital Models in Engineering. A Study on why and how engineers build and operate digital models for decision support",
J. Høyte, 1992:75, ISBN 82-7119-429-1, ISSN 0802-3271.

"Sparse Solution of Finite Element Equations",
A. C. Damhaug, 1992:76, ISBN 82-7119-430-5, ISSN 0802-3271.

"Some Aspects of Floating Ice Related to Sea Surface Operations in the Barents Sea",
S. Løset, 1992:95, ISBN 82-7119-452-6, ISSN 0802-3271.

"Modelling of Cyclic Plasticity with Application to Steel and Aluminium Structures",
O. S. Hopperstad, 1993:7, ISBN 82-7119-461-5, ISSN 0802-3271.

"The Free Formulation: Linear Theory and Extensions with Applications to Tetrahedral Elements with Rotational Freedoms",
G. Skeie, 1993:17, ISBN 82-7119-472-0, ISSN 0802-3271.

"Høyfast betongs motstand mot piggdekkslitasje. Analyse av resultater fra prøving i Veisliter'n",
T. Tveter, 1993:62, ISBN 82-7119-522-0, ISSN 0802-3271.

"A Nonlinear Finite Element Based on Free Formulation Theory for Analysis of Sandwich Structures",
O. Aamlid, 1993:72, ISBN 82-7119-534-4, ISSN 0802-3271.

"The Effect of Curing Temperature and Silica Fume on Chloride Migration and Pore Structure of High Strength Concrete",
C. J. Hauck, 1993:90, ISBN 82-7119-553-0, ISSN 0802-3271.

"Failure of Concrete under Compressive Strain Gradients",
G. Markeset, 1993:110, ISBN 82-7119-575-1, ISSN 0802-3271.

"An experimental study of internal tidal amphidromes in Vestfjorden",
J. H. Nilsen, 1994:39, ISBN 82-7119-640-5, ISSN 0802-3271.

"Structural analysis of oil wells with emphasis on conductor design",
H. Larsen, 1994:46, ISBN 82-7119-648-0, ISSN 0802-3271.

- "Adaptive methods for non-linear finite element analysis of shell structures",
K. M. Okstad, 1994:66, ISBN 82-7119-670-7, ISSN 0802-3271.
- "On constitutive modelling in nonlinear analysis of concrete structures",
O. Fyrilev, 1994:115, ISBN 82-7119-725-8, ISSN 0802-3271.
- "Fluctuating wind load and response of a line-like engineering structure with emphasis on motion-induced wind forces",
J. Bogunovic Jakobsen, 1995:62, ISBN 82-7119-809-2, ISSN 0802-3271.
- "An experimental study of beam-columns subjected to combined torsion, bending and axial actions",
A. Aalberg, 1995:66, ISBN 82-7119-813-0, ISSN 0802-3271.
- "Scaling and cracking in unsealed freeze/thaw testing of Portland cement and silica fume concretes",
S. Jacobsen, 1995:101, ISBN 82-7119-851-3, ISSN 0802-3271.
- "Damping of water waves by submerged vegetation. A case study of laminaria hyperborea",
A. M. Dubi, 1995:108, ISBN 82-7119-859-9, ISSN 0802-3271.
- "The dynamics of a slope current in the Barents Sea",
Sheng Li, 1995:109, ISBN 82-7119-860-2, ISSN 0802-3271.
- "Modellering av delmaterialenes betydning for betongens konsistens",
Ernst Mørtsell, 1996:12, ISBN 82-7119-894-7, ISSN 0802-3271.
- "Bending of thin-walled aluminium extrusions",
Birgit Søvik Opheim, 1996:60, ISBN 82-7119-947-1, ISSN 0802-3271.
- "Material modelling of aluminium for crashworthiness analysis",
Torodd Berstad, 1996:89, ISBN 82-7119-980-3, ISSN 0802-3271.
- "Estimation of structural parameters from response measurements on submerged floating tunnels",
Rolf Magne Larssen, 1996:119, ISBN 82-471-0014-2, ISSN 0802-3271.
- "Numerical modelling of plain and reinforced concrete by damage mechanics",
Mario A. Polanco-Loria, 1997:20, ISBN 82-471-0049-5, ISSN 0802-3271.
- "Nonlinear random vibrations - numerical analysis by path integration methods",
Vibeke Moe, 1997:26, ISBN 82-471-0056-8, ISSN 0802-3271.
- "Numerical prediction of vortex-induced vibration by the finite element method",
Joar Martin Dalheim, 1997:63, ISBN 82-471-0096-7, ISSN 0802-3271.
- "Time domain calculations of buffeting response for wind sensitive structures",
Ketil Aas-Jakobsen, 1997:148, ISBN 82-471-0189-0, ISSN 0802-3271.

- "A numerical study of flow about fixed and flexibly mounted circular cylinders",
Trond Stokka Meling, 1998:48, ISBN 82-471-0244-7, ISSN 0802-3271.
- "Estimation of chloride penetration into concrete bridges in coastal areas",
Per Egil Steen, 1998:89, ISBN 82-471-0290-0, ISSN 0802-3271.
- "Stress-resultant material models for reinforced concrete plates and shells",
Jan Arve Øverli, 1998:95, ISBN 82-471-0297-8, ISSN 0802-3271.
- "Chloride binding in concrete. Effect of surrounding environment and concrete composition",
Claus Kenneth Larsen, 1998:101, ISBN 82-471-0337-0, ISSN 0802-3271.
- "Rotational capacity of aluminium alloy beams",
Lars A. Moen, 1999:1, ISBN 82-471-0365-6, ISSN 0802-3271.
- "Stretch Bending of Aluminium Extrusions",
Arild H. Clausen, 1999:29, ISBN 82-471-0396-6, ISSN 0802-3271.
- "Aluminium and Steel Beams under Concentrated Loading",
Tore Tryland, 1999:30, ISBN 82-471-0397-4, ISSN 0802-3271.
- "Engineering Models of Elastoplasticity and Fracture for Aluminium Alloys",
Odd-Geir Lademo, 1999:39, ISBN 82-471-0406-7, ISSN 0802-3271.
- "Kapasitet og duktilitet av dybelforbindelser i trekonstruksjoner",
Jan Siem, 1999:46, ISBN 82-471-0414-8, ISSN 0802-3271.
- "Etablering av distribuert ingeniørarbeid; Teknologiske og organisatoriske erfaringer fra en norsk ingeniørbedrift",
Lars Line, 1999:52, ISBN 82-471-0420-2, ISSN 0802-3271.
- "Estimation of Earthquake-Induced Response",
Símon Ólafsson, 1999:73, ISBN 82-471-0443-1, ISSN 0802-3271.
- "Coastal Concrete Bridges: Moisture State, Chloride Permeability and Aging Effects",
Ragnhild Holen Relling, 1999:74, ISBN 82-471-0445-8, ISSN 0802-3271.
- "Capacity Assessment of Titanium Pipes Subjected to Bending and External Pressure",
Arve Bjørset, 1999:100, ISBN 82-471-0473-3, ISSN 0802-3271.
- "Validation of Numerical Collapse Behaviour of Thin-Walled Corrugated Panels",
Håvar Ilstad, 1999:101, ISBN 82-471-0474-1, ISSN 0802-3271.
- "Strength and Ductility of Welded Structures in Aluminium Alloys",
Mirosław Matusiak, 1999:113, ISBN 82-471-0487-3, ISSN 0802-3271.

"Thermal Dilation and Autogenous Deformation as Driving Forces to Self-Induced Stresses in High Performance Concrete",
Øyvind Bjøntegaard, 1999:121, ISBN 82-7984-002-8, ISSN 0802-3271.

"Some Aspects of Ski Base Sliding Friction and Ski Base Structure",
Dag Anders Moldestad, 1999:137, ISBN 82-7984-019-2, ISSN 0802-3271.

"Electrode reactions and corrosion resistance for steel in mortar and concrete",
Roy Antonsen, 2000:10, ISBN 82-7984-030-3, ISSN 0802-3271.

"Hydro-Physical Conditions in Kelp Forests and the Effect on Wave Damping and Dune Erosion. A case study on Laminaria Hyperborea",
Stig Magnar Løvås, 2000:28, ISBN 82-7984-050-8, ISSN 0802-3271.

"Random Vibration and the Path Integral Method",
Christian Skaug, 2000:39, ISBN 82-7984-061-3, ISSN 0802-3271.

"Buckling and geometrical nonlinear beam-type analyses of timber structures",
Trond Even Eggen, 2000:56, ISBN 82-7984-081-8, ISSN 0802-3271.

"Structural Crashworthiness of Aluminium Foam-Based Components",
Arve Grønsund Hanssen, 2000:76, ISBN 82-7984-102-4, ISSN 0809-103X.

"Measurements and simulations of the consolidation in first-year sea ice ridges, and some aspects of mechanical behaviour",
Knut V. Høyland, 2000:94, ISBN 82-7984-121-0, ISSN 0809-103X.

"Kinematics in Regular and Irregular Waves based on a Lagrangian Formulation",
Svein Helge Gjøvund, 2000:86, ISBN 82-7984-112-1, ISSN 0809-103X.

"Self-Induced Cracking Problems in Hardening Concrete Structures",
Daniela Bosnjak, 2000:121, ISBN 82-7984-151-2, ISSN 0809-103X.

"Ballistic Penetration and Perforation of Steel Plates",
Tore Børvik, 2000:124, ISBN 82-7984-154-7, ISSN 0809-103X.

"Freeze-Thaw resistance of Concrete. Effect of: Curing Conditions, Moisture Exchange and Materials",
Terje Finnerup Rønning, 2001:14, ISBN 82-7984-165-2, ISSN 0809-103X

"Structural behaviour of post tensioned concrete structures. Flat slab. Slabs on ground",
Steinar Trygstad, 2001:52, ISBN 82-471-5314-9, ISSN 0809-103X.

"Slipforming of Vertical Concrete Structures. Friction between concrete and slipform panel",
Kjell Tore Fosså, 2001:61, ISBN 82-471-5325-4, ISSN 0809-103X.

"Some numerical methods for the simulation of laminar and turbulent incompressible flows",
Jens Holmen, 2002:6, ISBN 82-471-5396-3, ISSN 0809-103X.

- “Improved Fatigue Performance of Threaded Drillstring Connections by Cold Rolling”,
Steinar Kristoffersen, 2002:11, ISBN: 82-421-5402-1, ISSN 0809-103X.
- "Deformations in Concrete Cantilever Bridges: Observations and Theoretical Modelling",
Peter F. Takács, 2002:23, ISBN 82-471-5415-3, ISSN 0809-103X.
- "Stiffened aluminium plates subjected to impact loading",
Hilde Giæver Hildrum, 2002:69, ISBN 82-471-5467-6, ISSN 0809-103X.
- "Full- and model scale study of wind effects on a medium-rise building in a built up area",
Jónas Thór Snæbjörnsson, 2002:95, ISBN82-471-5495-1, ISSN 0809-103X.
- “Evaluation of Concepts for Loading of Hydrocarbons in Ice-infested water”,
Arnor Jensen, 2002:114, ISBN 82-417-5506-0, ISSN 0809-103X.
- ”Numerical and Physical Modelling of Oil Spreading in Broken Ice”,
Janne K. Økland Gjøsteen, 2002:130, ISBN 82-471-5523-0, ISSN 0809-103X.
- ”Diagnosis and protection of corroding steel in concrete”,
Franz Pruckner, 20002:140, ISBN 82-471-5555-4, ISSN 0809-103X.
- “Tensile and Compressive Creep of Young Concrete: Testing and Modelling”,
Dawood Atrushi, 2003:17, ISBN 82-471-5565-6, ISSN 0809-103X.
- “Rheology of Particle Suspensions. Fresh Concrete, Mortar and Cement Paste with Various
Types of Lignosulfonates”,
Jon Elvar Wallevik, 2003:18, ISBN 82-471-5566-4, ISSN 0809-103X.
- “Oblique Loading of Aluminium Crash Components”,
Aase Reyes, 2003:15, ISBN 82-471-5562-1, ISSN 0809-103X.
- “Utilization of Ethiopian Natural Pozzolans”,
Surafel Ketema Desta, 2003:26, ISSN 82-471-5574-5, ISSN:0809-103X.
- “Behaviour and strength prediction of reinforced concrete structures with discontinuity
regions”, Helge Brå, 2004:11, ISBN 82-471-6222-9, ISSN 1503-8181.
- “High-strength steel plates subjected to projectile impact. An experimental and numerical
study”, Sumita Dey, 2004:38, ISBN 82-471-6282-2 (printed version), ISBN 82-471-6281-4
(electronic version), ISSN 1503-8181.
- “Alkali-reactive and inert fillers in concrete. Rheology of fresh mixtures and expansive
reactions.”
Bård M. Pedersen, 2004:92, ISBN 82-471-6401-9 (printed version), ISBN 82-471-6400-0
(electronic version), ISSN 1503-8181.

“On the Shear Capacity of Steel Girders with Large Web Openings”.
Nils Christian Hagen, 2005:9 ISBN 82-471-6878-2 (printed version), ISBN 82-471-6877-4 (electronic version), ISSN 1503-8181.

”Behaviour of aluminium extrusions subjected to axial loading”.
Østen Jensen, 2005:7, ISBN 82-471-6873-1 (printed version), ISBN 82-471-6872-3 (electronic version), ISSN 1503-8181.

”Thermal Aspects of corrosion of Steel in Concrete”.
Jan-Magnus Østvik, 2005:5, ISBN 82-471-6869-3 (printed version), ISBN 82-471-6868 (electronic version), ISSN 1503-8181.

”Mechanical and adaptive behaviour of bone in relation to hip replacement.” A study of bone remodelling and bone grafting.
Sébastien Muller, 2005:34, ISBN 82-471-6933-9 (printed version), ISBN 82-471-6932-0 (electronic version), ISSN 1503-8181.

“Analysis of geometrical nonlinearities with applications to timber structures”.
Lars Wollebæk, 2005:74, ISBN 82-471-7050-5 (printed version), ISBN 82-471-7019-1 (electronic version), ISSN 1503-8181.

“Pedestrian induced lateral vibrations of slender footbridges”,
Anders Rönquist, 2005:102, ISBN 82-471-7082-5 (printed version), ISBN 82-471-7081-7 (electronic version), ISSN 1503-8181.

“Initial Strength Development of Fly Ash and Limestone Blended Cements at Various Temperatures Predicted by Ultrasonic Pulse Velocity”,
Tom Ivar Fredvik, 2005:112, ISBN 82-471-7105-8 (printed version), ISBN 82-471-7103-1 (electronic version), ISSN 1503-8181.

“Behaviour and modelling of thin-walled cast components”,
Cato Dørum, 2005:128, ISBN 82-471-7140-6 (printed version), ISBN 82-471-7139-2 (electronic version), ISSN 1503-8181.

“Behaviour and modelling of selfpiercing riveted connections”,
Raffaele Porcaro, 2005:165, ISBN 82-471-7219-4 (printed version), ISBN 82-471-7218-6 (electronic version), ISSN 1503-8181.

”Behaviour and Modelling of Aluminium Plates subjected to Compressive Load”,
Lars Rønning, 2005:154, ISBN 82-471-7169-1 (printed version), ISBN 82-471-7195-3 (electronic version), ISSN 1503-8181.

”Bumper beam-longitudinal system subjected to offset impact loading”,
Satyanarayana Kokkula, 2005:193, ISBN 82-471-7280-1 (printed version), ISBN 82-471-7279-8 (electronic version), ISSN 1503-8181.

“Control of Chloride Penetration into Concrete Structures at Early Age”,
Guofei Liu, 2006:46, ISBN 82-471-7838-9 (printed version), ISBN 82-471-7837-0 (electronic version), ISSN 1503-8181.

“Modelling of Welded Thin-Walled Aluminium Structures”,
Ting Wang, 2006:78, ISBN 82-471-7907-5 (printed version), ISBN 82-471-7906-7 (electronic version), ISSN 1503-8181.

”Time-variant reliability of dynamic systems by importance sampling and probabilistic analysis of ice loads”,
Anna Ivanova Olsen, 2006:139, ISBN 82-471-8041-3 (printed version), ISBN 82-471-8040-5 (electronic version), ISSN 1503-8181.

“Fatigue life prediction of an aluminium alloy automotive component using finite element analysis of surface topography”,
Sigmund Kyrre Ås, 2006:25, ISBN 82-471-7791-9 (printed version), ISBN 82-471-7791-9 (electronic version), ISSN 1503-8181.

”Constitutive models of elastoplasticity and fracture for aluminium alloys under strain path change”,
Dasharatha Achani, 2006:76, ISBN 82-471-7903-2 (printed version), ISBN 82-471-7902-4 (electronic version), ISSN 1503-8181.

“Simulations of 2D dynamic brittle fracture by the Element-free Galerkin method and linear fracture mechanics”,
Tommy Karlsson, 2006:125, ISBN 82-471-8011-1 (printed version), ISBN 82-471-8010-3 (electronic version), ISSN 1503-8181.

“Penetration and Perforation of Granite Targets by Hard Projectiles”,
Chong Chiang Seah, 2006:188, ISBN 82-471-8150-9 (printed version), ISBN 82-471-8149-5 (electronic version), ISSN 1503-8181.

“Deformations, strain capacity and cracking of concrete in plastic and early hardening phases”,
Tor Arne Hammer, 2007:234, ISBN 978-82-471-5191-4 (printed version), ISBN 978-82-471-5207-2 (electronic version), ISSN 1503-8181.

“Crashworthiness of dual-phase high-strength steel: Material and Component behaviour”,
Venkatapathi Tarigopula, 2007:230, ISBN 82-471-5076-4 (printed version), ISBN 82-471-5093-1 (electronic version), ISSN 1503-8181.

“Fibre reinforcement in load carrying concrete structures”,
Åse Lyslo Døssland, 2008:50, ISBN 978-82-471-6910-0 (printed version), ISBN 978-82-471-6924-7 (electronic version), ISSN 1503-8181.

“Low-velocity penetration of aluminium plates”,
Frode Grytten, 2008:46, ISBN 978-82-471-6826-4 (printed version), ISBN 978-82-471-6843-1 (electronic version), ISSN 1503-8181.

“Robustness studies of structures subjected to large deformations”,
Ørjan Fyllingen, 2008:24, ISBN 978-82-471-6339-9 (printed version), ISBN 978-82-471-6342-9 (electronic version), ISSN 1503-8181.

“Constitutive modelling of morsellised bone”,
Knut Birger Lunde, 2008:92, ISBN 978-82-471-7829-4 (printed version), ISBN 978-82-471-7832-4 (electronic version), ISSN 1503-8181.

“Experimental Investigations of Wind Loading on a Suspension Bridge Girder”,
Bjørn Isaksen, 2008:131, ISBN 978-82-471-8656-5 (printed version), ISBN 978-82-471-8673-2 (electronic version), ISSN 1503-8181.

“Cracking Risk of Concrete Structures in The Hardening Phase”,
Guomin Ji, 2008:198, ISBN 978-82-471-1079-9 (printed version), ISBN 978-82-471-1080-5 (electronic version), ISSN 1503-8181.

“Modelling and numerical analysis of the porcine and human mitral apparatus”,
Victorien Emile Prot, 2008:249, ISBN 978-82-471-1192-5 (printed version), ISBN 978-82-471-1193-2 (electronic version), ISSN 1503-8181.

“Strength analysis of net structures”,
Heidi Moe, 2009:48, ISBN 978-82-471-1468-1 (printed version), ISBN 978-82-471-1469-8 (electronic version), ISSN 1503-8181.

“Numerical analysis of ductile fracture in surface cracked shells”,
Espen Berg, 2009:80, ISBN 978-82-471-1537-4 (printed version), ISBN 978-82-471-1538-1 (electronic version), ISSN 1503-8181.

“Subject specific finite element analysis of bone – for evaluation of the healing of a leg lengthening and evaluation of femoral stem design”,
Sune Hansborg Pettersen, 2009:99, ISBN 978-82-471-1579-4 (printed version), ISBN 978-82-471-1580-0 (electronic version), ISSN 1503-8181.

“Evaluation of fracture parameters for notched multi-layered structures”,
Lingyun Shang, 2009:137, ISBN 978-82-471-1662-3 (printed version), ISBN 978-82-471-1663-0 (electronic version), ISSN 1503-8181.

“Modelling of Dynamic Material Behaviour and Fracture of Aluminium Alloys for Structural Applications”,
Yan Chen, 2009:69, ISBN 978-82-471-1515-2 (printed version), ISBN 978-82-471-1516-9 (electronic version), ISSN 1503-8181.

“Nanomechanics of polymer and composite particles”,
Jianying He 2009:213, ISBN 978-82-471-1828-3 (printed version), ISBN 978-82-471-1829-0 (electronic version), ISSN 1503-8181.

“Mechanical properties of clear wood from Norway spruce”

Kristian Berbom Dahl 2009:250, ISBN 978-82-471-1911-2 (printed version) ISBN 978-82-471-1912-9 (electronic version), ISSN 1503-8181.

“Modeling of the degradation of TiB₂ mechanical properties by residual stresses and liquid Al penetration along grain boundaries”

Micol Pezzotta 2009:254, ISBN 978-82-471-1923-5 (printed version) ISBN 978-82-471-1924-2 (electronic version) ISSN 1503-8181.

“Effect of welding residual stress on fracture”

Xiabo Ren 2010:77, ISBN 978-82-471-2115-3 (printed version) ISBN 978-82-471-2116-0 (electronic version), ISSN 1503-8181.

“Pan-based carbon fiber as anode material in cathodic protection system for concrete structures”

Mahdi Chini 2010:122, ISBN 978-82-471-2210-5 (printed version) ISBN 978-82-471-2213-6 (electronic version), ISSN 1503-8181.

“Structural behaviour of deteriorated and retrofitted concrete structures”

Irina Vasililjeva Sæther 2010:171, ISBN 978-82-471-2315-7 (printed version) ISBN 978-82-471-2316-4 (electronic version) ISSN 1503-8181.

“Prediction of local snow loads on roofs”

Vivian Meløysund 2010:247, ISBN 978-82-471-2490-1 (printed version) ISBN 978-82-471-2491-8 (electronic version) ISSN 1503-8181.

“Behaviour and modelling of polymers for crash applications”

Virgile Delhaye 2010:251, ISBN 978-82-471-2501-4 (printed version) ISBN 978-82-471-2502-1 (electronic version) ISSN 1503-8181.

“Blended cement with reduced CO₂ emission – Utilizing the Fly Ash-Limestone Synergy”,

Klaartje De Weerd 2011:32, ISBN 978-82-471-2584-7 (printed version) ISBN 978-82-471-2584-4 (electronic version) ISSN 1503-8181.

“Chloride induced reinforcement corrosion in concrete” Concept of critical chloride content – methods and mechanisms.

Ueli Angst 2011:113, ISBN 978-82-471-2769-9 (printed version) ISBN 978-82-471-2763-6 (electronic version) ISSN 1503-8181.

“A thermo-electric-Mechanical study of the carbon anode and contact interface for Energy savings in the production of aluminium”.

Dag Herman Andersen 2011:157, ISBN 978-82-471-2859-6 (printed version) ISBN 978-82-471-2860-2 (electronic version) ISSN 1503-8181.

“Structural Capacity of Anchorage Ties in Masonry Veneer Walls Subjected to Earthquake”. The implications of Eurocode 8 and Eurocode 6 on a typical Norwegian veneer wall.

Ahmed Mohamed Yousry Hamed 2011:181, ISBN 978-82-471-2911-1 (printed version) ISBN 978-82-471-2912-8 (electronic ver.) ISSN 1503-8181.

“Work-hardening behaviour in age-hardenable Al-Zn-Mg(-Cu) alloys”.

Ida Westermann , 2011:247, ISBN 978-82-471-3056-8 (printed ver.) ISBN 978-82-471-3057-5 (electronic ver.) ISSN 1503-8181.

“Behaviour and modelling of selfpiercing riveted connections using aluminium rivets”.

Nguyen-Hieu Hoang, 2011:266, ISBN 978-82-471-3097-1 (printed ver.) ISBN 978-82-471-3099-5 (electronic ver.) ISSN 1503-8181.

“Fibre reinforced concrete”.

Sindre Sandbakk, 2011:297, ISBN 978-82-471-3167-1 (printed ver.) ISBN 978-82-471-3168-8 (electronic ver.) ISSN 1503:8181.

“Dynamic behaviour of cablesupported bridges subjected to strong natural wind”.

Ole Andre Øiseth, 2011:315, ISBN 978-82-471-3209-8 (printed ver.) ISBN 978-82-471-3210-4 (electronic ver.) ISSN 1503-8181.

“Constitutive modeling of solargrade silicon materials”

Julien Cochard, 2011:307, ISBN 978-82-471-3189-3 (printed ver.) ISBN 978-82-471-3190-9 (electronic ver.) ISSN 1503-8181.

“Constitutive behavior and fracture of shape memory alloys”

Jim Stian Olsen, 2012:57, ISBN 978-82-471-3382-8 (printed ver.) ISBN 978-82-471-3383-5 (electronic ver.) ISSN 1503-8181.

“Field measurements in mechanical testing using close-range photogrammetry and digital image analysis”

Egil Fagerholt, 2012:95, ISBN 978-82-471-3466-5 (printed ver.) ISBN 978-82-471-3467-2 (electronic ver.) ISSN 1503-8181.

“Towards a better understanding of the ultimate behaviour of lightweight aggregate concrete in compression and bending”.

Håvard Nedrelid, 2012:123, ISBN 978-82-471-3527-3 (printed ver.) ISBN 978-82-471-3528-0 (electronic ver.) ISSN 1503-8181.

“Numerical simulations of blood flow in the left side of the heart”

Sigrid Kaarstad Dahl, 2012:135, ISBN 978-82-471-3553-2 (printed ver.) ISBN 978-82-471-3555-6 (electronic ver.) ISSN 1503-8181.

“Moisture induced stresses in glulam”

Vanessa Angst-Nicollier, 2012:139, ISBN 978-82-471-3562-4 (printed ver.) ISBN 978-82-471-3563-1 (electronic ver.) ISSN 1503-8181.

“Biomechanical aspects of distraction osteogenesis”

Valentina La Russa, 2012:250, ISBN 978-82-471-3807-6 (printed ver.) ISBN 978-82-471-3808-3 (electronic ver.) ISSN 1503-8181.

“Ductile fracture in dual-phase steel. Theoretical, experimental and numerical study”
Gaute Gruben, 2012:257, ISBN 978-82-471-3822-9 (printed ver.) ISBN 978-82-471-3823-6 (electronic ver.) ISSN 1503-8181.

“Damping in Timber Structures”
Nathalie Labonnote, 2012:263, ISBN 978-82-471-3836-6 (printed ver.) ISBN 978-82-471-3837-3 (electronic ver.) ISSN 1503-8181.

“Biomechanical modeling of fetal veins: The umbilical vein and ductus venosus bifurcation”
Paul Roger Leinan, 2012:299, ISBN 978-82-471-3915-8 (printed ver.) ISBN 978-82-471-3916-5 (electronic ver.) ISSN 1503-8181.

“Large-Deformation behaviour of thermoplastics at various stress states”
Anne Serine Ognedal, 2012:298, ISBN 978-82-471-3913-4 (printed ver.) ISBN 978-82-471-3914-1 (electronic ver.) ISSN 1503-8181.

“Hardening accelerator for fly ash blended cement”
Kien Dinh Hoang, 2012:366, ISBN 978-82-471-4063-5 (printed ver.) ISBN 978-82-471-4064-2 (electronic ver.) ISSN 1503-8181.

“From molecular structure to mechanical properties”
Jiayang Wu, 2013:186, ISBN 978-82-471-4485-5 (printed ver.) ISBN 978-82-471-4486-2 (electronic ver.) ISSN 1503-8181.

“Experimental and numerical study of hybrid concrete structures”
Linn Grepstad Nes, 2013:259, ISBN 978-82-471-4644-6 (printed ver.) ISBN 978-82-471-4645-3 (electronic ver.) ISSN 1503-8181.

“Mechanics of ultra-thin multi crystalline silicon wafers”
Saber Saffar, 2013:199, ISBN 978-82-471-4511-1 (printed ver.) ISBN 978-82-471-4513-5 (electronic ver.) ISSN 1503-8181.

“Through process modelling of welded aluminium structures”
Anizahyati Alisibramulisi, 2013:325, ISBN 978-82-471-4788-7 (printed ver.) ISBN 978-82-471-4789-4 (electronic ver.) ISSN 1503-8181.

“Combined blast and fragment loading on steel plates”
Knut Gaarder Rakvåg, 2013:361, ISBN 978-82-471-4872-3 (printed ver.) ISBN 978-82-4873-0 (electronic ver.) ISSN 1503-8181.

“Characterization and modelling of the anisotropic behaviour of high-strength aluminium alloy”
Marion Fourmeau, 2014:37, ISBN 978-82-326-0008-3 (printed ver.) ISBN 978-82-326-0009-0 (electronic ver.) ISSN 1503-8181.

“Behaviour of threaded steel fasteners at elevated deformation rates”
Henning Fransplass, 2014:65, ISBN 978-82-326-0054-0 (printed ver.) ISBN 978-82-326-0055-7 (electronic ver.) ISSN 1503-8181.

“Sedimentation and Bleeding”

Ya Peng, 2014:89, ISBN 978-82-326-0102-8 (printed ver.) ISBN 978-82-326-0103-5 (electric ver.) ISSN 1503-8181.

“Impact against X65 offshore pipelines”

Martin Kristoffersen, 2014:362, ISBN 978-82-326-0636-8 (printed ver.) ISBN 978-82-326-0637-5 (electronic ver.) ISSN 1503-8181.

“Formability of aluminium alloy subjected to prestrain by rolling”

Dmitry Vysochinskiy, 2014:363,, ISBN 978-82-326-0638-2 (printed ver.) ISBN 978-82-326-0639-9 (electronic ver.) ISSN 1503-8181.

“Experimental and numerical study of Yielding, Work-Hardening and anisotropy in textured AA6xxx alloys using crystal plasticity models”

Mikhail Khadyko, 2015:28, ISBN 978-82-326-0724-2 (printed ver.) ISBN 978-82-326-0725-9 (electronic ver.) ISSN 1503-8181.

“Behaviour and Modelling of AA6xxx Aluminium Alloys Under a Wide Range of Temperatures and Strain Rates”

Vincent Vilamosa, 2015:63, ISBN 978-82-326-0786-0 (printed ver.) ISBN 978-82-326-0787-7 (electronic ver.) ISSN 1503-8181.

“A Probabilistic Approach in Failure Modelling of Aluminium High Pressure Die-Castings”

Octavian Knoll, 2015:137, ISBN 978-82-326-0930-7 (printed ver.) ISBN 978-82-326-0931-4 (electronic ver.) ISSN 1503-8181.

“Ice Abrasion on Marine Concrete Structures”

Egil Møen, 2015:189, ISBN 978-82-326-1034-1 (printed ver.) ISBN 978-82-326-1035-8 (electronic ver.) ISSN 1503-8181.

“Fibre Orientation in Steel-Fibre-Reinforced Concrete”

Giedrius Zirgulis, 2015:229, ISBN 978-82-326-1114-0 (printed ver.) ISBN 978-82-326-1115-7 (electronic ver.) ISSN 1503-8181.

“Effect of spatial variation and possible interference of localised corrosion on the residual capacity of a reinforced concrete beam”

Mohammad Mahdi Kioumars, 2015:282, ISBN 978-82-326-1220-8 (printed ver.) ISBN 978-82-326-1221-5 (electronic ver.) ISSN 1503-8181.

“The role of concrete resistivity in chloride-induced macro-cell corrosion”

Karla Horbostel, 2015:324, ISBN 978-82-326-1304-5 (printed ver.) ISBN 978-82-326-1305-2 (electronic ver.) ISSN 1503-8181.

“Flowable fibre-reinforced concrete for structural applications”

Elena Vidal Sarmiento, 2015:335, ISBN 978-82-326-1324-3 (printed ver.) ISBN 978-82-326-1325-0 (electronic ver.) ISSN 1503-8181.

“Development of chushed sand for concrete production with microproportioning” Rolands Cepuritis, 2016:19, ISBN 978-82-326-1382-3 (printed ver.) ISBN 978-82-326-1383-0 (electronic ver.) ISSN 1503-8181.

“Withdrawal properties of threaded rods embedded in glued-laminated timber elements” Haris Stamatopoulos, 2016:48, ISBN 978-82-326-1436-3 (printed ver.) ISBN 978-82-326-1437-0 (electronic ver.) ISSN 1503-8181.

“An Experimental and numerical study of thermoplastics at large deformation” Marius Andersen, 2016:191, ISBN 978-82-326-1720-3 (printed ver.) ISBN 978-82-326-1721-0 (electronic ver.) ISSN 1503-8181.

“Modeling and Simulation of Ballistic Impact” Jens Kristian Holmen, 2016:240, ISBN 978-82-326-1818-7 (printed ver.) ISBN 978-82-326-1819-4 (electronic ver.) ISSN 1503-8181.

“Early age crack assessment of concrete structures” Anja B. Estensen Klausen, 2016:256, ISBN 978-82-326-1850-7 (printed ver.) ISBN 978-82-326-1851-4 (electronic ver.) ISSN 1503-8181.

“Uncertainty quantification and sensitivity analysis for cardiovascular models” Vinzenz Gregor Eck, 2016:234, ISBN 978-82-326-1806-4 (printed ver.) ISBN 978-82-326-1807-1 (electronic ver.) ISSN 1503-8181.

“Dynamic behaviour of existing and new railway catenary systems under Norwegian conditions” Petter Røe Nåvik, 2016:298, ISBN 978-82-326-1935-1 (printed ver.) ISBN 978-82-326-1934-4 (electronic ver.) ISSN 1503-8181.

“Mechanical behaviour of particle-filled elastomers at various temperatures” Arne Ilseng, 2016:295, ISBN 978-82-326-1928-3 (printed ver.) ISBN 978-82-326-1929-0 (electronic ver.) ISSN 1503-8181.

“Nanotechnology for Anti-Icing Application” Zhiwei He, 2016:348, ISBN 978-82-326-2038-8 (printed ver.) ISBN 978-82-326-2019-5 (electronic ver.) ISSN 1503-8181.

“Conduction Mechanisms in Conductive Adhesives with Metal-Coated Polymer Spheres” Sigurd Rolland Pettersen, 2016:349, ISBN 978-82-326-2040-1 (printed ver.) ISBN 978-82-326-2041-8 (electronic ver.) ISSN 1503-8181.

“The interaction between calcium lignosulfonate and cement” Alessia Colombo, 2017:20, ISBN 978-82-326-2122-4 (printed ver.) ISBN 978-82-326-2123-1 (electronic ver.) ISSN 1503-8181.

“Behaviour and Modelling of Flexible Structures Subjected to Blast Loading” Vegard Aune, 2017:101, ISBN 978-82-326-2274-0 (printed ver.) ISBN 978-82-326-2275-7 (electronic ver.) ISSN 1503-8181.

“Behaviour of steel connections under quasi-static and impact loading”

Erik Løhre Grimsmo, 2017:159, ISBN 978-82-326-2390-7 (printed ver.) ISBN 978-82-326-2391-4 (electronic ver.) ISSN 1503-8181.

“An experimental and numerical study of cortical bone at the macro and Nano-scale”

Masoud Ramenzanzadehkoldeh, 2017:208, ISBN 978-82-326-2488-1 (printed ver.) ISBN 978-82-326-2489-8 (electronic ver.) ISSN 1503-8181.

“Optoelectrical Properties of a Novel Organic Semiconductor: 6,13-Dichloropentacene” Mao Wang, 2017:130, ISBN 978-82-326-2332-7 (printed ver.) ISBN 978-82-326-2333-4 (electronic ver.) ISSN 1503-8181.

“Core-shell structured microgels and their behavior at oil and water interface”

Yi Gong, 2017:182, ISBN 978-82-326-2436-2 (printed. ver.) ISBN 978-82-326-2437-9 (electronic ver.) ISSN 1503-8181.

“Aspects of design of reinforced concrete structures using nonlinear finite element analyses”

Morten Engen, 2017:149, ISBN 978-82-326-2370-9 (printed ver.) ISBN 978-82-326-2371-6 (electronic ver.) ISSN 1503-8181.

“Numerical studies on ductile failure of aluminium alloys”

Lars Edvard Dæhli, 2017:284, ISBN 978-82-326-2636-6 (printed ver.) ISBN 978-82-326-2637-3 (electronic ver.) ISSN 1503-8181.

“Modelling and Assessment of Hydrogen Embrittlement in Steels and Nickel Alloys”

Haiyang Yu, 2017:278, ISBN 978-82-326-2624-3 (printed. ver.) ISBN 978-82-326-2625-0 (electronic ver.) ISSN 1503-8181.

“Network arch timber bridges with light timber deck on transverse crossbeams”

Anna Weronika Ostrycharczyk, 2017:318, ISBN 978-82-326-2704-2 (printed ver.) ISBN 978-82-326-2705-9 (electronic ver.) ISSN 1503-8181.

“Splicing of Large Glued Laminated Timber Elements by Use of Long Threaded Rods”

Martin Cepelka, 2017:320, ISBN 978-82-326-2708-0 (printed ver.) ISBN 978-82-326-2709-7 (electronic ver.) ISSN 1503-8181.

“Thermomechanical behaviour of semi-crystalline polymers: experiments, modelling and simulation”

Joakim Johnsen, 2017:317, ISBN 978-82-326-2702-8 (printed ver.) ISBN 978-82-326-2703-5 (electronic ver.) ISSN 1503-8181.

“Small-Scale Plasticity under Hydrogen Environment”

Kai Zhao, 2017:356, ISBN 978-82-326-2782-0 (printed ver.) ISBN 978-82-326-2783-7 (electronic er.) ISSN 1503-8181.

“Risk and Reliability Based Calibration of Structural Design Codes”

Michele Baravalle, 2017:342, ISBN 978-82-326-2752-3 (printed ver.) ISBN 978-82-326-2753-0 (electronic ver.) ISSN 1503-8181.

“Dynamic behaviour of floating bridges exposed to wave excitation”

Knut Andreas Kvåle, 2017:365, ISBN 978-82-326-2800-1 (printed ver.) ISBN 978-82-326-2801-8 (electronic ver.) ISSN 1503-8181.

“Dolomite calcined clay composite cement – hydration and durability”

Alisa Lydia Machner, 2018:39, ISBN 978-82-326-2872-8 (printed ver.) ISBN 978-82-326-2873-5 (electronic ver.) ISSN 1503-8181.

“Modelling of the self-excited forces for bridge decks subjected to random motions: an experimental study”

Bartosz Siedziako, 2018:52, ISBN 978-82-326-2896-4 (printed ver.) ISBN 978-82-326-2897-1 (electronic ver.) ISSN 1503-8181.

“A probabilistic-based methodology for evaluation of timber facade constructions”

Klodian Gradeci, 2018:69, ISBN 978-82-326-2928-2 (printed ver.) ISBN 978-82-326-2929-9 (electronic ver.) ISSN 1503-8181.

“Behaviour and modelling of flow-drill screw connections”

Johan Kolstø Sønstabø, 2018:73, ISBN 978-82-326-2936-7 (printed ver.) ISBN 978-82-326-2937-4 (electronic ver.) ISSN 1503-8181.

“Full-scale investigation of the effects of wind turbulence characteristics on dynamic behavior of long-span cable-supported bridges in complex terrain”

Aksel Fenerci, 2018 100, ISBN 978-82-326-2990-9 (printed ver.) ISBN 978-82-326-2991-6 (electronic ver.) ISSN 1503-8181.

“Modeling and simulation of the soft palate for improved understanding of the obstructive sleep apnea syndrome”

Hongliang Liu, , 2018:101, ISBN 978-82-326-2992-3 (printed ver.) ISBN 978-82-326-2993-0 (electronic ver.) ISSN 1503-8181.

“Long-term extreme response analysis of cable-supported bridges with floating pylons subjected to wind and wave loads”.

Yuwang Xu, 2018:229, ISBN 978-82-326-3248-0 (printed ver.) ISBN 978-82-326-3249-7 (electronic ver.) ISSN 1503-8181.